Directed Phase Separation of Polymer Blends on Binary-Patterned Polymer Brushes

Claire Tamsin Wilshaw

Department of Chemistry

University of Sheffield

September 2009

A thesis presented for the degree of Doctor of Philosophy

Declaration

I certify that this thesis submitted for the degree of Doctor of Philosophy is the result of my own research, except where otherwise acknowledged. No portion of the work presented in this thesis has been submitted for another degree or qualification to this, or any other university or institution.

Signed

Claire Wilshaw

Department of Chemistry
The University of Sheffield
Sheffield
United Kingdom
September 2009

Abstract

Self-assembly of well-defined polymer microstructures is of interest for applications such as polymer solar cells, light emitting diodes, microelectronics and biosensors. Chemically patterned substrates can direct the phase separation of thin films of polymer blends, producing controlled morphologies. This has been demonstrated using patterned self-assembled monolayers. Binary-patterned polymer brushes provide a robust, chemically and topographically patterned surface which can interact with the blend, potentially resulting in interesting new behaviour, and greater control over phase separation.

Binary-patterned polystyrene/poly(methyl methacrylate) brushes were synthesised by a novel method. A self-assembled monolayer of triethoxysilane was patterned by exposure to ultraviolet light. This produced amine-terminated areas that could react with 2-bromoisobutyryl bromide to produce initiators for atom transfer radical polymerisation, allowing the synthesis of patterned polymer brushes. Dehalogenation of the first brush, followed by deprotection, modification and a second polymerisation produced binary-patterned brushes. Unpatterned and patterned polymer brushes were characterised using ellipsometry, x-ray photoelectron spectroscopy, contact angles, atomic force microscopy, lateral force microscopy, optical microscopy and secondary ion mass spectrometry. An alternative approach, based on direct microcontact printing of an atom transfer radical polymerisation initiator, 11-(2-bromo-2-methyl)propionyloxyundecyltrichlorosilane, was also investigated, although this approach was ultimately unsuccessful.

The behaviour of thin films of polystyrene/poly(methyl methacrylate) blends on silicon, patterned self-assembled monolayers and binary-patterned polymer brushes was studied. The morphologies were investigated using atomic force microscopy, optical microscopy, nuclear reaction analysis and secondary ion mass spectrometry, in order to determine the effect of the binary-patterned polymer brushes on the domain structure of the blend. The blend morphology was complex and reflected interactions between the blend and the brushes (as well as other factors). When the natural length scale of the blend is commensurate with the underlying pattern, phase separation may be spatially directed by the substrate.

Acknowledgements

I would like to thank my supervisor, Prof. Tony Ryan, for his continued faith in me, and patience, optimism and encouragement over the last four years.

Special thanks go to Dr Steve Edmondson and Dr Mike Tomlinson for helpful discussions and suggestions to do with the synthesis of polymer brushes. Thanks also to Prof. Graham Leggett and Shahrul Ahmad for providing me with NPPOC-silane coated samples and allowing me to extend their patterning method to allow the synthesis of binary patterned polymer brushes.

Thanks to all the technical and academic staff and other students who trained me to use particular techniques or helped me to analyse my samples, including Dr Cvetelin Vasilev, Dr Jamie Hobbs, Nic Mullin and Christa Webber (AFM), Dr Tracie Whittle (XPS and SIMS), Dr Andrew Parnell, Dr Sasha Heriot and Mike Weir (ellipsometry), Dr Mark Geoghegan, Dr Richard Thompson and Dr Parvaneh Mokarian-Tabari (NRA) and Dr Heath Bagshaw (SEM).

I would like to thank my colleagues in the Polymer Scattering Group past and present for friendship, patience, good humour, help with finding things in the lab, and always being prepared to answer questions or provide assistance. Thanks to Christine, Andy, Patrick, Shaomin, Sasha, Nadia, Carme, Rob, Pierre, Lorena, Adam, Josh, Keqin, Claire, Mel, Anne-Cecile, Sarah, Oscar, Yu Hao, Lewis, Craig, Susi, Gary, Joyce, Matt and Masa.

I am grateful to my family for their continued understanding, encouragement and support throughout the past four years. I would particularly like to thank my Mum, and my sister Vanessa for proofreading sections of this thesis. Thanks are also owed to my friends, mainly for putting up with me. I would especially like to thank Neil Chapman, Rachel Wilson, Clare Winter, Jeanie Worthington and Tom Fenton who gave up their time to help with proofreading.

Contents

Abbreviations

Terminology

AFM	Atomic Force Microscopy
AIBN	2,2'-azobisisobutyronitrile
Amine-silane	aminopropyltriethoxysilane
ATRP	Atom Transfer Radical Polymerisation
BMPUS	11-(2-bromo-2-methyl)propionyloxyundecyltrichlorosilane
bpy	2,2'-bipyridine
Bromoester-silane	3-(2-Bromoisobutyramido)propyl(triethoxy)silane
χ	Flory – Huggins interaction parameter
DMF	*N,N*-dimethylformamide
dnNbpy	4,4'-di-*n*-nonyl-2,2'-bipyridine
dPS	Deuterated polystyrene
FFM	Friction Force Microscopy
LCST	Lower Critical Solution Temperature
LFM	Lateral Force Microscopy
MMA	Methyl methacrylate
MSE	Mean Squared Error
μCP	Microcontact printing
N	Degree of polymerisation
NMP	Nitroxide Mediated Polymerisation
NPPOC-silane	{N-[2-(2-nitrophenyl)propan-1-oxycarbonyl]-3-aminopropyl} triethoxysilane
NRA	Nuclear Reaction Analysis
OTS	Octadecyltrichlorosilane
PMDETA	N,N,N',N'',N''-pentamethyldiethylenetriamine
PBD	Polybutadiene
PBr_xS	Partially brominated polystyrene or poly(styrene-co-4-bromostyrene)
PDMS	Poly(dimethylsiloxane)
PGMA	Poly(glycidyl methacrylate)
PMMA	Poly(methyl methacrylate)

1. Introduction

PNIPAM	Poly(N-isopropylacrylamide)
POEGMA	Poly[oligo(ethylene glycol)methacrylate]
PS	Polystyrene
PVME	Poly(vinyl methyl ether)
PVP	Poly(vinylpyridine)
R_a	Arithmetic average of the absolute values of the surface height deviations measured from the mean plane
R_g	Radius of gyration
Rms	Root mean square average of height deviations from the mean data plane
ROMP	Ring Opening Metathesis Polymerisation
ROP	Ring Opening Polymerisation
SALS	Small Angle Light Scattering
SAM	Self-Assembled Monolayer
SEM	Scanning Electron Microscopy
SIMS	Secondary Ion Mass Spectrometry
T_g	Glass transition temperature
THF	Tetrahydrofuran
UCST	Upper Critical Solution Temperature
XPS	X-ray Photoelectron Spectroscopy

Chapter 1

Introduction

The surface of a material controls its interaction with the environment, so thin coatings can dramatically alter and improve the properties of the material[1]. For example, conventional paint or varnish can be used to protect and waterproof wood. This has led to the coatings industry becoming a multibillion dollar business. However, there is increasing interest in functional coatings for a vast variety of different high tech applications[1]. Conventional polymer coatings are widely used to tailor surface properties such as wettability, biocompatibility, corrosion resistance, friction and adhesion[1,2]. A layer only a few ångstroms thick can completely hide the chemical nature of the underlying material and dictate the interaction of the system with the environment (for example, oxidised silicon has an advancing contact angle of < 20º; coating it with a self-assembled monolayer of octadecyltrichlorosilane (OTS) only 2 nm thick increases this to over 90º [3,4]). Simple coatings rely on intermolecular interactions between a disordered array of coating molecules and the substrate, so can fail by a variety of mechanisms including desorption, displacement, dewetting and delamination.

More robust coatings can be obtained by chemically bonding the coating molecules to the surface. Attachment of coating molecules to a surface by one end can lead to the formation of densely packed, well-defined layers that may have interesting and useful properties. Two such coatings are self-assembled monolayers (SAMs) and polymer brushes. SAMs form spontaneously by chemisorption and self-organisation of functionalised organic molecules on a suitable substrate[5]. Polymer brushes are long chain polymer molecules attached by one end to a surface or interface, with a density of attachment points high enough that the chains are obliged to stretch away from the surface/interface, sometimes much further than the typical unstretched size of a chain[6]. Polymer brushes have been extensively studied, particularly since the development of controlled radical polymerisation methods such as atom transfer radical polymerisation (ATRP). Controlled surface-initiated polymerisation from an initiator-functionalised SAM can be used to produce densely grafted polymer brushes and block copolymer

brushes of controlled thickness. These methods allow the production of mechanically and chemically robust coatings, with a high degree of synthetic flexibility towards the introduction of functional groups[2]. Functional and diblock copolymer brushes allow access to 'smart' or responsive surfaces which can change a physical property such as hydrophilicity or biocompatibility in response to an external trigger such as heat (polymers that have a lower critical solution temperature (LCST)), pH or salt concentration (polyelectrolytes)[2].

Microfabrication, the generation of small structures, is essential to much of modern science and technology; it supports information technology and permeates society through its role in microelectronics and optoelectronics[5]. The majority of commercial microfabrication is performed using photolithography, but this has several disadvantages. It is expensive, and only applicable to a limited range of photosensitive materials (photoresists), mainly on semiconductor substrates. The minimum feature size is defined by the wavelength of light used. It is also poorly suited for introducing specific chemical functionalities or producing three dimensional structures[5,7]. There is great interest in the development of alternative patterning techniques that can produce chemically and/or topographically patterned materials. Microcontact printing (μCP) can be used to form patterned SAMs, which can then be used as resists for selective etching or to self-assemble droplets of liquids on particular regions of the pattern[5,7,8]. This may lead to a range of applications, including uses in microelectronics and biosensors. Amplification of a patterned SAM into a patterned polymer brush (regions coated with polymer brush separated by regions of SAM-coated or bare substrate) or a binary-patterned polymer brush (adjacent regions of two chemically different polymer brushes) produces a more robust layer with fewer defects[9,10], and allows much greater control over the surface chemistry[11]. At the present time there have been few examples of the synthesis of binary-patterned polymer brushes, and little study of their properties.

Polymers are used in all areas of modern life and a vast range of polymers with very different properties have been synthesised. It would be useful, and commercially desirable, if new materials could be made by mixing two polymers, each with some of the required properties. This is not usually possible because most polymer blends which are mixtures of two (or more) polymers, are thermodynamically incompatible and

phase-separate[12,13]. Understanding and predicting the behaviour of polymer blends has been a subject of intensive study. The properties of a phase-separated blend are determined by the nature of the domain structure[14] and the strength of the interfaces between domains[13]. This can be controlled to some degree by changing the conditions e.g. blend composition, solvent, annealing temperature and time etc. In thin films of polymer blends, preferential attraction of one of the polymers to the substrate can affect the structure of the entire film, so changing the nature of the substrate can completely change the domain structure[15-17]. Patterned substrates can be used to direct the phase separation of thin films of polymer blends, giving control over the domain structure[18]. This pattern-directed phase separation has been demonstrated on patterned SAMs, and has been shown to have practical uses, for example the efficiency of polymer LEDs can be improved by controlling the domain structures of blends of semiconducting polymers[19-21]. However, there has been little study of the behaviour of polymer blends on patterned (or homogeneous) polymer brushes. Polymer brushes have different properties to SAMs, which may result in interesting new effects on these surfaces, and possibly increased control of phase separation.

The work presented in this thesis attempts to address some of the gaps in knowledge about the behaviour of polymer brushes and blends. The aims of this work were to synthesise binary-patterned polymer brushes and investigate the phase separation of a polymer blend on the patterned substrates. It was decided to concentrate on polystyrene (PS) and poly(methyl methacrylate) (PMMA), as there are many examples of the synthesis of PS and PMMA brushes, and they form an incompatible blend that has been well studied. It was decided to concentrate on brush synthesis by ATRP from an alkyltrichlorosilane-based initiator SAM. Silicon was chosen as the substrate, as it is used commercially (especially in the semiconductor/computer industry), has analogous surface chemistry to glass, silica particles and plasma-treated polymers.

The experimental work was split into several stages:

- Reproducible synthesis of smooth PMMA and PS brushes of controlled thickness.
- Production of patterned polymer brushes.

- Development of the patterning method to allow the synthesis of binary-patterned PS/PMMA brushes.
- Investigation of the behaviour of thin films of PS/PMMA blends on both homogeneous and patterned substrates to determine the effect of a binary-patterned polymer brush on the blend morphology.

The rest of this thesis presents and discusses the results of these experiments with reference to other relevant work.

1.1 Polymer Brushes

'Polymer brushes' can be formed by polymer micelles, block copolymers at fluid – fluid interfaces (e.g. vesicles and microemulsions), graft copolymers at fluid – fluid interfaces, adsorbed diblock copolymers and grafted polymers on a solid surface[22]. This thesis only considers brushes on solid substrates. These can be formed by physisorption, chemisorption or surface-initiated polymerisation.

1.1.1 Conformations of Polymers Attached to Interfaces

The behaviour of polymer chains attached by one end to a surface or interface is determined by the grafting density, σ, the number of chains grafted per unit area. If the grafting density is low, the distance between individual chains will be greater than their radius of gyration, R_g, so each chain will be isolated from its neighbours[13]. The conformation of the chains depends on the interaction of the polymer with the substrate. Where this is weak (or repulsive), a 'mushroom' morphology forms to minimise the polymer – substrate contact. This consists of typical random polymer coils attached to the surface by stems of varying size. If the polymer strongly adsorbs onto the surface, a flat 'pancake' will be formed[1]. This is shown schematically in Figure 1.1 a) and b).

Once the distance between the grafting points becomes less than R_g, the polymer chains begin to overlap[1,13]. The unfavourable interactions between adjacent molecules can

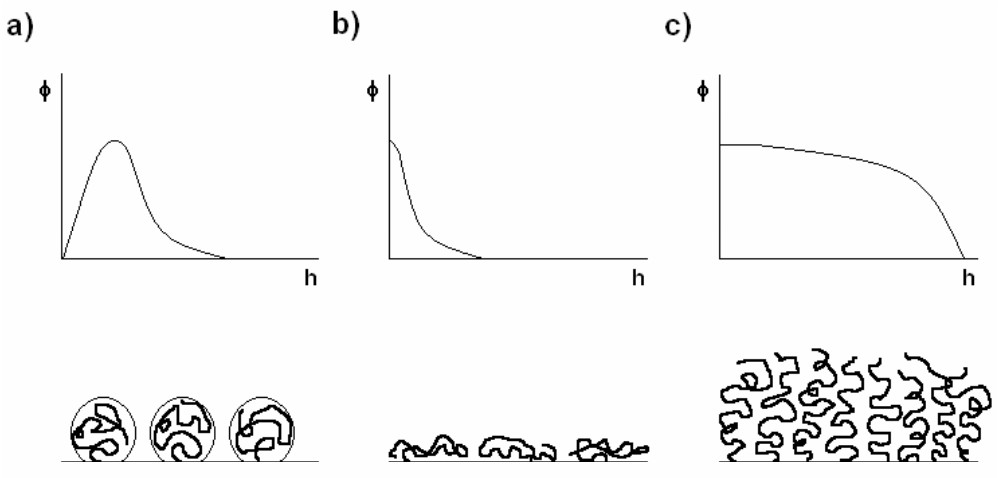

Figure 1.1 Segment density profiles (volume fraction, ϕ – height, h) and schematic illustrations of conformations of surface-attached polymers. a) mushroom, b) pancake, c) brush (parabolic brush density profile)[1].

be reduced by stretching away from the surface, but this decreases the number of possible polymer configurations, resulting in a reduction in the entropy of the system[1]. The polymer chains have two conflicting tendencies: to maximise their configurational entropy, which favours short, dense brushes, and to maximise wetting by solvent, which favours tall, sparse brushes[6]. Where the distance between grafting sites is smaller than the radius of gyration of the equivalent free polymer, both conditions cannot be met, and at equilibrium the polymer chains adopt a stretched configuration. This is referred to as a polymer brush[1,6,22] (see Figure 1. 1 c). The eventual thickness of the brush layer is a balance between two free energy costs – stretching, which reduces the configurational entropy, and overlap of neighbouring chains, which reduces the energetically favourable interaction with solvent molecules[6].

A simple model of brush behaviour was developed by Alexander[23] and de Gennes[24,25]. It considers a system of monodisperse polymer chains, with degree of polymerisation, N, and statistical segment (or monomer) size, a, tethered to a flat, non-adsorbing surface[22], and exposed to a solvent[6]. The free energy of the polymer brush, F, is a balance of the interaction energy between the statistical segments, F_{int}, and the energy difference between stretched and unstretched chains, caused by the entropy lost by stretching, F_{el} (elastic free energy) [1,22,26]:

$$F = F_{\text{int}} + F_{el} \qquad (1.1)$$

1. Introduction

The discussion that follows considers grafted polymer chains exposed to a good solvent. At relatively low grafting densities, conditions inside the brush are semidilute, and scaling arguments can be used to construct the dependence of the brush height on the grafting density and chain length[13]. A schematic diagram of the model is shown in Figure 1.2.

The average distance between attachment sites is given by[13,25]:

$$d = a\sigma^{-1/2} \qquad (1.2)$$

A grafted chain may be subdivided into 'blobs' of linear size d, each containing N_b monomer units. At small scales (e.g. less than d), the correlations are dominated by excluded volume effects[25]. This means that, within each blob, the chain segments behave as random coils[13,25], and:

$$d = aN_b^{3/5} \qquad (1.3)$$

In the region occupied by the grafted chains, the blobs behave as hard spheres and fill space, so the polymer volume fraction within the brush (ϕ_b) takes the form:[13,25]:

$$\phi_b \approx \frac{a^3 N_b}{d^3} \qquad (1.4)$$

(The symbol $\approx$ is used to mean 'approximately equal to', or 'equal to, within a numerical factor of order one'[26]).

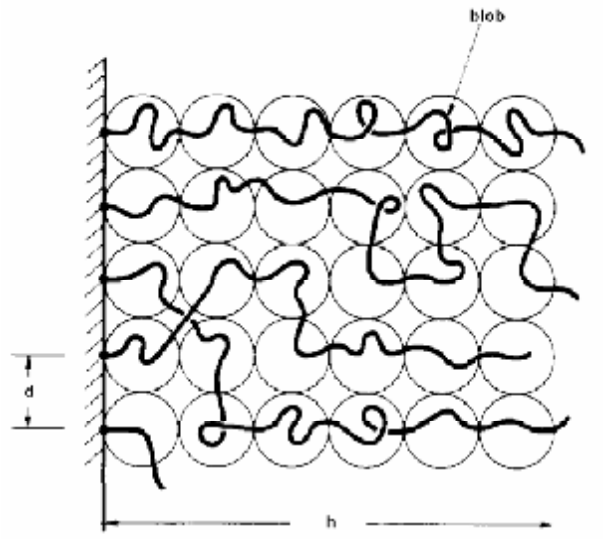

*Figure 1.2 Schematic illustration of the Alexander model[1,25,26] (reproduced with permission from de Gennes, P. G., Macromolecules, **1980**, 13, 1069-1075[25]. Copyright 1980 American Chemical Society).*

Substitution using equation (1.2) gives the relation between the volume fraction and the grafting density:

$$\phi_b \approx \frac{a^3 N_b}{(a\sigma^{1/2})^3}$$

$$\phi_b \approx N_b \sigma^{2/3} \qquad (1.5)$$

The thickness of the brush layer can then be calculated: the volume per grafted chain is hd^2, and it contains N monomers, so:

$$\phi_b \approx \frac{a^3 N}{hd^2} \qquad (1.6)$$

Substitution using equation (1. 2) gives:

$$\phi_b \approx \frac{Na^3}{ha^2\sigma^{1}} \qquad (1.7)$$

Substitution using equation (1.5) and rearrangement gives the approximate expression linking the brush thickness with the degree of polymerisation and grafting density[13,25]:

$$\frac{Na^3}{ha^2\sigma^{-1}} \approx N_b \sigma^{2/3}$$

$$h \approx \frac{Na\sigma^{1/3}}{N_b} \approx Na\sigma^{1/3} \qquad (1.8)$$

The most important feature of this expression is that the brush thickness increases linearly with N. In comparison, the radius of gyration of free polymer chains in solution in a good solvent is given by the Flory formula, so $R_g \propto N^{3/5}$[13]. Polymer molecules in a brush are strongly stretched and their properties may be expected to be quite different from those of free chains in solution[6].

For higher grafting densities, where the whole area of the interface is taken up by grafting sites, the Flory approximation can be used to obtain an explicit expression for the free energy[22] (NB. The scaling approach can also be used to obtain expressions for the free energy – see Halperin[26]). Two assumptions are made: firstly, the concentration of statistical segments within the brush is constant, so $\phi = \frac{Na^3}{d^2 h}$. Secondly, all the free chain ends are found at a distance, h, from the substrate[22,26]. The first simplifies the calculation of F_{int}, and the second yields a simple expression for F_{el}[26]. The Flory

approximation estimates the reduction in configurational entropy from results for an ideal random walk chain constrained to travel a distance h from the grafting surface to the outer edge of the brush. This form of the equation emphasises the physical origin of the stretching of tethered polymer chains[13]. The free energy per chain can be expressed by the following equation[22]:

$$\frac{F}{kT} \approx \frac{v\phi^2 d^2 h}{a^3} + \frac{h^2}{R_0^2} \qquad (1.9)$$

where v is a dimensionless excluded volume parameter, $v \approx 1 - 2\chi$, where χ is the Flory – Huggins interaction parameter[26], and $R_0 \approx N^{1/2} a$ is the radius of an ideal, unperturbed coil[22,26]. The first term represents the interaction energy between statistical segments and the second represents the elasticity of the Gaussian chains[22,26]. Minimisation with respect to h gives the following relation:

$$\frac{h}{a} \approx N\left(\frac{a}{d}\right)^{2/3} \approx N\sigma^{1/3} \qquad (1.10)$$

so this approach yields the same dependence of the layer thickness on N and σ as the scaling approach.

For polymer chains exposed to a theta solvent, the binary interaction between the statistical segments essentially disappears ($\chi = 1/2$ or v = 0) (in a theta solvent polymers exhibit ideal chain behaviour[27]). The expression must now account for three-body interactions:

$$\frac{F}{kT} \approx \frac{w\phi^3 d^2 h}{a^3} + \frac{h^2}{N a^2} \qquad (1.11)$$

where w is the dimensionless third virial coefficient. Minimisation with respect to h gives:

$$\frac{h}{a} \approx N\left(\frac{a}{d}\right) \approx N\sigma^{1/2} \qquad (1.12)$$

Similar arguments can be used to derive expressions for the behaviour of polymer chains exposed to poor solvents, and in the bulk state.

In conclusion, under all conditions (in the presence of a good solvent, a theta solvent or a poor solvent, or in the absence of solvent (melt conditions)), the polymer chains in tethered polymer brushes exhibit deformed configurations. The degree of deformation

depends on the environmental conditions to which the polymer chains are exposed[22]. However brush height always increases faster than the equivalent free chain dimension as N increases[6] and stretched configurations are found under equilibrium conditions[22]. The relationship between chain length and the dimensions of free and tethered chains under different conditions are summarised below:

	Tethered polymer chain	Free polymer chain
Good solvent	$h \approx N\sigma^{1/3}$	$R_g \approx N^{3/5}$
Theta solvent	$h \approx N\sigma^{1/2}$	$R_g \approx N^{1/2}$
Bulk state	$h \approx N^{2/3}$	$R_g \approx N^{1/2}$

Although this is a simple model, based solely on free energy arguments, it can be used to predict the experimentally observed scaling behaviour more or less completely, and can be used to roughly describe some of the key properties of polymer brushes[1] including the hydrodynamic properties, free energy per chain, and rough measurements of the stretching – repulsion balance[6]. These factors allow prediction of the hydrodynamic thickness, permeability, and force needed to compress a brush, as well as the lubrication properties that arise when two brushes are brought into near contact[22]. However, some important properties depend more sensitively on details of the brush structure such as the density profile of chains, the location of the free ends of the polymer chains, how the polymer chains segregate or mix in a system with either different chain lengths or different chemical compositions and how the polymer chains interpenetrate each other[22]. More sophisticated models have been devised to describe the detailed structure and behaviour of polymer brushes. For example the 'parabolic' brush model allows the free chain ends to be located at any distance from the substrate, and allows prediction of chain unit density profiles[6]. This, and other models, are discussed in more details in the references[6,13,26].

1.1.2 Types of Polymer Brushes

1.1.2.1 Physisorption

Brushes can be prepared by physisorption of block copolymers with 'sticky' segments. This can be done by a selective solvent approach, where the solvent is poor for one block, which collapses onto the substrate, and good for the other block, which stretches out to form the brush. Alternatively, there may be preferential adsorption if one block interacts strongly with the substrate[22]. Although this is a simple way to prepare polymer brushes, the polymer is only held onto the substrate by relatively weak intermolecular interactions such as van der Waals forces or hydrogen bonds. Desorption can occur on exposure to a good solvent for both blocks, and the brush can be displaced by other polymers or low molecular weight compounds. Also, thin polymer layers often dewet the substrate on heating above the glass transition temperature (T_g)[22]. A more versatile approach is to covalently bond the polymer to the substrate[22]. This is done by two main methods.

1.1.2.2 Grafting To

As shown in Figure 1.3, end-functionalised polymers can react with suitable functional groups on the substrate under appropriate conditions to form a tethered polymer brush[22]. End-functionalised polymers with narrow molecular weight distributions can be synthesised by living anionic, living cationic, living radical, group transfer and ring opening metathesis polymerisations. The substrate can be modified to contain suitable functional groups by coupling agents or SAMs etc[22]. However, there are some serious problems with the use of the 'grafting to' approach. Firstly, there are strict limits in the functional groups that can be present in the anchor group and/or in the polymer chain. Reactive groups in the polymer can lead to competing reactions with the substrate, or reactions between the anchor and the main polymer chains[1]. Secondly, the amount of polymer that can be immobilised is limited, both in terms of film thickness and grafting density, for both kinetic and thermodynamic reasons. As more and more polymer chains are grafted onto the surface, the polymer concentration at the substrate soon becomes higher than the concentration in solution (or in the bulk). Additional chains must diffuse against this concentration gradient to reach the surface. The rate of the

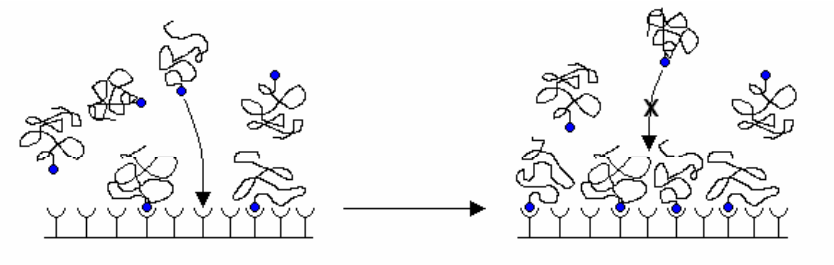

Figure 1.3 Grafting to. Initially, end-functionalised polymer molecules can react with reactive sites on the substrate to produce a grafted polymer layer. Once the concentration of the grafted layer exceeds the concentration of polymer in solution, addition of further chains becomes thermodynamically and kinetically unfavourable.

attachment reaction soon levels off, and attachment of further polymer becomes kinetically hindered and so very slow[1]. As the grafting density increases, the polymer chains must adopt a stretched conformation to avoid chain overlap. However, the loss of entropy during chain stretching is only offset by the formation of a single chemical bond, so attachment of further chains rapidly becomes thermodynamically unfavourable[1].

In a related approach, polymerisation is carried out in the presence of a substrate functionalised with monomers. When a growing polymer chain incorporates a surface bound monomer, it becomes attached to the surface, resulting in brush formation[1]. Unfortunately, the rate-limiting step is the surface-confined reaction, so the maximum grafting density is limited (as for the 'grafting to' approach)[1]. The random incorporation of the surface-bound monomers into the polymer may also lead to chain branching and chains that are attached to the surface at more than one point[1].

Some examples of physisorbed and grafted to brushes are discussed on page 52.

1.1.2.3 Grafting From/Surface-Initiated Polymerisation

A substrate with functional groups that can initiate polymerisation is exposed to a mixture containing monomer and catalyst, other reagents, solvents etc. Polymer chains can only grow from the initiator groups, so the reaction is surface-initiated, and (ideally) surface-confined, with no reaction occurring in solution[2]. When monomers approach the surface they react with the initiators, or add to growing chains. As the initial chains

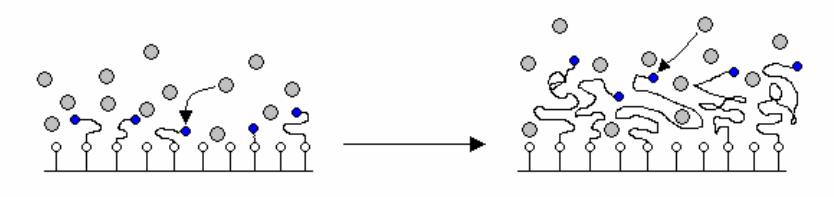

Figure 1.4 Grafting from/surface-initiated polymerisation. Surface-bound initiators can react with monomers in solution. As the polymer chains grow, monomer can continue to add to the active chain ends.

are very short, very high grafting densities can be achieved without steric hindrance. The polymer chains grow from the free ends, so monomer can continue to add to the growing chains without steric constraints. This method allows the production of dense, uniform brushes with highly stretched conformations and predictable and reproducible thicknesses. This is shown above in Figure 1.4.

This highly versatile approach has become the most popular technique for brush synthesis. Initiator groups can be immobilised onto the substrate by exposure to plasma or glow discharge in the presence of a gas or, more commonly, by forming an initiator-containing SAM[22]. In principle, almost any polymerisation can be used to 'grow' the brush. In order to achieve maximum control over brush density, polydispersity and composition, as well as allowing the production of block copolymer brushes, controlled polymerisation is highly desirable[2]. There have been reports of polymer brushes produced by conventional radical polymerisation, living ring-opening polymerisation (ROP), living anionic polymerisation, living cationic polymerisation, ring-opening metathesis polymerisation (ROMP), nitroxide-mediated polymerisation (NMP), reversible addition-fragmentation chain transfer (RAFT) polymerisation, and group transfer polymerisation[2,22]. Controlled radical polymerisations, most notably ATRP, have become the most popular methods, mostly because of their tolerance of a wide range of functional monomers and requirement of less stringent experimental conditions[2]. The synthesis of thiol- and silane-derivatised ATRP surface-bound initiators is easier than the 2,2'-azobisisobutyronitrile (AIBN) or nitroxide derivatives required for conventional free radical or nitroxide-mediated polymerisations[2]. ATRP and the formation of SAMs are discussed in more detail in the following sections.

1.1.3 Atom Transfer Radical Polymerisation

A polymerisation is said to be living when it proceeds in the absence of irreversible chain transfer and termination[28-30]. If there is complete and rapid initiation, and rapid exchange between reactive species, all the polymer chains grow at essentially the same rate, resulting in a linear increase in molecular weight with conversion and the production of polymers with low polydispersity (polydispersity = M_w/M_n). The degree of polymerisation can be controlled by varying the concentration of monomer relative to initiator. In the absence of termination, the reactive species are retained at the end of the polymerisation. Addition of fresh monomer results in continued polymerisation, and an increase in molecular weight (and the formation of block copolymers if a different monomer is used)[29,30]. Living polymerisations provide a route for the synthesis of polymers with well-defined structures including end-functionalised polymers, block copolymers, and star and comb polymers[29].

The first reported living polymerisation, living anionic polymerisation, was developed by Szwarc in the 1950s[31,32]. This approach can be used to produce well-defined polymers and block copolymers with very low polydispersities ($M_w/M_n < 1.1$). In this reaction the propagating species are stabilised anions. Under strictly aprotic conditions there is no formal termination step, so the active chain ends persist, even after complete monomer conversion. However, living anionic polymerisation can only be performed with a limited range of monomers – the monomer must contain substituents that can stabilise the negative charge (by delocalisation), and must not contain acidic, protic or strongly electrophilic groups that can react with bases or nucleophiles[30]. Living anionic polymerisation is also extremely sensitive to impurities, requiring the use of specialised glassware and the rigorous purification and drying of reagents[2,30]. This limits its use for the synthesis of polymer brushes[2].

Free radical polymerisation is the leading industrial method used to produce commercial polymers due to its relative synthetic ease and tolerance of functional groups and impurities[28,29], but it does not allow control of macromolecular structure[29] or molecular weight, and produces material of high polydispersity[33]. Controlled radical polymerisation is highly desirable, but difficult to achieve as radicals undergo very fast, near diffusion-controlled coupling and disproportionation reactions[29,34]. A more

controlled reaction could occur if there was a fast dynamic equilibrium formed between a very low concentration of active radicals and a vast majority of dormant chains. The low concentration of radicals minimises termination. Rapid exchange between active and dormant species allows a small number of radicals to propagate a large number of chains, and means that all the chains add monomer at essentially the same rate, giving control over molecular weight and polydispersity[29]. Since the mid-1990s several controlled radical polymerisations that fulfil these requirements have been developed.

In 1995 Wang and Matyjaszewski[35,36] and Kato *et al.*[34] independently developed ATRP, which is an extension of atom transfer radical addition (ATRA). ATRA is the transition metal-catalysed insertion of an alkene into the C-X bond of an alkyl halide (X represents a halogen atom). The transition metal complex reversibly abstracts the halogen atom from the alkyl halide, generating a radical which then reacts with the alkene, forming a C-C bond. The high efficiency of the transition metal-catalysed atom transfer reaction in producing the target product in good yield suggests that the process can effectively induce a low concentration of free radicals, resulting in reduced termination[35]. Both groups modified this reaction to allow more than one addition step to occur, resulting in a controlled radical polymerisation that could produce well-defined PS[35,36], poly(methyl acrylate)[35] and PMMA[34,35].

ATRP has been used produce a wide variety of polymers with good control over molecular weight and polydispersity. It has been used to synthesise polymers with controlled architectures including block copolymers[37-39], end-functionalised polymers[40-42], polymer brushes, and star, network and comb polymers[29].

The mechanism of ATRP is shown below (Scheme 1.1). Fast, efficient initiation establishes a constant concentration of growing radicals, which propagate a large number of polymer chains by rapid exchange between active and dormant species. Thermodynamically, the equilibrium must lie towards the side of the dormant chain ends to maintain a low enough steady-state concentration of radicals to minimise bimolecular termination. Kinetically, the exchange between dormant and active polymer chain ends must be fast, otherwise not all the chain ends will grow at the same rate, and polydispersity will increase[43].

Scheme 1.1 Mechanism of ATRP

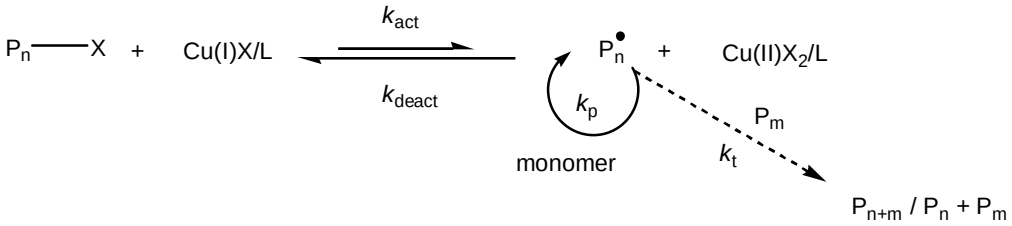

Overall

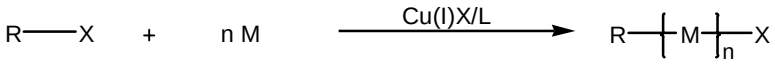

Initiation

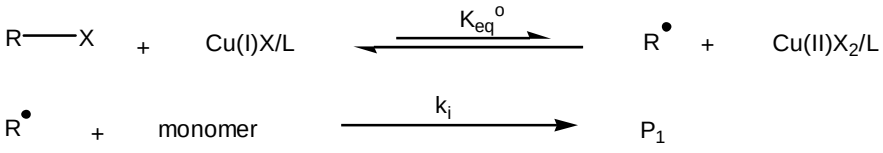

Propagation

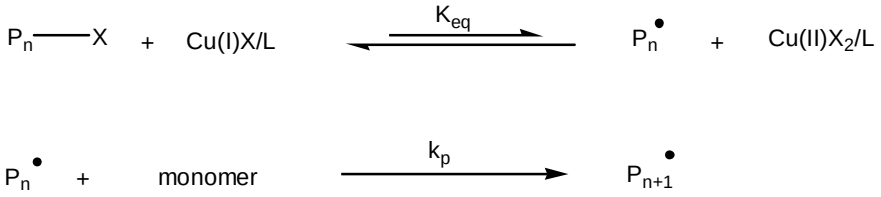

Termination

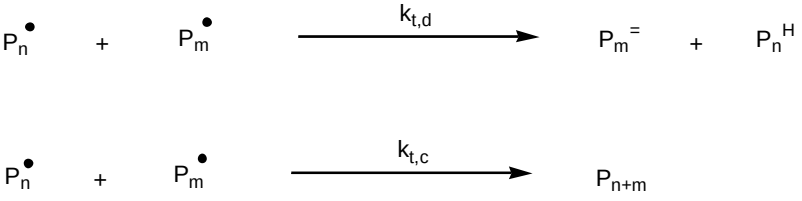

The rate law for ATRP is[29,44-46]:

$$K_{eq} = \frac{k_{act}}{k_{deact}} = \frac{[P_n^{\bullet}][Cu^{II}X_2]}{[Cu^{I}X][P_nX]} \quad (1.13)$$

$$R_p - k_{app}[M] - k_p[P_n^{\bullet}][M] - k_p K_{eq}[In]_0 \frac{[Cu^{I}X]}{[Cu^{II}X_2]}[M] \quad (1.14)$$

This means that the rate of polymerisation is first order with respect to the concentration of monomer[29,35].

Rearrangement and integration of this expression gives:

$$\ln\left(\frac{[M]_t}{[M]_0}\right) = -kt \quad (1.15)$$

where $[M]_0$ is the initial concentration of monomer, and $[M]_t$ is the concentration of monomer at time t. This can be used as a test for the controlled nature of an ATRP reaction: if a plot of $\ln([M]_t / [M]_0)$ against time is linear, it suggests that there is a constant concentration of radicals[28,35].

ATRP is not a true living polymerisation – termination is suppressed, but it can still occur, and in fact plays an important role in the early stages of the reaction. At the start of the polymerisation, the concentration of radicals and Cu(II) is close to zero. As Cu(I) reacts with the initiator, the concentration of both radicals and Cu(II) increases. During the initial stages of the polymerisation, the concentration of radicals is sufficiently large that the rate at which the radicals revert to the dormant state (Rate $k_{deact}[Cu^{II}X_2][R^{\bullet}]$) is slower than the rate at which they undergo termination (Rate $-k_t[R^{\bullet}]^2$). With each termination reaction, the concentration of Cu(II) increases, which shifts the position of equilibrium towards the dormant side, and reduces the concentration of radicals. Eventually the concentration of Cu(II) is high enough that the rate of termination becomes insignificant, and a controlled/"living" polymerisation starts to occur. This self-adjustment during the initial stages of the polymerisation is also known as the persistent radical effect[45,46]. An electron paramagnetic resonance spectroscopy study found that 4 – 6 % of Cu(I) was converted to Cu(II) during the early stages of an ATRP reaction[47]. Termination can occur by two mechanisms: combination, where two polymer radicals, P_n and P_m collide and form a bond, generating a longer chain, P_{n+m}. Alternatively, one radical can abstract a hydrogen atom from another, resulting in the

production of a hydrogen-terminated polymer chain, P_n^H, and an unsaturated, alkene-terminated polymer chain, $P_m^=$ (see Scheme 1.1).

ATRP has been reported for various monomers including (meth)acrylates, styrenes, (meth)acrylamides, certain dienes and acrylonitrile[28,48]. The monomer must contain substituents that can stabilise radicals, so at present ATRP cannot be used to polymerise less reactive monomers such as simple alkenes and vinyl acetate[28,29]. The structure of the monomer determines the position of the equilibrium between active and dormant species, K_{eq}, which controls the concentration of radicals, and the rate of propagation, R_p, which determines how fast they react (see Equations 1.13 and 1.14)[28,29]. This means that the optimum reaction conditions vary depending on the monomer, and changing the reaction conditions can greatly affect the polymerisation control. The catalyst, ligand, solvent and reaction temperature modify the position of equilibrium and the propagation rate, enabling controlled polymerisation[28,29].

The initiator is a species with a weakly-bound halogen atom that can be readily exchanged with the catalyst. A wide range of different (pseudo)halides with weak R-X bonds (C-X, N-X, S-X, O-X[45]) have been used to initiate ATRP[45], including halogenated alkanes, benzylic halides, α-haloesters, α-haloketones, α-halonitriles and sulfonyl halides[28]. The amount of initiator defines the total number of radicals generated, so the monomer: initiator molar ratio determines the final degree of polymerisation, N (and so the polymer molecular weight)[28,33,35,49]:

$$N = \frac{\left([\mathrm{M}]_0 - [\mathrm{M}]_t\right)}{[\mathrm{I}]_0} \qquad (1.16)$$

where $[I]_0$ is the initial concentration of initiator[33,44,45,50].

To obtain well-defined polymers with low polydispersities, the rate of initiation must be faster than the rate of propagation to ensure efficient generation of polymer chains[28,44]. This means that all the chains are established, and begin to add monomer at essentially the same time. The initiator must be appropriate for the monomer and catalyst system: for example, 1-phenylethyl chloride was found to be an efficient initiator for ATRP of styrene in diphenyl ether solution using CuCl or CuBr/4,4'-di-*n*-nonyl-2,2'-bipyridine (dnNbpy) as the catalyst[46]. However, it gave a poorly-controlled polymerisation of

MMA under similar conditions[44], due to the faster rate of propagation for MMA[28,48]. Various groups have studied the effect of initiator structure on ATRP of different monomers[33,44,45], producing a set of rules that describe initiator efficiency[28,44].

The catalyst, a transition metal complex, reversibly abstracts a halogen atom from the initiator or a dormant polymer chain and generates a free radical that can propagate the polymerisation[28]. In this process the metal atom undergoes one-electron oxidation and increases its coordination number by one. The catalyst can be used to adjust the position of the atom transfer equilibrium and the dynamics of exchange between active and dormant species[48]. Complexes of copper(I) halides with multidentate, nitrogen-containing ligands (such as 2,2'-bipyridine derivatives or alkyl amine ligands such as N,N,N',N'',N''-pentamethyldiethylenetriamine (PMDETA)) are the most popular ATRP catalysts, due to their versatility[48]. However, a wide range of transition metals including ruthenium(II), molybdenum(V), rhenium(V), iron(III), nickel(I) or (II), and palladium(0), complexed by a similar variety of nitrogen- or phosphorus-containing ligands (or other ligands) have been used successfully in ATRP[28,48]. The ligands control the solubility of the catalyst in the reaction medium and can be used to fine-tune its electronic properties (generally, more electron-donating ligands better stabilise the higher oxidation state of the metal and accelerate the polymerisation)[29].

Further fine-tuning of the initiator efficiency is possible by halogen exchange between the catalyst and the growing chains[28, 51]. In ATRP systems, alkyl bromide and chloride initiators are commonly used with the corresponding copper(I) halide catalyst. However, mixed halide systems (e.g. CuCl and RBr) have been shown to give better control of ATRP reactions than either CuBr/RBr or CuCl/RCl[51, 52]. The kinetic requirements for a controlled polymerisation are fast initiation followed by slow propagation, with fast, reversible deactivation of the majority of the polymer chains. The C-Br bond is weaker than C-Cl, which allows faster initiation. The growing chain is then deactivated by halide coupling. Model studies have shown that, in mixed halogen systems, predominantly C-Cl bonds are found in the dormant polymer chains, i.e. there is substantial halogen exchange in the early stages of the reaction, and alkyl chlorides are preferentially formed over alkyl bromides. The stronger C-Cl bond reduces the concentration of active polymer chains, resulting in slower propagation[52].

ATRP can be carried out in bulk, in solution or in heterogeneous media. ATRP of different monomers has been performed in solvents including benzene, toluene, anisole, diphenyl ether, acetone, ethylene carbonate, various alcohols and water[28,48]. The use of a solvent can have several effects on the polymerisation. For a controlled reaction to occur, the growing polymer chains must be soluble in the reaction mixture[53]. In some rare cases, the polymer is insoluble in its own monomer (e.g. acrylonitrile), and a solvent is essential[28,29,48]. Bulk ATRP is usually carried out at a temperature above the glass transition temperature of the polymer, but use of a suitable solvent allows lower temperatures to be used[48]. This can be particularly advantageous for the brush growth if temperature-sensitive initiators such as functionalised thiol SAMs are used[54]. In addition, the solvent dilutes the reaction mixture, reducing the concentration of radicals. Although this leads to slower polymerisation, it can reduce the amount of termination, improving control. This approach is commonly used for the ATRP of MMA, where the high value of K_{eq}, and so high concentration of radicals, can result in an uncontrolled polymerisation[48]. Finally, the catalyst complex may adopt different structures in different solvents, changing its level of activity[28,48,55]. However, the solvent must be chosen carefully to avoid side reactions, e.g. polar solvents are known to promote the elimination of HX from the dormant polystyrene chains, and so should be avoided in the ATRP of styrene[56].

1.1.3.1 Surface-Initiated ATRP

ATRP was first used to synthesise polymer brushes by Ejaz *et al.*[57], who used Langmuir-Blodgett techniques to produce a monolayer of a surface-bound initiator, which was then used for the surface-initiated polymerisation of MMA, generating PMMA brushes up to 70 nm thick. ATRP has become the most popular method for the synthesis of polymer brushes by surface-initiated polymerisation[2], and has been used to produce a wide variety of different polymer brushes[57-77], block copolymer brushes[78-82], patterned polymer brushes[54,68,83-90], and binary patterned polymer brushes[91-96]. As well as planar substrates such as gold or silicon wafers, brushes have also been synthesised on silica particles[97-100] and carbon nanotubes[101-103].

The amount of material present in a surface-bound layer is very small, which means that the concentration of the surface bound initiator is very low, and this has some

consequences for surface-initiated ATRP. As discussed above, termination in the early stages of ATRP leads to the build-up of Cu(II), which reduces the concentration of radicals until a steady state is reached. This persistent radical effect results in the termination of approximately 5 % of the polymer chains during the initial short, non-stationary process[46]. In solution reactions, the concentration of initiator is relatively high (usually equimolar to the catalyst), so termination can produce enough deactivator in solution to give a controlled polymerisation[53,63]. For the growth of polymer brushes, the effective concentration of the surface-bound initiator is too low for this mechanism to operate efficiently. Therefore, to get controlled brush growth, it is necessary to add either free initiator[57], or extra copper(II)[63,67,70] to reduce the concentration of active radicals enough to suppress termination. There are advantages and disadvantages to each approach. Adding free initiator generates polymer chains in solution as well as polymer brush. The free polymer can then be analysed, allowing measurement of the molecular weight and polydispersity. The disadvantage of this approach is that the free polymer tends to adsorb onto the brush, necessitating extensive solvent treatment, soxhlet extraction, sonication etc. to ensure it is removed. In some cases, it can even interfere with the surface polymerisation[53], or damage the brush surface[68]. The surface radical concentration, after the halogen exchange equilibrium is established, is directly proportional to the CuX: CuX_2 molar ratio[53], so adding Cu(II) directly reduces the concentration of active radicals, inhibiting termination[63]. Use of this approach makes sample purification easy: a simple rinse in solvent to remove excess reagents is all that is needed. However, there is no free polymer generated, so it is not possible to directly measure molecular weight and polydispersity.

Some groups have concentrated on direct measurement of molecular weight and polydispersity of polymer brushes, by growing them on large wafers or silica gel, then degrafting the polymer for analysis[69,73,79,97,104-106]. Husseman *et al.*[105] grew PS brushes on silica gel by NMP from an initiator containing a cleavable benzyl ether group. They added free initiator, so polymer was produced in solution at the same time as the polymer brushes. They observed a linear relationship between the molecular weight of the free polymer and the brush thickness (this has also been found for brushes produced by ATRP[57,67]). They also found closely corresponding molecular weight and polydispersity for the free polymer and the degrafted brush, suggesting that brush thickness is directly proportional to polymer molecular weight.

The low amount of surface-bound initiator also alters the reaction kinetics. Solution ATRP is first-order with respect to the concentration of monomer ([M])[29,35]:

$$Rate = \frac{-d[\mathrm{M}]}{dt} = k_p[\mathrm{M}][\mathrm{P}_n^{\bullet}] \quad (1.17)$$

In a surface-initiated reaction, the amount of polymer produced is negligible compared to the amount of monomer in solution (i.e. the monomer conversion is close to zero), so the reaction follows pseudozero-order kinetics and the rate does not depend on the concentration of monomer. Under these conditions the effective change in concentration of monomer with time is negligible. Instead, a plot of brush thickness (or molecular weight of free polymer) against time should be linear[70].

One of the criteria for a living polymerisation is the retention of the active species at the end of the reaction[30]. In the absence of termination, addition of fresh monomer should restart the polymerisation, resulting in chain extension. The living character of surface-initiated ATRP has been demonstrated by production of block copolymer brushes[2,67,69,78-82], or by chain extension on addition of a second portion of the same monomer. Kim *et al.*[79] were able to produce 'heptablock PMMA' by using a quenching and reinitiation approach: polymerisations were stopped by adding excess copper (II), favouring the production of dormant radicals. This was then washed off the brush, and the reaction could be restarted. Brush growth could also be stopped and restarted without quenching, although there was some termination, resulting in lower than expected layer thickness[79].

1.1.4 Self-Assembled Monolayers

Self-assembly is the spontaneous organisation of molecules (or meso scale objects) into stable, well-defined structures by non-covalent forces. SAMs are one of the best examples of non-biological self-assembly[7]. They were first studied by Bigelow *et al.*[107] who found that solutions of eicosyl alcohol ($C_{20}H_{41}OH$) in *n*-hexadecane formed coatings on glass or platinum that were oleophobic (e.g. they were not wet by the solution or the solvent), due to the adsorption of the long-chain alcohol molecules into a close-packed, orientated monolayer on the substrate. Since then it has been found that a wide range of functionalised long-chain organic molecules (of general form $Y(CH_2)_nX$)

can form SAMs on various substrates by chemisorption and self-organisation[5,7]. The final structure is close to, or at, thermodynamic equilibrium, so it tends to form spontaneously and reject defects[7].

SAMs can be formed by exposing a suitable substrate to a solution or vapour of a SAM-forming molecule, or by μCP. SAMs can be formed on a range of substrates by selecting an appropriate binding group, for example, thiols or disulfides on gold, silver, or copper; tri- or mono-chlorosilanes on silica, glass and plasma-oxidised polymers; and carboxylic acids on metal oxides[5]. The layer thickness can be adjusted by changing the number of CH_2 groups in the alkyl spacer, and functional groups such as fluorocarbons, esters, amines, amides, alcohols, nitriles and ethers can be added onto the chain, allowing modification of the interfacial and chemical properties of the surface[108] (though the presence of functional groups can alter the packing of the monolayer[109]). If necessary, the chemistry of the SAM can be modified by further reactions of terminal functional groups: for example, this can be used to introduce functional groups that would react with the 'anchoring' functionality and so interfere with SAM formation[110,111]. The formation of SAMs with suitable terminal functional groups allows the synthesis of polymer brushes by surface-initiated polymerisation.

The most studied and best characterised SAMs are formed by alkanethiolates – $CH_3(CH_2)_nS$- on gold substrates[5, 108, 7]. Alkanethiols or disulfides chemisorb spontaneously onto gold surfaces to form adsorbed alkanethiolates (this presumably occurs with the loss of hydrogen for thiols, though the fate of the hydrogen atom is still not known[5]). Alkanethiols with n > 11 form closely-packed, essentially two-dimensional organic quasi-crystals on gold surfaces[5]. In a high-quality complete monolayer, the alkyl chains extend from the surface in a nearly all-trans configuration, tilted on average ~ 33° from the surface normal[112,113] to maximise the van der Waals interactions between adjacent CH_2 groups[7,109,114] (shown in Figure 1.5 a). The adsorbed alkanethiolates form a hexagonal $\left(\sqrt{3}\times\sqrt{3}\right)$R30° lattice commensurate with the underlying gold structure[114] (this means that the intermolecular spacings in the SAM are $\sqrt{3}$ larger than those of the gold atoms, and the lattice is rotated 30° relative to the Au (111) lattice[109]). The adsorption and self-organisation is rapid – studies have shown that

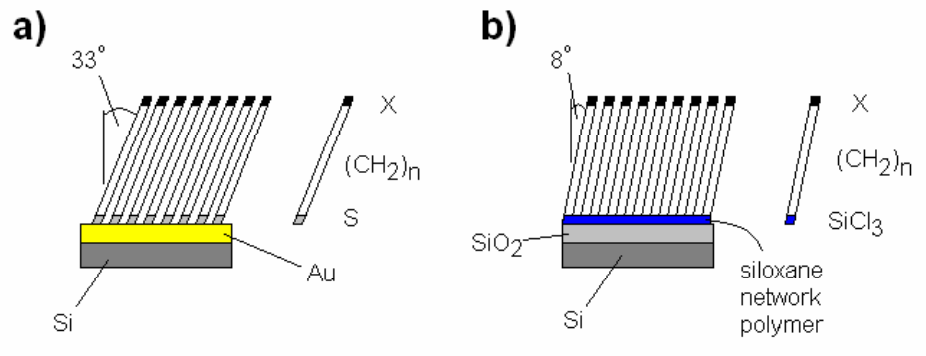

Figure 1.5 Schematic illustration showing the structure of a) alkylthiolate SAMs on gold substrates, and b) alkyltrichlorosilane SAMs on oxidised silicon substrates[5, 115].

well-ordered SAMs can be formed within a few minutes from solution[108], and in less than a second by μCP[114].

Alkyl chlorosilanes, $Cl_nH_{3-n}Si(CH_2)_xR$ and alkoxysilanes $(RO)_nH_{3-n}Si(CH_2)_xR$ form SAMs on hydroxyl-terminated surfaces such as oxidised silicon, glass, silica particles, Al_2O_3, and plasma-treated polymers[3,7,83]. It is generally thought that the SAM is formed via the production of silanol intermediates, which then react laterally with surface-bound hydroxyl groups and other silane molecules to give a network polymer that is covalently bound to the substrate[115,116]. The molecules align to form a highly orientated, crystalline-like structure, with the hydrocarbon chains tilted approximately 8º from the normal to the surface[115] (see Figure 1.5 b). Although silane SAMs can have densities approaching those found in bulk hydrocarbon crystals, they lack the long-range translational ordering found in thiol SAMs on gold[115].

The reaction of alkyltrichlorosilanes with –OH terminated surfaces is more complicated than the equivalent reaction of alkanethiols on gold, and has been a subject of considerable study[4,112,113,116-127]. Alkyltrichlorosilanes are capable of polymerising in the presence of water, which gives rise to a number of possible surface structures: covalent attachment and surface-induced polycondensation leading to horizontal polymerisation (self-assembly) or vertical polymerisation[117]. This is shown in Scheme 1.2 below.

Scheme 1.2 Possible products of the reaction of alkyltrichlorosilanes with silicon dioxide surfaces[117]

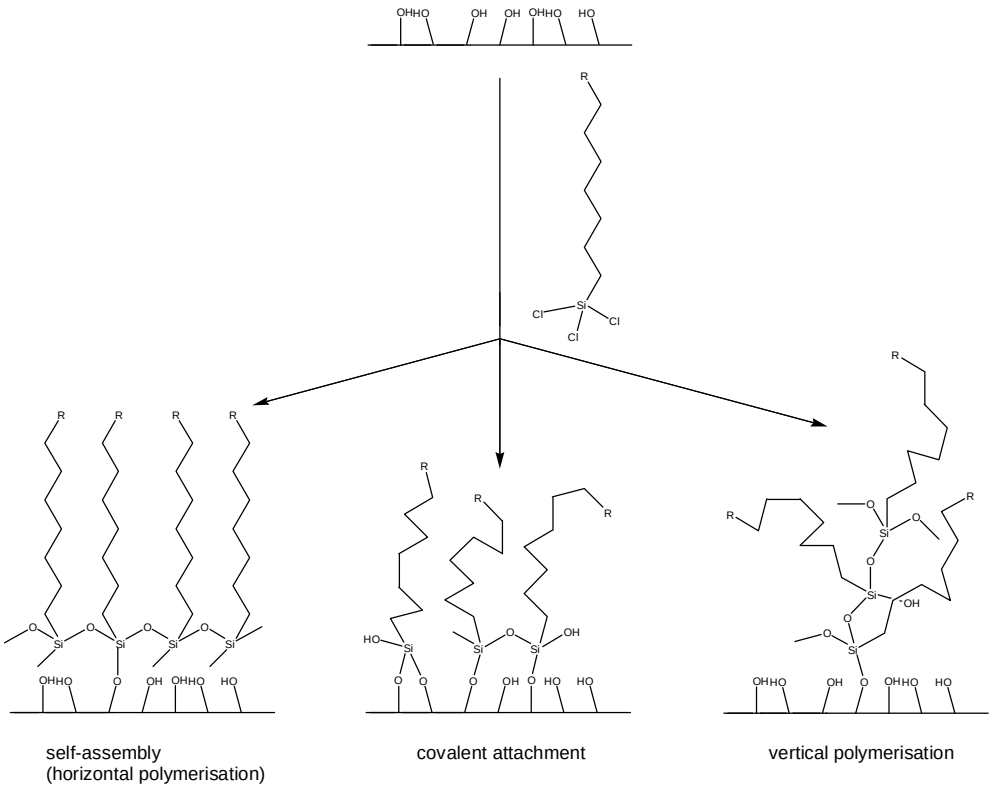

The structure formed is very sensitive to the deposition conditions, including temperature, solvent, amount of surface water, presence of base[118], concentration of trichlorosilane, and preparation method: solution, vapour or μCP[115].

There is consensus in the literature that water must be present to allow the formation of a well-ordered SAM, but there is some debate about whether silane molecules actually react with surface bound –OH groups. Hair and Trip[118] used infra-red spectroscopy to study the reaction of alkyltrichlorosilanes with silica. They found that OTS did not react with silica under strictly anhydrous conditions at room temperature. Under less stringent conditions, where some water was present adsorbed on the surface of the silica, the silane reacted with the molecular water, but there was no sign of reaction with surface bound –OH groups. Allara *et al.*[121] found that equivalent layers of OTS could be formed on SiO_2 and gold substrates in the presence of water, suggesting that there is an insignificant amount of bonding to the substrate. Sung *et al.*[124] produced SAMs of

alkyltrichlorosilanes on silicon nitride substrates, again suggesting that the presence of surface water is more important than reaction with surface silanol groups. Addition of an amine was found to alter the process: the amine forms strong hydrogen bonds to surface –OH groups. This increases the nucleophilicity of the surface –OH groups, allowing them to react directly with the silicon of the alkyltrichlorosilane[118].

1.2 Patterned SAMs and Polymer Brushes

1.2.1 Microcontact Printing

Patterned SAMs can be produced by a variety of methods, including photochemical methods (either photolithography or scanning near-field photolithography)[128,129], dip-pen nanolithography or nanoshaving/nanografting[128], but one of the simplest is μCP, first developed by Whitesides and Kumar in 1993[130]. An elastomeric stamp, usually made of poly(dimethylsiloxane) (PDMS), is prepared by cast moulding of a master with the desired relief structures. This stamp is exposed to an 'ink' – a solution of a chemical which can form SAMs on the desired substrate, dissolved in a suitable solvent. This can be done by directly applying the ink to the stamp, or indirectly, by transferring the ink from a flat 'stamp pad' (a flat piece of PDMS) so that only the raised parts of the stamp are inked. The stamp is applied to the substrate, transferring molecules of the ink onto the surface by direct contact, producing a patterned SAM. The remaining exposed surface can then be 'backfilled' by immersing the patterned substrate in a solution of a second SAM forming molecule, or left bare[5]. This is shown schematically in Figure 1.6.

The μCP of alkanethiols on gold (and silver) surfaces has been extensively studied[5,7,8,114,130-137]. Well-ordered SAMs with few defects can be produced much more rapidly by μCP than by adsorption from solution. One study even reported that alkanethiol SAMs were formed within 0.3 seconds by μCP[114]. Less is known about the mechanism of film formation of alkyltrichlorosilanes by μCP[138]. The end result is very sensitive to the deposition conditions, including the amount of water present in the

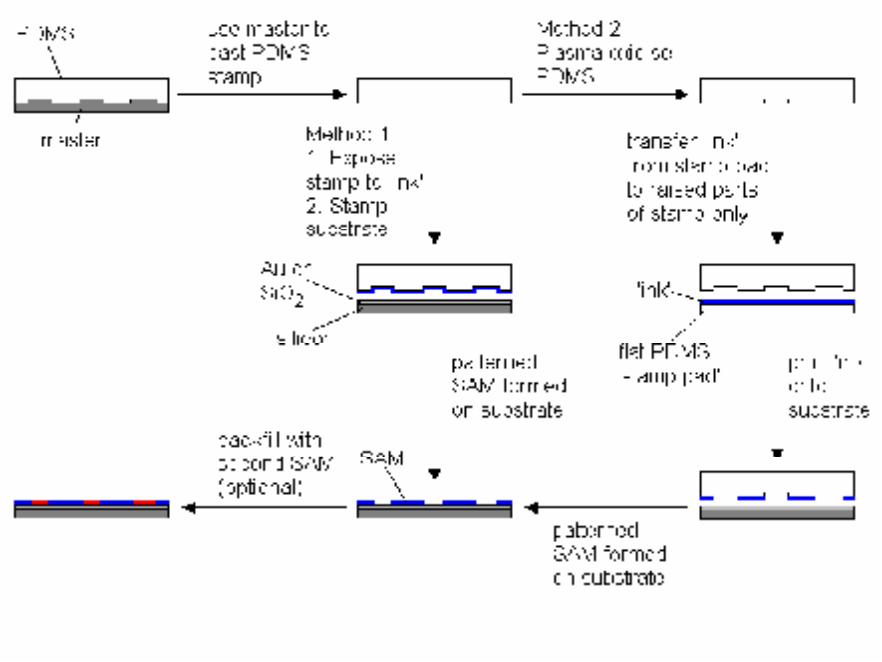

Figure 1.6 Microcontact printing[5,7,8,85,135,139]

reaction environment (in the solvents and reagents, on/in the stamp and in the ambient air), the temperature, the type and cleanliness of the substrate, the solvent used in the ink, the concentration of the active molecule in the ink[115,138], and the contact time[115]. Many of these variables are difficult to control, and can vary widely between different laboratories[115] (or even on different days in the same laboratory!).

Patterned SAMs, produced by μCP (or by other methods) can be employed as barrier layers, or to control wetting, dewetting, nucleation or deposition of other materials on the surface. Thiol SAMs have been used as resists for certain wet chemical etches, e.g. cyanide/ferricyanide. The gold is removed from the underlying substrate (usually silicon), apart from areas protected by the SAM. The remaining gold-coated regions can then be used as resists for the anisotropic etching of silicon, generating three dimensional patterns in silicon. Thiol SAMs have also been used as barriers for the electroless plating of nickel, although there were some problems due to the disruption of the thiol SAM at the raised temperatures needed (35 – 60 ºC). More thermally robust alkylsiloxane SAMs have been used as templates to control the nucleation and growth of metals and ceramics such as copper[140] or $LiNbO_3$[7] by selective chemical vapour deposition. Where a surface is patterned with regular arrays of hydrophilic and

hydrophobic SAM (usually done by printing a hydrophobic, methyl-terminated SAM, then backfilling with a SAM of different polarity), water will preferentially condense on the hydrophilic regions, and organics on the hydrophobic regions, due to the minimisation of interfacial tension. This produces a surface patterned with droplets of liquid, which may act as microreactors[8] or 'microfactories'. If the aqueous liquid contains dissolved salts, such as copper sulphate or potassium iodide[8], evaporation of water from the wetted areas can be used to produce arrays of salt micro- or nano-crystals of controlled shape and size[7, 8]. The organic phase can contain prepolymers, for example polyurethane[5], which can then be polymerised in situ by exposure to UV light, to self-assemble polymer microstructures[8]. Patterned SAMs can also be used to selectively bind particular species, which may lead to applications in biosensors and immunoassays. For example, oligo(ethylene glycol)-based SAMs were microcontact-printed with a pattern of biotin ligands. These were able to immobilise fluorescently-labelled antibodies or proteins, giving a direct visual response[141].

1.2.2 Patterned Polymer Brushes

Patterned polymer brushes are most commonly produced by μCP followed by surface-initiated polymerisation – often ATRP[54,68,83-86,88], although other methods including ROMP[10,142] and ROP[9] have been used. The usual approach is to print a pattern of a non-functionalised SAM, such as OTS or hexadecanethiol, then backfill with the initiator, probably because the μCP of these methyl-terminated molecules has been well studied and is reasonably well understood. It is also possible however to directly print an initiator SAM[83,85], which in principle allows μCP to be used for the synthesis of binary patterned polymer brushes.

Several other methods have also been used to produce patterned polymer brushes. Rühe and co-workers[143-145] used UV light to pattern polymer brushes in three different ways: either by etching exposed regions of a homogeneous brush, passivating exposed areas of an initiator layer or by UV-induced free radical polymerisation from a surface-attached initiator. These approaches could also be used to produce binary patterned polymer brushes (see below)[143-145]. Schmelmer *et al.*[146] used electron beam lithography to crosslink and chemically alter a SAM. The cross-linked regions could then be

converted into an initiator for free radical polymerisation. Lift-off electron-beam lithography has been used to produce a pattern of gold features on a silicon substrate, which were then modified with an initiator and used to grow poly(N-isopropylacrylamide) (PNIPAM) brushes by ATRP. The brushes were found to increase feature height and width, and decrease the spaces between the raised features, and were responsive to changes in solvent. It was suggested that nanopatterned polymer brushes with inducible phase transition behaviour, such as PNIPAM, could be exploited for protein-affinity separations and switches in microfluidic devices[89]. Brushes were also grown on chemical and topographical features by Hou *et al.*[90], who used local oxidation by AFM to produce patterns of oxidised silicon on a wafer protected by an OTS SAM. The silica dots were then modified with an ATRP initiator and used to grow PMMA brushes, amplifying the original features. Brushes have also been grown from the surface of features produced by contact moulding a UV curable photopolymer resin which contained groups that could initiate ATRP or NMP, allowing growth of brushes. This was shown to be able to produce features less than 60 nm across, and the spaces between features could be reduced by brush growth[87].

1.2.3 Binary-Patterned Polymer Brushes

A binary-patterned polymer brush consists of adjacent regions of two (or more) chemically different polymer brushes. They have been much less studied than patterned polymer brushes: at the present time (September 2009), there have been only 12 papers reporting their synthesis, and there has been little investigation of their properties. Further study and development of an efficient, general synthetic route are needed before these materials can be fully understood, and their potential properly assessed.

The first synthesis of binary-patterned polymer brushes was reported by Tovar *et al.*[143] in 1995: a homogeneous PS brush was grown by thermally-induced free radical polymerisation, then patterned by deep-UV photoablation in the presence of a mask. The exposed silicon substrate was then coated with fresh initiator and used to grow a second polymer brush by thermally-induced polymerisation[143,144]. The same research group has since used similar initiators to generate patterned polymer brushes by UV-induced polymerisation through a mask. A second brush was then grown on the rest of the surface by thermally-induced polymerisation from the remaining initiator. They

found that it was necessary to ensure that the first brush adopted a collapsed conformation during the polymerisation of the second monomer to block the remaining initiator groups and prevent the formation of mixed brushes[145]. In a similar approach, Zhou *et al.*[92] used ATRP to synthesise homogeneous polymer brushes, which were then etched with UV. The exposed surface was then recoated with initiator and used to grow a second brush. It was necessary to dehalogenate the first brush with sodium azide to 'kill' the polymer chains and prevent the unwanted formation of block copolymer brushes during the second polymerisation. Husemann *et al.*[147] produced binary-patterned poly(*tert*-butyl acrylate) (PtBA)/poly(acrylic acid) (PAA) brushes by spin coating a homogeneous PtBA brush with a layer of photoresist that contained bis(*tert*-butylphenyl)iodonium triflate. On exposure to UV light, this produced an acid that diffused into the brush and converted it to PAA. This approach is monomer-specific, and the loss of the tertiary butyl groups results in a decrease in chain volume, so there is a step of 10 – 20 nm between the domains – it would be useful if the thickness of each brush could be controlled independently. Maeng *et al.*[91] used electron-beam lithography to selectively dehalogenate areas of a homogeneous PS brush (produced by ATRP). The remaining halogen-capped chains were then extended by a further ATRP reaction to produce patterned PS/PS-*block*-PMMA brushes. An alternative approach is to assemble a pattern consisting of initiators for two different polymerisations: Xu and co-workers[95,96] used UV-induced hydrosilylation to attach an ATRP initiator to hydrogen-terminated silicon, either by irradiation through a mask[96], or by protection of regions of silicon oxide with a resist, followed by etching with HF[95]. A second initiator, for either RAFT[96] or NMP[95], was then attached to the silicon oxide regions of the surface. Binary-patterned polymer brushes could then be grown by sequential polymerisations (it was found that the brushes produced by ATRP did not react under RAFT or NMP polymerisation conditions, and vice versa).

There have only been two reports of the synthesis of binary-patterned polymer brushes without the use of UV light or electron-beams: Liu *et al.*[94] used capillary force lithography to form a physical barrier over some parts of an epoxy-based macroinitiator. ATRP of NIPAM, removal of the mask, and a second ATRP reaction produced binary-patterned brushes. It was found that the PS mask blocked the surface, preventing polymerisation from the covered areas (as long as no good solvents for PS were used). PNIPAM does not generally undergo a living reaction under ATRP conditions, so

dehalogenation was not necessary. However, if other polymers were used, this could be necessary to prevent the formation of block copolymer brushes. Finally, μCP has been used to print a thiol ATRP initiator onto gold substrates. It was found that it was not necessary to backfill the gold surface with a second SAM, so successive μCP – ATRP – dehalogenation reactions could be performed to produce up to quaternary-patterned polymer brushes. A feature of the patterned surfaces was the formation of 'nanogaps' (100 – 500 nm wide) between different brushes, due to incomplete contact of the PDMS stamp around existing raised brush features. This may be a disadvantage for some applications, but, if controllable, could provide a route for maskless patterning of (sub) 100 nm features[93].

The sequential microcontact printing method has since been used to produce patterns of two oppositely-charged polyelectrolyte brushes: poly[(methacryloyloxy)ethyl-trimethylammonium chloride] (PMETAC) and poly(methacryloyl ethyl phosphate) (PMEP). After treatment with suitable palladium-based catalysts, the patterned brushes provided templates for site specific electroless plating of copper (on PMETAC) and nickel (on PMEP), generating bimetallic patterns[148]. The same group also synthesised a binary-patterned polymer brush consisting of two different oligo(ethylene glycol)-based brushes. Hydroxyl-terminated poly[oligo(ethylene glycol)methacrylate] (POEGMA) brushes produced a reactive surface that could be modified to bind biomolecules such as biotin. Methyl-terminated POEGMA brushes provided an antifouling surface that was much more resistant to protein adsorption than a methyl-terminated SAM. Poly(methacrylic acid)/POEGMA brushes were also produced and used in similar selective adsorption experiments[149].

1.3 Applications of Polymer Brushes

The development of controlled surface-initiated polymerisations has allowed the synthesis of well-defined, densely-packed polymer brushes with a wide range of chemical functionality. This provides a versatile method to modify surface properties. The strong polymer – substrate interaction and the high density of polymer chains within the brush means that polymer brushes can have a high tolerance for temperature

changes, harsh chemical environments and radiation[84]. Preparation of a polymer brush-coated surface may be more complicated (and so expensive) than using a conventional coating (although the synthesis of coatings such as paints and varnishes may be very complex), so they are likely to be used under conditions where conventional coatings would not be stable, or to access particular functionality. Brushes produced by 'grafting from' have only been synthesised relatively recently, and currently have few commercial uses. Existing synthesis methods use large excesses of reagents for performing surface attachment reactions and cleaning brush surfaces. Improved reactions that use small excesses of reagents, and cleaning procedures that are fast, efficient and minimise solvent use are needed before brushes are considered seriously for industrial technology[150]. However, it has been suggested that brushes may find uses as colloidal stabilisers, adhesives and lubricants, to control surface properties such as friction, wettability and corrosion resistance and as functional surfaces in microfluidic systems, sensors, electronic and biological applications[22,68,150]. One of the areas of greatest interest is the development of 'smart' or responsive surfaces (for example block copolymer brushes that can change conformation to minimise unfavourable solvent interactions, producing switchable surfaces[69,80-82,91]). A few possible applications of homogeneous and patterned polymer brushes are discussed below.

The earliest, and to date, only commercial use of physisorbed or 'grafted to' polymer brushes was to stabilise colloidal suspensions. It was discovered in the 1950s that grafting polymer molecules to colloidal particles could prevent flocculation, as the polymer chains on different particles would avoid overlapping[22]. More recent uses for polymer brushes on particulate substrates have included the synthesis of organic/inorganic hybrid nanoparticles[98] and core – shell polymer nanocomposites[99]. Polymer brushes have also been found to improve the solubility of multiwalled carbon nanotubes in organic solvents[101,103].

Patterned polymer brushes have been used as resists for a wide range of wet etchants[9,54,68], and reactive ion etching[10]. In comparison with patterned SAMs, the brush forms a thicker, more durable layer (chemically, thermally and mechanically)[10]. In addition there are fewer defects, as the thicker brush layer covers defects in the underlying SAM[9].

One of the areas of greatest interest is the uses of polymer brushes that can selectively adsorb cells or proteins, or act as antifouling coatings, leading to uses in various biomedical applications such as the development of new types of biosensors and immunoassays. PNIPAM brushes have a LCST at ~ 35 ºC. Below the LCST, the polymer swells in water to create a relatively hydrophilic surface that resists the attachment of hydrophobic proteins. Above the transition temperature the polymer collapses, expelling the water and producing a much more hydrophobic surface[83,84,151]. It has been found that proteins could be reversibly adsorbed and released as a brush-coated substrate was heated and cooled using a micro hot plate[151]. De las Heras Alarcón *et al.*[86] demonstrated temperature-controlled adsorption and release of proteins from patterned PNIPAM brushes above and below the LCST respectively (although behaviour over longer times was more complicated). The brushes were also used to switchably adsorb Streptococcus mutans (a common species of oral bacterium that adheres to hydrophilic surfaces). As mentioned above (see p. 30), POEGMA brushes provide antifouling surfaces that resist the adsorption of proteins and cells[61,150]. However, hydroxyl-terminated POEGMA brushes contain reactive groups that can be modified to provide binding sites for particular proteins through specific chemical interactions (see p. 27 for an example of this)[61,149].

Poly(glycidyl methacrylate) (PGMA) brushes have been used as adhesives to bond quartz wafers together: a substrate coated with PGMA brush and a substrate coated with an aminopropyltriethoxysilane (APTES) SAM were pressed together and annealed at 300 ºC. This caused the epoxide group of the GMA to react with the amine group of APTES, covalently bonding the substrates together. This was found to give an invisible bonding layer, and allowed the use of rougher substrates than other methods such as anodic or fusion bonding. The solid nature of the adhesive could also be an advantage for use in microfluidic systems, where liquid adhesives could block the channels[60]. Patterned PGMA brushes have also been cross-linked and used to produce quasi-2D polymer objects which could then be released from the substrate by cathodic stripping. It was suggested that these objects could be exploited in applications such as polymeric nanoactuators, biomimetic systems and drug delivery vehicles[88].

Ito[152-154] and Iwata[155] and co-workers used stimuli-responsive polymer brushes to modify the flow properties of porous membranes. Both pH-[152,153,155] and redox-[154]

sensitive brushes have been shown to undergo conformation changes when exposed to appropriate environmental changes. This change in conformation resulted in the brushes acting as chemical gates that could regulate flow through porous membranes depending on the chemical conditions.

Patterned and homogeneous polymer brushes with liquid crystalline side chains have been used as alignment layers to control the orientation of molecules in liquid crystal thin films, which may lead to uses in displays and organic electronics applications[85].

Recently, Sontag *et al.*[156] reported the synthesis of polythiophene and poly(p-phenylene) brushes, two well known conducting polymers. Surface-grafted conductive polymers may help to improve the connectivity between metal or conducting oxide layers and conducting polymers in hybrid electronic devices such as solar cells, LEDs and sensors. They may also allow connections to be made between macroscopic electrodes and molecules or nanoscale objects in nanotechnology applications.

1.4 Phase Separation

1.4.1 Bulk Polymer Blends

Since synthetic polymers were first discovered, a massive range of materials with varied properties has been synthesised, and they have become ubiquitous. Although it may be possible to synthesise a polymer with the desired properties for a particular application, this can be expensive and time consuming. A simpler approach would be to mix two polymers, each having some of the desired properties, to make a material that fits the specification[12], but this is not usually possible because most polymer blends are thermodynamically incompatible and phase-separate[12,13]. If PS and PMMA are mechanically mixed, the result is a very brittle material with properties much worse than either of the pure polymers. The two polymers separate to form coarse domains of pure polymer, with no intimate mixing of the components and weak interfaces between the domains[13]. Phase-separated blends can still be useful: for example high impact polystyrene is a blend of PS with around 20 % polybutadiene (PBD). This phase-separates to produce a matrix of PS containing small (5 – 10 μm diameter) spherical

domains of rubbery PBD. These can absorb energy under stress, increasing the toughness of the brittle, glassy PS, while maintaining good stiffness[27,157].

Understanding and predicting the behaviour of polymer blends has been a subject of extensive study. The properties of a blend depend on whether it is miscible at a given composition and temperature, and, for immiscible systems, the nature of the domain morphology[14] and the strength of the interfaces between the domains[13].

Consider a system of two polymers, A and B. If a small amount of B is added to pure A, the blend will be miscible and form a single phase. As more B is added, the blend becomes unstable and separates into two phases, one rich in polymer A, the other rich in B. The miscibility of the system is also affected by temperature. Some blends phase-separate on heating, while others phase-separate as the temperature decreases[14]. The composition and temperature behaviour of a polymer blend can be shown in a phase diagram. Two examples are shown below.

In Figure 1.7 a) the miscibility increases with temperature, and at the Upper Critical Solution Temperature (UCST), the blend forms a single phase, e.g. PS/PMMA blends. In Figure 1.7 b) the polymers form a single phase at low temperatures, and phase-separate as the temperature is increased above the LCST e.g. PS/poly(vinyl methyl ether) (PVME) blends. This can occur if there are specific interactions between the

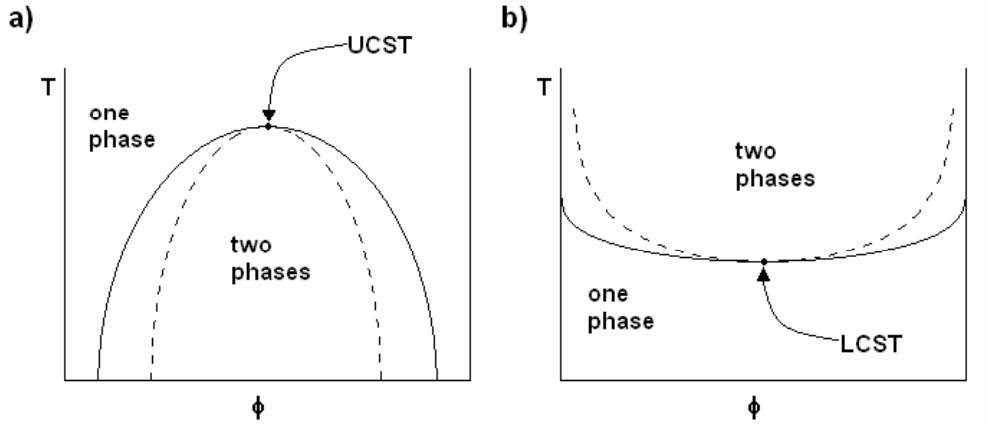

Figure 1.7 a) UCST type phase diagram, b) LCST type phase diagram. Solid lines show the binodal curve, broken lines show the spinodal curve[13,14,27].

polymers (such as hydrogen bonds), or if mixing results in a decrease in volume. As the temperature is increased, these attractive interactions eventually become disrupted, and the blend begins to phase-separate. Both these effects are relatively insensitive to composition, hence the fairly flat shape of the phase diagram[27] More complicated behaviour is also possible, resulting in phase diagrams with both UCST and LCST, or in some cases with neither feature[14]. In the figures, the region where a single phase is stable is separated from the two-phase region by the binodal or coexistence curve[13]. Within this, the spinodal line separates compositions that are unstable from those that are metastable with respect to small composition fluctuations[13].

The mixing of a blend is determined by the behaviour of the free energy of mixing as a function of temperature and composition (constant pressure is assumed, so it is the Gibbs free energy, ΔG_{mix}, that is relevant)[13]. Mixing can occur if the total free energy of the homogeneous system (G_{AB}) is less than that of two separate phases (G_A and G_B), so ΔG_{mix} is negative.

$$\Delta G_{mix} = G_{AB} - (G_A + G_B) \qquad (1.18)$$

This can be illustrated by looking at the free energy as a function of composition. In Figure 1.8 a), the total free energy of two separate phases with compositions ϕ_1 and ϕ_2 is G_i. The concave shape of the free energy profile means that, whatever the starting

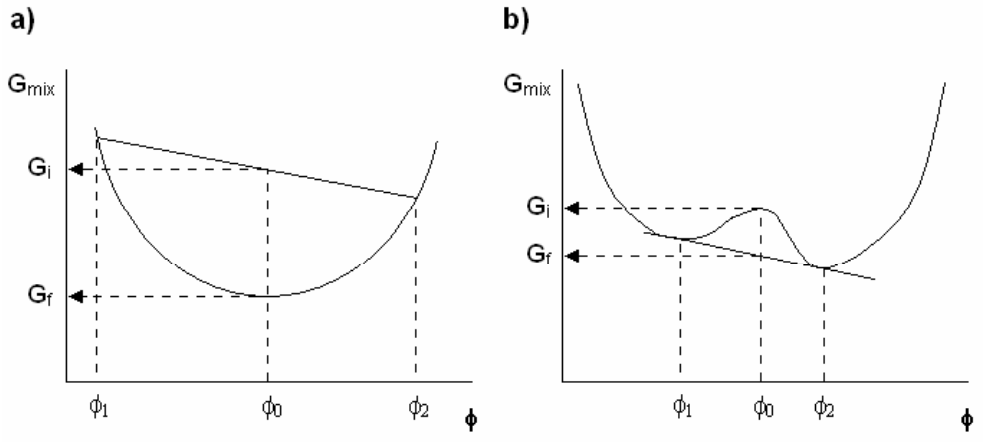

Figure 1.8 Gibbs free energy of mixing as a function of composition. a) The two species are miscible for all compositions; b) the two species are immiscible for compositions between ϕ_1 and ϕ_2. See text for further details[13].

conditions, the free energy can be reduced to G_f by forming a single phase (with composition ϕ_0), so the system is fully miscible[13]. In Figure 1.8 b), within a certain range of compositions the free energy profile is convex. In this range, the free energy of the system can be reduced by forming two phases of compositions ϕ_1 and ϕ_2. The lowest possible free energy is obtained when the phase-separated compositions are defined by the points at which a line is tangential to the free energy curve in two places; these two limits define the limits of composition within which a single phase is not stable[13].

1.4.1.1 Flory – Huggins Theory

The Flory – Huggins theory can be used to determine the mixing properties of two polymers as a function of composition and temperature[13,27]. It is a mean field lattice model and an extension of the regular solution model commonly used for liquids. It provides an expression for the change in Gibbs free energy on mixing two dissimilar polymers, A and B. Initially, consider a system with n_A moles of polymer A in a container of volume V_A and n_B moles of polymer B in a volume V_B. Mixing may be initiated by removing the barrier between the containers, giving a total volume, $V = V_A + V_B$. For mixing to occur, the Gibbs free energy of mixing, ΔG_{mix}, must be negative.

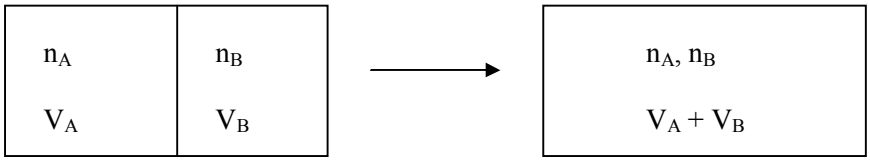

ΔG_{mix} can be represented as the sum of two contributions[27]:

$$\Delta G_{mix} = -T\Delta S_t + \Delta G_{loc} \qquad (1.19)$$

Mixing leads to an increase in the translational (or configurational) entropy, S_t, so ΔS_t is always negative and favours mixing[14]. However, $\Delta S_t \propto \frac{1}{N}$, where N is the degree of polymerisation of a polymer, so for high molecular weight polymers, it is very small in magnitude[14]. ΔG_{loc} refers to a change in the local interactions and motions of the monomers. This can be further split into the enthalpy change of mixing, ΔH_{mix}, and the entropy change, ΔS_{loc}, due to changes in the number of available conformations, for

example due to shrinkage or expansion in the total volume on mixing, so $\Delta G_{loc} = \Delta H_{mix} - T\Delta S_{loc}$. ΔG_{loc} may be positive or negative depending on the nature of the monomer – monomer interactions[27]. For most polymers, the Van der Waals attractive energies between equal monomers are stronger than those between unlike pairs, so $\Delta G_{loc} > 0$ and opposes mixing[27]. The small negative value of ΔS_t, and the larger positive value of ΔG_{loc} mean that ΔG_{mix} is usually positive, so most polymer pairs are immiscible, and compatibility is only found if there are specific interactions such as hydrogen bonds[27]. NB. the equations presented below assume that ΔG_{loc} is solely of energetic origin.

Expressions can be produced for ΔS_t and ΔG_{loc}:

$$\frac{\Delta S_t}{R} - n_A \ln \frac{V}{V_A} + n_B \ln \frac{V}{V_B} \tag{1.20}$$

If the volume fraction of component i, $\phi_i = \frac{V_i}{V}$, then:

$$\frac{\Delta S_t}{R} = -n_A \ln \phi_A - n_B \ln \phi_B \tag{1.21}$$

The change in local interactions is expressed by:

$$\Delta G_{loc} = RT \frac{V}{V_c} \chi \phi_A \phi_B \tag{1.22}$$

Where ϕ_A is the volume fraction of polymer A and V_c is an arbitrary reference volume, usually chosen to be the volume occupied by one of the monomer units. χ is the Flory – Huggins interaction parameter, which defines in an empirical manner the change in local free energy per reference unit. Another way to describe this is that χ is the energy change (in units of RT) when a segment of polymer A is taken from an environment of pure A and swapped with a segment of B in an environment of pure B.

Combining these expressions gives:

$$\begin{aligned} \Delta G_{mix} &= -T\Delta S_t + \Delta G_{loc} \\ &= RT\left(n_A \ln \phi_A + n_B \ln \phi_B + \frac{V}{V_c} \chi \phi_A \phi_B \right) \end{aligned} \tag{1.23}$$

By defining the number of moles of polymer i, $n_i - \frac{V\phi_i}{V_i}$, the molar number of reference units, $n_c = \frac{V}{V_c}$, the degree of polymerisation of a polymer i, $N_i = \frac{V_i}{V_c}$, and substituting these into the equation, it can be rewritten as:

$$\Delta G_{mix} = RTn_c \left(\frac{\phi_A}{N_A} \ln \phi_A + \frac{\phi_B}{N_B} \ln \phi_B + \chi \phi_A \phi_B \right) \quad (1.24)$$

This is the Flory – Huggins equation (see Jones[13] and Strobl[27] for a more complete derivation/description). This allows discussion of the properties of a polymer blend in terms of the value of χ: where it is positive, a blend will undergo phase separation, where it is negative, it will be miscible[13,27]. The Flory – Huggins equation can be used to derive expressions for the spinodal and binodal curves and compute phase diagrams, or these can be measured experimentally and used to determine χ[14]. For systems where, ΔG_{loc} is mainly of energetic origin, $\chi \propto \frac{1}{T}$ so χ decreases with increasing temperature, resulting in increased miscibility and UCST behaviour. Where entropic factors have a more significant effect, χ may increase with temperature, producing LCST behaviour[13,27]. For example, mixing two polymers with some type of attractive interaction may lead to a reduction in the volume of the system, lowering the entropy. This reduction in entropy usually increases with temperature, and eventually overcomes the initial attractive interactions[27] (see Figure 1.7 b). In reality, χ may be a complex function of the degrees of polymerisation, volume fraction and temperature[14], resulting in the wide range of phase diagrams observed experimentally.

1.4.1.2 Mechanisms of Phase Separation

When a blend is quenched into the two-phase part of the phase diagram it will begin to phase-separate. This can be done by changing the temperature or by evaporation of a common solvent from a solution of both polymers, for example during spin coating. For bulk homopolymer blends, phase separation leads to the formation of an isotropic, disordered phase morphology with a characteristic length scale that increases over time with no specific equilibrium value[158]. The mechanism of phase separation, and the morphologies formed depend on the conditions. If the blend is quenched inside the

spinodal line, it will be unstable with respect to small composition fluctuations and will immediately and spontaneously begin to phase-separate (see Figure 1.9)[13]. This spinodal decomposition results in the formation of two structurally equivalent interpenetrating phases[27]. Concentration fluctuations of different sizes grow at different rates. Fluctuations grow in amplitude by diffusion of material from the troughs to the peaks (formally a negative concentration gradient). This suppresses the growth of long wavelength composition variations[13]. Short wavelength fluctuations are dissipated by thermal motion so also grow slowly. This leads to a characteristic spinodal wavelength of fluctuations which grows fastest, and is the dominant length scale in the early stages of phase separation (the domains later coarsen as phase separation progresses)[13].

If the blend is quenched into the metastable region between the binodal and spinodal lines, a single phase is globally unstable with respect to separation into two phases, but small composition fluctuations lead to an increase in free energy (see Figure 1.9)[13]. There is an energy barrier, which can only be overcome by a large fluctuation which directly leads to the formation of a nucleus of a new equilibrium phase (of a certain critical size). This can then grow by conventional diffusion of polymer chains towards areas of lower concentration[13,27]. This nucleation and growth leads to the formation of spherical domains of the minority phase dispersed in a matrix of the majority phase[27]. It

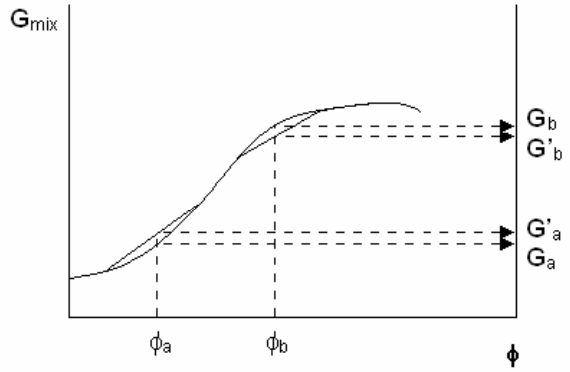

Figure 1.9 Magnification of Figure 1.8 b) between ϕ_1 and ϕ_0. The free energy profile shows that separation into two phases is globally energetically favourable. For a single phase of composition ϕ_a, small fluctuations in composition result in an increase in free energy from G_a to G'_a, and the system is metastable (within the binodal curve). For a single phase of composition ϕ_b, any fluctuations lead to a lowering of free energy from G_b to G'_b, so the system is unstable with respect to small composition fluctuations and will immediately and spontaneously begin to phase-separate by spinodal decomposition[13]. The curvature of the free energy curve can be determined from the value of the second differential, $d^2G/d\phi^2$.

is worth noting that for most polymer systems, the rate of homogeneous nucleation is vanishingly small, and the presence of impurities such as dust, and interaction of the polymers with the container walls play an important role in heterogeneous nucleation[13].

1.4.2 Surface-Directed Spinodal Decomposition

The presence of the polymer – air and polymer – substrate interfaces breaks the symmetry of phase separation. The lower surface free energy component of the blend is enriched at the air interface to minimise the total surface energy[16,159]. For example, the surface of 50/50 PS/PVME blends may be over 95 % PVME at the air interface, due to the lower surface energy of PVME[13,160,161]. In many cases there is also preferential segregation of one of the polymers to the substrate, again to minimise the interfacial energy with the boundary surface[162]. As the film thickness is decreased (to less than ~ 1 μm[162]), the preferential attraction of the blend components to the interfaces begins to significantly affect phase separation throughout the polymer layer.

During bulk spinodal decomposition, random composition fluctuations are amplified with a strong selection of fluctuations of a certain wavelength. This results in an isotropic structure consisting of a superposition of composition waves of roughly constant wavelength, but random phase and direction[163]. Interaction of the polymers with the free surface (and the substrate) pins the direction and phase of the composition waves, so they propagate from the surface of the film into the bulk[164]. This surface-directed spinodal decomposition can result in the formation of well-defined layered morphologies. This was first shown experimentally by Jones *et al.*[165] for a blend of poly(ethylenepropylene)/perdeuterated poly(ethylenepropylene) (PEP/dPEP). Forward-recoil spectrometry analysis showed the presence of a dPEP-rich surface layer and the formation of a composition wave propagating into the bulk, and coarsening over time[165]. Similar behaviour has been found in a range of blends such as deuterated polystyrene/poly(α-methyl styrene (dPS/PαMS)[164], PS/PBD[163],and deuterated polystyrene/poly(styrene-co-4-bromostyrene) (dPS/PBr$_x$S)[166]. The spinodal waves originating from the surface and substrate can interfere with each other resulting in the formation of complicated multilayered structures[167]. Constructive interference results in the production of almost perfectly ordered lamellar structures[167]. Where there is destructive interference of the spinodal waves, lateral structure consisting of droplets of

either of the two phases can develop. This can be understood as the compromising reaction of the system to competing surface fields which tend to enrich the particular layer in both polymers at the same time[167]. For example, Geoghegan *et al.*[163] found that dPS/PBD blends on silicon substrates formed dPS-rich layers at the surface and substrate, with a laterally phase-separated, PBD-rich layer in between. Bruder and Brenn[166] found that a stable layered structure could only be found where both interfaces were completely wet by one of the blend components[166,167]. For films that are thinner than the characteristic wavelength of composition fluctuations (typically 200 - 300 nm), surface-directed spinodal decomposition is suppressed and lateral phase separation occurs within the plane of the film[168].

1.4.3 Phase Separation in Thin Films

Understanding and controlling the morphology of phase-separated thin blend films has been a subject of extensive study, due to the potential commercial applications. Suggested uses include dielectric coatings[17,169], lubricants[16,169], lithographic photoresist masks[169], polymer LEDs[158,170], photovoltaic devices (solar cells)[170,171], antireflection coatings[172,173], photographic materials[17], paint systems[17], gas separating membranes[158], polymer photodiodes[158] and coatings to control blood compatibility[16]. Antireflective coatings for glass can improve the efficiency of solar cells and increase the quality of lens systems. Their manufacture requires materials of very low refractive index (~ 1.22), which cannot be achieved using conventional dielectric coatings. One solution to this is to use a nanoporous film. If the pore size is significantly smaller than the wavelength of light, the effective refractive index of the nanoporous medium is given by an average over the film[172]. Thin films of low molecular weight PS/PMMA (both M_w ~ 10,000 g mol^{-1}) phase-separate to produce domains that are approximately 100 nm across. Selective dissolution of PS by cyclohexane produces nanoporous films which were found to make highly effective antireflective coatings[172,173]. The properties could be tuned by altering the amount of PMMA in the blend[173]. Exceptionally low refractive index coatings were obtained by selective removal of PS and partial removal of PMMA[172].

It is thought that the performance of titanium dioxide/conjugated polymer solar cells could be improved by generating an interdigitated structure of 10 – 50 nm domains of

titanium dioxide and polymer. PS/PMMA blends (PS M_w 280,000 g mol^{-1}, PMMA M_w 120,000 g mol^{-1}) were used as a template for the synthesis of nanoscale pillars of titanium dioxide on glass and titanium dioxide substrates. The blend composition and concentration was optimised to produce isolated PMMA domains in a PS matrix. The PMMA domains were removed, and the resulting pores were infiltrated with a sol – gel mixture. Thermal treatment removed the remaining PS and produced crystalline titanium dioxide pillars. Although the structures were not of the desired height and diameter, tuning of the method could allow the production of structures suitable for use in interdigitated solar cells, which may lead to improved power conversion efficiencies[171].

Polymer thin films are commonly prepared by spin coating, which is shown schematically in Figure 1.10 b. The polymers are dissolved in a common solvent and the solution is deposited on a spinning substrate. Most of the solution is flung off, leaving a thin fluid layer on the substrate. This layer then thins, firstly by fluid flow and then by solvent evaporation. As the solvent evaporates, the concentration of the

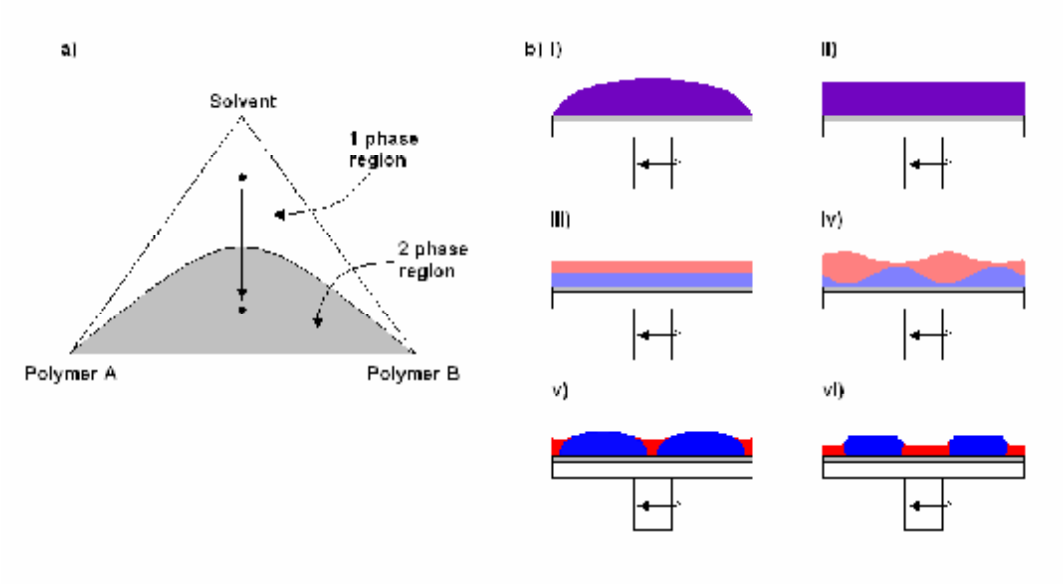

Figure 1.10 a) Ternary phase diagram for two polymers dissolved in a common solvent[174]. b) Schematic diagram of film formation and phase separation during spin coating; i), ii) the initial spin-off process where both polymer and solvent are removed; iii) the film separates into two layers and the film thins due to solvent evaporation; iv) the interface between the phases destabilises; v), vi) a laterally phase-separated structure forms and develops[175]. In this case, the blue polymer is less soluble in the common solvent and so solidifies first, the blue polymer also has lower surface tension, resulting in a rounded domain shape[15].

solution increases until the polymer – polymer interactions become significant and the blend begins to phase-separate (see Figure 1.10 a)[13,164,174,176].

At the intermediate point when the phases are still liquid due to their solvent content, the sample surface is essentially flat due to the small difference in surface tension between the two phases. Even though the solvents used in spin coating dissolve both polymers, the relative solubility of the two polymers in these solvents vary. For example, toluene is a better solvent for PS than for PMMA[15]. Therefore during spin coating of a PS/PMMA blend, the PS-rich phase retains more solvent than the PMMA-rich phase. As the solvent evaporates, the PMMA-rich phase becomes virtually solvent free when the PS-rich phase is still swollen with toluene. Further evaporation results in the collapse of the PS domains to produce a topographically structured surface[15]. The domain structure continues to develop until one or both of the polymers becomes glassy, preventing further changes[176,177]. The rapid evaporation of solvent means that the final phase morphology may be far from thermodynamic equilibrium[15]. Annealing above the glass transition temperature can lead to changes in surface composition and topography[159], although there may be kinetic barriers which prevent relaxation towards equilibrium[15].

Phase separation in thin films is much more complicated than in the bulk. The initial morphology of a spin-coated polymer blend film is determined by the chemistry of the polymers and their molecular weights, the blend composition, nature of the substrate, film thickness (controlled by the solution concentration), cast solvent, chain end groups and the presence of block copolymer additives[177-179]. The final morphology is also affected by the annealing time and temperature[177,178]. Different preparation methods may also result in different morphologies[180]. Some of these factors will be discussed in more detail below, mainly with reference to PS/PMMA blends.

Changing the composition of the blend, e.g. the volume fraction of the polymers, ϕ, necessarily leads to changes in the phase-separated morphology. This has been reported by a large number of studies, both for PS/PMMA blends[16,171-173,180-183], and other polymers[176,184,185]. There are a wide range of possible morphologies, depending on the polymers used and the preparation conditions, so it is difficult to make generalisations

about structure. However, starting from pure polymer A, and adding increasing amounts of polymer B, it can be expected that at first there will be a matrix made up of the A-rich phase, with isolated domains of B. As the amount of B increases, at some point an interconnected structure will form, then there will be a stage where B forms the matrix, and A forms isolated domains. However, other morphologies can also occur, for example, minimisation of surface energy can lead to the formation of bilayers when there is strong surface or substrate segregation (see p. 46).

Polymer blends with a wide range of molecular weights have been investigated, but there has been little systematic study of how this affects the process of phase separation. Most researchers simply choose two polymers, usually with fairly similar molecular weights, and then investigate other factors. There is some evidence that the use of lower molecular weight polymers results in a reduction in domain size[172,186]. Reduction of molecular weight also reduces the viscosity of the polymers[181] (and reduces T_g[187]), which results in more rapid approach towards equilibrium during annealing[181,188]. Where there are large differences in molecular weight between the two polymers there can be more dramatic effects. For example, Tanaka *et al.*[189] observed a surface excess of low molecular weight PMMA in blends with high molecular weight PS due to entropic effects, even though PMMA has higher surface energy.

As discussed previously, preferential segregation of the polymers to the surface and substrate results in a change from bulk phase separation to surface-directed spinodal decomposition to lateral phase separation as the film thickness is reduced. In very thin films, lateral domains reappear, then there are further changes in morphology as the film thickness approaches the size of the individual polymer molecules.[16,160,161,177,179,182]. Polymer blend films with a thickness less than twice the radius of gyration of the higher molecular weight polymer are defined as two-dimensional ultrathin blend films[160,178]. A flexible polymer chain in an ultrathin blend film is in a non-equilibrium state, since the conformational entropy of an individual chain is less than in the three-dimensional solid state[160]. This means that the number of pair interactions between foreign segments is reduced compared to in the bulk state, so χ_{2D} becomes smaller than χ_{3D}. This increases the miscibility of the two polymers and may result in very thin films becoming homogeneous[16]. Secondly, reducing the film thickness can result in a change in the

cloud point[160,161]. This can be sufficient to alter the mechanism of phase separation from spinodal decomposition to nucleation and growth[161]. Finally, in extremely thin films, the polymer chains are very constrained, with little entanglement between chains, so begin to behave as individual molecular chains[16]. This can eventually overcome the improved miscibility due to the lower value of χ_{2D}, and lead to the reappearance of a phase-separated structure[16].

For thin blend films, preferential segregation of one of the phases to the substrate can affect the morphology of the entire film, so changing the nature of the substrate can completely change the morphology[15-17]. For PS/PMMA blends on (oxidised) silicon, there is a fairly strong attractive interaction between the carbonyl groups of PMMA and polar silanol groups on the substrate surface[16], which leads to the formation of a continuous PMMA layer wetting the substrate[15], and both PS and PMMA domains at the free surface[15-17]. On gold, an intermediate surface energy substrate, it is not as strongly favourable to have PMMA at the substrate, so a greater area of the surface is covered by PMMA-rich domains[15-17]. If the substrate is hydrophobic (octadecylmercaptan SAM[15], siliconised cover glass[16] or cobalt[17]) the substrate – surface interfacial energy can now be minimised by the selective adsorption of PS (lower surface free energy[16]), which results in a much greater amount of PMMA at the air interface[16], and in some cases formation of a PS – PMMA bilayer[15].

The solvent used for spin coating can have significant effects on the final domain morphology[15,177,181]. In most cases, one of the polymers is more soluble than the other in the common solvent. The less soluble polymer solidifies earlier in the spin coating process, while the other polymer is still swollen with solvent, resulting in a topographically structured surface with raised domains of the less soluble component[15] (see Figure 1.10). This effect can also lead to the less soluble polymer forming a continuous layer covering the substrate, even where this is thermodynamically unfavourable[159,181]. During spin coating, phase separation progresses until the morphology is frozen in by vitrification of one (or both) of the polymers. The longer the polymers have to phase-separate, the closer the morphology will be to equilibrium. This time is determined by the vapour pressure of the solvent (along with other factors such as the spin speed and the solution concentration), so Cui *et al.*[177] found very

different morphologies for the same PS/PMMA blend spin-coated from dichloromethane, tetrahydrofuran (THF), toluene and ethyl benzene, even though they are all better solvents for PS than PMMA. Ethyl benzene was the least volatile solvent studied, so the observed structure was expected to be closer to equilibrium due to the longer interval before the polymers became glassy.

Polymer blend films produced by spin coating may not be at thermodynamic equilibrium due to rapid solvent evaporation during film formation[159,178,180,190]. The solvent effects may be removed or reduced by annealing the as-cast films under appropriate conditions[159,180,190]. Annealing refers to heating the system to a temperature above the glass transition temperature of both polymers, and in the two-phase part of the phase diagram, which allows the morphology to develop towards equilibrium (although there may be kinetic barriers that prevent relaxation towards equilibrium[15]). The effect of annealing on thin films of various polymer blends has been reported by a large number of researchers[15,17,159,161,178,181,185,186,188,190-192]. For PS/PMMA blends on hydrophilic substrates (such as oxidised silicon and mica), the more polar PMMA is strongly attracted to the substrate and forms a wetting layer on annealing[181]. This results in the formation of a transient bilayer structure. The stability of such a structure can be calculated using Young's equation:

$$S_{PS} = \gamma_{PS} - \gamma_{PMMA} - \gamma_{PS/PMMA} \qquad (1.25)$$

Where S_{PS} is the spreading coefficient for PS, γ_{PS} and γ_{PMMA} are the surface energies of PS and PMMA, and $\gamma_{PS/PMMA}$ is the interfacial tension. At normal annealing temperatures, $\gamma_{PS/PMMA}$ is larger than the difference in surface energies, so S_{PS} is negative, and the bilayer is unstable. The system tries to minimise the interfacial area rather than the surface area of a specific polymer[181], so the late stage of phase separation is dominated by the dewetting of PS on top of the PMMA layer[178]. This results in the formation of the equilibrium morphology of PS droplets in a PMMA matrix[181], though in many cases kinetic factors mean that the equilibrium morphology will never be reached[178,181].

1.4.4 Pattern-Directed Phase Separation

Phase-separated polymer blends have many potential applications (see p. 41). The domain size and morphology can be controlled by the choice of suitable polymers and preparation conditions, but in most cases there is no long-range order and there are a range of domain shapes, sizes and spacings. For some applications it would be useful if phase separation could be directed, allowing the production of structures of predetermined shapes and length scales.

The lateral morphology of a phase-separated polymer blend film can be controlled by breaking the symmetry of the substrate by chemical (and/or topographical) patterning[18]. Spin coating of a polymer blend onto a chemically patterned substrate offers a one step deposition process in which phase domains rich in each of the blend components are formed and spontaneously self-organise[193]. This pattern-directed phase separation is driven by preferential adsorption of each polymer to different areas of the patterned surface (see Figure 1.11)[18].

An example of the ordered structures that can be produced by pattern-directed phase separation is shown in Figure 1.12[193].

Pattern-directed phase separation was first investigated by Krausch *et al.*[194], who found that an array of alternating 1 μm wide lines of chromium and hydrogen-terminated silicon was replicated by spin coating it with a PS/partially brominated polystyrene (PBr_xS) blend[194]. Since then, extensive study has helped to identify the key factors for successful pattern replication. The nature of the substrate is very important – for example there was no evidence of pattern replication when the PS/PBr_xS blend mentioned above was deposited on a pattern of chromium and oxidised silicon[194]. For successful pattern replication, there must be preferential segregation of at least one of

Figure 1.11 Schematic diagram showing pattern-directed phase separation. A polymer blend is spin-coated onto a patterned substrate. Preferential adsorption of the polymers results in replication of the substrate pattern by the phase-separated domains.

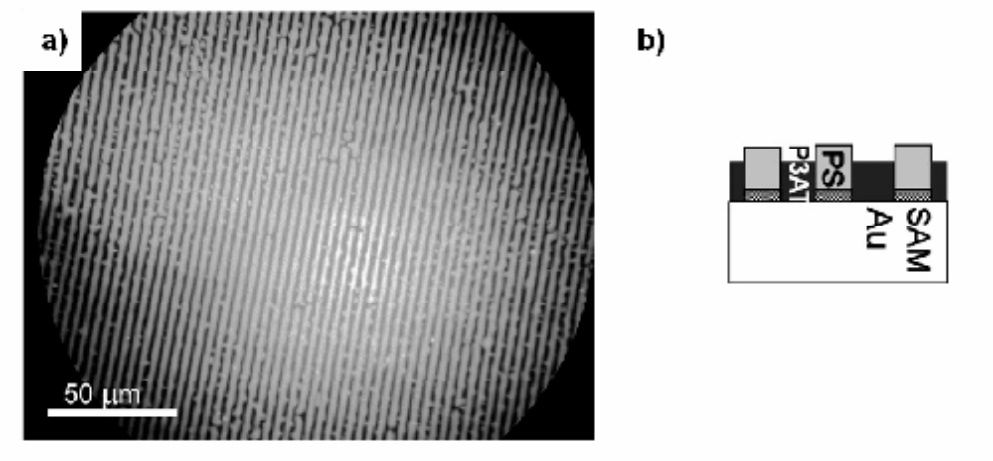

Figure 1. 12 Example of pattern-directed phase separation: a) Fluorescence microscopy image of PS/poly(3-dodecylthiophene) (P3DDT) blend film spin coated from chloroform onto a patterned substrate consisting of alternating 2 µm wide lines of gold and hexadecane thiol SAM, showing pattern replication over a wide area, b) Schematic representation of the phase separated morphology on the patterned substrate. Reproduced from Jaczewska et al., Soft Matter, 2009, 5, 234-241, http://dx.doi.org/10.1039/b811429c[193], by permission of the Royal Society of Chemistry.

the polymers to one of the substrates[158,195]. This can be detected by the formation of a bilayer when the blend is spin-coated onto a homogeneous substrate. If the substrate – polymer attraction is strong enough, this can force the domain structure to follow the substrate pattern.

Secondly, the periodicity of the substrate pattern must be comparable to the natural length scale for phase separation (on a homogeneous substrate) for the conditions used[19].

The natural domain size of a thin polymer blend film can be adjusted by changing the film thickness[18,196]. During spin coating, phase separation begins when the polymer – polymer interactions become significant[13,164,174,176], and ends when the polymers become glassy[176,177]. For thicker films, solvent drying and phase coarsening take place over a longer period of time, leading to an increase in domain size with film thickness[196]. Domain size can also be tuned by changing the blend composition[18]. The characteristic length scale of phase separation for a laterally structured sample is usually determined by analysis of the diffuse isotropic ring of the Fourier transform of AFM

images[18,168,193]. Where the length scale of the substrate pattern and the blend match, there can be nearly perfect alignment over macroscopic areas[193,195]. Where there is a mismatch, there will be the formation of defects. Bridges between lines form when the pattern is smaller than the characteristic length scale[158,197], and secondary polymer domains when the pattern is larger than the characteristic length scale[195]. However, it is not necessarily that simple: Cui *et al.*[198] found perfect pattern replication for a PS/PVP blend spin coated onto OTS/oxidised silicon patterns, even when the length scale of the patterns was over three times larger than the characteristic length scale of phase separation. They concluded that this was because the substrate – polymer interactions dominated over the interfacial tension between the two polymers[198]. Conversely, Cyganik *et al.*[197] found that spin coating a dPS/PVP blend onto a COOH-/CH_3-terminated patterned SAM resulted in worse pattern replication than on a gold/CH_3-terminated SAM, despite the larger difference in surface energy between the two areas of the pattern. This was thought to be due to a more favourable interaction between gold and PVP than between the COOH-terminated monolayer and PVP[197].

Finally, the match of the blend composition to the patterned area fraction should be considered. This has a relatively complicated effect, as changing the blend composition changes the characteristic length scale of phase separation[18]. Where the pattern size is comparable to the characteristic length, matching the area fraction of the pattern to the blend composition may allow the ordering to propagate throughout the film[194]. However, matching the pattern periodicity to the characteristic length scale of phase separation is more important since good pattern replication can be obtained when this condition is satisfied, even if the area fraction is very different to the blend composition[18].

Most of the work on pattern-directed phase separation has focussed on the use of μCP to produce patterned SAMs as it offers a quick, (relatively) simple route to the production of suitably sized, almost flat, chemically patterned substrates. There has been extensive study of the behaviour of a range of polymer blends on patterned SAMs and other impenetrable chemically patterned substrates (e.g. alternating lines of metals etc), including PS/PVP[18,195,198-201], dPS/PVP[158,197], dPS/PBD[168,202,203], PVP/PBr_xS[158,195,197], Poly(9,9-di-*n*-octylfluorene-*alt*-benzothiadiazole/Poly(9,9'-dioctylfluorene)

(F8BT/PFO)[19], F8BT/Poly(9,9-di-*n*-octylfluorene-*alt*-(1,4-phenylene-((4-*sec*-butyl phenyl)imino)-1,4-phenylene) (TFB)[20], PS/poly(3-alkylthiophene) (P3AT)[193,201] and dPS/PMMA/PVP[196]. There have also been various theoretical studies modelling the behaviour of polymer blends on patterned surfaces[202,204-206]. Only one report of phase separation of PS/PMMA on patterned surfaces was found. Jerome *et al*. [169] used phase-separated PS/PMMA films as templates to produce gold/silicon patterns by argon ion etching. 50/50 PS/PMMA blends were then spin-coated and annealed on the chemical patterns, but there was little evidence for pattern-directed phase separation/pattern replication (although the patterned surfaces definitely affected the domain morphology).

There has been some study of the behaviour of polymer thin films on substrates that are both chemically and topographically patterned. Raised patterns produced by μCP of OTS can be used to direct dewetting of thin films of PS into regular arrays[207]. Rockford[208], Geoghegan[209] and co-workers investigated the behaviour of thin PS films[209] and PS/PMMA blends[208] on patterned surfaces produced by annealing miscut silicon single crystal wafers, and then evaporating gold at glancing angle. PS/PMMA blends formed micron-scale irregularly-shaped domains on these substrates. At small scales, close to the substrate there was selective adsorption of PS onto the gold-coated regions of the substrate, but the patterning did not extend to the air interface. However, the length scale of the substrate patterns (~ 60 nm) was significantly smaller than the characteristic domain size (~ 1 μm), so complete pattern replication would not be expected. This is supported by models of thin blend films on patterns with periodicity less than the initial wavelength of spinodal decomposition (λ_{sp}), which show macrophase separation at the free surface as the patterns are too small[204].

1.4.4.1 Applications of Pattern-Directed Phase Separation

The ability to pattern surfaces on a microscopic length scale is important for technological applications such as the fabrication of microelectronic circuits and digital storage media[195]. Pattern-directed phase separation is one technique that could be used to produce microstructured materials for use in polymer LEDs[19], non-linear optical devices[194], polymer-based microelectronic circuits[195,210], optoelectronic devices[211] and templating in lithographic processes[211]. For example, Fichet *et al*.[19] used a patterned SAM to direct the phase separation of a F8BT/PFO blend into a regular array of

domains. This was then used to make polymer LEDs, which were twice as efficient (external and power conversion efficiencies) as devices made from unpatterned blends, due to the efficient outcoupling of waveguided light within the device (e.g. the domain boundaries reduce total internal reflection of light within the polymer layer)[19,21]. Similar performance improvements were observed in LEDs made from patterned F8BT/TFB blends – charge carrier injection was confined to the TFB-rich domains, which led to higher electroluminescence efficiency[20].

Bulk heterojunction solar cells are fabricated by blending conjugated polymers with fullerenes. The ideal morphology consists of vertical domains with an average interspacial distance equal to or less than the exciton diffusion length. The interdigitated structure must be aligned perpendicular to the electrodes to provide direct pathways for efficient charge transportation. Chen, Lin and Ko[212] used pattern-directed phase separation to control the phase separation of a blend of poly(3-hexylthiophene) (P3HT) and (6,6)-phenyl-C_{61}-butyric acid methyl ester (PCBM) (PCBM is a fullerene derivative, not a polymer, but the blend still undergoes phase separation). As the pattern size was reduced, the power conversion efficiency of the solar cells improved. The smaller domain size resulted in more complete phase separation during spin coating (e.g. higher percentage P3HT in the P3HT-rich phase etc). This increased the hole mobility, due to the improved ordering of the P3HT chains.

1.4.5 Polymers on Polymer Brushes

There has been little study of the behaviour of polymers on homogeneous or patterned polymer brushes, probably because of the extra synthesis steps required to produce these substrates, and their more complex behaviour. The use of brushes allows access to a greater range of chemical functionality including the ability to create a surface that consists of the same monomers as found in a particular polymer blend or copolymer. The use of random copolymer brushes allows tuning of surface affinities, from neutral surfaces to those that are strongly selective for each polymer[213]. Polymer chains undergo a large loss of conformational entropy at solid interfaces, which can result in dewetting. Polymer molecules can interact with the penetrable brush surface, which can reduce the driving force for dewetting, improve adhesion and ensure that polymer – brush interactions are averaged over a large volume[213]. Finally, brushes form a

macromolecular barrier, which, unlike SAMs, can rearrange to screen defects, and offer improved resistance to etching[9].

Several groups have investigated the behaviour of thin films of PS on substrates coated with PS brush[214-217]. For example, Maas *et al.*[214] studied the effect of varying the grafting density of a 'grafted to' brush and the molecular weight of the free polymer. At low grafting densities, the polymer did not wet the brush because of the lack of attraction between polymer and substrate. At intermediate grafting densities, the polymer film was stable on the brush surface (complete wetting). As the grafting density of the brush was increased further, and for fairly high molecular weight free polymer, the free melt was gradually expelled from the brush, resulting in a return to partial wetting[214]. Voronov and Shafranska[216] found similar behaviour with brushes prepared by free radical polymerisation from a surface-bound initiator.

Edwards *et al.*[218] grafted OH-terminated PS and random PS – PMMA copolymers to silicon, then used extreme UV interference lithography and oxygen plasma etching to produce a pattern of alternating lines of oxidised silicon and polymer brush. These substrates were found to direct the phase separation of a PS-*block*-PMMA copolymer. The PMMA block was attracted to the polar silicon, and the PS to the brush. As the percentage of PS in the brush was increased, perfect ordering was found for pattern periodicities further away from the natural length scale[218]. Stoykovich *et al.*[219] used a similar approach to graft OH-terminated PS to silicon. The PS brush was then patterned by oxygen plasma treatment to produce a binary patterned brush. Exposure to oxygen plasma caused a significant change in contact angle, and an increased amount of oxygen in the brush[219], suggesting that there was partial breakdown and removal of the PS. It is debatable whether the 'oxygenated brush' was actually a true polymer brush, but it is clear that a chemically patterned surface was produced. The patterned substrates were used to direct phase separation of PS/PS-*block*-PMMA/PMMA ternary blends, and could again produce perfectly ordered linear domains for length scales within 10 nm of the natural length scale. Features such as sharp corners could also be replicated, providing that the domain size at the apex of the corner was no more than 10 nm larger than the natural length scale of the blend[219]. Fukunaga *et al.*[162] produced a binary polymer brush by spin-coating silicon with a thin layer of PS-*block*-P2VP-*block*-PtBMA) triblock copolymer. The polar PVP middle block physisorbs onto the silicon,

and the PS and PtBMA end blocks microphase-separate, resulting in a patterned brush surface. Spin-coating this with a PS/PtBMA blend resulted in a significant reduction in domain size compared to the morphology found on silicon substrates. The affect of the patterned substrate on phase separation was found to strongly depend on film thickness.

1.5 Objectives of Thesis and Outline of Work

No previous work investigating the phase separation of a binary polymer blend on a binary-patterned polymer brush was found in the literature. The rest of this thesis presents work aimed to address this omission via the synthesis of binary patterned PS/PMMA brushes, and the investigation of phase separation of PS/PMMA blends on these substrates. The remainder of the thesis introduces the relevant surface analysis techniques, with the results presented in four chapters: *Synthesis of polymer brushes*, *Synthesis of patterned polymer brushes by μCP*, *Synthesis of binary-patterned polymer brushes* (by patterning a photosensitive SAM), and *Pattern-directed phase separation* (studying the phase separation of a PS/PMMA blend on silicon, patterned SAMs and binary-patterned polymer brushes). The final chapter presents the conclusions and discusses subjects for further study.

1.6 References

(1) Rühe, J. In *Polymer Brushes: Synthesis, Characterization, Applications*; Advincula, R. C., Ed.; Wiley-VCH: Weinheim, 2004.
(2) Huck, W. T. S.; Edmondson, S.; Osborne, V. L. *Chemical Society Reviews* **2004**, *33*, 14-22.
(3) Xia, Y.; Mrksich, M.; Kim, E.; Whitesides, G. M. *Journal of the American Chemical Society* **1995**, *117*, 9576-9577.
(4) Angst, D. L.; Simmons, G. W. *Langmuir* **1991**, *7*, 2236-2242.
(5) Xia, Y.; Whitesides, G. M. *Angewandte Chemie, International Edition* **1998**, *37*, 550-575.
(6) Milner, S. T. *Science* **1991**, *251*, 905-914.
(7) Xia, Y.; Whitesides, G. M. *Annual Review of Materials Science* **1998**, *28*, 153-184.
(8) Kumar, A.; Biebuyck, H. A.; Whitesides, G. M. *Langmuir* **1994**, *10*, 1498-1511.
(9) Husemann, M.; Mecerreyes, D.; Hawker, C. J.; Hedrick, J. L.; Shah, R.; Abbott, N. L. *Angewandte Chemie, International Edition* **1999**, *38*, 647-649.
(10) Jeon, N. L.; Choi, I. S.; Whitesides, G. M.; Kim, N. Y.; Laibinis, P. E.; Harada, Y.; Finnie, K. R.; Girolami, G. S.; Nuzzo, R. G. *Applied Physics Letters* **1999**, *75*, 4201-4203.
(11) Zhou, F.; Huck, W. T. S. *Physical Chemistry Chemical Physics* **2006**, *8*, 3815-3823.
(12) Eastwood, E.; Viswanathan, S.; O'Brien, C. P.; Kumar, D.; Dadmun, M. D. *Polymer* **2005**, *46*, 3957-3970.
(13) Jones, R. A. L.; Richards, R. W. *Polymers at Surfaces and Interfaces*; Cambridge University Press: Cambridge, 1999.
(14) Balsara, N. P. In *Physical Properties of Polymers Handbook*; Mark, J. E., Ed.; AIP Press: New York, 1996.
(15) Walheim, S.; Böltau, M.; Mlynek, J.; Krausch, G.; Steiner, U. *Macromolecules* **1997**, *30*, 4995-5003.
(16) Tanaka, K.; Takahara, A.; Kajiyama, T. *Macromolecules* **1996**, *29*, 3232-3239.
(17) Winesett, D. A.; Ade, H.; Sokolov, J.; Rafailovich, M.; Zhu, S. *Polymer International* **2000**, *49*, 458-462.
(18) Andrew, P.; Huck, W. T. S. *Soft Matter* **2007**, *3*, 230-237.
(19) Fichet, G.; Corcoran, N.; Ho, P. K. H.; Arias, A. C.; MacKenzie, J. D.; Huck, W. T. S.; Friend, R. H. *Advanced Materials* **2004**, *16*, 1908-1912.
(20) Yim, K.-H.; Zheng, Z.; Friend, R. H.; Huck, W. T. S.; Kim, J.-S. *Advanced Functional Materials* **2008**, *18*, 2897-2904.
(21) Corcoran, N.; Ho, P. K. H.; Arias, A. C.; Mackenzie, J. D.; Friend, R. H.; Fichet, G.; Huck, W. T. S. *Applied Physics Letters* **2004**, *85*, 2965-2967.
(22) Zhao, B.; Brittain, W. J. *Progress in Polymer Science* **2000**, *25*, 677-710.
(23) Alexander, S. *Journal de Physique* **1977**, *38*, 983-987.
(24) De Gennes, P. G. *Journal de Physique* **1976**, *37*, 1445-1452.
(25) De Gennes, P. G. *Macromolecules* **1980**, *13*, 1069-1075.
(26) Halperin, A.; Tirrell, M.; Lodge, T. P. *Advances In Polymer Science* **1992**, *100*, 31-71.
(27) Strobl, G. *The Physics of Polymers: Concepts for Understanding Their Structures and Behaviour*; Third ed.; Springer: Berlin, 2007.

(28) Matyjaszewski, K.; Xia, J. *Chemical Reviews* **2001**, *101*, 2921-2990.
(29) Patten, T. E.; Matyjaszewski, K. *Advanced Materials* **1998**, *10*, 901-915.
(30) Hsieh, H. L.; Quirk, R. P. *Anionic Polymerisation: Principles and Practical Applications*; Marcel Dekker, Inc.: New York, 1996.
(31) Szwarc, M. *Nature* **1956**, *178*, 1168-1169.
(32) Szwarc, M.; Levy, M.; Milkovich, R. *Journal of the American Chemical Society* **1956**, *78*, 2656-2657.
(33) Wang, T.-L.; Liu, Y.-Z.; Jeng, B.-C.; Cai, Y.-C. *Journal of Polymer Research* **2005**, *12*, 67-75.
(34) Kato, M.; Kamigaito, M.; Sawamoto, M.; Higashimura, T. *Macromolecules* **1995**, *28*, 1721-1723.
(35) Wang, J.-S.; Matyjaszewski, K. *Macromolecules* **1995**, *28*, 7901-7910.
(36) Wang, J.-S.; Matyjaszewski, K. *Journal of the American Chemical Society* **1995**, *117*, 5614-15.
(37) Karanam, S.; Goossens, H.; Klumperman, B.; Lemstra, P. *Macromolecules* **2003**, *36*, 3051-3060.
(38) Karanam, S.; Goossens, H.; Klumperman, B.; Lemstra, P. *Macromolecules* **2003**, *36*, 8304-8311.
(39) Sun, X.; Zhang, H.; Huang, X.; Wang, X.; Zhou, Q.-F. *Polymer* **2005**, *46*, 5251-5257.
(40) Tsarevsky, N. V.; Matyjaszewski, K. *Macromolecules* **2002**, *35*, 9009-9014.
(41) Coessens, V.; Nakagawa, Y.; Matyjaszewski, K. *Polymer Bulletin* **1998**, *40*, 135-142.
(42) Matyjaszewski, K.; Nakagawa, Y.; Gaynor, S. G. *Macromolecular Rapid Communications* **1997**, *18*, 1057-1066.
(43) Patten, T. E.; Xia, J.; Abernathy, T.; Matyjaszewski, K. *Science* **1996**, *272*, 866-868.
(44) Matyjaszewski, K.; Wang, J.-L.; Grimaud, T.; Shipp, D. A. *Macromolecules* **1998**, *31*, 1527-1534.
(45) Wang, J.-L.; Grimaud, T.; Matyjaszewski, K. *Macromolecules* **1997**, *30*, 6507-6512.
(46) Matyjaszewski, K.; Patten, T. E.; Xia, J. *Journal of the American Chemical Society* **1997**, *119*, 674-680.
(47) Matyjaszewski, K.; Kajiwara, A. *Macromolecules* **1998**, *31*, 548-550.
(48) Matyjaszewski, K.; Davis, T. P. *Handbook of Radical Polymerization*; John Wiley & Sons, Inc.: Hoboken, 2002.
(49) Matyjaszewski, K.; Nakagawa, Y.; Jasieczek, C. B. *Macromolecules* **1998**, *31*, 1535-1541.
(50) Odian, G. *Principles of Polymerization*; 4th ed.; John Wiley and Sons, Inc: Hoboken, New Jersey, 2004.
(51) Matyjaszewski, K.; Wang, J.-L.; Grimaud, T.; Shipp, D. A. *Macromolecules* **1998**, *31*, 1527-1534.
(52) Matyjaszewski, K.; Shipp, D. A.; Wang, J.-L.; Grimaud, T.; Patten, T. E. *Macromolecules* **1998**, *31*, 6836-6840.
(53) Tomlinson, M. R. Surface-Grafted Polymer and Copolymer Assemblies with Gradient in Molecular Weight and Composition, PhD thesis, North Carolina State University, 2005.
(54) Shah, R. R.; Merreceyes, D.; Husemann, M.; Rees, I.; Abbott, N. L.; Hawker, C. J.; Hedrick, J. L. *Macromolecules* **2000**, *33*, 597-605.

(55) Pintauer, T.; Reinohl, U.; Feth, M.; Bertagnolli, H.; Matyjaszewski, K. *Eur. J. Inorg. Chem.* **2003**, 2082-2094.
(56) Matyjaszewski, K.; Davis, K.; Patten, T. E.; Wei, M. *Tetrahedron* **1997**, *53*, 15321-15329.
(57) Ejaz, M.; Yamamoto, S.; Ohno, K.; Tsujii, Y.; Fukuda, T. *Macromolecules* **1998**, *31*, 5934-5936.
(58) Wang, Y.; Hu, S.; Brittain, W. J. *Macromolecules* **2006**, *39*, 5675-5678.
(59) Ryan, A. J.; Crook, C. J.; Howse, J. R.; Topham, P.; Jones, R. A. L.; Geoghegan, M.; Parnell, A. J.; Ruiz-Perez, L.; Martin, S. J.; Cadby, A.; Menelle, A.; Webster, J. R. P.; Gleeson, A. J.; Bras, W. *Faraday Discussions* **2004**, *128*, 55-74.
(60) Zhao, J.; Shang, Z.; Gao, L. *Sensors and Actuators, A: Physical* **2007**, *A135*, 257-261.
(61) Tugulu, S.; Arnold, A.; Sielaff, I.; Johnsson, K.; Klok, H.-A. *Biomacromolecules* **2005**, *6*, 1602-1607.
(62) Topham, P. D.; Howse, J. R.; Crook, C. J.; Parnell, A. J.; Geoghegan, M.; Jones, R. A. L.; Ryan, A. J. *Polymer International* **2006**, *55*, 808-815.
(63) Huang, W.; Kim, J.-B.; Bruening, M. L.; Baker, G. L. *Macromolecules* **2002**, *35*, 1175-1179.
(64) Yu, W. H.; Kang, E. T.; Neoh, K. G.; Zhu, S. *Journal of Physical Chemistry B* **2003**, *107*, 10198-10205.
(65) Yu, W. H.; Kang, E. T.; Neoh, K. G. *Langmuir* **2004**, *20*, 8294-8300.
(66) Yamamoto, S.; Ejaz, M.; Tsujii, Y.; Fukuda, T. *Macromolecules* **2000**, *33*, 5608-5612.
(67) Matyjaszewski, K.; Miller, P. J.; Shukla, N.; Immaraporn, B.; Gelman, A.; Luokala, B. B.; Siclovan, T. M.; Kickelbick, G.; Vallant, T.; Hoffmann, H.; Pakula, T. *Macromolecules* **1999**, *32*, 8716-8724.
(68) Jones, D. M.; Huck, W. T. S. *Advanced Materials* **2001**, *13*, 1256-1259.
(69) Kong, X.; Kawai, T.; Abe, J.; Iyoda, T. *Macromolecules* **2001**, *34*, 1837-1844.
(70) Edmondson, S.; Huck, W. T. S. *Journal of Materials Chemistry* **2004**, *14*, 730-734.
(71) Yamamoto, S.; Ejaz, M.; Tsujii, Y.; Matsumoto, M.; Fukuda, T. *Macromolecules* **2000**, *33*, 5602-5607.
(72) Xu, F. J.; Cai, Q. J.; Kang, E. T.; Neoh, K. G. *Langmuir* **2005**, *21*, 3221-3225.
(73) Kim, J.-B.; Bruening, M. L.; Baker, G. L. *Journal of the American Chemical Society* **2000**, *122*, 7616-7617.
(74) Raghuraman, G. K.; Dhamodharan, R.; Prucker, O.; Rühe, J. *Macromolecules* **2008**, *41*, 873-878.
(75) Huang, W.; Baker, G. L.; Bruening, M. L. *Angewandte Chemie, International Edition* **2001**, *40*, 1510-1512.
(76) Sha, K.; Li, D. S.; Li, Y.; Wang, S.; Wang, J. *Journal of Materials Science* **2007**, *42*, 4916-4925.
(77) Bao, Z.; Bruening, M. L.; Baker, G. L. *Macromolecules* **2006**, *39*, 5251-5258.
(78) Osborne, V. L.; Jones, D. M.; Huck, W. T. S. *Chemical Communications* **2002**, 1838-1839.
(79) Kim, J.-B.; Huang, W.; Bruening, M. L.; Baker, G. L. *Macromolecules* **2002**, *35*, 5410-5416.
(80) Granville, A. M.; Boyes, S. G.; Akgun, B.; Foster, M. D.; Brittain, W. J. *Macromolecules* **2004**, *37*, 2790-2796.

(81) Boyes, S. G.; Brittain, W. J.; Weng, X.; Cheng, S. Z. D. *Macromolecules* **2002**, *35*, 4960-4967.
(82) Boyes, S. G.; Akgun, B.; Brittain, W. J.; Foster, M. D. *Macromolecules* **2003**, *36*, 9539-9548.
(83) Farhan, T.; Huck, W. T. S. *European Polymer Journal* **2004**, *40*, 1599-1604.
(84) Tu, H.; Heitzman, C. E.; Braun, P. V. *Langmuir* **2004**, *20*, 8313-8320.
(85) Hamelinck, P. J.; Huck, W. T. S. *Journal of Materials Chemistry* **2005**, *15*, 381-385.
(86) de las Heras Alarcón, C.; Farhan, T.; Osborne, V. L.; Huck, W. T. S.; Alexander, C. *Journal of Materials Chemistry* **2005**, *15*, 2089-2094.
(87) von Werne, T. A.; Germack, D. S.; Hagberg, E. C.; Sheares, V. V.; Hawker, C. J.; Carter, K. R. *Journal of the American Chemical Society* **2003**, *125*, 3831-3838.
(88) Edmondson, S.; Huck, W. T. S. *Advanced Materials* **2004**, *16*, 1327-1331.
(89) Ahn, S. J.; Kaholek, M.; Lee, W.-K.; LaMattina, B.; LaBean, T. H.; Zauscher, S. *Advanced Materials* **2004**, *16*, 2141-2145.
(90) Hou, S.; Li, Z.; Li, Q.; Liu, Z. F. *Applied Surface Science* **2004**, *222*, 338-345.
(91) Maeng, I. S.; Park, J. W. *Langmuir* **2003**, *19*, 9973-9976.
(92) Zhou, F.; Jiang, L.; Liu, W.; Xue, Q. *Macromolecular Rapid Communications* **2004**, *25*, 1979-1983.
(93) Zhou, F.; Zheng, Z.; Yu, B.; Liu, W.; Huck, W. T. S. *Journal of the American Chemical Society* **2006**, *128*, 16253-16258.
(94) Liu, Y.; Klep, V.; Luzinov, I. *Journal of the American Chemical Society* **2006**, *128*, 8106-8107.
(95) Xu, F. J.; Song, Y.; Cheng, Z. P.; Zhu, X. L.; Zhu, C. X.; Kang, E. T.; Neoh, K. G. *Macromolecules* **2005**, *38*, 6254-6258.
(96) Xu, F. J.; Kang, E. T.; Neoh, K. G. *Journal of Materials Chemistry* **2006**, *16*, 2948-2952.
(97) Pyun, J.; Jia, S.; Kowalewski, T.; Patterson, G. D.; Matyjaszewski, K. *Macromolecules* **2003**, *36*, 5094-5104.
(98) Pyun, J.; Jia, S.; Kowalewski, T.; Patterson, G. D.; Matyjaszewski, K. *Macromolecules* **2003**, *36*, 6952.
(99) Lei, Z.; Bi, S. *Materials Letters* **2007**, *61*, 3531-3534.
(100) Zhang, K.; Li, H.; Zhang, H.; Zhao, S.; Wang, D.; Wang, J. *Materials Chemistry and Physics* **2006**, *96*, 477-482.
(101) Kong, H.; Gao, C.; Yan, D. *Journal of Materials Chemistry* **2004**, *14*, 1401-1405.
(102) Matrab, T.; Chancolon, J.; L'Hermite, M. M.; Rouzaud, J.-N.; Deniau, G.; Boudou, J.-P.; Chehimi, M. M.; Delamar, M. *Colloids and Surfaces, A: Physicochemical and Engineering Aspects* **2006**, *287*, 217-221.
(103) Baskaran, D.; Mays, J. W.; Bratcher, M. S. *Angewandte Chemie, International Edition* **2004**, *43*, 2138-2142.
(104) Prucker, O.; Rühe, J. *Macromolecules* **1998**, *31*, 592-601.
(105) Husseman, M.; Malmström, E. E.; McNamara, M.; Mate, M.; Mecerreyes, D.; Benoit, D. G.; Hedrick, J. L.; Mansky, P.; Huang, E.; Russell, T. P.; Hawker, C. J. *Macromolecules* **1999**, *32*, 1424-1431.
(106) Wang, Y.-P.; Pei, X.-W.; He, X.-Y.; Yuan, K. *European Polymer Journal* **2005**, *41*, 1326-1332.
(107) Bigelow, W. C.; Pickett, D. L.; Zisman, W. A. *Journal of Colloid Science* **1946**, *1*, 513-538.

(108) Xia, Y.; Qin, D.; Yin, Y. *Current Opinion in Colloid & Interface Science* **2001**, *6*, 54-64.
(109) Delamarche, E.; Michel, B.; Biebuyck, H. A.; Gerber, C. *Advanced Materials* **1996**, *8*, 719-729.
(110) Balachander, N.; Sukenik, C. N. *Langmuir* **1990**, *6*, 1621-1627.
(111) Fryxell, G. E.; Rieke, P. C.; Wood, L. L.; Engelhard, M. H.; Williford, R. E.; Graff, G. L.; Campbell, A. A.; Wiacek, R. J.; Lee, L.; Halverson, A. *Langmuir* **1996**, *12*, 5064-5075.
(112) Hoffmann, H.; Mayer, U.; Brunner, H.; Krischanitz, A. *Journal of Molecular Structure* **1995**, *349*, 305-308.
(113) Hoffmann, H.; Mayer, U.; Brunner, H.; Krischanitz, A. *Vibrational Spectroscopy* **1995**, *8*, 151-157.
(114) Larsen, N. B.; Biebuyck, H.; Delamarche, E.; Michel, B. *Journal of the American Chemical Society* **1997**, *119*, 3017-3026.
(115) Jeon, N. L.; Finnie, K.; Branshaw, K.; Nuzzo, R. G. *Langmuir* **1997**, *13*, 3382-3391.
(116) Hoffmann, H.; Mayer, U.; Krischanitz, A. *Langmuir* **1995**, *11*, 1304-1312.
(117) Fadeev, A. Y.; McCarthy, T. J. *Langmuir* **2000**, *16*, 7268-7274.
(118) Hair, M. L.; Tripp, C. P. *Colloids and Surfaces, A: Physicochemical and Engineering Aspects* **1995**, *105*, 95-103.
(119) Brzoska, J. B.; Azouz, I. B.; Rondelez, F. *Langmuir* **1994**, *10*, 4367-4373.
(120) Finnie, K. R.; Haasch, R.; Nuzzo, R. G. *Langmuir* **2000**, *16*, 6968-6976.
(121) Allara, D. L.; Parikh, A. N.; Rondelez, F. *Langmuir* **1995**, *11*, 2357-2360.
(122) Parikh, A. N.; Allara, D. L.; Azouz, I. B.; Rondelez, F. *Journal of Physical Chemistry* **1994**, *98*, 7577-7590.
(123) Tripp, C. P.; Hair, M. L. *Langmuir* **1992**, *8*, 1120-1126.
(124) Sung, M. M.; Kluth, G. J.; Maboudian, R. *Journal of Vacuum Science & Technology, A: Vacuum, Surfaces, and Films* **1999**, *17*, 540-544.
(125) Vallant, T.; Brunner, H.; Mayer, U.; Hoffmann, H.; Leitner, T.; Resch, R.; Friedbacher, G. *Journal of Physical Chemistry B* **1998**, *102*, 7190-7197.
(126) Vallant, T.; Kattner, J.; Brunner, H.; Mayer, U.; Hoffmann, H. *Langmuir* **1999**, *15*, 5339-5346.
(127) Maoz, R.; Sagiv, J. *Journal Of Colloid And Interface Science* **1984**, *100*, 465-496.
(128) Leggett, G. J. *Chemical Society Reviews* **2006**, *35*, 1150-1161.
(129) Sun, S.; Leggett, G. J. *Nano Letters* **2007**, *7*, 3753-3758.
(130) Kumar, A.; Whitesides, G. M. *Applied Physics Letters* **1993**, *63*, 2002-2004.
(131) Wilbur, J. L.; Kumar, A.; Biebuyck, H. A.; Kim, E.; Whitesides, G. M. *Nanotechnology* **1996**, *7*, 452-457.
(132) Qin, D.; Xia, Y.; Xu, B.; Yang, H.; Zhu, C.; Whitesides, G. M. *Advanced Materials* **1999**, *11*, 1433-1437.
(133) Xia, Y.; Whitesides, G. M. *Langmuir* **1997**, *13*, 2059-2067.
(134) Xia, Y.; Tien, J.; Qin, D.; Whitesides, G. M. *Langmuir* **1996**, *12*, 4033-4038.
(135) Libioulle, L.; Bietsch, A.; Schmid, H.; Michel, B.; Delamarche, E. *Langmuir* **1999**, *15*, 300-304.
(136) Delamarche, E.; Donzel, C.; Kamounah, F. S.; Wolf, H.; Geissler, M.; Stutz, R.; Schmidt-Winkel, P.; Michel, B.; Mathieu, H. J.; Schaumburg, K. *Langmuir* **2003**, *19*, 8749-8758.
(137) Delamarche, E.; Schmid, H.; Bietsch, A.; Larsen, N. B.; Rothuizen, H.; Michel, B.; Biebuyck, H. *Journal of Physical Chemistry B* **1998**, *102*, 3324-3334.

(138) Harada, Y.; Girolami, G. S.; Nuzzo, R. G. *Langmuir* **2004**, *20*, 10878-10888.
(139) Pompe, T.; Fery, A.; Herminghaus, S.; Kriele, A.; Lorenz, H.; Kotthaus, J. P. *Langmuir* **1999**, *15*, 2398-2401.
(140) Jeon, N. L.; Nuzzo, R. G.; Xia, Y.; Mrksich, M.; Whitesides, G. M. *Langmuir* **1995**, *11*, 3024-3026.
(141) Lahiri, J.; Ostuni, E.; Whitesides, G. M. *Langmuir* **1999**, *15*, 2055-2060.
(142) Harada, Y.; Girolami, G. S.; Nuzzo, R. G. *Langmuir* **2003**, *19*, 5104-5114.
(143) Tovar, G.; Paul, S.; Knoll, W.; Prucker, O.; Rühe, J. *Supramolecular Science* **1995**, *2*, 89-98.
(144) Prucker, O.; Habicht, J.; Park, I.-J.; Rühe, J. *Materials Science & Engineering, C-Biomimetic and Supramolecular Systems* **1999**, *8-9*, 291-297.
(145) Konradi, R.; Rühe, J. *Langmuir* **2006**, *22*, 8571-8575.
(146) Schmelmer, U.; Jordan, R.; Geyer, W.; Eck, W.; Golzhauser, A.; Grunze, M.; Ulman, A. *Angewandte Chemie, International Edition* **2003**, *42*, 559-563.
(147) Husemann, M.; Morrison, M.; Benoit, D.; Frommer, J.; Mate, C. M.; Hinsberg, W. D.; Hedrick, J. L.; Hawker, C. J. *Journal of the American Chemical Society* **2000**, *122*, 1844-1845.
(148) Liu, Z.; Hu, H.; Yu, B.; Chen, M.; Zheng, Z.; Zhou, F. *Electrochemistry Communications* **2009**, *11*, 492-495.
(149) Liu, Z.; Khan, N.; Hu, H.; Yu, B.; Liu, J.; Chen, M.; Zhou, F. *Macromolecular Rapid Communications* **2008**, *29*, 1937-1943.
(150) Caster, K. C. In *Polymer brushes: synthesis, characterization, applications*; Advincula, R. C., Ed.; Wiley-VCH: Weinheim, 2004.
(151) Huber, D. L.; Manginell, R. P.; Samara, M. A.; Kim, B.-I.; Bunker, B. C. *Science* **2003**, *301*, 352-354.
(152) Ito, Y.; Park, Y. S.; Imanishi, Y. *Journal of the American Chemical Society* **1997**, *119*, 2739-2740.
(153) Ito, Y.; Ochiai, Y.; Park, Y. S.; Imanishi, Y. *Journal of the American Chemical Society* **1997**, *119*, 1619-1623.
(154) Ito, Y.; Nishi, S.; Park, Y. S.; Imanishi, Y. *Macromolecules* **1997**, *30*, 5856-5859.
(155) Iwata, H.; Hirata, I.; Ikada, Y. *Macromolecules* **1998**, *31*, 3671-3678.
(156) Sontag, S. K.; Marshall, N.; Locklin, J. *Chemical Communications* **2009**, 3354-3356.
(157) http://pslc.ws/mactest/iblend.htm.
(158) Budkowski, A.; Bermasik, A.; Cyganic, P.; Rysz, J.; Brenn, R. *e-Polymers* **2002**, Paper No 6, 1-21.
(159) Ton-That, C.; Shard, A. G.; Daley, R.; Bradley, R. H. *Macromolecules* **2000**, *33*, 8453-8459.
(160) Tanaka, K.; Yoon, J.-S.; Takahara, A.; Kajiyama, T. *Macromolecules* **1995**, *28*, 934-938.
(161) El-Mabrouk, K.; Belaiche, M.; Bousmina, M. *Journal of Colloid and Interface Science* **2007**, *306*, 354-367.
(162) Fukunaga, K.; Elbs, H.; Krausch, G. *Langmuir* **2000**, *16*, 3474-3477.
(163) Geoghegan, M.; Jones, R. A. L.; Payne, R. S.; Sakellariou, P.; Clough, A. S.; Penfold, J. *Polymer* **1994**, *35*, 2019-2027.
(164) Geoghegan, M.; Jones, R. A. L.; Clough, A. S. *Journal of Chemical Physics* **1995**, *103*, 2719-2724.
(165) Jones, R. A. L.; Norton, L. J.; Kramer, E. J.; Bates, F. S.; Wiltzius, P. *Physical Review Letters* **1991**, *66*, 1326-1329.

(166) Bruder, F.; Brenn, R. *Physical Review Letters* **1992**, *69*, 624-627.
(167) Krausch, G.; Dai, C. A.; Kramer, E. J.; Marko, J. F.; Bates, F. S. *Macromolecules* **1993**, *26*, 5566-5571.
(168) Nisato, G.; Ermi, B. D.; Douglas, J. F.; Karim, A. *Macromolecules* **1999**, *32*, 2356-2364.
(169) Jerome, J.; Zhu, S.; Seo, Y. S.; Ho, M.; Pernodet, N.; Gambino, R.; Sokolov, J.; Rafailovich, M. H.; Zaitsev, V.; Schwarz, S.; DiNardo, R. *Macromolecules* **2004**, *37*, 6504-6510.
(170) Chappell, J.; Lidzey, D. G.; Jukes, P. C.; Higgins, A. M.; Thompson, R. L.; O'Connor, S.; Grizzi, I.; Fletcher, R.; O'Brien, J.; Geoghegan, M.; Jones, R. A. L. *Nature Materials* **2003**, *2*, 616-621.
(171) Liu, D.; Yang, P. Y.; Luscombe, C. K. *Journal Of Physical Chemistry C* **2008**, *112*, 7886-7894.
(172) Walheim, S.; Schaffer, E.; Mlynek, J.; Steiner, U. *Science* **1999**, *283*, 520-522.
(173) Li, H. M.; Wang, Z.; Chen, X. C.; Xie, Z. D.; Shu, D. J.; Wang, M.; Peng, R. W.; Ming, N. B. *European Physical Journal-Applied Physics* **2009**, *45*, 20501/1-4.
(174) Jukes, P. C.; Heriot, S. Y.; Sharp, J. S.; Jones, R. A. L. *Macromolecules* **2005**, *38*, 2030-2032.
(175) Heriot, S. Y.; Jones, R. A. L. *Nature Materials* **2005**, *4*, 782-786.
(176) Higgins, A. M.; Martin, S. J.; Thompson, R. L.; Chappell, J.; Voigt, M.; Lidzey, D. G.; Jones, R. A. L.; Geoghegan, M. *Journal of Physics: Condensed Matter* **2005**, *17*, 1319-1328.
(177) Cui, L.; Ding, Y.; Li, X.; Wang, Z.; Han, Y. *Thin Solid Films* **2006**, *515*, 2038-2048.
(178) Li, X.; Han, Y.; An, L. *Applied Surface Science* **2004**, *230*, 115-124.
(179) Seo, Y.-S.; Kim, E.; Kwon, S. Y.; Jing, H.; Shin, K. *Ultramicroscopy* **2008**, *108*, 1186-1190.
(180) Li, Y. X.; Yang, Y. M.; Yu, F. S.; Dong, L. S. *Journal Of Polymer Science Part B: Polymer Physics* **2006**, *44*, 9-21.
(181) Harris, M.; Appel, G.; Ade, H. *Macromolecules* **2003**, *36*, 3307-3314.
(182) Ton-That, C.; Shard, A. G.; Teare, D. O. H.; Bradley, R. H. *Polymer* **2000**, *42*, 1121-1129.
(183) Sugihara, H.; Oya, K.; Murase, H.; Akabori, K.; Tanaka, K.; Kajiyama, T.; Takahara, A. *Applied Surface Science* **2008**, *254*, 3180-3183.
(184) Raghavan, D.; VanLandingham, M.; Gu, X.; Nguyen, T. *Langmuir* **2000**, *16*, 9448-9459.
(185) Müller-Buschbaum, P.; Gutmann, J. S.; Stamm, M. *Macromolecules* **2000**, *33*, 4886-4895.
(186) Li, X.; Han, Y.; An, L. *Polymer* **2003**, *44*, 8155-8165.
(187) Callaghan, T. A.; Paul, D. R. *Macromolecules* **1993**, *26*, 2439-2450.
(188) Wang, H.; Composto, R. J. *Journal of Chemical Physics* **2000**, *113*, 10386-10397.
(189) Tanaka, K.; Takahara, A.; Kajiyama, T. *Macromolecules* **1998**, *31*, 863-869.
(190) Ugur, S.; Pekcan, O. *Journal of Applied Polymer Science* **2006**, *100*, 2104-2110.
(191) Li, X.; Han, Y.; An, L. *Polymer* **2003**, *44*, 5833-5841.
(192) Winesett, D. A.; Zhu, S.; Sokolov, J.; Rafailovich, M.; Ade, H. *High Performance Polymers* **2000**, *12*, 599-602.
(193) Jaczewska, J.; Budkowski, A.; Bernasik, A.; Raptis, I.; Moons, E.; Goustouridis, D.; Haberko, J.; Rysz, J. *Soft Matter* **2009**, *5*, 234-241.

(194) Krausch, G.; Kramer, E. J.; Rafailovich, M. H.; Sokolov, J. *Applied Physics Letters* **1994**, *64*, 2655-2657.
(195) Böltau, M.; Walheim, S.; Mlynek, J.; Krausch, G.; Steiner, U. *Nature* **1998**, *391*, 877-879.
(196) Cyganik, P.; Budkowski, A.; Steiner, U.; Rysz, J.; Bernasik, A.; Walheim, S.; Postawa, Z.; Raczkowska, J. *Europhysics Letters* **2003**, *62*, 855-861.
(197) Cyganik, P.; Bernasik, A.; Budkowski, A.; Bergues, B.; Kowalski, K.; Rysz, J.; Lekki, J.; Lekka, M.; Postawa, Z. *Vacuum* **2001**, *63*, 307-313.
(198) Cui, L.; Zhang, Z.; Li, X.; Han, Y. *Polymer Bulletin* **2005**, *55*, 131-140.
(199) Li, X.; Xing, R. B.; Zhang, Y.; Han, Y. C.; An, L. J. *Polymer* **2004**, *45*, 1637-1646.
(200) Raczkowska, J.; Bernasik, A.; Budkowski, A.; Cyganik, P.; Rysz, J.; Raptis, I.; Czuba, P. *Surface Science* **2006**, *600*, 1004-1011.
(201) Wei, J. H.; Coffey, D. C.; Ginger, D. S. *Journal of Physical Chemistry B* **2006**, *110*, 24324-24330.
(202) Karim, A.; Douglas, J. F.; Lee, B. P.; Glotzer, S. C.; Rogers, J. A.; Jackman, R. J.; Amis, E. J.; Whitesides, G. M. *Physical Review E: Statistical Physics, Plasmas, Fluids, and Related Interdisciplinary Topics* **1998**, *57*, R6273-R6276.
(203) Ermi, B. D.; Nisato, G.; Douglas, J. F.; Rogers, J. A.; Karim, A. *Physical Review Letters* **1998**, *81*, 3900-3903.
(204) Kielhorn, L.; Muthukumar, M. *Journal of Chemical Physics* **1999**, *111*, 2259-2269.
(205) Yan, L.-T.; Li, J.; Li, Y.; Xie, X.-M. *Macromolecules* **2008**, *41*, 3605-3612.
(206) Li, J.-L.; Yan, L.-T.; Xie, X.-M. *Polymer* **2009**, *50*, 2172-2180.
(207) Zhang, Z.; Wang, Z.; Xing, R.; Han, Y. *Surface Science* **2003**, *539*, 129-136.
(208) Rockford, L.; Liu, Y.; Mansky, P.; Russell, T. P.; Yoon, M.; Mochrie, S. G. J. *Physical Review Letters* **1999**, *82*, 2602-2605.
(209) Geoghegan, M.; Wang, C.; Rehse, N.; Magerle, R.; Krausch, G. *Journal of Physics: Condensed Matter* **2005**, *17*, S389-S402.
(210) Higgins, A. M.; Jones, R. A. L. *Nature* **2000**, *404*, 476-479.
(211) Shou, Z.; Chakrabarti, A. *Polymer* **2001**, *42*, 6141-6152.
(212) Chen, F.-C.; Lin, Y.-K.; Ko, C.-J. *Applied Physics Letters* **2008**, *92*, 023307/1-023307/3.
(213) Mansky, P.; Liu, Y.; Huang, E.; Russell, T. P.; Hawker, C. *Science* **1997**, *275*, 1458-1460.
(214) Maas, J. H.; Fleer, G. J.; Leermakers, F. A. M.; Stuart, M. A. C. *Langmuir* **2002**, *18*, 8871-8880.
(215) Reiter, G.; Auroy, P.; Auvray, L. *Macromolecules* **1996**, *29*, 2150-2157.
(216) Voronov, A.; Shafranska, O. *Langmuir* **2002**, *18*, 4471-4477.
(217) Sharma, S.; Rafailovich, M. H.; Sokolov, J.; Liu, Y.; Qu, S.; Schwarz, S. A.; Eisenberg, A. *High Performance Polymers* **2000**, *12*, 581-586.
(218) Edwards, E. W.; Montague, M. F.; Solak, H. H.; Hawker, C. J.; Nealey, P. F. *Advanced Materials* **2004**, *16*, 1315-1319.
(219) Stoykovich, M. P.; Müller, M.; Kim, S. O.; Solak, H. H.; Edwards, E. W.; de Pablo, J. J.; Nealey, P. F. *Science* **2005**, *308*, 1442-1446.

Chapter 2

Major Analytical Methods

2.1 Introduction

The goals of this project were to synthesise binary patterned polymer brushes and investigate the influence of patterned substrates on the phase separation of a polymer blend. Consequently, reactions to produce or modify SAMs and polymer brushes were essential. However, molecules covalently bonded to a substrate cannot be analysed by routine methods such as NMR and size exclusion chromatography.

The amount of material present in a surface-bound polymer brush is very small: for a PMMA brush with a theoretical degree of polymerisation (*N*) of 100, and an area per polymer chain of ~ 100 $Å^2$ [1], the surface coverage can be estimated to be ~ 2 ng/cm^2. Even if the polymer brush or SAM can be degrafted from the substrate, this makes it challenging to collect enough material to analyse (though there are examples in the literature of degrafting polymer brushes grown on large wafers or silica gel and subsequent GPC analysis of the free polymer[1-8]). One of my colleagues, Keqin Xu, has investigated growing polymer brushes on colloidal particles in order to increase the amount of polymer that can be collected.

Finally, the properties, reactivity and morphology of surface-bound molecules are different to in the bulk state or in solution. For example, polymer chains adopt a highly stretched conformation in a brush due to the proximity of other chains, compared to the random coils found in solution and bulk. This makes it important to study the properties of the materials in situ.

This section will briefly introduce the main techniques used to measure the morphology, thickness and chemistry of polymer brushes, SAMs and polymer blends. Each method is discussed with reference to the systems used in this project. A full description of

each method is beyond the scope of this report – for more information the reader is directed to the references for each section.

2.2 Atomic Force Microscopy

Atomic force microscopy (AFM) is a type of scanning probe microscopy (SPM): a group of techniques that measure the interaction of a probe with the surface of a sample to obtain information about its properties. The first SPM technique was scanning tunnelling microscopy (STM), developed by Binning and Rohrer in 1981. It can be used to image the topography of conducting samples with atomic resolution. A voltage is applied between the probe (usually a platinum-iridium or tungsten wire) and the sample. As the probe approaches the surface, electrons begin to tunnel across the gap. The tunnelling current varies exponentially with the probe – sample separation, allowing an image of the sample surface to be built up[9,10].

AFM, first developed in 1986, allows imaging of the topography of a wide range of materials including insulators and soft or delicate samples such as cells and polymers. The probe is a sharp tip, with a diameter of ~ 10 nm (or less) at the end, attached to a long thin cantilever (usually 100 – 150 μm long). The tip is moved back and forwards across the surface by a piezoelectric scanner to build up an image of the desired area. Intermolecular interactions deflect the tip, causing the cantilever to bend. The movement of the cantilever can be measured and used to build up an image of the topography of the sample. In contrast to conventional microscopy, where the resolution is limited by the wavelength of light, the resolution of AFM (and other SPM techniques) is defined by the diameter of the tip, which allows the routine imaging of features as small as tens of nanometres across (and smaller if special tips are used)[10].

The first AFM used a STM to measure the position of the cantilever[11]. In modern instruments, a laser beam is reflected off the back of the cantilever onto a position sensitive photodetector. Interaction of the tip with the sample alters the position of the cantilever, which results in deflection of the laser beam, and a change in the output of the photodetector. Software is used to convert the voltage changes into an image of the sample[9,11]. A schematic diagram of an AFM is shown in Figure 2.1 below:

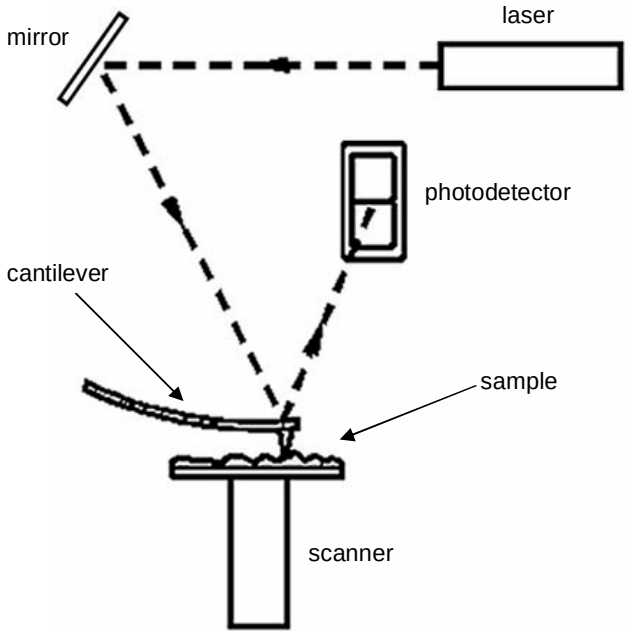

Figure 2.1 Schematic diagram of an AFM (reproduced from [10], image courtesy of Veeco Instruments Inc).

The three basic AFM techniques measure the attractive or repulsive intermolecular interactions at different parts of the force – distance curve (Figure 2.2):

Contact mode operates by measuring the repulsion between the atoms of the tip and the sample. A constant force is applied to hold a flexible silicon nitride cantilever in contact with the surface. As the tip is scanned over the surface, variations in height cause measurable deflection of the cantilever, which is used to build up an image. A feedback loop is used to maintain a constant cantilever deflection or 'set point'. Contact mode imaging can damage the surface of soft samples. In addition, under ambient conditions most samples are covered by a thin layer of adsorbed water (and other species). This tends to wick around the tip, applying a strong attractive force that can hold the tip in contact with the sample[10,11]. This can be avoided by performing the measurements in liquid. Furthermore, scanning the tip across the sample surface can lead to the build-up of electrostatic charge, contributing to the attractive force between the tip and the sample. All these factors mean that a certain minimum normal force must be applied to the sample, but this creates a substantial frictional force as the probe

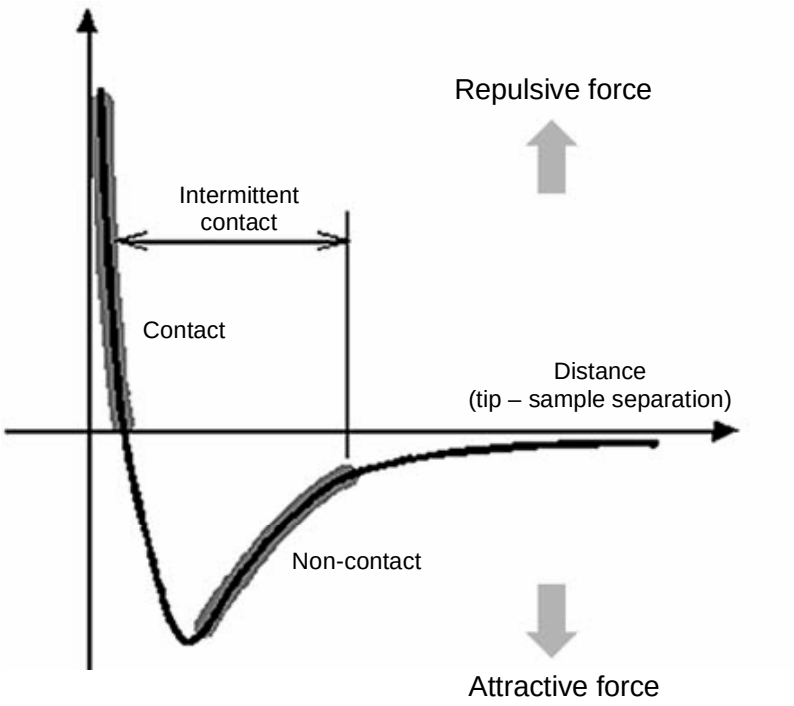

Figure 2.2 Force – distance curve showing tip – sample interactions (reproduced from [10], image courtesy of Veeco Instruments Inc).

scans over the sample, which can damage the sample, dull the cantilever probe and distort the resulting data[11].

In non-contact mode, the tip is maintained a small distance above the surface, and the attractive Van der Waals interactions between the tip and the sample are measured. The forces measured are much weaker than for contact mode, so a very sensitive detection system is required. Non-contact mode imaging is difficult to perform: a high degree of precision is needed to prevent the tip becoming trapped in the surface fluid layer or hovering beyond the effective range of the forces it attempts to measure[11] (although imaging under vacuum, or in liquid can limit these effects). Because of this it is probably the least popular type of AFM.

Tapping, or intermittent contact mode solves some of the problems of contact and non-contact mode. A stiff cantilever made of single crystal silicon is oscillated at close to its resonant frequency at constant amplitude, so that it intermittently contacts the sample surface. Changes in the sample topography change the amplitude of oscillation, which

is detected as a change in the output of the photodetector. The feedback loop then moves the tip until the original 'set point' amplitude is reached. The output of the feedback loop (i.e. the movement of the scanner in the z direction) is used to produce the height image[9].

Because the tip only contacts the sample intermittently, and is only moved laterally when it is not in contact with the surface, it can be used to image soft or easily damaged materials such as biological samples. The oscillation of the cantilever is also large enough to overcome the adhesive forces caused by adsorbed water on the sample[11].

Phase images can be acquired simultaneously with topography information, and can give additional information about the chemistry, adhesion, friction, viscoelasticity, hardness and contamination of the sample. To produce a phase image, the phase of the periodic oscillation of the cantilever is measured relative to the oscillating driving signal (see Figure 2.3 below). Changes in phase can be used to identify changes in the properties of the sample, in some cases giving improved contrast than shown by topography[10-12].

Lateral Force Microscopy (LFM) or Friction Force Microscopy (FFM) is a variant of contact mode which can be used to image samples with changes in chemical/physical properties, but low topographical contrast, such as patterned SAMs. As the tip is

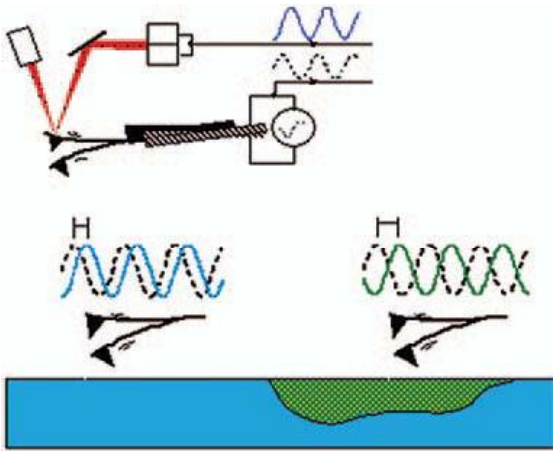

Figure 2.3 Schematic diagram showing phase imaging (reproduced from [10], image courtesy of Veeco Instruments Inc).

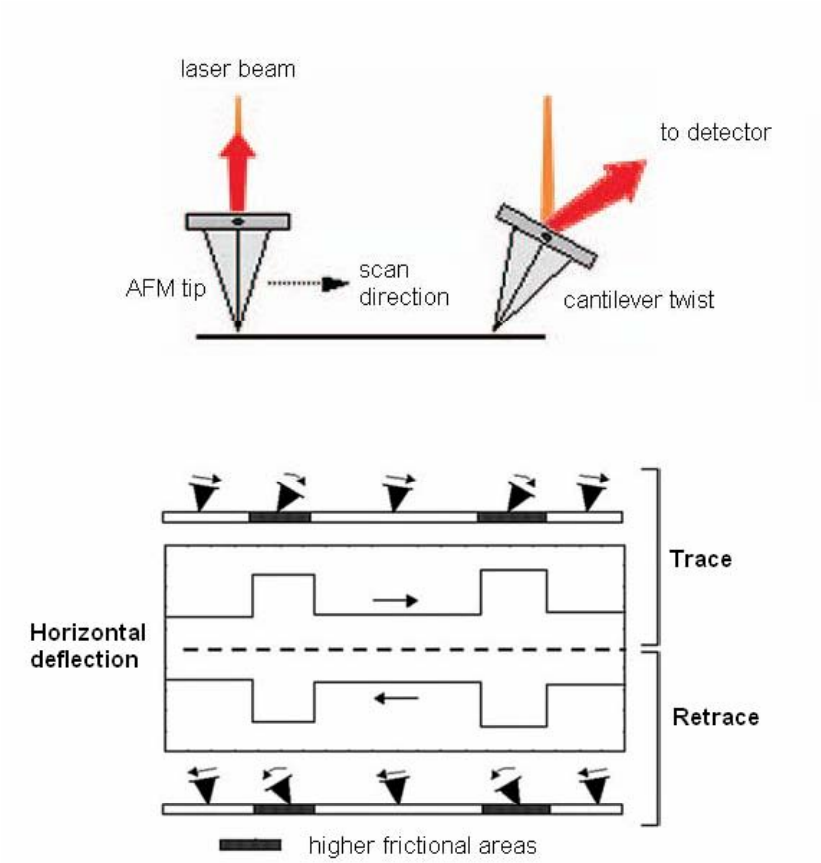

Figure 2.4 Example of the frictional forces on the tip during a scan (reproduced from [10], image courtesy of Veeco Instruments Inc).

scanned across the sample, changes in the frictional properties of the surface cause the cantilever to twist. This causes lateral deflection of the laser beam which can be measured by the photodetector. The torsion is greatest if the sample is scanned at 90º to the cantilever axis. Height features also cause the cantilever to twist, due to delay in the feedback loop, so also produce a signal. When scanned in the opposite direction, the friction changes cause the cantilever to twist in the opposite direction (see Figure 2.4). Changes in height produce the same response whatever the scan direction. Subtracting the trace from the retrace data (or vice versa) removes the height artefacts, producing an image of the frictional properties of the sample[9,10].

In the following chapters, tapping mode imaging was used extensively to image and measure polymer brushes, patterned samples and polymer blends. FFM was used to

produce images of patterned SAMs, which showed no height or phase contrast in tapping mode. There is more information about AFM, including how to produce an image of a sample, and descriptions of other AFM techniques, in the references[9-13].

2.3 Ellipsometry

Ellipsometry is a non-contact, non-destructive method which can be used to measure the thickness, refractive index and other optical properties of thin films[14] with thicknesses from less than a nanometre to several microns. Ellipsometry consists of measuring and interpreting the change in polarisation that occurs following reflection from (or transmission through) a sample[15].

2.3.1 Polarisation

Light can be described as a transverse electromagnetic wave propagating through space. The polarisation of the wave describes the behaviour of the electric field vector ($\mathfrak{E}$) in the plane x, y, perpendicular to the direction of propagation z[16]. The usual approach is to resolve the electric field vector into its x and y component. The amplitude and relative phase of the two orthogonal components define the nature of polarisation. Unpolarised light has random orientation and phase of the electric field components. Linear polarisation occurs when the two orthogonal electric field waves have equal amplitudes and are in phase. When the x and y components are 90 º out of phase and equal in amplitude, it is described as circular polarisation. Looking along the direction of travel, the electric field vector would trace out a spiral around the z axis; an end on view would show the vector tracing out a circle over time. Elliptical polarisation occurs when the orthogonal components have unequal amplitude and any phase difference[17]. Following the direction of travel, the electric field vector would be seen as a 'skewed' spiral, and projected it forms an ellipse. Different types of polarisation are illustrated in Figure 2.5 below.

2.3.2 Ellipsometry Measurement and Theory

The interaction of polarised light with a sample results in a change in its polarisation. All ellipsometers contain a light source with a polariser to produced polarised light. The reflected light is passed through an analyser (a second polariser), before hitting a detector. The amount of light allowed to pass through to the detector depends on the orientation of the analyser relative to the electric field ellipse coming from the sample. The response of the detector is compared to the known input polarisation to determine the change in polarisation. There are several different ellipsometer configurations: in the rotating analyser ellipsometer (RAE) configuration, linearly polarised light is

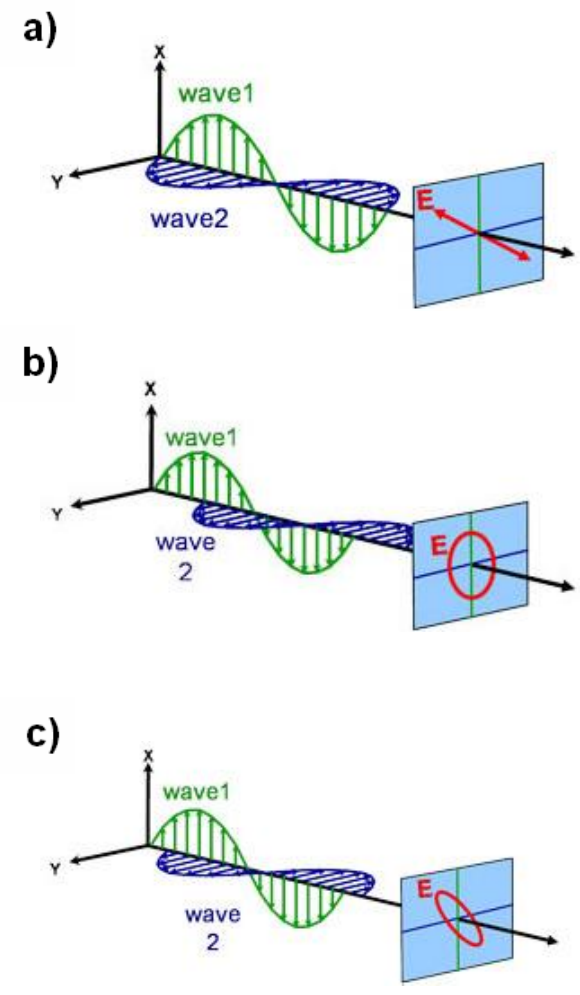

Figure 2.5 Different types of polarisation: x and y components of the electric field vector show (a) linear; (b) circular; and (c) elliptical polarisation (reproduced from [17], image courtesy of J A Woollam Co., Inc).

incident on the sample. Reflection from the surface changes the phase and amplitude by a different amount for the s and p components, so the reflected beam becomes elliptically polarised. The reflected beam is passed through a continuously rotating analyser. The amount of light allowed to pass depends on the orientation of the analyser relative to the electric field ellipse coming from the sample. The detector converts light to electronic signal to determine the reflected polarisation. This information is compared to the known input polarisation to determine the polarisation change caused by the sample[17] (see Figure 2.6).

A two-layer system will now be considered in more detail. Linearly polarised light passing through a medium of refractive index n_0 (usually air) is incident on the bare surface of a material with refractive index n_1. The path of the incident and reflected light waves defines the plane of incidence. The angles of incidence (θ_i), reflection (also θ_i) and refraction (θ_r) (all measured relative to the surface normal) describe the trajectory of the light. The electric field vector (ε) can be split into two components; parallel (ε_p) and perpendicular (ε_s) to the plane of incidence. Interaction with the surface causes both the phase and amplitude of the reflected light components (r) to change, so it becomes elliptically polarised (and attenuated)[15]. This is shown below in Figure 2.7.

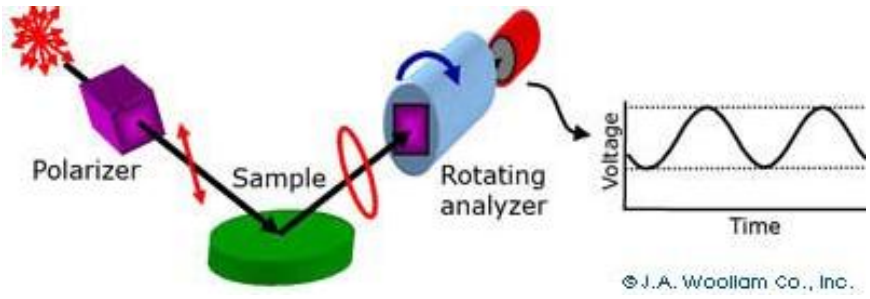

Figure 2.6 RAE measurement: a polarizer defines the incoming polarization and a rotating analyser after the sample measures the outgoing light. The detector converts light to a voltage whose dependence yields the measurement of the reflected polarization (reproduced from [17], image courtesy of J A Woollam Co., Inc).

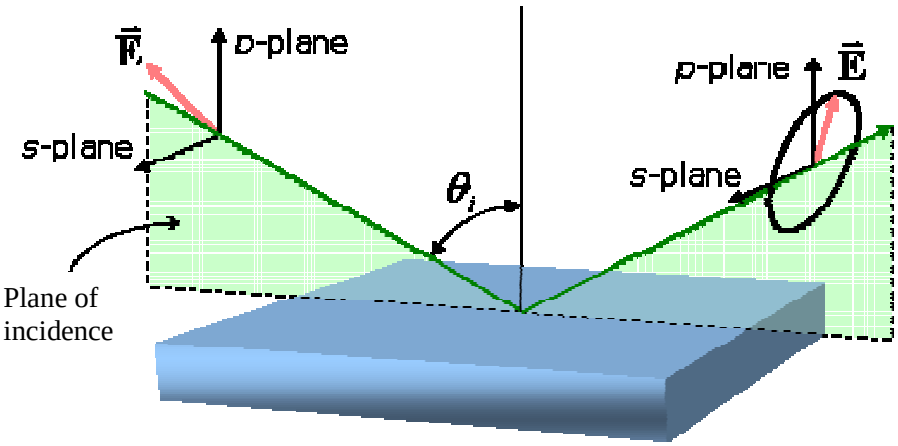

Figure 2.7 Plane of incidence and change in polarisation following reflection from a surface (reproduced from [18], with permission of the authors).

Comparison of the initial and final state of polarisation produces the fundamental ellipsometry equation:

$$\rho = \frac{r_p}{r_s} = \frac{\varepsilon_{rp}/\varepsilon_{ip}}{\varepsilon_{rs}/\varepsilon_{is}} = \tan\psi \exp(i\Delta) \qquad (2.1)$$

The complex reflection coefficient (ρ): the ratio of the amplitudes of the parallel and perpendicular parts of the reflectivity, r_p and r_s, is a complex number. This is usually split into two parameters: ψ, related to the amplitude ratio, and Δ, the phase difference, which are actually measured by the ellipsometer.

A similar equation can be written for a thin film on a substrate. For this more complex (but more useful) situation ψ and Δ depend on the wavelength of the light, the angle of incidence, the complex refractive indices, *n* and *k*, for the film and the substrate, and the film thickness[15]. The equation can be solved in terms of the thickness and refractive index of the intermediate layer. A model is constructed and used to calculate the predicted response from Fresnel's equations (which describe each material with thickness and optical constants). A sensible estimate of film properties is used as the starting point. The calculated values are then compared to the experimental data, and the unknown material properties are varied to improve the fit. Typically an estimator like the mean square error (MSE) is used to quantify the difference between curves. The unknown parameters are varied until the minimum MSE is reached. Care is needed

when selecting the starting thickness and MSE structural conditions to ensure that the true film thickness is found[17].

Spectroscopic ellipsometry provides amplitude and phase change information across the wavelength spectrum (samples in this project were measured for wavelengths from 300 to 700 nm). This allows a more extensive and precise determination of optical constants, and solves some of the correlation effects that can affect single wavelength ellipsometric measurements. However, the use of a range of wavelengths also complicates the results, as *n* and *k* vary with wavelength. The Cauchy approximations can be used to overcome these problems[15]: e.g. for refractive index:

$$n(\lambda) = A + \frac{B}{\lambda^2} + \frac{C}{\lambda^4} \qquad (2.2)$$

Where $n(\lambda)$ is the refractive index at wavelength λ, and *A*, *B* and *C* are constants (*A* is the refractive index at infinite wavelength).

More information about ellipsometry can be found in the references[14,15,17-21].

In this project, ellipsometry was used in a very simple way to determine the thickness of polymer brush and SAM layers. Two different ellipsometers were used: a single wavelength RAE ellipsometer (Gaertner Scientific 116B) and a spectroscopic (variable wavelength) phase-modulated ellipsometer (Jobin Yvon Uvisel). The layer thicknesses were obtained in slightly different ways (see p. 93 for details), but both rely on a model to convert ψ and Δ to layer thicknesses.

Brush thickness can also be measured directly by AFM: a scalpel blade was used to scratch the sample, removing a thin strip of brush from the substrate. The scratch was then imaged using tapping mode AFM. The software was used to flatten the image, and then measure the height difference between the bottom of the scratch and the undisturbed film (this measures the brush thickness and the initiator SAM together). At least ten measurements were averaged to give a value for the brush thickness. An example showing a single measurement is shown in Figure 2.8 below.

Both ellipsometry and AFM measurements can be subject to errors: for ellipsometry this can be caused by use of unsuitable parameters in the model; for AFM, the scratch

may also damage the underlying silicon, or not completely remove the polymer layer (leading to an overestimate or underestimate of brush thickness respectively). Comparison of the ellipsometric and AFM thicknesses for different PMMA and PS brushes revealed that the differences were relatively small (maximum difference 4.3 nm) – see Table 2.1. AFM tended to give a higher layer thickness than ellipsometry. The reasonable agreement between the two methods suggests that either could give a good estimate of brush thickness. It is much more time consuming to image a scratched sample by AFM, so for the rest of the work presented in this thesis, ellipsometry was used to measure brush thickness.

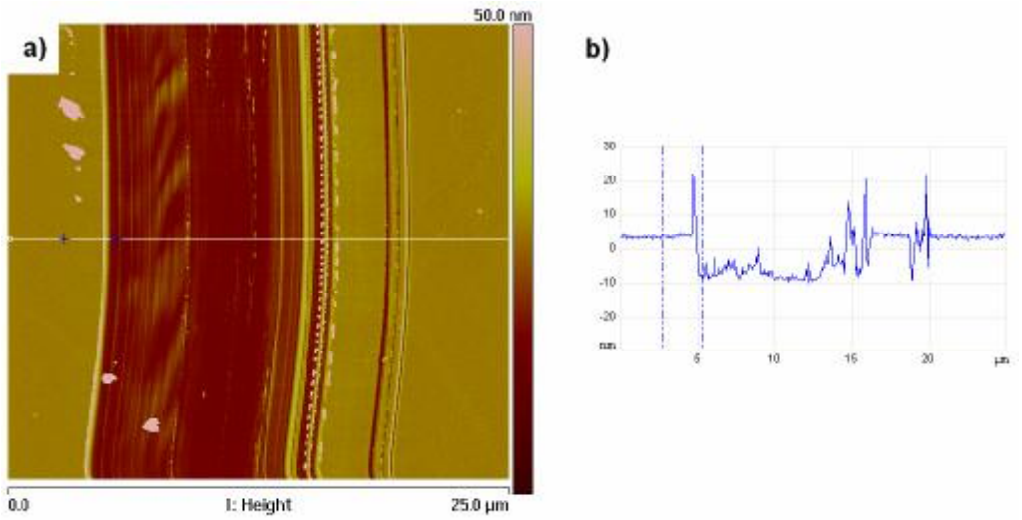

Figure 2.8 Tapping mode AFM image (25 x 25 µm) of a scratched PMMA brush (PMMA B in table below), showing an example of a section used to calculate brush thickness. Horizontal distance between marks 2.59 µm, vertical distance 11.89 nm.

Table 2.1 Comparison of polymer brush thicknesses measured by ellipsometry and AFM.

Sample Reference	Ellipsometric Brush Thickness/ nm[a]	AFM Brush Thickness/ nm[b]
PMMA A	7.5 ± 0.3	7.4 ± 0.6
PMMA B	11.9 ± 0.8	14.1 ± 0.7
PMMA C	2.6 ± 0.4	4.1 ±0.8
PS A	13.8 ± 0.3	17.0 ± 0.6
PS B	20.1 ± 0.8[c]	24.5 ± 1.3

[a]Ellipsometric thickness = total thickness – oxide thickness (measured separately), ± one standard deviation. Thicknesses reported here include the polymer brush layer and the initiator SAM layer. [b]AFM thickness determined from average of ten sections across a flattened AFM image ± one standard deviation. [c]PS B was measured using the spectroscopic ellipsometer, model parameters as p. 94, ± MSE.

2.4 X-ray Photoelectron Spectroscopy

X-ray photoelectron spectroscopy (XPS), also known as electron spectroscopy for chemical analysis (ESCA), is a relatively non-destructive technique which can measure and quantify the atoms present within approximately 10 nm of the surface of a sample, and give some information about their chemical environment. XPS is based on the photoelectric effect, first explained by Einstein in 1905. An x-ray photon of energy hν can interact with an atom, causing electronic excitation, and resulting in the ejection of a core (or valence) electron without energy loss (see Figure 2.9). The energy of the emitted electron is described by:

$$E_K = h\nu - E_B - \phi_{sp} \qquad (2.3)$$

where E_K is the kinetic energy of the emitted electron, E_B is the electron binding energy (which is characteristic of a particular orbital and atom), and ϕ_{sp} is the work function of the spectrometer.

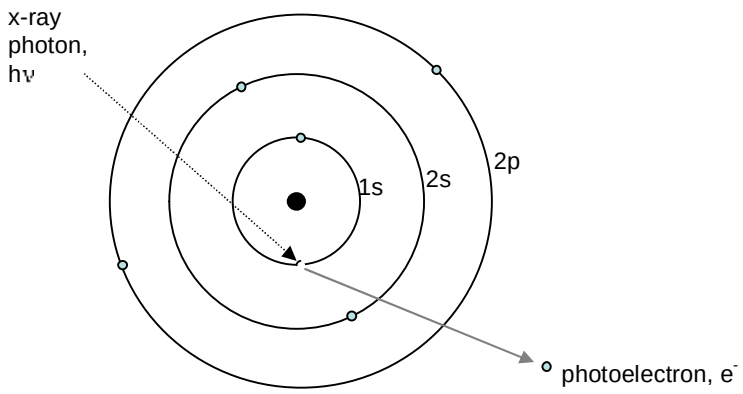

Figure 2.9 X-ray induced photoemission of an oxygen 1s electron[22].

XPS analysis was developed by Kai Siegbahn in the 1950s, and became commercially available in the 1970s. The sample is held under high vacuum and irradiated with x-rays. The kinetic energy of the emitted electrons is measured and used to calculate the binding energy.

In a modern XPS, an aluminium or magnesium anode is used to generate monochromatic x-rays, which are focussed onto the sample surface. These produce x-rays of sufficient energy to excite photoemission from at least one core level for any atom (except hydrogen). The ejected photoelectrons are collected and their energy distribution is measured using an electrostatic hemispherical analyser. Emission of electrons from the surface of an insulator leads to the development of a positive charge, which over time decreases the kinetic energy of the emitted electrons (resulting in an apparent increase in binding energy). This is corrected by the use of an electron flood gun (a high current, low energy electron source).

The spectrum is produced as a plot of electron intensity against binding energy. X-ray irradiation causes the emission of electrons by several different mechanisms, which all contribute to the observed spectrum. Electrons emitted without undergoing energy loss produce the main photoelectric peaks. The binding energy of an electron depends on the type of atom and orbital (electrons in orbitals closer to the nucleus will be more tightly bound) and the bonding of the atom, which alters its electronic structure. Overlaps between elemental peaks are rare, so measurement of the binding energy

allows unambiguous identification of the elements present. Subtraction of the background allows measurement of peak areas, which can used to calculate the abundances of different atoms in the sample. Different chemical environments cause small changes (typically < 10 eV) in the binding energy of the core electrons. These 'chemical shifts' can be measured in high resolution spectra, and then curve-fitted to give information about the surface chemistry of the material.

X-rays penetrate several microns into the sample, and stimulate electron emission throughout the sample. The probability of an electron escaping the sample without undergoing an energy loss event decreases with depth, which explains the surface sensitivity of XPS. Electrons emitted from the surface zone which have lost some energy due to inelastic interactions produce a continuous background observed in all spectra. The background intensity increases with increasing binding energy (decreasing kinetic energy). Other spectral features include Auger series, valence band features, shake-up and shake-off satellites and plasmon loss peaks. Shake-up satellites are commonly found in systems containing aromatic structures. Irradiation of an atom can promote a valence electron from an occupied energy level to a higher unoccupied level (e.g. a π to π^* transition), reducing the energy of the emitted photoelectrons, and producing a peak at higher binding energy than the main C 1s peak. This was observed in the spectra of polystyrene brushes.

The discussion above is very simplified: subtraction of the background spectrum and referencing of the binding energy scale are not trivial, and can affect the results. Surface roughness and inhomogeneity of the sample with depth also affect the measurements in a complex way. For a more detailed description of XPS, the reader is directed towards the references[22-24], in particular for more complete descriptions of background subtraction, curve fitting, and other spectral features.

2.5 Scanning Electron Microscopy

Scanning Electron Microscopy can be used to produce high resolution images of conductive samples, allowing visualisation of features as small as ~ 2 nm. The images produced have excellent depth of focus and are simple to interpret because they resemble conventional photographs. A beam of moderate energy electrons (usually less than 50 keV) is focussed to produce a narrow spot, 2 – 10 nm diameter, which is rastered across the surface. The incident primary electrons are inelastically scattered through a teardrop-shaped interaction volume, resulting in the emission of secondary electrons, backscattered electrons, Auger electrons, x-rays, and light (cathodoluminescence) and also induce a current through the sample (see Figure 2.10 a). Each of these is produced by interactions at different depths within the sample, and can be used to obtain different information about its topography and physical and chemical properties. Many SEMs contain several detectors to allow more information about the sample to be obtained. This is discussed in more detail in the references[15,25,26]. The images presented in Chapter 4 are secondary electron images, so the other signals are not discussed here.

In a typical SEM, electrons are thermionically emitted from a tungsten or lanthanum hexaboride filament (or a field emission gun), drawn to an anode and focussed into a narrow beam by two sets of condenser lenses. Scanning coils are used to raster the electron beam over the surface. The emitted electrons and x-rays are collected and analysed by suitable detectors. The whole system is held under vacuum to allow

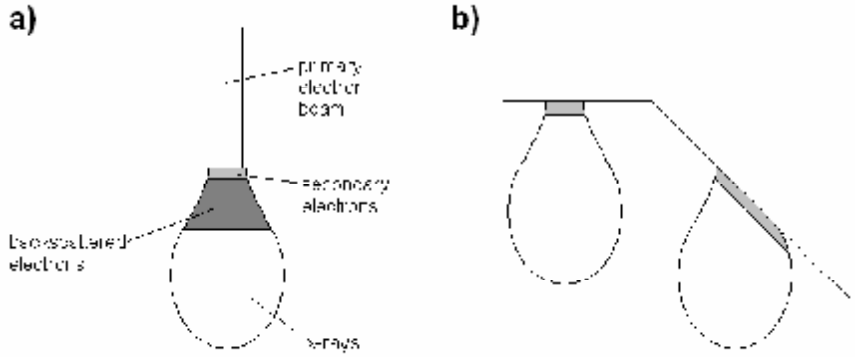

Figure 2.10 a) The electron interaction volume and regions from which secondary electrons, backscattered electrons and x-rays can be detected b) effect of surface topography on electron emission

transmission of electrons both to and from the sample. Secondary electrons are usually detected by an Everhart-Thornley detector: a scintillator/photomultiplier combination. The scintillator is surrounded by a metal grid which is biased to a potential of a few hundred volts. This prevents the scintillator interfering with the primary electron beam, and attracts secondary electrons, collecting even those that were not originally moving towards the detector (for flat samples, almost all the secondary electrons are captured).

Secondary electrons are produced by inelastic collisions between the energetic primary electrons and valence/conduction band electrons in the sample. Only a small amount of energy is transferred to the secondary electrons, so only those produced within the top few ångstroms can escape from the surface of the sample (although secondary electrons are produced throughout the interaction volume). This also explains why sloping surfaces and edges appear brighter in SEM images: the portion of the interaction volume at the surface is larger when the sample is tilted (see Figure 2.10 b) below). Secondary electron images have excellent depth of focus, and clearly show sample topography as they resemble conventional light images. When a sample is diffusely illuminated light arrives from all directions, so whatever the orientation of the surface some light is reflected towards the eye. In SEM, the primary electrons are incident from above, but they are all attracted towards the detector. Although the direction is reversed, the appearance of the images is very similar (see Figure 2.11).

Irradiation of an insulating sample with electrons leads to the build-up of negative charge, which repels the incoming electrons and results in image distortion (there are equivalent problems with positive charge in XPS and SIMS). This is not a problem if

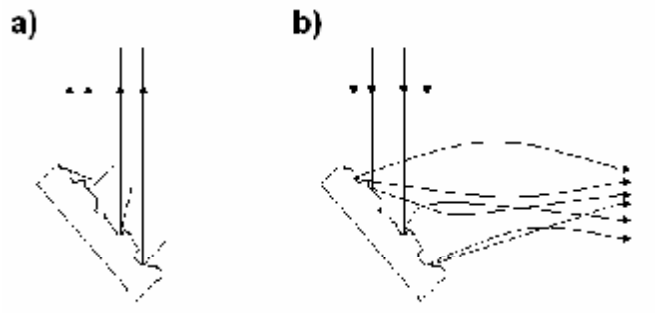

Figure 2.11 a) An object viewed from above with diffuse illumination. b) Equivalent situation for secondary electron imaging in SEM.

the sample surface is conductive, and the sample is earthed. Charge build-up can be prevented by sputter-coating insulating samples with a thin layer of gold (or carbon). SEM was used to image PDMS stamps and patterned polymer brushes. PDMS stamps were coated with gold before imaging; patterned polymer brushes on silicon were found to be sufficiently conductive to avoid charging without surface treatment.

2.6 Secondary Ion Mass Spectrometry

Secondary Ion Mass Spectrometry can be used to identify and image the distribution of particular species (ions) on a sample. The sample is bombarded by a beam of high energy ions (or neutral atoms). This causes a complex cascade of fragmentation and ionisation resulting in the emission of neutral species, and a much smaller amount of positive and negative secondary ions. These are extracted and analysed using a mass spectrometer. Different materials produce different characteristic ions which can be used to identify the composition of the surface. It is extremely surface selective: most of the signal comes from the top nanometre or so of the sample, and it is very sensitive: species present at parts per million or femtomolar concentration on the surface can be detected, with lateral resolution down to 60 nm.

Initially SIMS was used for depth profiling: the destructive primary ion beam was used to analyse the elemental composition of materials as a function of depth. This dynamic SIMS mode is used extensively throughout the semiconductor industry. Static SIMS, allowing true surface analysis, was first developed by Benninghoven in the 1960s[27]. A very low primary ion current is used to allow spectral data to be collected in a timescale that is short compared to the lifetime of the surface layer. Static conditions can be defined so that successive measurements of the same area of the sample produce the same spectrum. To obtain this, the total ion dose must be limited. Calculations based on the area affected by a simple ion impact suggest that all the surface atoms of a sample will be affected by an ion dose of around 10^{13} ions/cm^2 [24]. For all the SIMS data presented in this thesis, the total ion dose for each measurement was limited to 10^{12} ions/cm^2, and each measurement was performed on a different area of the sample.

All SIMS instruments contain a source of primary ions (or atoms), a mass spectrometer and an electron source (for charge compensation), all enclosed in a vacuum chamber. There are many possible variations within this. Most modern SIMS instruments use a liquid metal ion source to produce the primary ions, commonly Ga^+ (although in this work a field emission bismuth cluster ion source was used), and a Time of Flight (ToF) mass spectrometer to collect and analyse the secondary ions. In a ToF mass spectrometer, the secondary ions are accelerated to 3 – 5 keV over a very short distance, so they all have virtually the same kinetic energy (E_K). As $E_K = \frac{1}{2}mv^2$, ions of different mass have different velocities, so the time of flight through a field-free drift tube, and arrival at the detector depends on the mass of the ion, allowing the spectrum to be produced. ToF mass spectrometry allows the whole spectrum to be acquired in parallel, minimising the ion dose needed. Ion bombardment and the emission of secondary electrons cause the sample to become positively charged. Over time, this would suppress the emission of negative ions, and increase the energy of the emitted positive ions. To prevent this, it is necessary to provide a source of electrons to control the surface potential. However, electron beams can also produce secondary ions, distorting the measurement. For ToF SIMS, a very short pulse of primary ions is directed at the sample, and the extraction voltage is raised to allow capture of the secondary ions. During the data analysis period, the extraction voltage is dropped to zero, and a long pulse of low energy electrons is directed at the sample to correct the

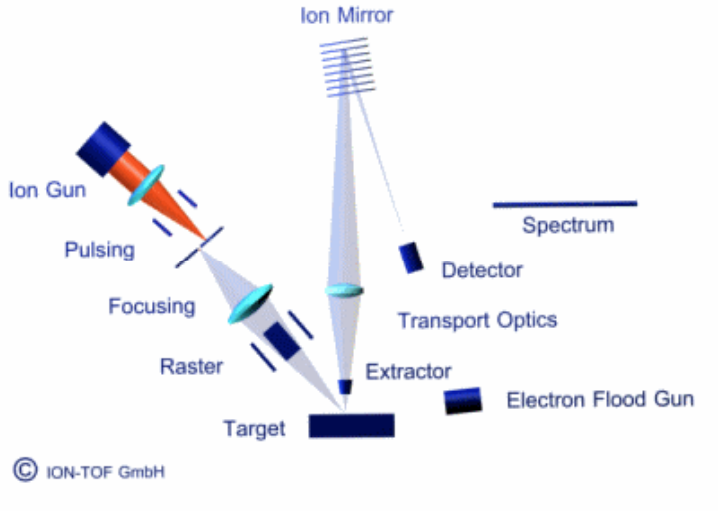

Figure 2.12 Schematic diagram of a secondary ion mass spectrometer (reproduced from[28], image courtesy of Ion-ToF).

charge. There is then a pause before the extraction voltage is raised, and the next pulse of ions sent, to avoid the extraction of any ions produced by electron impact. A diagram of a ToF SIMS is shown in Figure 2.12. The relevant literature contains a more complete description of SIMS instrumentation[24,28-30].

SIMS can be used to map the distribution of particular ions over the sample and build up images. The primary ion beam is focussed to produce a small spot at the surface (as small as ~ 60 nm), and the beam is rastered over the sample. ToF MS allows the entire mass spectrum to be measured at each pixel, allowing retrospective analysis after acquiring the complete positive and negative ion spectra for each pixel.

The formation, fragmentation and ionisation of secondary particles is complicated and not fully understood. There are two main processes: sputtering and ionisation. Sputtering is the process by which secondary particles are emitted from the surface as a result of high energy primary particle impact. Various models have been used to explain the key mechanisms. The linear cascade model (developed by Sigmund) is based on elastic collisions between point particles. The incident particle transfers its energy to the target atoms, initiating a cascade of collisions between atoms within about 3 nm of the surface. Some of these collisions return to the surface and cause the emission of sputtered particles. This can occur up to 10 nm away from the initial impact site.

Sputtering produces mainly neutral species (~ 99 %), with a small amount of positive and negative ions. Ionisation can occur by several different processes, including direct emission of preformed cations and anions, ionisation of neutral clusters by attachment of small ions such as hydrogen, halogens or metal ions, or ionised species can undergo unimolecular fragmentation before they reach the mass spectrometer. The probability of ionisation varies by several orders of magnitude for different ions, both across the periodic table and depending on the chemical environment of the surface. This makes quantification of SIMS very challenging.

The complex nature of SIMS spectra and their high sensitivity to surface contamination make it difficult to assign all the peaks present. A common approach is to ‘fingerprint’ the material by comparing the SIMS spectrum to a reference spectrum. SIMS of

polymers results in well-defined fragmentation patterns (frequently from cleavage of the polymer backbone or loss of pendant groups). These were identified using the Handbook of SIMS[31]. For polymer films and polymer brushes, a selection of characteristic ions was chosen, and used to identify PS and PMMA in all samples. For chemicals where there was no reference spectrum (e.g. most of the SAMs), chemical intuition was used to identify likely fragment ions. The SIMS data presented in this thesis are ion images. For each sample, a list of candidate ions was identified, and each ion image was examined. A selection of these ions, mainly those that clearly showed the surface pattern and changes in chemistry, are presented in the following chapters[24,29,30].

2.7 References

(1) Husseman, M.; Malmström, E. E.; McNamara, M.; Mate, M.; Mecerreyes, D.; Benoit, D. G.; Hedrick, J. L.; Mansky, P.; Huang, E.; Russell, T. P.; Hawker, C. J. *Macromolecules* **1999**, *32*, 1424-1431.

(2) Kim, J.-B.; Huang, W.; Bruening, M. L.; Baker, G. L. *Macromolecules* **2002**, *35*, 5410-5416.

(3) Kim, J.-B.; Bruening, M. L.; Baker, G. L. *Journal of the American Chemical Society* **2000**, *122*, 7616-7617.

(4) Kong, X.; Kawai, T.; Abe, J.; Iyoda, T. *Macromolecules* **2001**, *34*, 1837-1844.

(5) Prucker, O.; Rühe, J. *Macromolecules* **1998**, *31*, 592-601.

(6) Wang, Y.-P.; Pei, X.-W.; He, X.-Y.; Yuan, K. *European Polymer Journal* **2005**, *41*, 1326-1332.

(7) Pyun, J.; Jia, S.; Kowalewski, T.; Patterson, G. D.; Matyjaszewski, K. *Macromolecules* **2003**, *36*, 5094-5104.

(8) Pyun, J.; Jia, S.; Kowalewski, T.; Patterson, G. D.; Matyjaszewski, K. *Macromolecules* **2003**, *36*, 6952.

(9) *MultiMode SPM Instruction Manual NanoScope Software Version 5*; Veeco Instruments Inc., 2004.

(10) http://www.veeco.com/pdfs/library/SPM_Guide_0829_05_166.pdf.

(11) www.chembio.uoguelph.ca/educmat/chm729/afm/general.htm.

(12) Vasilev, C., AFM Training - talk (personal communication).

(13) *Scanning Probe Microscopy Training Notebook*; Veeco Instruments Inc., 2003.

(14) http://users.aber.ac.uk/tej/ellipso.html; Jenkins, T., Ed.; University of Wales, Aberystwth.

(15) Ohring, M. *Materials Science of Thin Films: Deposition and Structure*; Academic Press: San Diego, 2002.

(16) Smith, F. G.; King, T. A.; Wilkins, D. *Optics and Photonics: An Introduction*; Second ed.; John Wiley and Sons, Ltd: Chichester, UK, 2007.

(17) www.jawoollam.com/tutorial_1.html.

(18) http://www.uta.edu/optics/research/ellipsometry/ellipsometry.htm.

(19) Sharp, J. S. Swelling and Adsorption Phenomena in Thin Polymer Films and at Interfaces, PhD thesis, University of Sheffield, 2001.

(20) Jones, R. A. L.; Richards, R. W. *Polymers at Surfaces and Interfaces*; Cambridge University Press: Cambridge, 1999.

(21) http://ecee.colorado.edu/~bart/book/ellipsom.htm; Zeghbroeck, B. V., Ed., 1997.

(22) Ratner, B.; Castner, D. In *Surface Analysis - The Principal Techniques*; Vickerman, J. C., Ed.; John Wiley and Sons: Chichester, 1997.

(23) http://www.casaxps.com/help_manual/manual_updates/xps_spectra.pdf.

(24) Briggs, D. *Surface Analysis of Polymers by XPS and Static SIMS*; First ed.; Cambridge University Press: Cambridge, 1998.

(25) Goodhew, P. J.; Humphreys, J.; Beanland, R. *Electron Microscopy and Analysis*; Third ed.; Taylor and Francis: London, 2001.

(26) http://mse.iastate.edu/microscopy/home.html Iowa State University, Materials Science and Engineering Department.

(27) Benninghoven, A. *Physica Status Solidi* **1969**, *34*, K169-K171.

(28) http://www.ion-tof.com/technique-timeofflight-IONTOF-TOF-SIMS-TIME-OF-FLIGHT-SURFACE-ANALYSIS.htm.

(29) Vickerman, J. C.; Swift, A. In *Surface Analysis - The Principal Techniques*; Vickerman, J. C., Ed.; John Wiley and Sons: Chichester, 1997.
(30) http://eng.technoinfo.ru/catalog/2.html.
(31) Briggs, D.; Brown, A.; Vickerman, J. C. *Handbook of Secondary Ion Mass Spectrometry (SIMS)*; John Wiley and Sons: Chichester, 1989.

Chapter 3

Synthesis of Polymer Brushes

3.1 Introduction

The aims of this project were to synthesise a binary patterned PS/PMMA brush, and to investigate the phase separation of a polymer blend on the chemically-patterned surface. The first step towards this goal was the reproducible synthesis of smooth PMMA and PS brushes of controlled thickness.

It was decided to focus on brush growth by surface-initiated ATRP from silicon substrates. ATRP is a controlled radical polymerisation that has been used extensively to synthesise polymer brushes. It can be used to polymerise a wide range of functional monomers with control over molecular weight and low polydispersity, and also allows the synthesis of block copolymers. ATRP is particularly popular for brush growth because it is relatively straightforward to synthesise silane or thiol derivatised ATRP initiators that can form SAMs on silicon or gold substrates respectively[1]. It was decided to use silicon as the substrate as it is used commercially (especially in the semiconductor/computer industry), and has analogous surface chemistry to glass, silica particles and plasma-treated polymers. In addition, alkyltrichlorosilane SAMs form a robust, thermally stable layer (in contrast to thiol SAMs on gold, which undergo degradation at relatively low temperatures[2], or on exposure to air[3]). However, the self-assembly of alkyltrichlorosilanes on silicon is more complicated than the analogous formation of SAMs from alkanethiols on gold substrates, and in particular is very sensitive to the amount of water present in the reaction environment. This will be discussed in more detail in Chapter 4.

11-(2-bromo-2-methyl)propionyloxyundecyltrichlorosilane (BMPUS) was synthesised according to the literature method[4], and characterised by NMR, mass spectrometry and elemental analysis. This was then allowed to self-assemble on oxidised silicon, producing a surface-bound ATRP initiator which was then used to grow PMMA and PS

brushes. The chemical differences between the two monomers meant that different reaction conditions were needed to polymerise them. Several different methods were tested for each monomer, and the resulting polymer brushes were analysed by ellipsometry, AFM and XPS. The results are presented and discussed below.

3.2 Materials

Methyl methacrylate (Aldrich, 99 %) and styrene (Aldrich, ≥ 99 %) were dried over calcium hydride, then vacuum distilled prior to use. Distilled monomers were stored in sealed flasks in the freezer, and used within 24 hours (styrene), or 5 days (MMA).

Copper(I) chloride and copper(I) bromide were purified by stirring with at least three portions of glacial acetic acid under nitrogen. The acetic acid was decanted off the solid residue, which was then washed with petroleum ether and ethanol, followed by thorough drying in a vacuum oven at room temperature[4,5]. They could be stored under nitrogen for 3 – 4 months before cumulative exposure to atmospheric oxygen caused significant oxidation, detectable by a colour change from white/grey to green.

2,2'-Bipyridine (Aldrich, ≥ 99 %) was recrystallised from hot *n*-hexane, and filtered when hot to remove brown solid impurities, yielding white, needle-shaped crystals.
^{1}H NMR: ($CDCl_3$, 250 MHz), δ: 7.23 (2H, t, J = 8 Hz), 7.73 (2H, t of d), 8.32 (2H, d, J = 8 Hz), 8.61 (2H, s). This was a good match to the reference spectrum[6].

Anhydrous THF, toluene and *n*-hexane were obtained from a Solvent Purification System (Innovative Technology Inc., SPS-400-6 and SPS-200-6). Typical water contents were 23-27 ppm for THF, 16 ppm for toluene, and 8 ppm for *n*-hexane.

Single crystal silicon wafers were obtained from Compart Technology Ltd (100 mm diameter, 525 μm thick, boron-doped, <100> face polished).

Triethylamine (Aldrich, 99 %) was filtered through a 0.45 μm PTFE filter (Whatman or Acrodisc) immediately before use.

All other reagents were obtained from Aldrich and used as received.

3.3 Experimental Methods

Glass and plastic syringes were used extensively to transfer liquid reagents between containers. Before use, they were purged three times with nitrogen gas, to displace the residual air in the syringe needle.

3.3.1 Synthesis of 10-undecen-1-yl 2-bromo-2-methylpropionate

10-Undecen-1-ol (8.52 g, 50 mmol) and dry THF (50 ml) were added to a dry two-necked flask equipped with a stirrer bar, nitrogen inlet/outlet, and a suba seal. The mixture was left stirring for 10 minutes under flowing nitrogen, then pyridine (4.2 ml, 50 mmol) was added by syringe. The flask was cooled in an ice bath for 5 minutes, then 2-bromoisobutryl bromide (6.2 ml, 50 mmol) was added dropwise. After 30 minutes, the ice bath was removed, and the yellowish mixture was left to react at room temperature overnight.

This yielded a cream solid suspended in a brownish liquid, which was diluted with 100 ml *n*-hexane, then washed with 100 ml of 2 mol dm^{-3} hydrochloric acid and twice with water. The brownish liquid was dried with sodium sulphate and the solvent was removed under reduced pressure to give a pale brown oil. The crude product was purified by flash column chromatography (silica gel, 25:1 hexane: ethyl acetate), to give 10-undecen-1-yl 2-bromo-2-methylpropionate (13.62 g, 43 mmol) as a pale yellow oil in 85 % yield[4].

^{1}H NMR ($CDCl_3$, 250 MHz), δ: 1.28-1.41 (12H, br, m), 1.61-1.72 (2H, m), 1.92 (6H, s), 1.98-2.07 (2H, q), 4.15 (2H, t, J = 7 Hz), 4.89-5.02 (2H, br, m), 5.72-5.89 (1H, br, m).

^{13}C NMR ($CDCl_3$, 250 MHz), δ: 25.78, 28.34, 28.92, 29.09, 29.15, 29.38, 29.42, 30.80 (CH/CH_3), 33.81, 66.18, 114.15, 139.21 (CH/CH_3). All signals are CH_2/C unless otherwise stated.

3.3.2 Synthesis of 11-(2-bromo-2-methyl)propionyloxyundecyl trichlorosilane

10-Undecen-1-yl 2-bromo-2-methylpropionate (13.62 g, 43 mmol) was added to a dry two-necked flask equipped with a magnetic stirrer, nitrogen inlet/outlet and a suba seal. This was left to stir for 20 minutes under flowing nitrogen, then trichlorosilane (43.4 ml, 0.43 mol) was added by syringe and the flask was cooled in an ice bath for at least 10 minutes. Platinum(0)-1,3-divinyl-1,1,3,3-tetramethyldisiloxane complex solution 0.1 mol dm^{-3} in xylenes (0.05 ml, equivalent to 5 mmol Pt) ('Pt', also known as Karstedt's catalyst) was added dropwise over 10 minutes. The mixture was left to slowly warm to room temperature, and then to react overnight, to ensure that the reaction was complete[4].

The crude reaction mixture was purified by high vacuum distillation using a short path distillation apparatus. Initially, the excess trichlorosilane was removed under high vacuum at room temperature over several hours (and collected in a second flask). The product was then distilled: it was necessary to use a yellow flame (temperature > 220 ºC) to achieve distillation, even at 3 x 10^{-5} Torr pressure. 11-(2-Bromo-2-methyl)propionyloxyundecyltrichlorosilane was collected as a yellow oil.

^{1}H NMR ($CDCl_3$, 250 MHz), δ: 1.18-1.43 (16H, br, m), 1.54-1.74 (4H, br, m), 1.93 (6H, s), 4.17 (2H, t, J = 7 Hz).

^{13}C NMR ($CDCl_3$, 250 MHz), δ: 22.25, 24.31, 25.77, 28.34, 28.99, 29.14, 29.29, 29.44, 30.79 (CH/CH_3), 31.80, 55.98 (very weak), 66.14. All signals are CH_2/C unless otherwise stated.

^{29}Si NMR ($CDCl_3$, 500 MHz), δ: 12.95.

Mass Spectrum: The mass spectrum of this compound is complicated, with groups of peaks due to the presence of different isotopes of bromine, chlorine, silicon (and carbon) within the initiator. There is a group of peaks from m/z 452 – 462, which correspond to the mass ion (m/z 452 fits $C_{15}H_{28}O_2Si^{35}Cl_3{}^{79}Br$, m/z 460 fits $C_{15}H_{28}O_2Si^{37}Cl_3{}^{81}Br$). The next intense peaks occur at m/z 286 – 291, which could correspond to the loss of the α-bromoester group ($C_4H_6O_2Br$ – m/z 165 or 167 depending on bromine isotope). Below this, there are many peaks down to m/z 55.

Elemental Analysis:

Element	% (by mass) predicted	% (by mass) measured
C	39.61	41.33
H	6.22	6.86
Br	17.57	15.09
Cl	23.39	20.23

3.3.3 Preparation of Initiator SAM on Silicon Wafers

Silicon wafers cut into 1 cm^2 pieces were cleaned and rendered hydrophilic by heating to 80 °C for 10 minutes in 100 vol hydrogen peroxide (50 ml), 37 wt % ammonia solution (50 ml) and deionised water (250 ml) (RCA clean). The cleaned wafers were rinsed with copious quantities of distilled water, dried with nitrogen, then heated to 120 °C under vacuum for two hours to remove any remaining traces of water.

The cleaned, dried wafers were added to a PTFE dish with a tight-fitting lid, polished face up, then covered with BMPUS (22.5 μl) in dry toluene (15 ml), and triethylamine (1.5 ml), and left overnight. The wafers were then removed from the initiator solution and washed twice with toluene, once with acetone and finally with ethanol, for at least 10 minutes in each solvent, before being dried and stored[5].

3.3.4 Brush Growth Reactions: General Points

ATRP is tolerant of a wide range of functional groups present in the monomer, solvent and initiator[7], but it is rather sensitive to the presence of oxygen[8]. To obtain a well

controlled, reproducible polymerisation, thorough deoxygenation of all reagents was necessary. This was done by bubbling nitrogen gas (from a needle inlet) through the reaction liquid, for at least 10 minutes to displace dissolved oxygen.

Brush growth reactions were performed in custom-made 4- or 8-necked flasks that allowed up to eight initiator-coated wafers to be reacted at any one time with all the wafers in identical chemical environments[5]. For all reactions, the 8-necked flask was set up in the same way: initiator-coated wafers were put into stainless steel wire holders, with the shiny side facing downwards. The wire was then pushed through a suba seal, and the whole assembly was put into one neck of the clean dry flask. This was repeated, leaving one neck equipped with a plain suba seal (see Figure 3.1 below). The whole apparatus was then purged with flowing nitrogen for at least 30 minutes before the premixed reagents were added by syringe. Once all reagents had been added, the nitrogen flow was increased, and the blank suba seal was replaced with one with a wafer holder and initiator-coated wafer. The same procedure was used to remove wafers from the flask after the desired reaction time, to allow immediate rinsing of the reaction mixture off the wafers. As long as the nitrogen flow was high, this did not result in

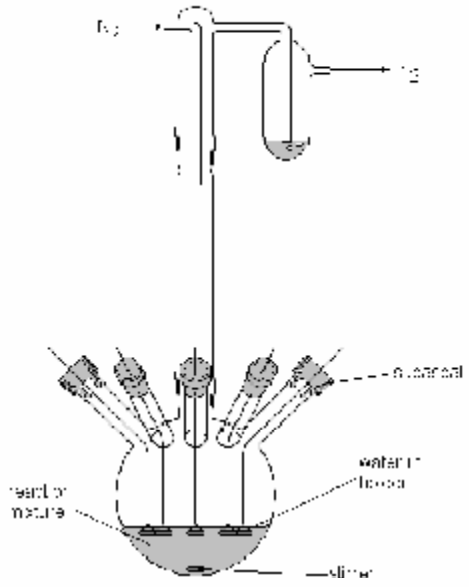

Figure 3.1 8-necked reaction vessel used to perform multiple brush growth experiments under identical conditions[5]. Reproduced from Topham et. al, Polymer International, ***2006****, 55, 808-815[5],* *by permission of John Wiley & Sons, Inc. http://www3.interscience.wiley.com/journal/117946201/grouphome/home.html*

noticeable oxidation of the polymerisation solution (detectable as a colour change, e.g. for PMMA brushes, the dark brown reaction mixture changed colour to turquoise on exposure to air).

Alternatively, the reaction could be performed in carousel tubes (Radleys Scientific): an initiator-coated wafer was placed shiny face down in each carousel tube. Tubes were sealed with rubber septa and purged with nitrogen for at least 10 minutes. Reagents were degassed and mixed in a round-bottomed flask to produce a homogeneous polymerisation solution. Then 5 – 6 ml of this solution was added to each tube by syringe. Quantities of reagents were adjusted according to the number (and size) of substrates to be reacted. Wafers were left to react without stirring for the desired reaction time.

3.3.5 Synthesis of Poly(methyl methacrylate) Brushes

Methyl methacrylate (25.03 g, 0.25 mol), 20 ml methanol and 5 ml water were added to a round-bottomed flask equipped with a suba seal and a magnetic stirrer. The mixture was degassed for 15 minutes, with stirring. 2,2'-Bipyridine (0.98 g, 6.25 mmol), copper(II) bromide (0.028 g, 0.125 mmol), and copper(I) chloride (0.25 g, 2.5 mmol) were added, and degassing continued for 10 minutes. The homogeneous, dark brown solution was then transferred to the 8-necked flask by syringe. The wafers were immersed in the reaction mixture, and left to react under a positive pressure of nitrogen at room temperature (approximately 20 ºC), for up to 9 hours[9]. After the desired reaction time, the wafers were removed from the flask and rinsed twice in 4: 1 methanol: water, then once in dichloromethane.

3.3.6 Synthesis of Polystyrene Brushes: Anisole, PMDETA

Styrene (20.907 g, 0.20 mol) and 27 ml anisole were added to a dry round-bottomed flask equipped with a magnetic stirrer and degassed for 15 minutes, with stirring. The flask was then opened to allow addition of PMDETA (0.73 g, 4.2 mmol), $CuBr_2$ (0.045 g, 0.2 mmol) and CuBr (0.29 g, 2.0 mmol). The flask was sealed, and degassing continued, as the mixture was heated up to 90 ºC in an oil bath, and until the solids had dissolved giving a homogeneous solution. The pale green solution was then transferred

to the nitrogen-filled 8-necked flask by syringe. The wafers were immersed in the reaction mixture, and left to react under a positive pressure of nitrogen at 90 ºC[10,11]. After the desired reaction time, the wafers were removed from the flask, and rinsed in portions of toluene, distilled water and finally acetone, before being dried and stored.

3.3.7 Synthesis of Polystyrene Brushes: Cyclohexanone, PMDETA

Styrene (20.90 g, 0.20 mol) and cyclohexanone (28 ml) were added to a dry round-bottomed flask equipped with a magnetic stirrer, and degassed for 10 minutes. PMDETA (0.73 g, 4.2 mmol) was added, and degassing continued for a further 10 minutes. The 8-necked flask was set up with initiator-coated wafers, and purged with flowing nitrogen for 10 minutes, before CuBr (0.29 g, 2.0 mmol) or CuCl (0.199 g, 2.0 mmol) and $CuBr_2$ (0.045 g, 0.20 mmol) were added. The flask was then left under flowing nitrogen. Styrene, cyclohexanone and PMDETA were transferred into the 8-necked flask by syringe. The pale turquoise-coloured reaction mixture was heated to 90 ºC in an oil bath, then the reaction was started by immersing the initiator-coated wafers[12]. After the desired reaction time, the wafers were removed from the flask and sequentially rinsed in portions of cyclohexanone, acetone and dichloromethane.

3.3.8 Synthesis of Polystyrene Brushes: Bulk, dnNbpy

Styrene (22.725 g, 0.218 mol) and $CuBr_2(dnNbpy)_2$ (0.1135 g, 0.10 mmol) were added to a dry round-bottomed flask equipped with a magnetic stirrer and degassed, with stirring, until a pale purple/maroon solution formed (about 10 minutes). The flask was opened and dnNbpy (1.81 g, 4.43 mmol) and CuBr (0.4875 g, 2.18 mmol) were added and degassing continued until all the solids had dissolved (~ 15 minutes) leaving a brown solution. The reaction mixture was transferred into the 8-necked flask by syringe, and heated to 100 ºC[4]. Polymerisation was started by immersing the initiator-coated wafers into the reaction mixture. Wafers were reacted for the desired length of time, then withdrawn from the reaction flask, and immediately rinsed twice with toluene, then with acetone, water, methanol or ethanol and finally with THF.

3.3.9 Synthesis of Copper (II) bromide bis-(4,4'-di-n-nonyl-2,2'-bipyridine)

$CuBr_2$ (0.25 g, 1.1 mmol) and dnNbpy (0.92 g, 2.3 mmol) were added to a round bottomed flask, along with 10 ml THF and 10 ml acetonitrile. The resulting green solution was allowed to stir under nitrogen for 90 minutes. The flask was attached to a high vacuum line, and the solution degassed by two freeze – vacuum – thaw cycles. The solvents were then removed by vacuum distillation (trap to trap distillation), and the solids left to dry under high vacuum overnight. Bright green $CuBr_2(dnNbpy)_2$ was obtained in 45 % yield, and used without further purification[4].

3.3.10 Dehalogenation of Polymer Brushes

Polymer brush-coated wafers were placed shiny face down in carousel tubes. Tubes were sealed with rubber septa, covered with silver foil and purged with nitrogen for at least 10 minutes. In a separate flask a saturated solution of sodium azide in *N,N*-dimethylformamide (DMF) was made up and 5 – 6 ml of this solution was added to each carousel tube by syringe. Wafers were left to react at 50 ºC for at least 48 hours. Wafers were then rinsed with DMF, sonicated in water for 15 minutes and rinsed with methanol and THF.

3.4 Characterisation

3.4.1 Ellipsometry

Ellipsometry measurements were performed with a Gaertner Scientific 116B ellipsometer with a 633 nm He/Ne laser set at an angle of incidence of 70°. The resulting values were fitted using a single layer model with the refractive index set to 1.5 for PMMA brushes and 1.59 for PS on a silicon substrate of $n = 3.875$, $k = 0.018$. The silicon oxide, initiator SAM and polymer layer were all measured together. The thickness of the oxide layer and SAM were measured on separate reference wafers, and then subtracted from the other measurements to give the thickness of the polymer brush layer. Measurements were made at five randomly chosen spots on the sample surface,

to allow calculation of the mean thickness and standard deviation. All values of brush thickness given in this report have been corrected for the thickness of the SAM and oxide layer (which was 33 – 40 Å, depending on the batch of wafers used).

3.4.2 Spectroscopic Ellipsometry

Measurements were performed using a Jobin Yvon Uvisel Spectroscopic phase modulated ellipsometer. Measurements were performed in two different configurations, with an angle of incidence of 70º. A measurement was taken every 10 nm over a range of wavelengths from 300 – 700 nm. Each spot was integrated for 1000 ms.

WVase software was then used to model the brushes, and convert the raw ellipsometry data into a value for the layer thickness. A 3-layer model was used:

Layer	**Layer Name**	**Thickness**
Substrate	SI-ASP	1 mm
Oxide	SIO2	2 nm
Initiator SAM and polymer brush	CAUCHY	Fit Refractive index (An): 1.5 for PMMA and SAMs 1.59 for PS

The model gives a value for the layer thickness, and its mean square error (MSE). All values of brush thickness given in this thesis have been corrected for the thickness of the SAM and oxide layer.

3.4.3 Atomic Force Microscopy

Tapping mode and LFM AFM images were acquired using a Multimode AFM with an Extended Nanoscope 3A controller and Nanoscope V5.12r4 software. The images presented in this thesis were produced using Nanoscope V6.11r1 software. Tapping mode images were produced using single crystal silicon cantilevers obtained from Olympus (Micro Cantilever AC 160TS), with a resonant frequency of approximately 300 kHz, spring constant of 42 N/m and a tip radius of 10 nm.

3.4.4 Contact angles

Equilibrium contact angles were measured using a home-made set-up: 2 μl drops of water were placed onto the surface to be analysed, and allowed to equilibrate/spread for two minutes. Magnified photographs of the droplets were taken. Once the photographs had been cropped and converted to black and white, the contact angle could be calculated using the DropSnake plugin for ImageJ software. At least two droplets were measured for each sample (giving four separate contact angles), and two separate samples were measured for each type of surface, allowing calculation of the average contact angle and standard deviation.

3.4.5 NMR

^{1}H and ^{13}C NMR spectra were acquired using Bruker AV1-250 or AC-250 spectrometers, at 250 MHz. The ^{29}Si spectrum was acquired on a Bruker DRX-500 spectrometer at 500 MHz. All samples were dissolved in deuterated chloroform.

3.4.6 XPS

XPS spectra were collected on a Kratos Axis Ultra X-ray Photoelectron Spectrometer (Kratos Ltd, Manchester) operated with a base pressure of 10^{-9} mbar. The X-ray source was a monochromated Al source. The X-ray emission current was set at 10 mA and the anode high throughput (acceleration voltage) was 15 kV. All survey scans were collected at a pass energy of 160 eV and a step size (resolution) of 1.0 eV. Narrow scans of the Br 3d, N 1s and Cl 2p regions were collected at a pass energy of 160 eV, with a step size of 0.1 eV. C 1s spectra were collected at a pass energy of 20 eV, with a step size of 0.1 eV. All samples were run as insulators. All spectra were charge-corrected to saturated hydrocarbon at 285 eV. Data were analysed using CasaXPS software (www.casaxps.com), with the help of the searchable XPS database available at www.lasurface.com. XPS spectra were acquired and analysed by Tracie Whittle.

3.4.7 Mass Spectrometry

The mass spectrum was measured on a VG Autospec, Magnetic Sector Mass Spectrometer, using electron ionisation (EI +).

3.4.8 Size Exclusion Chromatography

Analysis of polystyrene samples were obtained using a Knauer apparatus (K-501 HPLC pump) fitted with two PL gel mixed C 300 x 7.5 mm (particle size 5 μm) columns running at room temperature with a THF flow rate of 1 ml/minute, having refractive index detector (Knauer K-2301), and calibrated using linear polystyrene standards (from 1200 – 900,000 g mol^{-1}).

3.5 Results and Discussion

3.5.1 Synthesis of the Initiator

The initiator, 11-(2-bromo-2-methyl)propionyloxy)undecyltrichlorosilane, was synthesised in two steps, broadly according to the method described by Matyjaszewski *et al.*[4] (see Scheme 3.1):

Firstly, 10-undecen-1-ol was reacted with 2-bromoisobutyryl bromide in the presence of pyridine to produce the ester 10-undecen-1-yl 2-bromo-2-methylpropionate. Addition of 2-bromoisobutyryl bromide resulted in a rapid exothermic reaction generating an opaque cream solid (pyridine hydrobromide) suspended in a brown liquid. The brown colour was thought to be due to bromine containing species generated by thermal degradation of 2-bromoisobutyryl bromide. This was felt to be undesirable, so in subsequent reactions, the reaction mixture was cooled in an ice bath during the addition of the 2-bromoisobutyryl bromide, then allowed to slowly warm to room temperature. The final appearance of the reaction mixture was the same whether the reaction mixture was cooled or not. After purification, the product was obtained as a pale yellow oil, estimated to be 99 % pure by NMR. This could be stored in the fridge, with no sign of degradation (by NMR) for at least 18 months.

10-Undecen-1-yl 2-bromo-2-methylpropionate was then hydrosilylated with trichlorosilane catalysed by Karstedt's catalyst. Addition of the catalyst resulted in the rapid evolution of hydrogen gas and was strongly exothermic. To control this, the reaction mixture was cooled in an ice bath for 90 minutes after the addition of the

Scheme 3.1 Synthesis of 11-(2-bromo-2-methyl)propionyloxy)undecyltrichlorosilane, a surface-attachable ATRP initiator

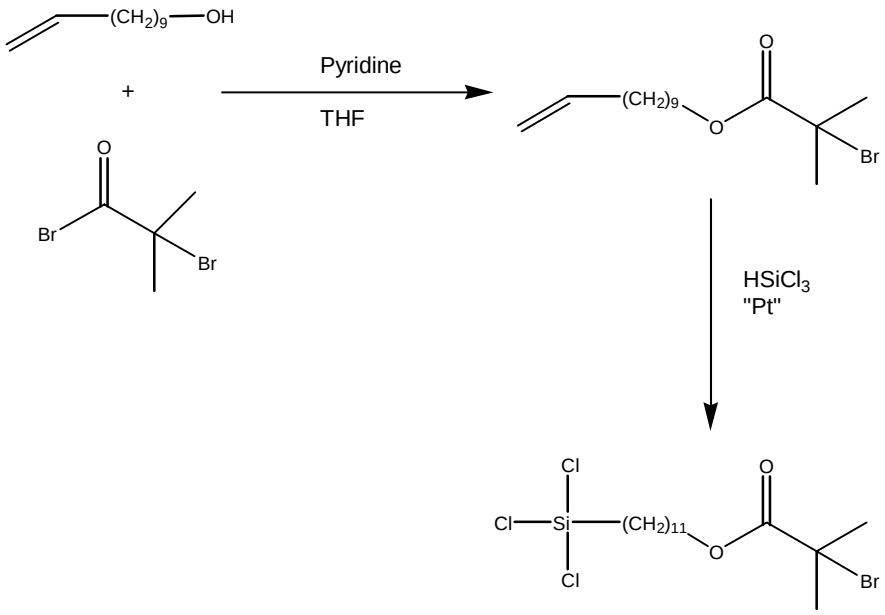

catalyst, then allowed to slowly warm to room temperature and react for at least 12 hours. The literature describes filtering the product through a plug of silica gel to remove the catalyst[4]. This was not done, as BMPUS would react with the silanol groups present on the surface of the silica, resulting in significant loss of the product. Instead, the crude BMPUS was purified by high vacuum distillation. Firstly, the excess trichlorosilane was removed under high vacuum at room temperature. The initiator was then distilled using a short path distillation apparatus. The previously reported boiling point of the initiator was 80 – 85 ºC at 2.0 x 10^{-2} Torr [4]. However, the boiling point was found to be much higher than this: even with extensive heating at 140 ºC, 3 x 10^{-5} Torr no product could be collected. It was necessary to use a yellow flame (temperature > 220 ºC) to distil the initiator. This aggressive heating caused the platinum catalyst to decompose, leaving a black residue. BMPUS was analysed by ^{1}H, ^{13}C and ^{29}Si NMR, mass spectrometry and elemental analysis, and found to be 96 % pure by NMR. Alkyl trichlorosilanes are very water-sensitive, but BMPUS could be stored under nitrogen in a Young's flask for up to a year, before cumulative exposure to traces of moisture caused it to degrade.

3.5.2 Preparation of Initiator SAM on Silicon Wafers

This was done using a standard literature method[5,9]: pieces of silicon wafers were treated with ammonia and hydrogen peroxide. This removes surface organic contaminants, and ensures the presence of a high concentration of surface hydroxide groups, making the surface very hydrophilic. After thorough drying, the wafers were then exposed to a dilute solution of the initiator (1.5 μl/ml) in dry toluene, in the presence of triethylamine. A SAM is formed via hydrolysis of the trichlorosilane group and reaction of the –OH terminated product with silanol groups on the surface of the silicon wafers and other BMPUS molecules, generating a cross-linked siloxane network. The triethylamine mops up the acidic by-products of this reaction, giving a smoother surface layer[9]. The thickness of this layer was measured as approximately 1 nm, although this was quite variable between batches of BMPUS-coated wafers. The reaction is more complicated than described above, and will be discussed in more detail in Chapter 4.

3.5.3 Polymer Brushes

The initial stage of this project involved finding suitable methods to synthesise PMMA and PS brushes. It was important to find methods that could reliably and reproducibly generate smooth, dense brushes of predetermined thickness, to allow the future production of binary patterned brushes. ATRP is the most widely used technique for the synthesis of polymer brushes, allowing the production of a wide range of well-defined polymers from surface-immobilised initiators, under experimentally accessible conditions[1]. ATRP is a controlled/'living polymerisation', which can produce polymers with predictable molecular weights[13-16] and narrow molecular weight distributions ($1.05 < M_w/M_n < 1.5$)[16-19]. The mechanism (see Scheme 3.2) relies on establishing a rapid dynamic equilibrium between a very low concentration of active free radicals and a large majority of dormant chains[14,18]. The low concentration of radicals minimises termination, and the rapid exchange between active and dormant species ensures that all the chains add monomer at essentially the same rate[8].

Scheme 3.2 Mechanism of Copper-Mediated ATRP[18,20,21]

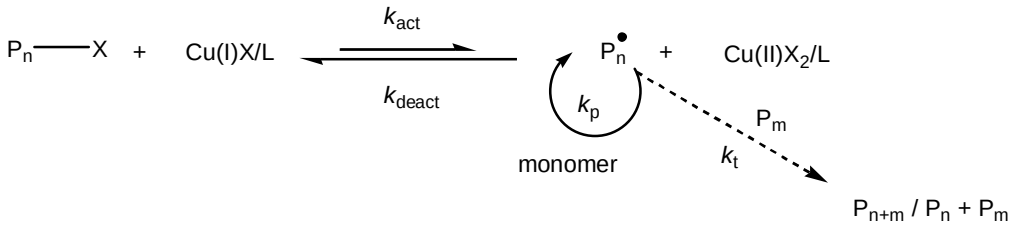

The controlled nature of an ATRP reaction depends on the position of the equilibrium between active and reversibly-deactivated radicals ($K_{eq} = k_{act}/k_{deact}$) and the rate of propagation (k_p). Each monomer has a specific value of K_{eq} which determines the concentration of active radicals and k_p which determines how fast they react[8,18]. This means that the optimum reaction conditions vary depending on the monomer, and changing conditions may have totally different effects on different systems. The role of the catalyst, ligands, solvent, temperature and additives are to adjust the position of this equilibrium and the propagation rate to ensure that the reaction is controlled[8,18]. MMA is more reactive under ATRP conditions than styrene[22], so quite different conditions are required to allow controlled synthesis of each polymer.

For both monomers, a well-controlled, reproducible polymerisation was desirable. The literature was used to identify suitable methods, which were tested by investigating the reaction kinetics and analysing the surface chemistry. In a controlled/'living' reaction, termination is limited, so there is an (almost) constant concentration of active radicals, which results in first-order kinetics with respect to the concentration of monomer. In a surface-initiated polymerisation, the amount of polymer produced is negligible, so the concentration of monomer, and the rate of polymerisation remains approximately constant throughout the reaction. Under these conditions, a linear increase in brush thickness with time indicates a controlled reaction with a constant concentration of propagating radicals.

A polymerisation is said to be living when it proceeds in the absence of irreversible chain transfer and termination[8,18,23]. Although ATRP is not a true living polymerisation, the majority of the polymer chains do not undergo termination during the reaction, and are retained as dormant, halogen-capped species. Addition of fresh monomer (and

catalyst etc.) restarts the reaction, resulting in an increase in molecular weight or brush thickness. Chain extension, or 'self blocking' experiments were used as another test of the 'livingness' of the reaction. In addition, XPS was used to analyse the surface chemistry, directly confirming the presence of bromine (and chlorine) on the surface.

In contrast to truly living polymerisations, such as living anionic polymerisation, termination plays an important role in ATRP. During the early stages of an ATRP reaction, the concentration of radicals is relatively high, and bimolecular termination occurs at a significant rate. With each termination, the concentration of copper(II) increases, which shifts the position of the atom transfer equilibrium back towards the dormant side, and eventually reduces the concentration of radicals to a level where termination becomes insignificant[8,20]. In solution reactions, the concentration of initiator is relatively high (usually equimolar to the catalyst), so termination can produce enough deactivator in solution to give a controlled polymerisation[24,25]. For polymer brushes, the effective concentration of the surface-bound initiator is too low for this mechanism to operate efficiently. Therefore, to get controlled brush growth, it is necessary to add either free initiator[26] (which produces polymer in solution), or extra copper(II)[4,9,25] (added deactivator) to reduce the concentration of active radicals enough to suppress termination. For these experiments, the added deactivator approach was chosen, as removal of free polymer requires purification by techniques such as soxhlet extraction. This could affect the first brush or the exposed initiator SAM, which would further complicate the synthesis of binary-patterned polymer brushes.

ATRP can be performed under a wide range of conditions, but it was decided to focus on homogeneous polymerisation methods. A heterogeneous reaction could lead to the deposition of solid material onto or within the brush, and on exposed regions of the substrate. It would be difficult to ensure the complete removal of these residues, especially if they penetrated into the brush or reacted with the silicon, and these contaminants could then interfere with subsequent synthetic steps.

To allow later use of the methods for the synthesis of binary-patterned polymer brushes, it was necessary to find methods for the growth of PMMA and PS brushes that gave:

- Reproducible and reliable production of polymer brushes

- Linear increase in brush thickness with time[27]
- Retention of active chain ends.
- Surface-confined reaction (e.g. no polymer generated in solution)
- Reaction under homogeneous conditions.

3.5.4 PMMA Brushes

The ATRP equilibrium constant for MMA is among the largest of any monomer, so PMMA can be produced using a wide range of ATRP catalysts, even very weak systems. Under some conditions, the value of K_{eq} can be too high to allow a fully controlled reaction, e.g. the concentration of radicals is not low enough to suppress termination[22]. Most polymerisations of MMA by ATRP are carried out in solution at temperatures below 90 ºC. A solvent dilutes the reaction mixture, reducing the concentration of radicals, which can improve the control. In addition, it solubilises the growing PMMA which has a fairly high glass transition temperature[22] (M_w 2400 T_g 77 ºC, M_w 4500 T_g 99 ºC[28]).

Early in the development of ATRP it was found to be tolerant of polar and protic additives[20,29]. Since then Armes, Huck and other groups have developed 'aqueous ATRP' for the synthesis of a wide range of hydrophilic and hydrophobic polymers in water, or mixtures of polar solvents and water[7,30-38]. This method has also been used extensively for the synthesis of polymer brushes[9,11,25,27,39-51]. Water and other polar solvents accelerate ATRP. For example aqueous ATRP of oligo(ethylene glycol) methacrylate is faster than bulk polymerisation, despite the higher concentrations of reagents present in the bulk system[7]. Similar effects have been found for brush growth: surface-initiated polymerisation of glycidyl methacrylate (GMA) in a 2: 1 mixture of DMF and water produces 28 nm thick brushes in 6 hours, compared to only 6 nm for an equivalent reaction with pure DMF as the solvent[43]. It is thought that the catalyst changes structure depending on the polarity of the reaction medium. In non-polar systems, it is thought to adopt a neutral, binuclear structure with bridging halide ligands. In polar solvents, the structure changes to the more active, mononuclear, cationic $[Cu(I)bpy_2]^+$, resulting in faster reactions[7].

The use of aqueous systems allows ATRP to be performed in reasonable amounts of time at room temperature using (relatively) environmentally-friendly solvents. This allows the production of polymer brushes on temperature-sensitive substrates such as thiol SAMs on gold[1]. Low temperatures also suppress side reactions such as thermal autopolymerisation and cross-linking, transesterification and elimination reactions[1,41]. However, too much water can lead to a loss of control: aquation and hydrolysis can displace halide ligands from copper complexes, reducing the concentration of the deactivator[36,37]. For hydrophobic monomers, the amount of water also needs to be balanced to give a homogeneous mixture of monomer, solvent and water.

Initial experiments were performed, testing several different aqueous ATRP systems. The most promising method was the 'aqueous ATRP' system used by Edmondson and Huck[9] to produce poly(glycidyl methacrylate) (PGMA) brushes and PGMA – PMMA random copolymer brushes. The reagents used were MMA (monomer), copper (I) chloride (catalyst), bpy (ligand) and copper (II) bromide (added deactivator) in a 100: 1: 2: 0.05 molar ratio. Polymerisation was initiated by the bromoisobutyrate functional groups bound to the silicon surface. The solvent was a 4: 1 mixture of methanol and water, in a 1: 1 (v/v) ratio with the monomer. This gave a homogeneous reaction mixture that dissolved PMMA. All reactions were performed at room temperature[9,24]. This produced smooth PMMA brushes (typically $R_a < 0.5$ nm – an example is shown in Figure 3.2), with a reasonably linear increase in brush thickness with reaction time. However, results were not very repeatable, and the reaction could not reach the degree of control originally reported for aqueous ATRP of MMA[9,27,52].

This poor reproducibility had two causes: the reaction mixture was hydrophilic, so droplets of liquid adhered to the surface of the wafers after they were lifted out of the solution. This allowed polymerisation to continue for an indefinite length of time (until the reagents in the surface drop were exhausted), resulting in inaccurate reaction times (it is also possibly that the residue of the reaction mixture could cause problems in subsequent reactions[24]). This was prevented by removing wafers from the 8-necked flask under a high flow of nitrogen, allowing immediate rinsing. Providing that the flow of nitrogen was high, this could be done without significant ingress of oxygen into the flask. Secondly, dissolved oxygen was not completely removed from the reaction

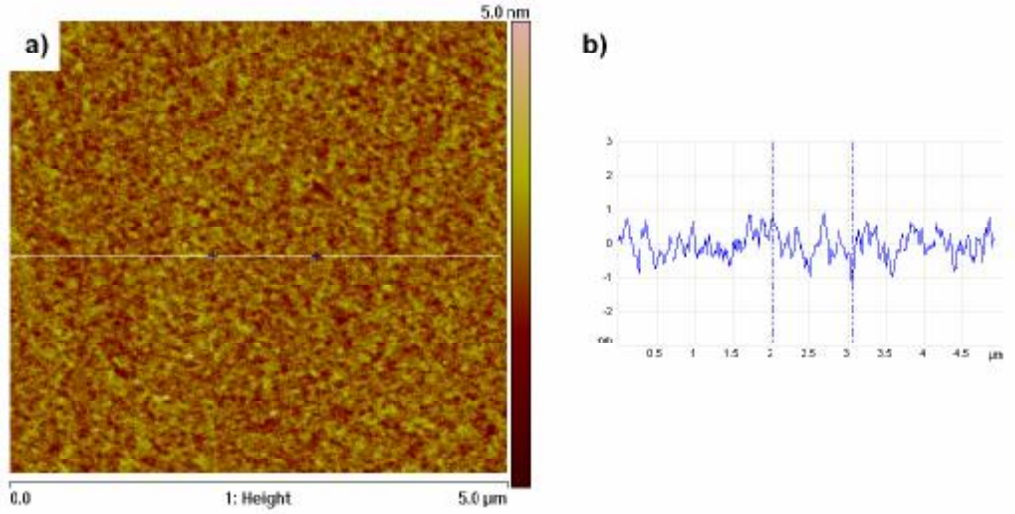

Figure 3.2 Tapping mode AFM of a typical PMMA brush, 5 x 5 µm, R_a 0.278 nm, Rms 0.352 nm, and a typical height profile across the brush surface, maximum height difference 2.018 nm. NB. R_a and rms (R_q) are measurements of surface roughness. R_a is the arithmetic average of the absolute values of the surface height deviations measured from the mean plane. Rms is the root mean square average of height deviations taken from the mean data plane.

system. Oxygen rapidly traps propagating radicals[53], and thorough deoxygenation of reagents is necessary for a controlled reaction. The method was modified slightly: MMA, methanol and water were added to a dry round-bottomed flask, and degassed by bubbling nitrogen through the liquids from a needle inlet for around 10 minutes. The other reagents were then added, and degassing continued until all the reagents had dissolved (usually 10 – 15 minutes). The reaction mixture was then transferred into the 8-necked flask by nitrogen purged syringe (a cannula could also be used), and the reaction started by immersing the wafers into the reaction mixture. These changes to the method gave a well-controlled, reproducible method for the growth of PMMA brushes with thicknesses up to 15 nm. Typical results are shown in Figure 3.3.

As discussed above, in a 'living' ATRP reaction, termination is suppressed, and the dormant, halogen-capped chain ends are retained, allowing the polymerisation to be restarted[18,54]. To test this, PMMA brushes were grown for set lengths of time, then removed from the reaction mixture, and rinsed. After measuring the ellipsometric thickness, the wafers were replaced in the reaction mixture, and left to react for an additional period of time. The second reaction resulted in an increase in film thickness,

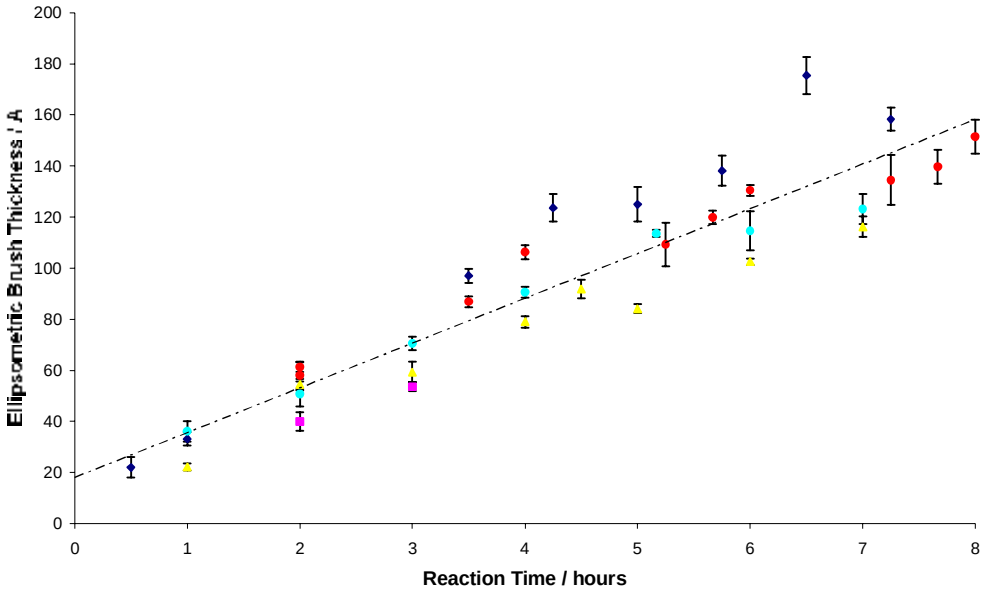

Figure 3.3 Plot of the evolution of polymer layer thickness from a modified silicon surface as a function of reaction time. Conditions: methyl methacrylate, methanol, water 5: 4: 1 by volume, CuCl 1 %, $CuBr_2$ 0.05 %, bpy 2.5 % (mole % relative to MMA), room temperature. Different data series for reactions done on different days under the same conditions: ◆ 6.8.2006, ■ 15.8.2006, ▲ 17.8.2006, ● 17.10.2006, ● 10.5.2007. Line of best fit for all data included to guide the eye (R^2 = 0.87). Error bars indicate one standard deviation.

which correlated well with brushes grown for equivalent amounts of time without interruption. The grow – measure – regrow process was repeated up to 4 times on a single wafer – the results are shown in Figure 3.4. Wafers which had been stored for several weeks could be reacted again, with a linear increase in thickness, indicating the stability of the halide-capped chain ends. This provided further evidence of the absence of termination, and the pseudo-living nature of the polymerisation.

AFM and ellipsometry do not provide any information about the chemistry of the surface layer (although AFM phase images give some qualitative information about chemical inhomogeneities across a sample). XPS is a surface-specific analysis technique which allows direct identification and quantification of elements present within approximately the top 10 nm of the material. The sample is exposed to a beam of x-rays, which can electronically excite any atom except hydrogen, leading to the ejection of photoelectrons: quantised, core level electrons which are characteristic of particular atoms (and chemical environments). Electrons emitted from the sample

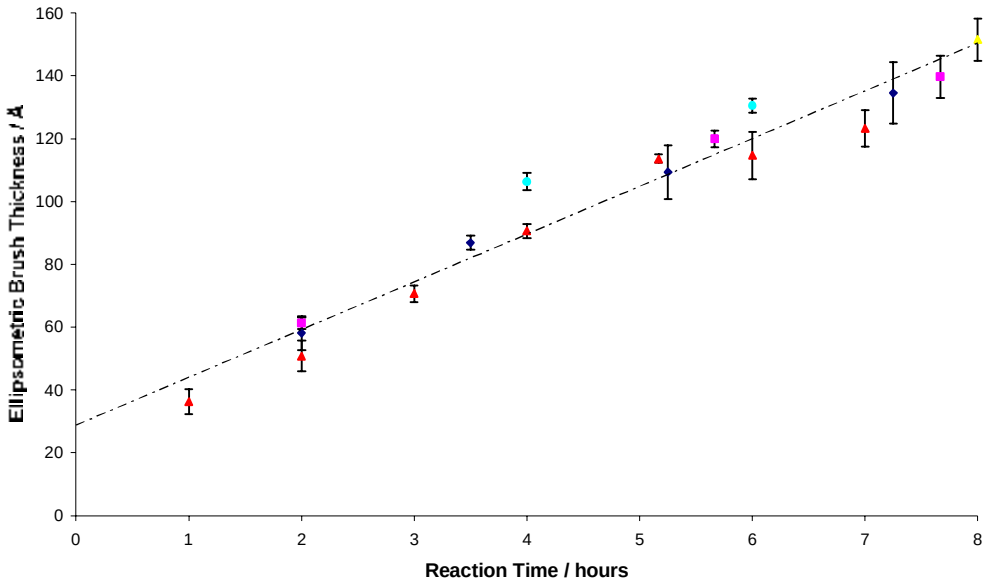

Figure 3.4 Regrowth of PMMA brushes on silicon. ♦,■, ▼, ▲ separate initiator functionalised wafers that have been removed from the reaction mixture, analysed, then allowed to react further. Thicknesses of PMMA brush grown without interruption are included for comparison (▲). Line of best fit for all the data included to guide the eye (R^2 = 0.95). Reaction conditions as Figure 3.3, error bars indicate one standard deviation. This data is also presented in Figure 3.3.

without undergoing an energy loss event form the main, identifiable photoelectric peaks (this emission is unlikely if the atom is more than 10 nm from the surface, hence the surface sensitivity). Electrons which have lost some energy due to inelastic interactions form a continuous background[55]. Two types of scan are commonly used: the survey scan covers a wide range of binding energies, and is used mainly to identify (and quantify) the atoms present. High resolution scans of a particular peak can be used to identify different chemical environments within the substance, helping with the identification of organic substances. For example, high resolution scans of the C 1s region are presented below, and used to help identify the presence of PMMA or PS brushes.

The XPS survey scan of a PMMA brush, 10.9 nm thick (see Figure 3.5) indicates the presence of carbon, oxygen, chlorine, bromine and silicon. The low thickness of the brush means that silicon from the substrate can be detected. The ratio of carbon: oxygen was 2.8: 1. Assuming that all the polymer chains in the brush had $N = 100$, each

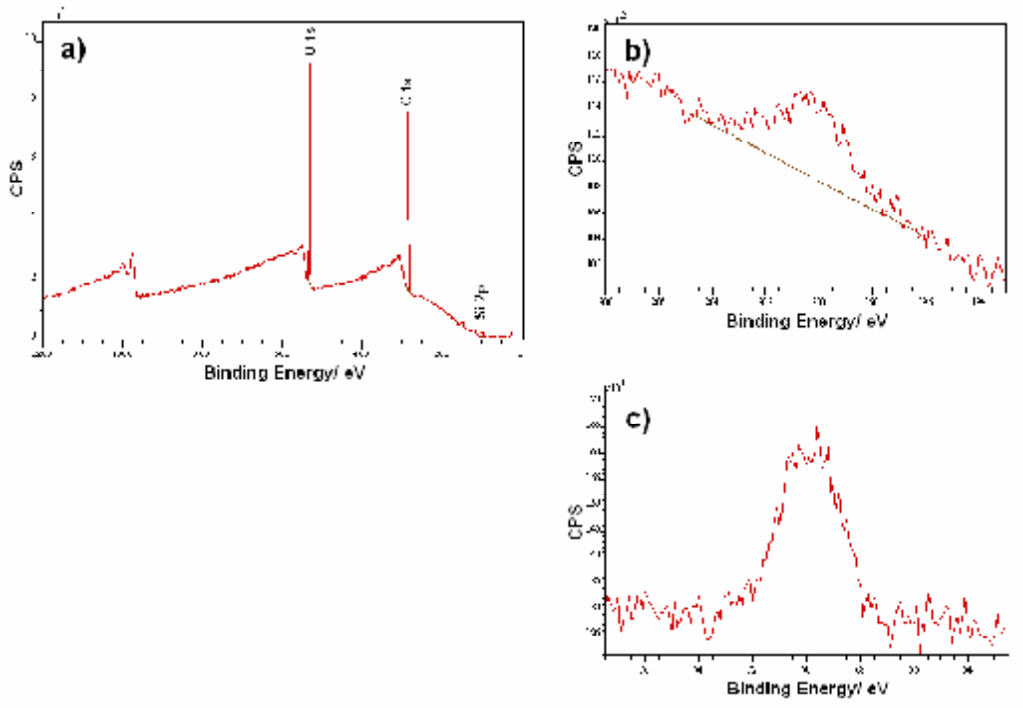

Figure 3.5 XPS of PMMA brush; a) survey scan, b) magnified view of Cl 2p region of survey scan, c) magnified view of Br 3d region of survey scan.

with a single initiator group, the ratio of C: O would be 2.54: 1. The excess carbon could indicate that the polymer has a lower than predicted degree of polymerisation, or alternatively that there is a considerable amount of unreacted initiator present (which has a C: O ratio of 7.5: 1). This would fit with calculations of the grafting densities of polymer brushes which suggest that each growing polymer chain blocks 10 – 12 initiator groups[52,56]. The presence of both chlorine and bromine gave direct evidence that the halogen capped chain ends were retained.

Several studies[21,57-59] have suggested that a mixed halogen system (an alkyl bromide initiator and a copper chloride catalyst) can give improved control of the ATRP of MMA. For a controlled polymerisation, the rate of initiation must be faster than the rate of propagation[21,57]. The position of equilibrium for the initiation and propagation steps must be shifted towards the dormant state[57], and the deactivation step should be rapid to maintain a low concentration of active radicals, and so limit termination and side reactions[21]. In a mixed halogen system, the weaker C-Br bonds in the initiator promote rapid initiation. The majority of the chains then react with the catalyst to produce Cl capped chains[21,57,59]. This exchange process results in the formation of Cu(II)-Br bonds,

which are weaker than Cu(II)-Cl bonds, and increase the rate of deactivation[21]. Matyjaszewski *et al*. [57] used gas chromatography and ^{1}H NMR to follow halogen exchange in model systems:

$$RBr + CuCl/2L \rightleftharpoons RCl + CuBr/2L \qquad (3.1)$$

They found that, regardless of the starting conditions, the position of equilibrium gave 80-90 % RCl (the different values depend on the nature of the R group, and the measurement technique).

In this case, the mixed halogen system used to produce PMMA brushes gave a well-controlled polymerisation of MMA. The XPS spectrum showed that both bromine and chlorine were present in a ratio of 1: 2.35. This meant that approximately 70 % of the polymer chains were chlorine-terminated, which fits well with the results from the model study discussed above. Halogen exchange has not been directly measured for PMMA, either for free polymer or brushes. This confirms that the polymer behaves in a similar manner to the small molecule alkyl halide models.

The high resolution spectrum of the C 1s region is shown below in Figure 3.6. Curve fitting (using a normal PMMA curve fit) revealed four different carbon environments in an approximate 2: 1: 1: 1 ratio. These could be assigned to saturated hydrocarbon (C-C) (C1), -C*-C(=O) (C2), alkoxy carbon (C*-O-C(=O), (C3) and carbonyl carbon (-C(=O)OR, C4) respectively. The different carbon environments present in PMMA are illustrated on the spectrum.

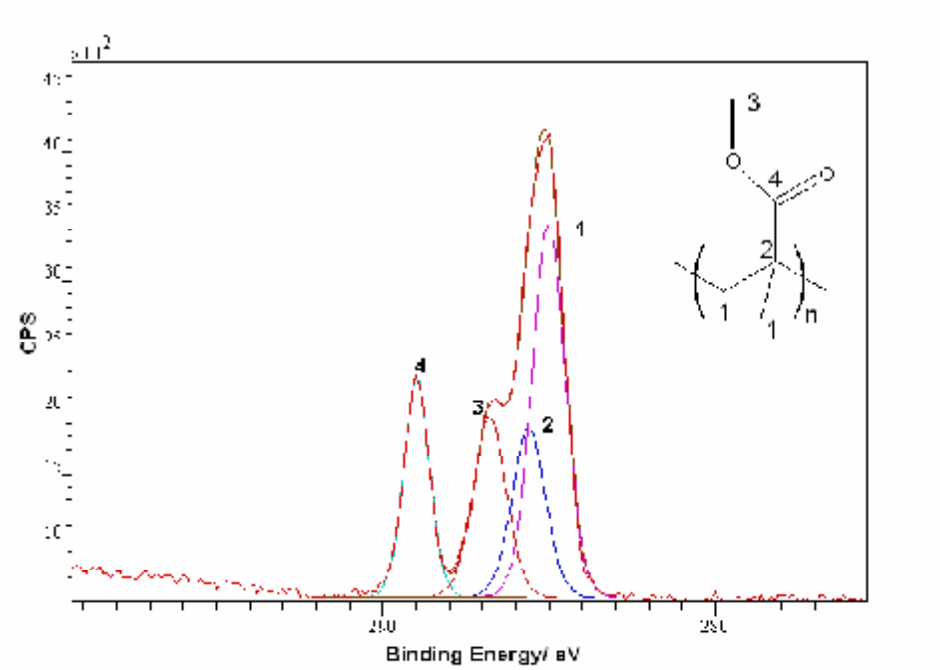

Figure 3.6 High resolution XPS scan of C 1s region of PMMA brush, showing curve fit, with carbon environments identified and quantified.

3.5.5 Polystyrene Brushes

PS brushes have been synthesised using a range of polymerisations including ATRP[4], NMP[60], reverse ATRP[61] and conventional free radical polymerisation[62,63]. It was decided to focus on producing PS brushes by surface-initiated ATRP. As mentioned earlier, styrene is less reactive than MMA under ATRP conditions[22]. Elimination of HX from the polymer end groups plays a significant role in the ATRP of styrene, limiting the maximum molecular weight and resulting in a slower reaction and increased polydispersity at higher molecular weights. Model studies showed that elimination was minimised when the concentration of monomer was high (i.e. bulk polymerisation) and the concentration of Cu(II) was as low as possible to retain control of the polymerisation. Polar solvents were found to promote significant decomposition of the end groups[64]. Because of this, styrene is most commonly polymerised in the bulk although (relatively) non-polar solvents are also used[8]. Reactions are usually performed at temperatures between 90 and 130 ºC. This allows reactions to be carried out in a reasonable length of time, and is above the glass transition temperature of PS[22] (M_w

2950 T_g 74 ºC, M_w 9200 T_g 96 ºC[28]). Lower temperatures (e.g. 90 ºC) may lead to better control over molecular weight by reducing the amount of thermal self-initiation[22].

Reaction under homogeneous conditions was desirable to prevent the deposition of solid residues onto or in the brush. It also ensures that the effective concentration of copper (II) is high enough to give rapid exchange between active and dormant chains, ensuring that all the chains grow at the same rate[8,65]. Copper – bpy complexes are not completely soluble in most styrene-solvent mixtures, leading to heterogeneous reactions. Solubility can be improved by using alkyl-modified bipyridines such as dnNbpy or multidentate amine ligands such as PMDETA and 1,1,4,7,10,10-hexamethyltriethylenetetramine (HMTETA) (these are cheaper and more tunable than bipyridines, give less strongly coloured copper complexes and can lead to higher polymerisation rates)[66].

There are fewer references describing the production of PS brushes by ATRP compared to PMMA. Several different systems were investigated to find a method that gave well-controlled, reproducible growth of smooth PS brushes. First it was decided to try a method based on that of Granville *et al.*[10], who synthesised PS brushes from BMPUS coated silicon (these were then used to produce block copolymer brushes by chain extension with methyl acrylate[67], *tert*-butyl acrylate[68] or pentafluorostyrene[10]). The original method used 2-bromoisobutyrate as a sacrificial initiator, in a 0.8 mole ratio relative to copper (I) bromide. It was decided to replace this with 10 mole % $CuBr_2$, to promote a controlled reaction without generating free polymer. The molar ratios were also altered to give the same theoretical degree of polymerisation as for PMMA brushes – i.e. 100: 1: 2.1: 0.1 styrene: copper bromide: PMDETA: $CuBr_2$.

Some of the test reactions gave a linear increase in thickness with time (up to reaction times of ~ 25 hours), indicating some degree of control, but reproducibility was poor – the most linear examples are shown in Figure 3.7 below.

According to the references, the polymerisation mixture becomes homogeneous when it is heated to 90 ºC[10]. It was found that even after extended stirring at 90 ºC there was always some solid material left in the flask. During the reactions a dark-coloured solid precipitate (thought to be copper complexes) was deposited on the wire wafer holders,

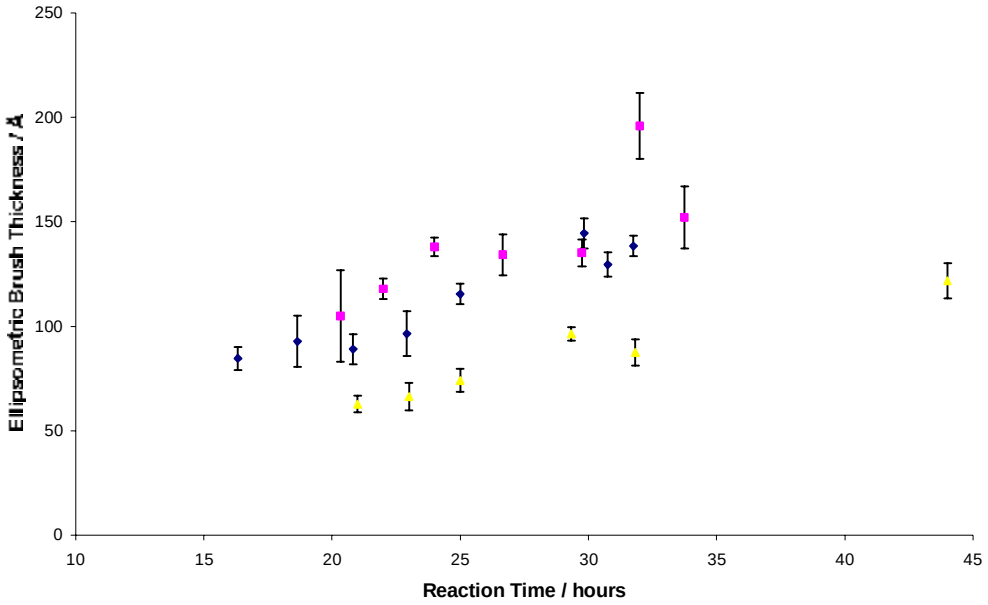

Figure 3.7 Plot of the evolution of polymer layer thickness from a modified silicon surface as a function of reaction time. Conditions: styrene, anisole, 23:27 (v/v). CuBr 1 %, PMDETA 2.1 %, $CuBr_2$, 0.1 %, (mole % relative to styrene), 90 ºC. Different data series for reactions done on different days under the same conditions: ♦ 11.10.2006, ■ 1.11.2006, ▲, 29.11.2006. Error bars indicate one standard deviation.

the initiator-coated wafers and sometimes on the walls of the 8-necked flask. It is possible that the addition of $CuBr_2$ and the alteration of the reaction stoichiometry prevented the formation of a homogeneous reaction mixture. The limited control and reproducibility however, suggests that the active concentration of catalyst and deactivator decreased over time. The poor reproducibility between reactions could also be explained by variation in the amount of material deposited in different reactions. The solid material seemed to be removed by soaking the wafers in water – where this was successfully done, the brush surface was smooth. However, in other cases, the brush surface was rough, presumably due to incomplete removal of the solid residue. Typical AFM images of smooth and rough PS brushes are shown in Figure 3.8.

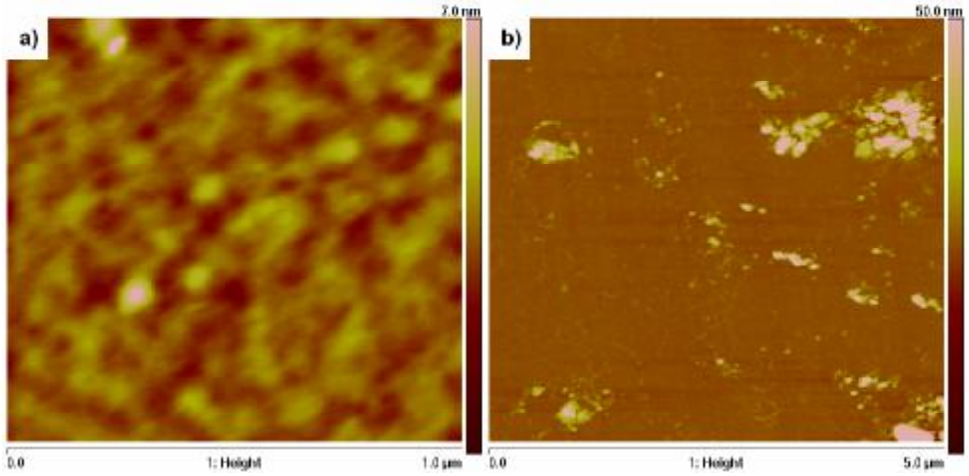

Figure 3.8 Tapping mode AFM images of polystyrene brushes. a) 1 x 1 µm, smooth brush, rms 0.518 nm, R_a 0.388 nm, b) 5 x 5 µm, rough sample, with surface features, rms 4.741 nm, R_a 1.881 nm.

Another method was evaluated, using cyclohexanone as the solvent, CuCl or CuBr as the catalyst, with PMDETA and $CuBr_2$ at 90 ºC. This was adapted from the method used by Xu *et al.*[12] to polymerise styrene with a triphenylmethyl chloride initiator – very different in structure from BMPUS. The reaction mixture was homogeneous, but ellipsometry showed that the brush thickness increased rapidly at first, then levelled out and stopped growing, and reproducibility was very poor (results not shown). The reaction mixture became more viscous over time; it was decided to test if this was due

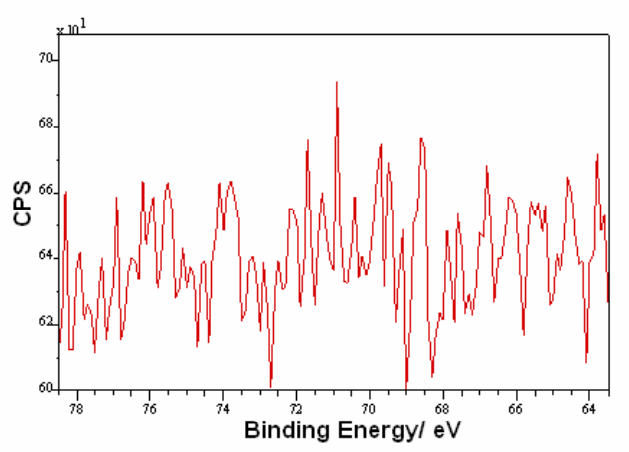

Figure 3.9 XPS of PS brush produced by ATRP in cyclohexanone solution catalysed by CuBr: magnified view of Br 3d region of survey scan, showing the absence of bromine on the sample surface

to polymerisation in solution. The reaction mixture was dissolved in THF and stirred with silica to remove copper residues, then precipitated in methanol. Whatever the catalyst, free polymer was obtained (and analysed by GPC: CuBr: M_n 27,200, M_w/M_n 1.55. CuCl: M_n 8600, M_w/M_n 2.01). As there was no free initiator present in solution, this must be produced by chain transfer and/or thermal autopolymerisation. XPS analysis of a sample produced using CuBr showed the presence of PS, but there was no detectable bromine peak (the Br 3d region of the spectrum is shown above in Figure 3.9). These results suggest that the polymerisation followed a conventional (or only partially controlled) free radical mechanism, with chain transfer to solvent producing free polymer and termination, leading to the loss of the 'living' chains.

Matyjaszewski *et al*.[4] reported the production of PS brushes on silicon wafers by well-controlled, homogeneous ATRP. The reaction was performed in bulk, using CuBr, dnNbpy and $CuBr_2(dnNbpy)_2$ at 100 ºC. Brush growth under bulk conditions is wasteful, because greater amounts of reagents are needed to maintain the same molar ratios, but conversion to polymer is minute. This was a particular concern because of the relatively high cost of dnNbpy. However, this method reliably produced PS bushes with a linear increase in thickness with time, and reasonable reproducibility. It was possible to regrow brushes, resulting in a total film thickness equivalent to samples grown without interruption and providing further evidence for the living nature of the reaction. Some results are shown below in Figure 3.10 (● shows samples that were regrown).

AFM showed that this method produced smooth PS brushes: a typical image is shown in Figure 3.11 below.

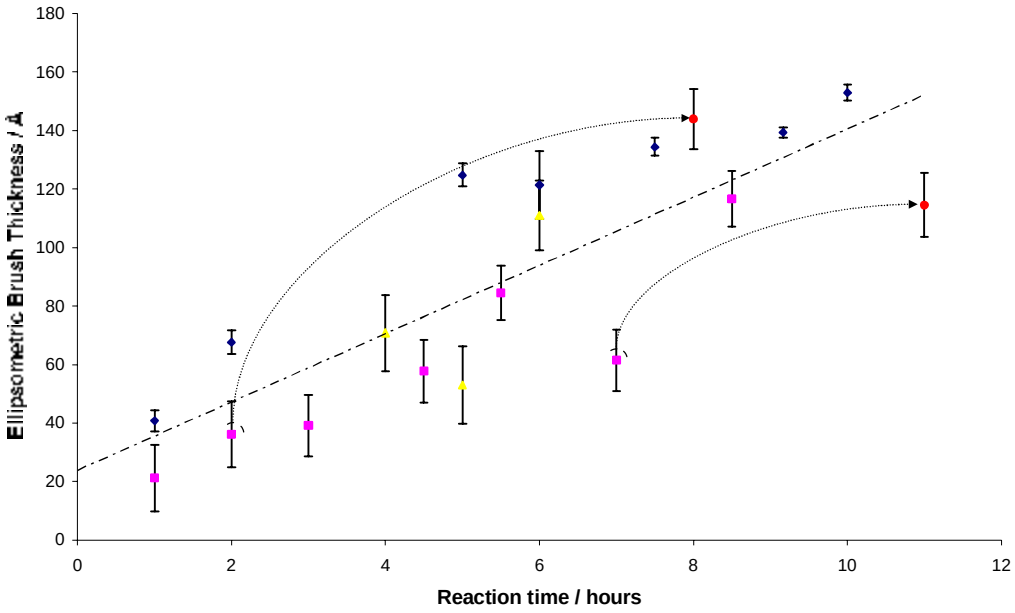

Figure 3.10 Plot of the evolution of polymer layer thickness from a modified silicon surface as a function of reaction time. Conditions: styrene, CuBr 1 %, dnNbpy 2 %, $CuBr_2(dnNbpy)_2$ 0.05 %, (mole % relative to styrene), 100 ºC. Different data series for reactions done on different days under the same conditions: ♦ 4.4.2007, ■ 19.11.2008, ▲ 24.11.2008, ● 24.11.2008: cumulative reaction time for regrown samples; arrows indicate which samples were regrown. Line of best fit for all data included to guide the eye (R^2 = 0.68). Error bars represent the MSE (except ♦: error bars represent one standard deviation).

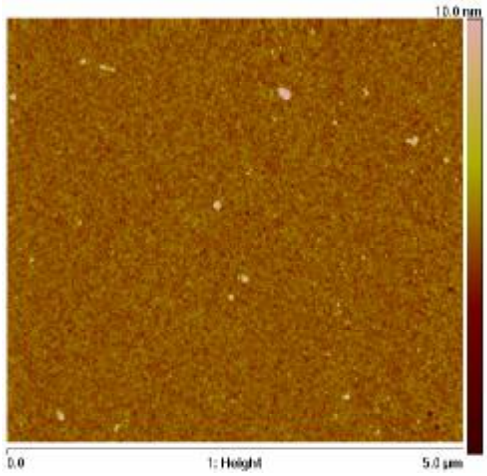

Figure 3.11 Tapping mode AFM image of PS brush grown for 6 hours. 5 x 5 µm, R_a 0.348 nm, rms 0.597 nm.

XPS analysis showed peaks due to silicon, oxygen (from the substrate), carbon and bromine. The presence of a bromine peak provided further evidence for the controlled nature of the polymerisation. The high resolution C 1s spectrum was curve-fitted to two carbon environments, aromatic carbon (C1) and saturated carbon (C2), based on standard PS spectra (see Figure 3.12). The ratio of C1: C2 was 2.1: 1, compared to the 1.7: 1 predicted from the structure of PS. It is not clear why there was this discrepancy, however, the C 1s spectrum of a PS brush grown using the cyclohexanone method had almost exactly the expected ratio, although the polymerisation was not controlled, and the brushes were not halogen terminated (see p. 111).

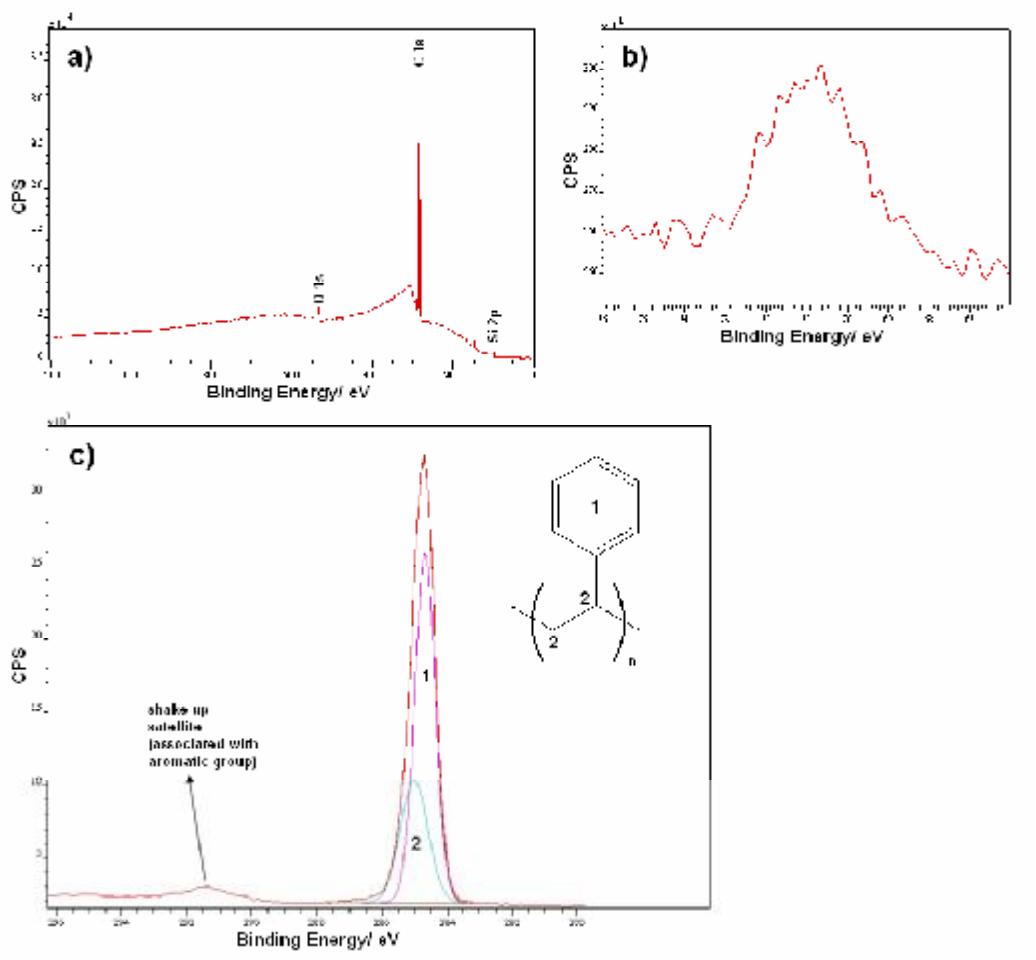

Figure 3.12 XPS of bromine-terminated PS brush; a) survey scan, b) magnified view of Br 3d region of survey scan, c) high resolution spectrum of C 1s region.

3.5.6 Dehalogenation of Polymer Brushes

The presence of halogen-capped polymer chains confirms that controlled ATRP is occurring, but they present a problem for the production of binary-patterned brushes. When the second reaction is performed, polymerisation will occur from the initiator, and from the dormant chains of the first brush, resulting in the formation of patterned polymer/block copolymer brushes. To prevent this, it is necessary to dehalogenate/terminate (or 'kill') the first brush[11]. Bromine-terminated SAMs[69-71] polymer brushes[11,45] and free poly(methyl acrylate)[72] have been successfully dehalogenated by nucleophilic substitution with sodium azide. Methods were tested by reacting samples of polymer brush with sodium azide, then attempting to regrow the brush. Changes in thickness were measured using ellipsometry.

Dehalogenation of PMMA brushes was attempted using several different sets of reaction conditions[11,45,69,70]. All the reactions resulted in a small decrease in the brush thickness, which was thought to be due to a change in brush conformation after exposure to DMF and sodium azide. The second polymerisation resulted in a significant increase in brush thickness, even when the samples were exposed to saturated sodium azide in DMF at room temperature for 72 hours. XPS analysis of a sample reacted under milder conditions (0.12 mol dm^{-3} NaN_3 in DMF, room temperature, 48 hours) suggested that there had been no reaction, as there was no detectable nitrogen signal, and no obvious decrease in the intensity of the Br 3d peak. However, the second polymerisation reaction seemed to give a lower increase in thickness than predicted from the reaction time, so it is possible that some of the halogen groups were removed. The reaction of azide with alkyl halides goes via a S_N2 mechanism. The reactivity of a molecule towards nucleophiles is strongly affected by the degree of substitution of the electrophilic carbon. For example, a secondary alkyl halide, 2-bromopentane, is more than 500 times more reactive than a tertiary group, tertiary-butyl bromide[73]. The nature of the leaving group is also important: bromine is a much better leaving group than chlorine[73]. The end group of PMMA synthesised by ATRP is a tertiary alkyl halide (see Figure 3.13). PMMA brushes were synthesised using a mixed halogen system, so the chains were terminated by a mixture of chlorine and bromine (see p. 106). This suggests that the end groups were relatively unreactive

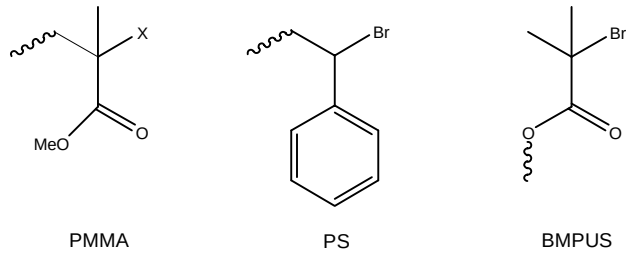

Figure 3.13 Structures of end groups of polymer brushes and BMPUS.

towards nucleophiles, and that not all the halogen groups were removed under the conditions used. An additional consideration is that the surface-bound reactions undergo considerable kinetic retardation compared to equivalent reactions in solution, accentuating these effects[70].

It was decided to try dehalogenation of PS brushes: the end group of PS forms a less hindered secondary alkyl halide (see Figure 3.13), and all the polymer chains were bromine-terminated. PS brushes were grown for different lengths of time, then some of

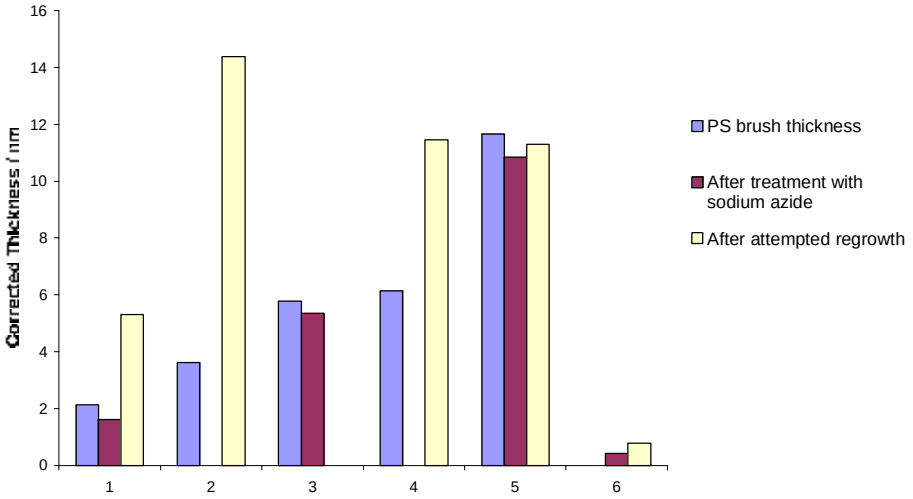

Figure 3.14 Reaction of PS brushes with sodium azide. Plot of changes of ellipsometric brush thickness through various reactions. Conditions: growth of PS brushes: styrene, CuBr 1 %, dnNbpy 2 %, $CuBr_2(dnNbpy)_2$ 0.05 %, (mole % relative to styrene), 90 ºC. Reaction times: 1, 2, 4.5, 7, 8.5, 0 hours for wafers 1 – 6 respectively. Dehalogenation: saturated NaN_3 in DMF, 50 ºC, 63 h, all samples except 2 and 4. Second polymerisation, conditions as above, additional reaction times: 6, 6, 0, 4, 6, 6 hours for wafers 1 - 6 respectively.

them were reacted with saturated sodium azide in DMF at 50 ºC for 63 hours, resulting in a small decrease in brush thickness. The samples were then placed in a second polymerisation solution. The samples that had been exposed to sodium azide (samples 1 and 5) had a much smaller increase in thickness than those that had simply been stored (samples 2 and 4), suggesting that the dehalogenation was at least partially successful (sample 1 still showed a significant increase in thickness during the second reaction): the results are shown in Figure 3.14 above.

XPS analysis (Figure 3.15) showed complete loss of the Br 3d peak after reaction with excess azide. Nitrogen could be detected on the sample, but only as a trace signal. However, Lee *et al*.[69] found that azide-terminated monolayers were very susceptible to x-ray damage, with the N 1s photoemission almost disappearing after a single high resolution scan. BMPUS-coated samples were also reacted with sodium azide, then exposed to polymerisation conditions (sample 6 in Figure 3.14). There was no significant increase in layer thickness, and no halogen signal could be detected by XPS. The high resolution N 1s scan (shown in Figure 3.16) showed a clear doublet, with peaks at around 405 and 401 eV, characteristic of an azide terminal group[69,71,74]. BMPUS is a tertiary alkyl halide, so this suggests that the dehalogenation of PMMA was inhibited by the chlorine-terminated chains. It is also possible that the end groups of polymer brush are more sterically hindered than BMPUS. This seems unlikely, as a polymer brush should be more flexible than a SAM, but it could occur if the chain ends were buried within the brush.

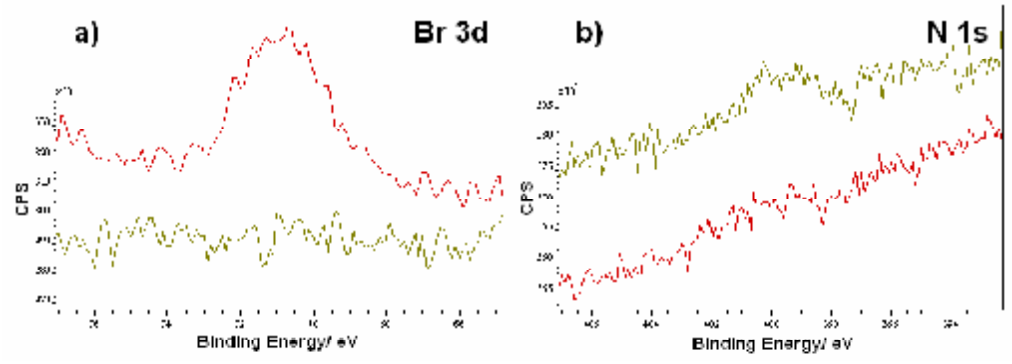

Figure 3.15 XPS of a) Br 3d and b) N 1s regions for samples of PS brush before (red traces) and after (green traces) reaction with sodium azide. Conditions: saturated NaN_3 in DMF, 50 ºC, > 48 h).

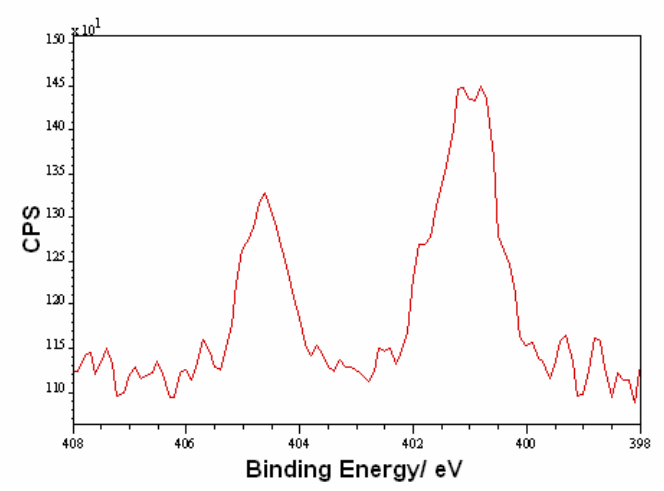

Figure 3.16 High resolution XPS of the N 1s region for a sample of BMPUS after treatment with sodium azide (saturated NaN_3 in DMF, 50 ºC, > 48 hours).

3.6 Summary

PMMA and PS brushes were synthesised on silicon substrates by surface-initiated ATRP from a BMPUS SAM. Well-controlled, homogeneous polymerisation methods were established that gave linear increases in brush thickness with time and acceptable reproducibility. Chain extension experiments and XPS gave further evidence for the controlled /'living' character of these polymerisations.

To allow these methods to be used for the synthesis of binary-patterned polymer brushes it will be necessary to terminate the first brush to prevent the unwanted formation of block copolymer brushes during the second ATRP reaction. Bromine-terminated PS brushes were effectively dehalogenated by reaction with sodium azide, but the same conditions did not 'kill' PMMA brushes, which were synthesised using a mixed halogen system and had both bromine- and chlorine- terminated chains. This means that it will be necessary to grow the PS brush first. However, if this later causes problems, PMMA could be produced by an alternative method, avoiding the use of a mixed halogen system.

3.7 References

(1) Huck, W. T. S.; Edmondson, S.; Osborne, V. L. *Chemical Society Reviews* **2004**, *33*, 14-22.
(2) Shah, R. R.; Merreceyes, D.; Husemann, M.; Rees, I.; Abbott, N. L.; Hawker, C. J.; Hedrick, J. L. *Macromolecules* **2000**, *33*, 597-605.
(3) Willey, T. M.; Vance, A. L.; van Buuren, T.; Bostedt, C.; Terminello, L. J.; Fadley, C. S. *Surface Science* **2005**, *576*, 188-196.
(4) Matyjaszewski, K.; Miller, P. J.; Shukla, N.; Immaraporn, B.; Gelman, A.; Luokala, B. B.; Siclovan, T. M.; Kickelbick, G.; Vallant, T.; Hoffmann, H.; Pakula, T. *Macromolecules* **1999**, *32*, 8716-8724.
(5) Topham, P. D.; Howse, J. R.; Crook, C. J.; Parnell, A. J.; Geoghegan, M.; Jones, R. A. L.; Ryan, A. J. *Polymer International* **2006**, *55*, 808-815.
(6) Pouchert, C. J.; Behnke, J. In *The Aldrich Library of ^{13}C and ^{1}H FT NMR Spectra*; First ed.; Aldrich Chemical Company, Inc., 1993; Vol. 3.
(7) Wang, X. S.; Armes, S. P. *Macromolecules* **2000**, *33*, 6640-6647.
(8) Patten, T. E.; Matyjaszewski, K. *Advanced Materials* **1998**, *10*, 901-915.
(9) Edmondson, S.; Huck, W. T. S. *Journal of Materials Chemistry* **2004**, *14*, 730-734.
(10) Granville, A. M.; Boyes, S. G.; Akgun, B.; Foster, M. D.; Brittain, W. J. *Macromolecules* **2004**, *37*, 2790-2796.
(11) Zhou, F.; Zheng, Z.; Yu, B.; Liu, W.; Huck, W. T. S. *Journal of the American Chemical Society* **2006**, *128*, 16253-16258.
(12) Xu, Y.; Lu, J.; Xu, Q.; Wang, L. *European Polymer Journal* **2005**, *41*, 2422-2427.
(13) Matyjaszewski, K.; Wang, J.-L.; Grimaud, T.; Shipp, D. A. *Macromolecules* **1998**, *31*, 1527-1534.
(14) Wang, J.-L.; Grimaud, T.; Matyjaszewski, K. *Macromolecules* **1997**, *30*, 6507-6512.
(15) Odian, G. *Principles of Polymerization*; 4th ed.; John Wiley and Sons, Inc: Hoboken, New Jersey, 2004.
(16) Wang, T.-L.; Liu, Y.-Z.; Jeng, B.-C.; Cai, Y.-C. *Journal of Polymer Research* **2005**, *12*, 67-75.
(17) Wang, J.-S.; Matyjaszewski, K. *Macromolecules* **1995**, *28*, 7901-7910.
(18) Matyjaszewski, K.; Xia, J. *Chemical Reviews* **2001**, *101*, 2921-2990.
(19) Matyjaszewski, K.; Nakagawa, Y.; Jasieczek, C. B. *Macromolecules* **1998**, *31*, 1535-1541.
(20) Matyjaszewski, K.; Patten, T. E.; Xia, J. *Journal of the American Chemical Society* **1997**, *119*, 674-680.
(21) Matyjaszewski, K.; Wang, J.-L.; Grimaud, T.; Shipp, D. A. *Macromolecules* **1998**, *31*, 1527-1534.
(22) Matyjaszewski, K.; Davis, T. P. *Handbook of Radical Polymerization*; John Wiley & Sons, Inc.: Hoboken, 2002.
(23) Hsieh, H. L.; Quirk, R. P. *Anionic Polymerisation: Principles and Practical Applications*; Marcel Dekker, Inc.: New York, 1996.

(24) Tomlinson, M. R. Surface-Grafted Polymer and Copolymer Assemblies with Gradient in Molecular Weight and Composition, PhD thesis, North Carolina State University, 2005.
(25) Huang, W.; Kim, J.-B.; Bruening, M. L.; Baker, G. L. *Macromolecules* **2002**, *35*, 1175-1179.
(26) Ejaz, M.; Yamamoto, S.; Ohno, K.; Tsujii, Y.; Fukuda, T. *Macromolecules* **1998**, *31*, 5934-5936.
(27) Jones, D. M.; Huck, W. T. S. *Advanced Materials* **2001**, *13*, 1256-1259.
(28) Callaghan, T. A.; Paul, D. R. *Macromolecules* **1993**, *26*, 2439-2450.
(29) Nishikawa, T.; Ando, T.; Kamigaito, M.; Sawamoto, M. *Macromolecules* **1997**, *30*, 2244-2248.
(30) Wang, X. S.; Jackson, R. A.; Armes, S. P. *Macromolecules* **2000**, *33*, 255-257.
(31) Ashford, E. J.; Naldi, V.; O'Dell, R.; Billingham, N. C.; Armes, S. P. *Chemical Communications* **1999**, 1285-1286.
(32) Robinson, K. L.; Khan, M. A.; de Banez, M. V.; Wang, X. S.; Armes, S. P. *Macromolecules* **2001**, *34*, 3155-3158.
(33) Wang, X. S.; Lascelles, S. F.; Jackson, R. A.; Armes, S. P. *Chemical Communications* **1999**, 1817-1818.
(34) Ma, I. Y.; Lobb, E. J.; Billingham, N. C.; Armes, S. P.; Lewis, A. L.; Lloyd, A. W.; Salvage, J. *Macromolecules* **2002**, *35*, 9306-9314.
(35) Krishnan, R.; Srinivasan, K. S. V. *Macromolecules* **2003**, *36*, 1769-1771.
(36) Chatterjee, U.; Jewrajka, S. K.; Mandal, B. M. *Polymer* **2005**, *46*, 1575-1582.
(37) Jewrajka, S. K.; Chatterjee, U.; Mandal, B. M. *Macromolecules* **2004**, *37*, 4325-4328.
(38) McDonald, S.; Rannard, S. P. *Macromolecules* **2001**, *34*, 8600-8602.
(39) Farhan, T.; Huck, W. T. S. *European Polymer Journal* **2004**, *40*, 1599-1604.
(40) Osborne, V. L.; Jones, D. M.; Huck, W. T. S. *Chemical Communications* **2002**, 1838-1839.
(41) Huang, W.; Baker, G. L.; Bruening, M. L. *Angewandte Chemie, International Edition* **2001**, *40*, 1510-1512.
(42) Tu, H.; Heitzman, C. E.; Braun, P. V. *Langmuir* **2004**, *20*, 8313-8320.
(43) Yu, W. H.; Kang, E. T.; Neoh, K. G. *Langmuir* **2004**, *20*, 8294-8300.
(44) Bao, Z.; Bruening, M. L.; Baker, G. L. *Macromolecules* **2006**, *39*, 5251-5258.
(45) Zhou, F.; Jiang, L.; Liu, W.; Xue, Q. *Macromolecular Rapid Communications* **2004**, *25*, 1979-1983.
(46) de las Heras Alarcón, C.; Farhan, T.; Osborne, V. L.; Huck, W. T. S.; Alexander, C. *Journal of Materials Chemistry* **2005**, *15*, 2089-2094.
(47) Zhang, K.; Li, H.; Zhang, H.; Zhao, S.; Wang, D.; Wang, J. *Materials Chemistry and Physics* **2006**, *96*, 477-482.
(48) Tugulu, S.; Arnold, A.; Sielaff, I.; Johnsson, K.; Klok, H.-A. *Biomacromolecules* **2005**, *6*, 1602-1607.
(49) Liu, Y.; Klep, V.; Luzinov, I. *Journal of the American Chemical Society* **2006**, *128*, 8106-8107.
(50) Xu, F. J.; Song, Y.; Cheng, Z. P.; Zhu, X. L.; Zhu, C. X.; Kang, E. T.; Neoh, K. G. *Macromolecules* **2005**, *38*, 6254-6258.
(51) Xu, F. J.; Kang, E. T.; Neoh, K. G. *Journal of Materials Chemistry* **2006**, *16*, 2948-2952.
(52) Jones, D. M.; Brown, A. A.; Huck, W. T. S. *Langmuir* **2002**, *18*, 1265-1269.
(53) Matyjaszewski, K.; Dong, H.; Jakubowski, W.; Pietrasik, J.; Kusumo, A. *Langmuir* **2007**, *23*, 4528-4531.

(54) Kim, J.-B.; Huang, W.; Bruening, M. L.; Baker, G. L. *Macromolecules* **2002**, *35*, 5410-5416.
(55) http://www.casaxps.com/help_manual/manual_updates/xps_spectra.pdf.
(56) Kim, J.-B.; Bruening, M. L.; Baker, G. L. *Journal of the American Chemical Society* **2000**, *122*, 7616-7617.
(57) Matyjaszewski, K.; Shipp, D. A.; Wang, J.-L.; Grimaud, T.; Patten, T. E. *Macromolecules* **1998**, *31*, 6836-6840.
(58) Karanam, S.; Goossens, H.; Klumperman, B.; Lemstra, P. *Macromolecules* **2003**, *36*, 8304-8311.
(59) Schellekens, M. A. J.; de Wit, F.; Klumperman, B. *Macromolecules* **2001**, *34*, 7961-7966.
(60) Husseman, M.; Malmström, E. E.; McNamara, M.; Mate, M.; Mecerreyes, D.; Benoit, D. G.; Hedrick, J. L.; Mansky, P.; Huang, E.; Russell, T. P.; Hawker, C. J. *Macromolecules* **1999**, *32*, 1424-1431.
(61) Sedjo, R. A.; Mirous, B. K.; Brittain, W. J. *Macromolecules* **2000**, *33*, 1492-1493.
(62) Feng, J.; Haasch, R. T.; Dyer, D. J. *Macromolecules* **2004**, *37*, 9525-9537.
(63) Prucker, O.; Habicht, J.; Park, I.-J.; Rühe, J. *Materials Science & Engineering, C-Biomimetic and Supramolecular Systems* **1999**, *8-9*, 291-297.
(64) Matyjaszewski, K.; Davis, K.; Patten, T. E.; Wei, M. *Tetrahedron* **1997**, *53*, 15321-15329.
(65) Karanam, S.; Goossens, H.; Klumperman, B.; Lemstra, P. *Macromolecules* **2003**, *36*, 3051-3060.
(66) Xia, J.; Matyjaszewski, K. *Macromolecules* **1997**, *30*, 7697-7700.
(67) Boyes, S. G.; Brittain, W. J.; Weng, X.; Cheng, S. Z. D. *Macromolecules* **2002**, *35*, 4960-4967.
(68) Boyes, S. G.; Akgun, B.; Brittain, W. J.; Foster, M. D. *Macromolecules* **2003**, *36*, 9539-9548.
(69) Lee, M.-T.; Ferguson, G. S. *Langmuir* **2001**, *17*, 762-767.
(70) Fryxell, G. E.; Rieke, P. C.; Wood, L. L.; Engelhard, M. H.; Williford, R. E.; Graff, G. L.; Campbell, A. A.; Wiacek, R. J.; Lee, L.; Halverson, A. *Langmuir* **1996**, *12*, 5064-5075.
(71) Haensch, C.; Hoeppener, S.; Schubert, U. S. *Nanotechnology* **2008**, *19*, 035703/1-035703/7.
(72) Coessens, V.; Nakagawa, Y.; Matyjaszewski, K. *Polymer Bulletin* **1998**, *40*, 135-142.
(73) McMurry, J. *Organic Chemistry*; Fourth ed.; Brooks/Cole Publishing Company: Pacific Grove, 1996.
(74) Al-Bataineh, S. A.; Britcher, L. G.; Griesser, H. J. *Surface Science* **2006**, *600*, 952-962.

Chapter 4

Synthesis of Patterned Polymer Brushes by Microcontact Printing

4.1 Introduction

Microstructured and microfabricated materials are essential for much of modern technology, as a vital part of microelectronics and optoelectronics. Most commercial manufacture of such materials is done using photolithography[1]. However, there are disadvantages to this approach, so alternative patterning techniques are being investigated, giving access to new types of micropatterned materials, such as patterned SAMs. These can be made using microcontact printing (μCP): a SAM-forming molecule is deposited onto the substrate by direct contact with a relief-patterned elastomeric stamp. Patterned SAMs can be used as etch resists[1,2], or as templates to control the deposition of metals or to direct self-assembly of patterns of liquid droplets[2] (see p. 26 for further details). However, SAMs have several limitations: they form by self-assembly, so it is practically impossible to obtain large area defect-free monolayers[3], and pattern transfer is not as reliable as can be obtained routinely using photolithography[4]. SAMs form a very thin layer, and are not robust enough to be used as resists for dry processes such as reactive ion etching[5].

The amplification of a patterned SAM into a patterned polymer brush produces a macromolecular barrier which can mask defects within the underlying monolayer. The thicker, more robust layer is resistant to a wider range of etchants[5,6]. The use of polymers also allows much greater control over the chemical composition of the film: although a large range of functional groups can be incorporated in a SAM, these groups can only be introduced at the surface. In theory, any monomer can be used to prepare a polymer brush,

allowing the introduction of functional groups all along the polymer backbone, and, by the synthesis of block copolymer brushes, in spatially controlled architectures[3]. This gives access to interesting new patterned materials such as temperature-responsive, pH-sensitive or block copolymer brushes. Further amplification into a binary-patterned polymer brush may allow access to an even greater range of interesting materials with novel properties.

One of the goals of this project was to synthesise a binary-patterned polymer brush. At the start of this project (March 2005), this had only been done by methods requiring a photolithographic step[7-11]. It was felt to be desirable to develop an alternative approach, based on the use of μCP, and in principle, applicable to any polymer brush. The proposed method was to produce a patterned BMPUS SAM, then use it to grow a polymer brush by ATRP. The first brush would then be dehalogenated (to prevent the formation of block copolymers), and the remaining areas of the substrate coated with fresh initiator and used to grow the second brush. This is shown schematically in Figure 4.1 below.

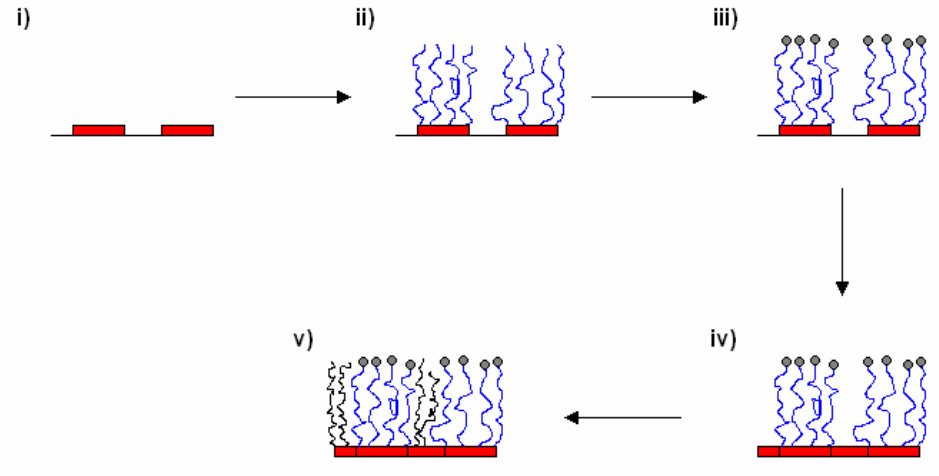

Figure 4.1 Proposed synthesis of a binary-patterned polymer brush by μCP and surface-initiated ATRP. i) μCP of BMPUS, ii) ATRP of first polymer brush, iii) dehalogenation of first brush, iv) backfill bare regions of substrate with BMPUS, v) grow second brush.

Methods for the synthesis of PMMA and PS brushes and the dehalogenation of PS brushes were discussed in Chapter 3. The next target was μCP of BMPUS and the production of patterned polymer brushes.

The formation of SAMs has been a subject of extensive study, and is well understood for alkylthiolate SAMs on gold substrates. Unfortunately, thiol SAMs are not stable to ambient conditions, and can undergo significant degradation within a day[12]. Alkyltrichlorosilanes can self-assemble on a wide range of substrates: oxidised silicon, silica particles, plasma-treated polymers[13], and, with suitable preparation, gold[14] and silicon nitride[15]. The self-assembly process is much more complicated and more sensitive to conditions than the gold/thiol system. Well controlled self-assembly is needed to produce a robust, dense initiator layer for the growth of patterned polymer brushes. Attempts were made to optimise the printing conditions to allow the reproducible production of dense, defect-free patterned polymer brushes. Patterned SAMs and polymer brushes were studied using AFM, SEM and optical microscopy.

4.2 Materials

Three different masters were used to make PDMS stamps:

1. Custom-made gallium arsenide master (EPSRC National Centre for III-V Technologies, University of Sheffield): arrays of squares, circles and triangles approx 100 μm across and 50 μm high, with varying spacing between the features. PDMS replicas of this master were made by Dr Shaomin Mai.
2. Blazed diffraction grating (Edmund Optics Ltd.), consisting of angled grooves, 1200/mm (approximately 833 nm per groove), blaze angle 36º 52′. The relief features were made of epoxy coated with aluminium.
3. An AFM calibration grid (TGZ04 silicon calibration grating, Mikro Masch) with square section lines, period 3 μm, step height 1040 nm. The master was made of silicon, with silicon dioxide steps, coated with a thin layer of silicon nitride.

PDMS stamps were made using Sylgard 184 silicone elastomer kit (Dow Corning), consisting of base and curing agent supplied in a 10: 1 ratio.

Anhydrous dichloromethane, toluene and *n*-hexane were obtained from a Solvent Purification System (Innovative Technology Inc., SPS-400-6 and SPS-200-6). Typical water contents were 9 ppm for dichloromethane, 16 ppm for toluene and 8 ppm for *n*-hexane.

All other reagents were prepared as described in Chapter 3, or used as received.

4.3 Experimental Methods

Homogeneous BMPUS SAMs and PMMA brushes were synthesised using the methods described in Chapter 3.

4.3.1 Preparation of PDMS Stamps

PDMS base (15 g) and curing agent (1.5 g) were added to a round-bottomed flask and degassed by stirring under low vacuum until the viscous mixture was homogeneous, and had stopped producing bubbles (~ 15 minutes). Pieces of poly(tetrafluoroethylene) (PTFE) were used to make a support for the master in a plastic petri dish. The degassed PDMS was carefully poured into the petri dish, and the master was placed face down in the PDMS, resting on the PTFE supports. The dish was transferred to a vacuum oven at 50 ºC and put under vacuum for ~ 2 minutes to encourage the PDMS to fill all the channels of the master, then left to cure at atmospheric pressure for at least 4 hours. Once the PDMS had set, it was removed from the petri dish and trimmed with a scalpel blade to leave the PDMS replica of the master[2,4].

4.3.2 Preparation of Master 3

Concentrated sulphuric acid (70 ml) was carefully added to 100 vol hydrogen peroxide (30 ml) (Piranha solution). The mixture reacts exothermically and bubbles violently. **Warning:** Piranha solution should be handled with extreme care. In some circumstances, most probably when it has been mixed with significant quantities of oxidisable organic material it has detonated unexpectedly[5]. After 1 hour, the master was removed from the piranha solution, rinsed with deionised water, then rendered hydrophilic by heating to 80 °C for 10 minutes in 100 vol hydrogen peroxide (50 ml), 37 wt% ammonia solution (50 ml) and deionised water (250 ml). The cleaned master was rinsed with copious quantities of deionised water, surface dried with nitrogen, then heated to 120 °C under vacuum for four hours to remove any traces of water.

The master was put into a PTFE dish with a tight fitting lid, covered with 20 ml dry dichloromethane and 12 μl OTS and left to react for 1 hour 10 minutes. The master was then rinsed with dichloromethane, then ethanol and finally with water[16].

4.3.3 Microcontact Printing

4.3.3.1 Method 1

Silicon wafers were cleaned and rendered hydrophilic as described in Chapter 3. BMPUS (0.8 ml) was added to dry toluene (32 ml) under nitrogen in a Young's flask. This BMPUS solution (25 μl/ml v/v) could be stored and used again. A small portion of the BMPUS solution was placed in a sample tube, then painted onto the surface of the PDMS stamp with a cotton bud. The stamp was dried with a stream of nitrogen, then placed on a freshly-cleaned piece of silicon, pressed gently to ensure complete contact, and left for between 10 and 120 seconds. The patterned wafers were then rinsed twice with toluene, once with acetone and finally with ethanol.

4.3.3.2 Method 2: Use of a Stamp Pad

Silicon wafers were cleaned and rendered hydrophilic as described in Chapter 3. A featured PDMS stamp and a plain, flat piece of PDMS (the ink pad) were plasma-oxidised with oxygen plasma, under varying conditions (see p. 134 for details). BMPUS (5 ml) was added to 20 ml dry *n*-hexane under nitrogen. A drop of the BMPUS solution was placed onto the ink pad, left for 5 seconds, then the excess liquid was blown off the surface, and the ink pad dried with a stream of nitrogen gas. The featured stamp was placed on the ink pad, pressed lightly to ensure complete contact, and left for 30 – 60 seconds. The stamp was then immediately placed on a piece of cleaned, surface oxidised silicon, pressed lightly and left for 30 – 60 seconds. The printed wafers were rinsed twice with *n*-hexane, once with acetone and finally with ethanol[17].

4.4 Characterisation

Characterisation by ellipsometry, XPS, and tapping mode AFM were performed as described in Chapter 3.

4.4.1 Scanning Electron Microscopy

Scanning electron microscopy was performed using a Camscan Mk 2 SEM with an X and Y motorised stage, 7 nm resolution in secondary electron (SE) mode, and SE, BSE and SC detectors.

4.4.2 Optical Microscopy/Differential Condensation

Images were collected with an Olympus BX50 microscope, using a Prior Lite high intensity illuminator (Prior Scientific) as an external light source (NB. This only works for relatively low magnifications, where the focal length is high enough to allow the external light source to illuminate the sample sufficiently). Samples were cooled using a Linkam THMS 600 Heating and Freezing Stage controlled by Linksys software. Transitory condensation figures were produced

by cooling the samples in the ambient air. The cooling conditions had to be fine-tuned for each measurement – presumably due to changes in humidity and air temperature near the microscope.

4.5 Results and Discussion

4.5.1 Preparation of PDMS Stamps

PDMS is the most commonly used material to make stamps for μCP[18]. It is usually purchased in kit form (e.g. Sylgard 184) which consists of PDMS base (vinyl silane-terminated PDMS prepolymers), and a curing agent/catalyst, which contains short PDMS chains (cross-linkers), and a platinum-based catalyst. When the components are mixed, vinyl silane groups in the prepolymers react with silane hydrogens in the cross-linkers in the presence of the platinum catalyst, to form a cross-linked PDMS elastomer[18], as shown in Scheme 4.1.

PDMS stamps for μCP were made by mixing PDMS base and curing agent in a 10: 1 ratio, degassing to remove air bubbles, then pouring over a master: a substrate with suitably sized relief features. The PDMS was cured at 50 ºC for at least 4 hours, although other curing temperatures and times have been used by other workers[2,18-21]. The flexible nature of the elastomer meant that it could be released easily from the mould structures[22]. Three different structures were used as masters to make PDMS stamps.

A wide range of different structured materials have been used as masters to make stamps for μCP. Some groups used masters without any preparation[2,4,23]. Others coated masters with alkyl-[19], or fluoro- [18,20,22,24] functionalised SAMs, to ensure that the PDMS stamp could be cleanly removed from the master after curing. The first two masters were used to make stamps without any preparation (they had already been used to produce stamps by other members of the group without any problems). It was decided to prepare the third master by coating it with OTS. The master was cleaned and surface-oxidised, then placed in a 1.5 mM

Scheme 4.1 Structure of PDMS prepolymers, and cross-linking reaction to generate PDMS elastomers[25]

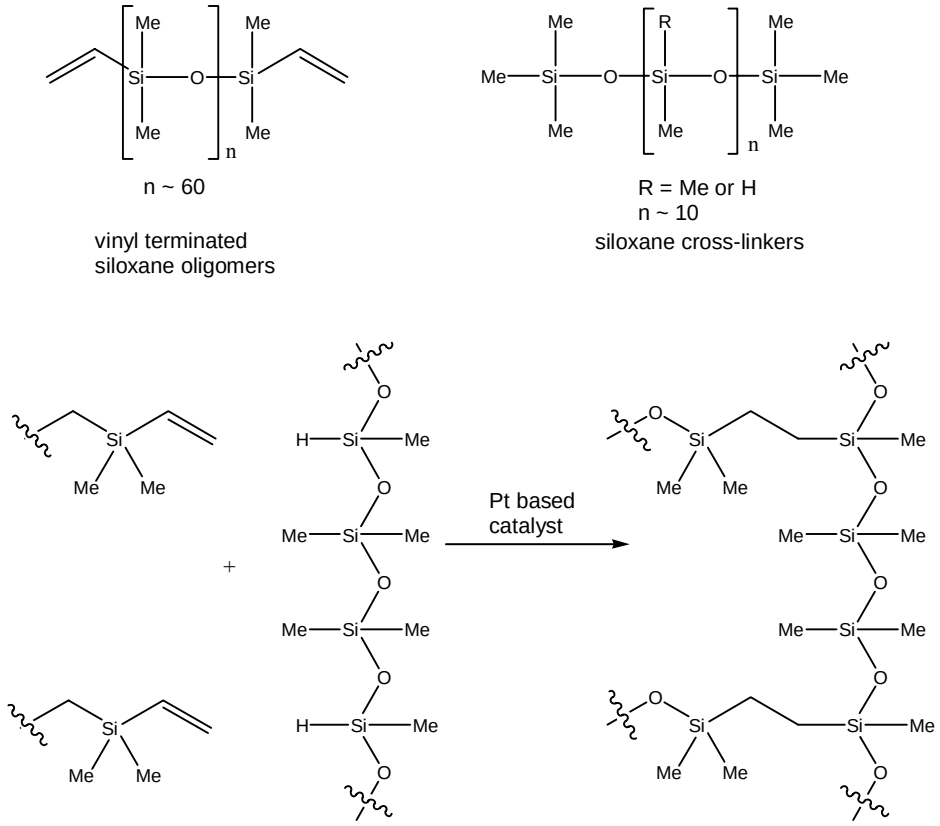

solution of OTS in dichloromethane. After this treatment, the master was used to make good quality PDMS stamps which could be released easily from the mould.

An elastomeric stamp is required for μCP. PDMS can conform to the surface of the substrate over a large area, even if it is non-planar on the sub-micrometre scale. Its low interfacial energy means that most molecules do not adhere to, or react with the stamp. Cross-linked PDMS is elastic and durable, so stamps can be released easily from complex and fragile surfaces, and stamps can be used many times without degradation. PDMS is homogeneous, isotropic and optically transparent down to 300 nm (this allows in situ ultra-violet curing of suitable polymers)[1,22]. Finally, its surface properties can be readily modified, most commonly by plasma treatment[22,26], sometimes followed by chemical attachment of desired functional groups[27-29].

The PDMS stamps were imaged using SEM. The stamps replicated the features of the masters over large areas, although there were defects on both small and large scales (cracks, surface roughness, tears and holes). As the focus of this project was the production of binary-patterned brushes, these defects were not considered to be a problem. Some examples of typical images are shown in Figure 4.2 below.

Feature sizes were measured from the SEM images, and compared to the reported values for each master. The measured values were all close to the reported feature sizes. For the third master, SEMs were recorded at different angles, and trigonometry was used to calculate the feature height. The average feature height was calculated to be 933 nm, compared to the reported feature height of the master (1040 nm). The difference is probably due to inaccuracies in the measurement technique, though PDMS is known to shrink by approximately 1 % during curing[22]. For this project, the fidelity of replication of

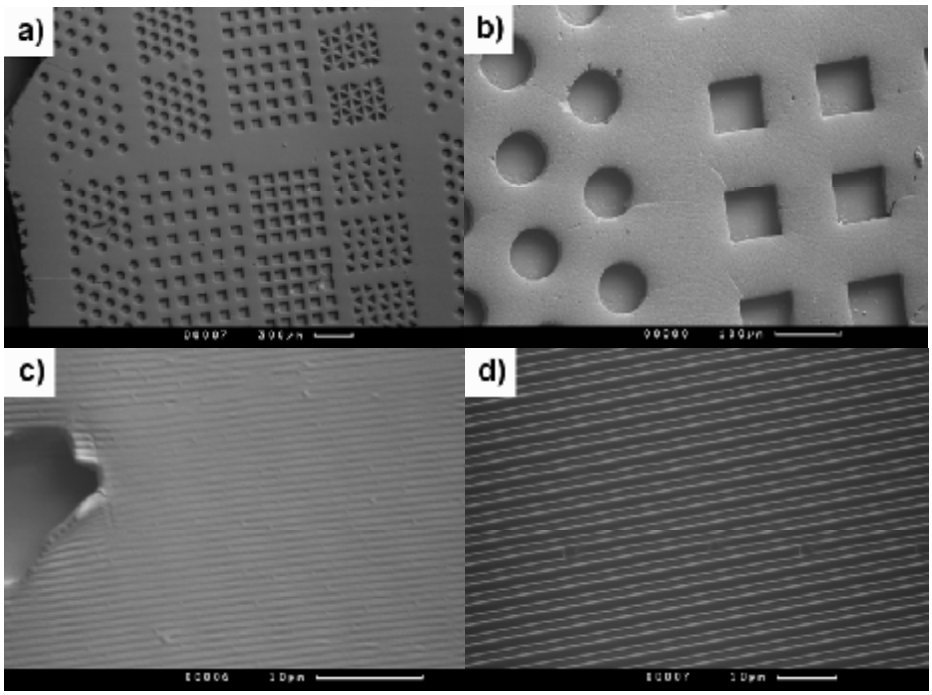

Figure 4.2 SEM micrographs of PDMS stamps, scale bars as shown. (a), (b) Stamp 1, some surface roughness and cracking is visible. (c) Stamp 2, (d) Stamp 3. Scale bars as shown.

the master was not important. What was required was a stamp with features that could be visualised by AFM and other techniques, and sufficient relief to reduce reactive spreading and prevent sagging.

All three stamps were used to produce patterned SAMs and polymer brushes. Stamp 1 was used in the early stages of the project, but the features were too large to image by AFM. Patterned SAMs were visualised indirectly by cooling samples under ambient conditions, and recording the transitory condensation patterns (an example is shown below in Figure 4.3). Patterned polymer brushes produced using this stamp were imaged using SEM (see p. 141). The second stamp was a replica of a blazed diffraction grating, which had a much smaller pattern size that could easily be visualised by AFM. However, the angled nature of the features was felt to be a potential problem: Xia *et al.*[30] used blazed diffraction gratings to produce stamps for μCP. They found that attractive forces between stamp and substrate resulted in deformation of the stamp, so the printed area was much larger than the bare areas. This would not be ideal for the formation of binary-patterned brushes, as excessive pressure and/or contact time could easily result in loss of the pattern. The comparatively small size and low height of the features could encourage diffusion of silane vapour from the ink into the voids between the stamp features, followed by deposition onto areas of silicon not contacted by the stamp[31,32]. To overcome these potential problems, a third master was obtained and used to make PDMS stamps with a pattern of

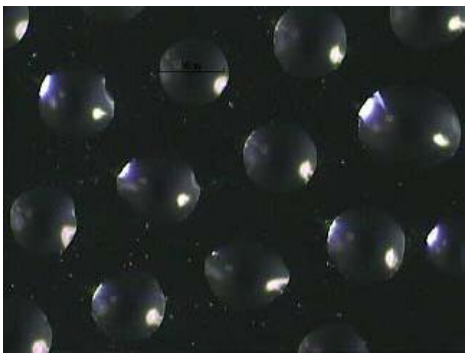

Figure 4.3 Optical micrograph of transitory condensation pattern formed by cooling a printed SAM under ambient conditions.

square section lines, period ~ 3 μm, height ~ 1 μm. This feature size could be easily imaged using AFM and other techniques, and the height of the lines would hopefully limit the amount of silane spreading.

4.5.2 Non-patterned Initiator SAMs

SAMs are formed spontaneously by chemisorption and self-organisation of functionalised long chain organic molecules onto the surface of an appropriate substrate, for example alkanethiolates on gold substrates, and alkyl trichlorosilanes on silicon. Densely packed, ordered layers can be produced by adsorption from solution, exposure to vapour or by μCP[1,22].

Functionalised SAMs have been used for the growth of polymer brushes by several different surface-initiated polymerisation methods. For example, Husseman *et al*.[33] used an alkoxyamine-functionalised SAM to initiate NMP of styrene, Feng *et al*.[34] synthesised an AIBN-based thiol which was used to grow mixed PS/PMMA brushes by photoinitiated free radical polymerisation. However, ATRP has become the most popular method for brush growth, as it is easier to synthesise initiator-functionalised thiols or silanes[35]. For example, ω-mercaptoundecyl bromoisobutyrate, $HS(CH_2)_{11}OCOC(CH_3)_2Br$, has been widely used for the synthesis of unpatterned[36-38], patterned[39,40] and binary patterned polymer brushes[41] on gold substrates.

As discussed in Chapter 3, it was decided to focus on the synthesis of polymer brushes on silicon substrates by ATRP from BMPUS, an α-bromoester functionalised alkyltrichlorosilane. In addition to this initiator, other similar silanes have also been used for the synthesis of unpatterned[42-50] and patterned[13,17,51] polymer brushes. The reaction of alkyltrichlorosilanes with –OH terminated substrates is very sensitive to the deposition conditions[32,52], and the trifunctional nature of the alkyltrichlorosilane group also means that there is more than one possible surface structure (see p. 23).

4. Synthesis of Patterned Polymer Brushes by μCP

Unpatterned BMPUS SAMs were produced using a common literature method: silicon wafers were cleaned and rendered hydrophilic, then dried and exposed to a dilute solution of the initiator silane in toluene, in the presence of triethylamine[43,45]. Several studies have suggested that alkyltrichlorosilane SAMs form by hydrolysis of the trichlorosilane groups and polymerisation of the resulting silanol groups to produce a cross-linked siloxane network, without significant bonding to surface –OH groups[14,15,52]. However, addition of an amine was found to alter the process: the amine forms strong hydrogen bonds to surface –OH groups, increasing their nucleophilicity, and allowing them to react directly with the silicon of the alkyltrichlorosilane[52]. The reaction was performed under 'semi-dry' conditions: dry solvents were used, and the silicon substrates were dried at 120 ºC under vacuum (though this may still leave 1 – 2 monolayers of residual water on the surface[53]). The substrates were then left to react with the initiator solution exposed to a limited amount of ambient, moisture-containing, air. Under similar conditions, Edmondson and Huck[43] found that adding triethylamine to the initiator solution improved the quality of surface-attached layers of a similar molecule. Without base, large particles of cross-linked siloxanes were deposited on the surface. The method used was found to produce a smooth initiator layer (an example is shown in Figure 4.4), which could then be used to produce polymer brushes (see Chapter 3 for details of brush growth).

Some samples were prepared using different methods: silicon substrates were also oxidised by exposure to UV/ozone for 30 minutes, then dried and exposed to the initiator solution as above. The drying step could be omitted without any apparent change in the quality or function of the initiator SAM (this fits well with the discussion above). Finally, an initiator layer was also produced by immersing freshly oxidised silicon in a solution of 1.25 μl initiator in 10 ml cold toluene, and leaving it to react for 5 – 15 hours in the freezer[50]. This also gave a smooth active initiator layer, although it was approximately 0.8 nm thicker than the SAMs produced at room temperature.

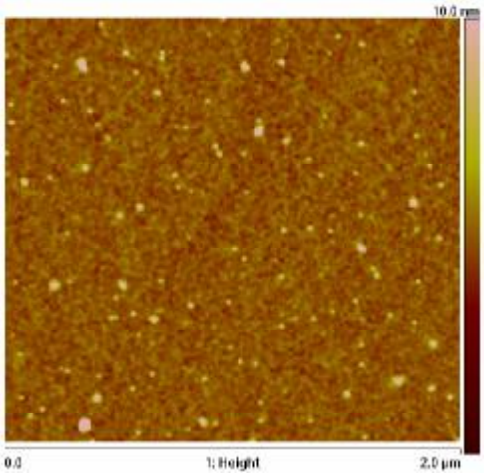

Figure 4.4 Tapping mode AFM of BMPUS SAM, 2 x 2 μm. Rms 0.678 nm, R_a 0.345 nm.

The XPS of BMPUS-coated silicon is shown in Figure 4.5 below. It revealed the presence of silicon, oxygen (mainly from the substrate), carbon and bromine. The ratio of C: Br was 25: 1, higher than 15: 1 predicted from the structure of BMPUS. However, bromine-terminated monolayers are known to be susceptible to x-ray-induced damage[54], which could explain the discrepancy. The high resolution spectrum of the C 1s region was curve-fitted to four different carbon environments in a ratio of 9: 1: 2: 1. These can be assigned to saturated hydrocarbon (C1, chain CH_2 groups and methyl groups adjacent to Br), C*-C-O-C(=O) (C2), C*-O-C(=O) and C(=O)-C*-Br (C3) and –O-C(=O) (C4) (see Figure 4.5 c) for details of the assignment of the different environments). The structure of BMPUS has 11 aliphatic chain carbons (C1). The lower than predicted abundance of C1 is a common feature of ordered systems such as SAMs. The signal for carbons nearer the substrate is somewhat attenuated compared to the signal from surface carbons due to the lower probability of the photoelectrons escaping the surface without undergoing an energy loss event[55].

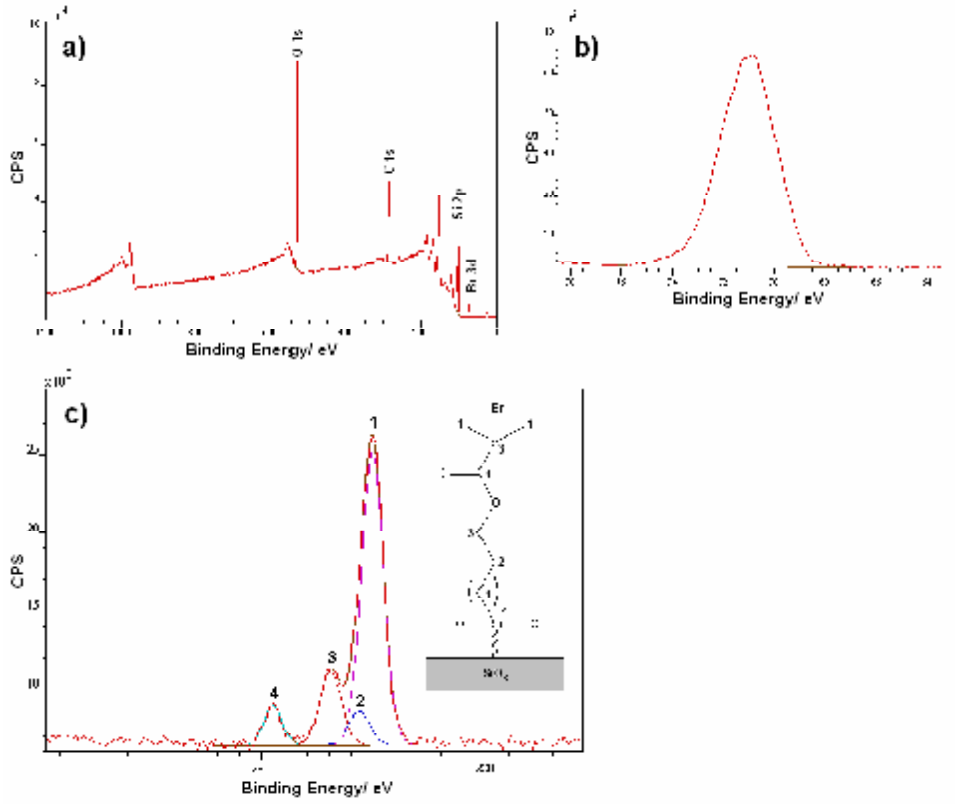

Figure 4.5 XPS of BMPUS SAM on silicon; a) survey scan, b) magnified view of Br 3d region of survey scan, c) high resolution spectrum of C 1s region

4.5.3 Patterned SAMs and Polymer Brushes

The PDMS stamps were used for μCP of BMPUS. μCP of simple alkyltrichlorosilanes has been well studied[31,32,56-58]. If a pattern of a functionalised silane is required (e.g. for the synthesis of patterned polymer brushes), the most common approach is to print a solution of a simple alkyltrichlorosilane, such as OTS[5,31,32,51,56-60], then 'backfill' the unpatterned areas with a solution of a second alkyltrichlorosilane with the desired functional group[5,51,59]. However, this approach would prevent the production of binary patterned polymer brushes, so it was necessary to print BMPUS. There are examples in the literature of μCP of functionalised alkyltrichlorosilanes[13,17], including examples of the printing of shorter chain α-bromoesters, and their use to produce patterned polymer brushes[13,17]; however, no examples of the μCP of BMPUS were found. As discussed in Chapter 1, the formation of

alkyltrichlorosilane SAMs by μCP is very sensitive to the deposition conditions, including the amount of water present in the reaction environment (in the solvents and reagents, on/in the stamp and in the ambient air), the temperature, the type and cleanliness of the substrate, the solvent used in the ink, the concentration of the active molecule in the ink[32,58], and the contact time[32]. Many of these variables are difficult to control, and can vary widely between different laboratories[32] (or even on different days). This makes optimisation of conditions something of a difficult and black art! Because of this, it was necessary to try a range of different conditions to attempt to optimise the process. After growth of the first brush, the desired result was a clearly patterned surface, made up of smooth, dense polymer brush, with little or no brush outside the printed regions.

In initial experiments, a solution of BMPUS in dry toluene was painted onto the stamps with a cotton bud. The stamp was either left until it appeared dry, or dried with nitrogen for 30 s, then applied to a prepared piece of silicon for varying contact times. Excess reagents were removed by rinsing in toluene, acetone and ethanol. Printing was tried with concentrations of 'ink' between 0.15 % and 20 % (v/v), and contact times between 10 and 120 seconds. Samples were then used to grow PMMA brushes, which were analysed by AFM.

The results of these experiments were disappointing: the most convincing patterns were produced by printing 2.5 % (v/v) initiator solution for 60 s. Although the samples were definitely patterned, with linear features with a period of approximately 800 nm, the patterns were faint and obviously made up of discontinuous islands of material (up to 25 nm high). One of the best examples is shown in Figure 4.6.

It was thought that the 'islands' were formed by deposition of cross-linked siloxane particles produced by polymerisation of BMPUS on exposure to moisture from the atmosphere and stamp. These features were then amplified by brush growth from the unevenly distributed, dense initiator regions.

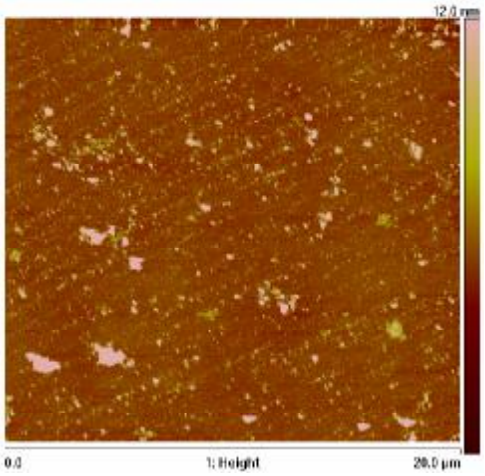

Figure 4.6 Tapping mode AFM of patterned PMMA brush, 20 x 20 μm. Conditions: Stamp 2, 2.5 % initiator in toluene, printing time 60 s. PMMA brush, reaction time 8 hours (for PMMA brush growth conditions see Chapter 3).

A second approach was tried, based on a method used to print a similar alkyltrichlorosilane; 2-bromo-2-methylpropionic acid 3-trichlorosilanylpropyl ester[17]. 5 μl of BMPUS was dissolved in 20 ml dry *n*-hexane. A drop of this solution was placed on a flat piece of PDMS (the ink pad). After 5 – 10 seconds, the excess material was blown off the surface with a stream of nitrogen. The featured stamp was placed on the ink pad, pressed very gently to ensure conformal contact, and left for 30 s. The featured stamp was then transferred to a prepared piece of silicon, lightly pressed, and again left for 30 s[17]. This resulted in very faint, but apparently even, patterns (not shown).

The low brush thickness was not surprising considering the extremely low concentration of the initiator solution (equivalent to 0.25 μl/ml or 0.025 % v/v) – 100 times more dilute than the 'ink' which gave the patterns in Figure 4.6. It was decided to try oxidising the stamp and ink pad with an oxygen plasma. This is used to increase the hydrophilicity of PDMS to allow hydrophilic 'inks' to wet the stamp, and improve the quality of printing[26-29]. Plasma oxidation acts on the siloxane chains of the PDMS, producing a thin, glassy silica-like layer at the surface[26,27,29]. The 'ink' used is hydrophobic, so this preparation should not be necessary to wet the surface of the PDMS. It is more likely that the glassy silica

layer at the surface acts as a barrier, preventing loss of the minute amounts of BMPUS by diffusion into the stamp, and so increasing the transfer of initiator to the silicon surface. This method gave clearly patterned polymer brushes: an example is shown in Figure 4.7.

In the first experiments the PDMS stamp and ink pad were plasma-oxidised for 120 s at a power of 300 W at 0.8 Torr. This was loosely based on conditions found by Langowski and Uhrich[26] to prevent the transfer of low molecular weight siloxane fragments to surfaces and retain a smooth or rippled PDMS surface with no cracks. The plasma oxidiser used in these experiments was not designed for use with organic substrates, and it was not possible to access the gas pressures used in the reference; it was also difficult to predetermine the parameters (except exposure time). The relatively long exposure time did produce patterned brushes, but several samples show defects which appear to be due to cracking of the glassy layer on the surface of the stamp (some examples are shown in Figure 4.8). An attempt was made to investigate the effect of different plasma oxidation conditions. Pieces of PDMS were exposed to an oxygen plasma for different lengths of time (as discussed above, it was difficult to control the other parameters), then contact angles were measured. Untreated

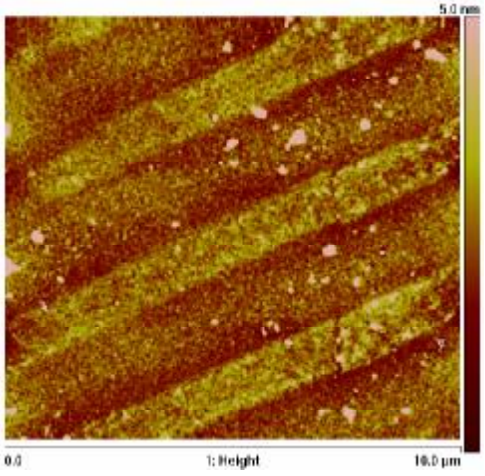

Figure 4.7 Tapping mode AFM of PMMA brush, 10 x 10 μm. Conditions: ink pad method, with a plasma-oxidised stamp, plasma exposure time 120 s. PMMA brush: reaction time 10 hours.

PDMS has an average contact angle of ~ 73º. Exposure to plasma for as little as 10 seconds was found to decrease the contact angle by ~ 20º. The contact angle tended to decrease further with increasing exposure time, although this was not a linear trend, and there were some exceptions. It was anticipated that a shorter plasma oxidation would give a thinner, and hopefully more flexible, glassy surface layer. Patterned polymer brushes were successfully produced using

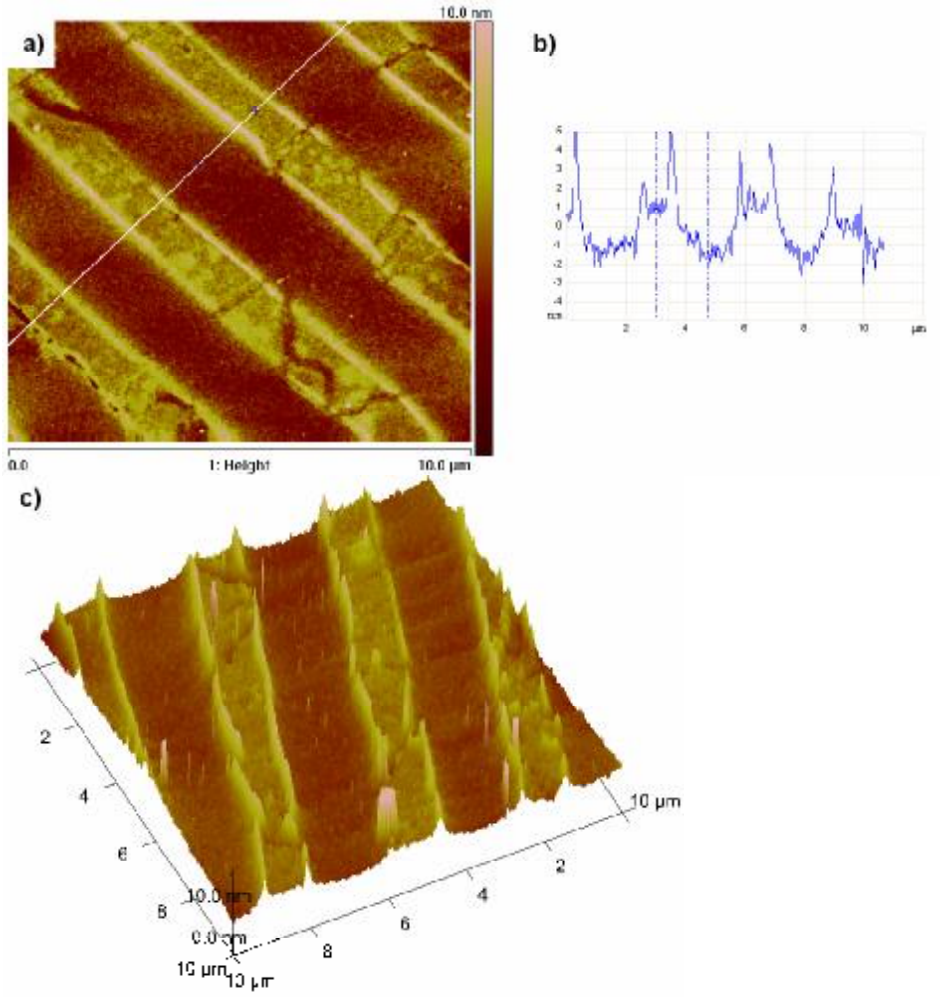

Figure 4.8 Tapping mode AFMs of patterned PMMA brushes showing cracking and hillocks. a), b) stamp and ink pad plasma-oxidised for 120 s, n-hexane method, stamp in contact with stamp pad 30 s, stamp in contact with Si 30 s, PMMA brush grown for 7 hours , b) height profile (location shown by white line in a), height difference between markers: 2.97 nm, maximum height difference ~ 6.73 nm. c) three-dimensional view of a different sample, ink pad and stamp plasma-oxidised for 120 s, n-hexane method, stamp in contact with stamp pad 30 s, stamp in contact with Si 30 s, PMMA grown 11 hours.

stamps which were plasma-oxidised for 20 s, and there was no sign of surface cracking.

A second defect, which can also be seen in Figure 4.8, was the formation of raised 'rims' at the edges of the printed regions. Imperfect casting and solvent-induced swelling means that PDMS stamps are not exact replicas of the master, and usually have rounded edges. If there is any excess ink it undergoes capillary condensation towards the edges of the raised features of the stamp, resulting in the formation of rims at the edges of the printed features[19]. In this case, the excess BMPUS can then react with atmospheric moisture, generating a stable, cross-linked hillock which was still visible after the growth of polymer brush. It seems surprising that these formed considering the low concentration of the active molecule in the ink. It is possible, however, that the higher concentration of initiator results in a higher grafting density, and so thicker brush (more stretched polymer chains) at the edges of the pattern.

Excess ink and contact times can lead to diffusion/spreading of the trichlorosilane into regions not contacted by the stamp[32]. This 'reactive spreading' was observed at longer contact times (e.g. 120 s). The process is quite complex, with several different mechanisms operating at the same time. Delamarche *et al.*[61] described the processes involved as part of work on optimising μCP of alkanethiols on gold – the reader is referred to their work for a fuller explanation.

SEM was also used to image patterned brushes (see Figure 4.9). The patterns could be seen clearly, but there was extensive cracking and islands of material outside the printed regions. It is worth noting that the low height of the patterned brushes (from the AFM images) is around the minimum height resolution of the SEM, so it was not possible to produce clearer images.

Printing was tried with different plasma oxidation conditions, ink concentrations and contact times, to try to find conditions which would give a defect-free initiator layer that could produce patterned polymer brushes. A balance was

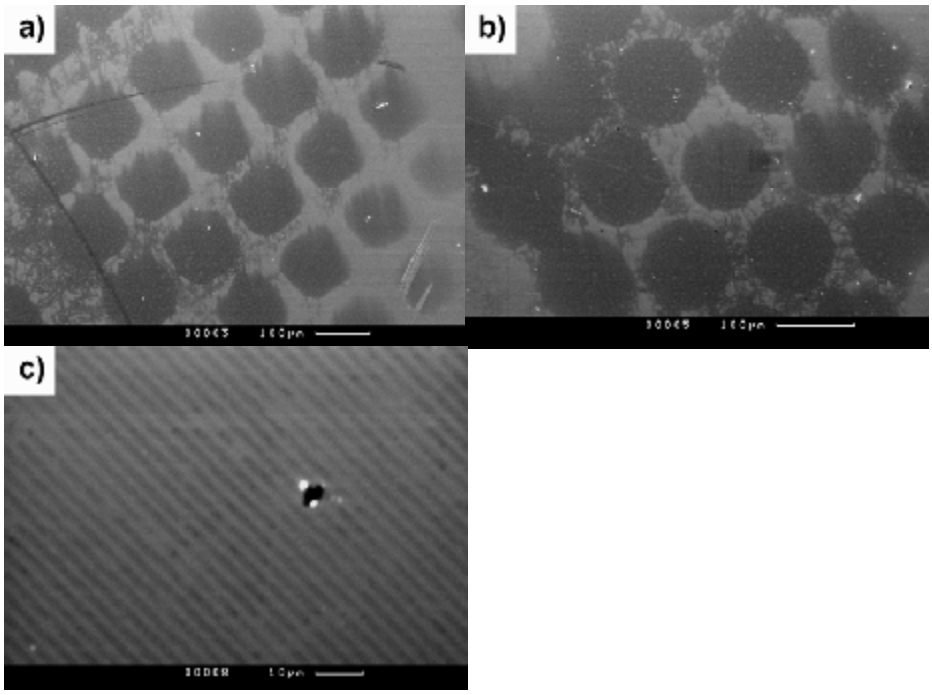

Figure 4.9 SEM images of patterned PMMA brushes, scale bars as shown. (a), (b) large scale patterns produced using stamp 1 showing cracking and reactive spreading, (c) small scale pattern produced using stamp 2.

needed between too much ink, leading to hillock formation and brush growth outside the printed areas, and too little ink, giving a discontinuous layer made up of islands of brush. Another factor is the amount of water in the reaction environment. Water plays an important role in the formation of alkyltrichlorosilane SAMs. Insufficient humidity leads to lower film growth rates and lower mass coverage[58], but excessive moisture can lead to cross-linking of the initiator in solution. Humidity was not controlled or monitored in these experiments, which were performed in an open laboratory, so this could explain some of the variation between samples.

A final piece of the puzzle was the low thickness of the patterned polymer brushes – the maximum thickness was < 5 nm, compared to ~ 15 nm for non-patterned brushes grown for similar reaction times. It is possible that the low concentration of BMPUS in the ink produced a homogeneous, but submonolayer coverage of initiator. When exposed to polymerisation conditions, the low

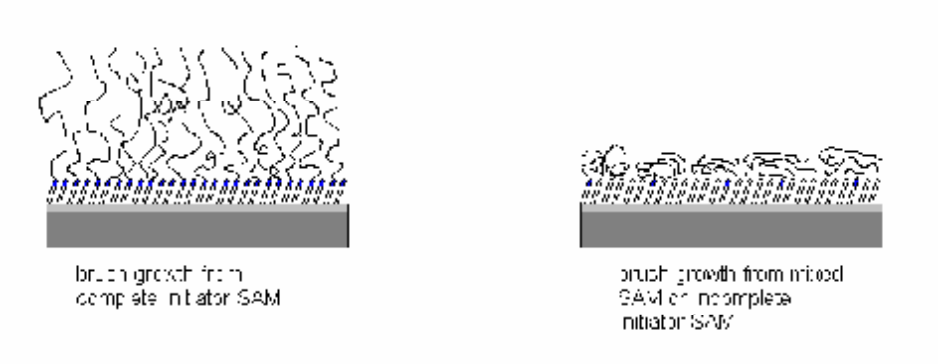

Figure 4.10 Different chain morphologies produced by polymer growth from complete and incomplete initiator SAMs[36].

density of initiating sites meant that the polymer chains did not adopt the highly stretched conformation of a true polymer brush, but instead spread across the surface in a 'pancake' morphology. Similar effects have been observed for polymer brushes grown from SAMs where the initiator is diluted by a non-functionalised analogue[36]. This is shown schematically in Figure 4.10.

4.6 Summary

The μCP of alkyltrichlorosilanes on oxidised surfaces is more difficult than printing thiols on gold. Film formation in μCP is affected by many variables, including the amount of water present in the reaction environment, temperature, type and cleanliness of substrate, solvent, concentration of the ink[32,58], contact time[32] and method used (such as use of a ink pad)[19]. It proved impossible to control and optimise all these factors to reliably produce defect-free patterns of dense polymer brush. This prevented further development towards the production of binary-patterned brushes. Zhou *et al.*[41] used an analogous approach to produce up to quaternary-patterned brushes on gold substrates. ω-Mercaptoundecyl bromoisobutyrate was printed, and used to grow polymer brushes by ATRP. Sequential printing and brush growth with different stamps and monomers produced up to quaternary-patterned brushes.

4. Synthesis of Patterned Polymer Brushes by μCP

A further problem, not anticipated at the start of the project was the need to activate/oxidise the silicon to provide sufficient silanol groups for the initiator to interact with. Polymer brushes could not be grown from silicon wafers that were not oxidised by RCA or UV/ozone before reaction with the initiator solution. However, exposure of a patterned brush to such oxidising conditions would probably alter the structure of the polymer, or remove it. It is possible that the surface activation of the silicon may be retained through the first polymerisation, allowing backfilling with BMPUS. Alternatively, PS is known to be more resistant to air plasma etching than PMMA[62], and may be able to withstand brief exposure to reactivate the silicon surface. A final option would be to use two different polymerisation techniques. For example, a pattern of ATRP initiator could be produced by μCP, then a NMP initiator-functionalised silane could be used to backfill the surface. A binary-patterned brush could then be produced by sequential ATRP and NMP. This approach was used by Zhao and He[63] to produce mixed PMMA/PS brushes, and a related approach has since been used to synthesise binary-patterned brushes, although the patterned initiator layer was not produced by μCP[9].

4.7 References

(1) Xia, Y.; Whitesides, G. M. *Annual Review of Materials Science* **1998**, *28*, 153-184.
(2) Kumar, A.; Biebuyck, H. A.; Whitesides, G. M. *Langmuir* **1994**, *10*, 1498-1511.
(3) Zhou, F.; Huck, W. T. S. *Physical Chemistry Chemical Physics* **2006**, *8*, 3815-3823.
(4) Shah, R. R.; Merreceyes, D.; Husemann, M.; Rees, I.; Abbott, N. L.; Hawker, C. J.; Hedrick, J. L. *Macromolecules* **2000**, *33*, 597-605.
(5) Jeon, N. L.; Choi, I. S.; Whitesides, G. M.; Kim, N. Y.; Laibinis, P. E.; Harada, Y.; Finnie, K. R.; Girolami, G. S.; Nuzzo, R. G. *Applied Physics Letters* **1999**, *75*, 4201-4203.
(6) Husemann, M.; Mecerreyes, D.; Hawker, C. J.; Hedrick, J. L.; Shah, R.; Abbott, N. L. *Angewandte Chemie, International Edition* **1999**, *38*, 647-649.
(7) Husemann, M.; Morrison, M.; Benoit, D.; Frommer, J.; Mate, C. M.; Hinsberg, W. D.; Hedrick, J. L.; Hawker, C. J. *Journal of the American Chemical Society* **2000**, *122*, 1844-1845.
(8) Zhou, F.; Jiang, L.; Liu, W.; Xue, Q. *Macromolecular Rapid Communications* **2004**, *25*, 1979-1983.
(9) Xu, F. J.; Song, Y.; Cheng, Z. P.; Zhu, X. L.; Zhu, C. X.; Kang, E. T.; Neoh, K. G. *Macromolecules* **2005**, *38*, 6254-6258.
(10) Tovar, G.; Paul, S.; Knoll, W.; Prucker, O.; Rühe, J. *Supramolecular Science* **1995**, *2*, 89-98.
(11) Prucker, O.; Habicht, J.; Park, I.-J.; Rühe, J. *Materials Science & Engineering, C-Biomimetic and Supramolecular Systems* **1999**, *8-9*, 291-297.
(12) Willey, T. M.; Vance, A. L.; van Buuren, T.; Bostedt, C.; Terminello, L. J.; Fadley, C. S. *Surface Science* **2005**, *576*, 188-196.
(13) Farhan, T.; Huck, W. T. S. *European Polymer Journal* **2004**, *40*, 1599-1604.
(14) Allara, D. L.; Parikh, A. N.; Rondelez, F. *Langmuir* **1995**, *11*, 2357-2360.
(15) Sung, M. M.; Kluth, G. J.; Maboudian, R. *Journal of Vacuum Science & Technology, A: Vacuum, Surfaces, and Films* **1999**, *17*, 540-544.
(16) Fragneto, G.; Lu, J. R.; McDermott, D. C.; Thomas, R. K.; Rennie, A. R.; Gallagher, P. D.; Satija, S. K. *Langmuir* **1996**, *12*, 477-486.
(17) Hamelinck, P. J.; Huck, W. T. S. *Journal of Materials Chemistry* **2005**, *15*, 381-385.
(18) Choi, K. M. *Journal of Physical Chemistry B* **2005**, *109*, 21525-21531.
(19) Pompe, T.; Fery, A.; Herminghaus, S.; Kriele, A.; Lorenz, H.; Kotthaus, J. P. *Langmuir* **1999**, *15*, 2398-2401.
(20) Deng, T.; Ha, Y.-H.; Cheng, J. Y.; Ross, C. A.; Thomas, E. L. *Langmuir* **2002**, *18*, 6719-6722.
(21) Libioulle, L.; Bietsch, A.; Schmid, H.; Michel, B.; Delamarche, E. *Langmuir* **1999**, *15*, 300-304.

(22) Xia, Y.; Whitesides, G. M. *Angewandte Chemie, International Edition* **1998**, *37*, 550-575.
(23) Wilbur, J. L.; Kumar, A.; Biebuyck, H. A.; Kim, E.; Whitesides, G. M. *Nanotechnology* **1996**, *7*, 452-457.
(24) Burgin, T.; Choong, V.-E.; Maracas, G. *Langmuir* **2000**, *16*, 5371-5375.
(25) Whitesides, G. M., Soft Lithography (I) - lecture slides, Harvard University.
(26) Langowski, B. A.; Uhrich, K. E. *Langmuir* **2005**, *21*, 6366-6372.
(27) Donzel, C.; Geissler, M.; Bernard, A.; Wolf, H.; Michel, B.; Hilborn, J.; Delamarche, E. *Advanced Materials* **2001**, *13*, 1164-1167.
(28) He, Q.; Liu, Z.; Xiao, P.; Liang, R.; He, N.; Lu, Z. *Langmuir* **2003**, *19*, 6982-6986.
(29) Delamarche, E.; Donzel, C.; Kamounah, F. S.; Wolf, H.; Geissler, M.; Stutz, R.; Schmidt-Winkel, P.; Michel, B.; Mathieu, H. J.; Schaumburg, K. *Langmuir* **2003**, *19*, 8749-8758.
(30) Xia, Y.; Tien, J.; Qin, D.; Whitesides, G. M. *Langmuir* **1996**, *12*, 4033-4038.
(31) Finnie, K. R.; Haasch, R.; Nuzzo, R. G. *Langmuir* **2000**, *16*, 6968-6976.
(32) Jeon, N. L.; Finnie, K.; Branshaw, K.; Nuzzo, R. G. *Langmuir* **1997**, *13*, 3382-3391.
(33) Husseman, M.; Malmstroem, E. E.; McNamara, M.; Mate, M.; Mecerreyes, D.; Benoit, D. G.; Hedrick, J. L.; Mansky, P.; Huang, E.; Russell, T. P.; Hawker, C. J. *Macromolecules* **1999**, *32*, 1424-1431.
(34) Feng, J.; Haasch, R. T.; Dyer, D. J. *Macromolecules* **2004**, *37*, 9525-9537.
(35) Huck, W. T. S.; Edmondson, S.; Osborne, V. L. *Chemical Society Reviews* **2004**, *33*, 14-22.
(36) Jones, D. M.; Brown, A. A.; Huck, W. T. S. *Langmuir* **2002**, *18*, 1265-1269.
(37) Huang, W.; Kim, J.-B.; Bruening, M. L.; Baker, G. L. *Macromolecules* **2002**, *35*, 1175-1179.
(38) Kim, J.-B.; Huang, W.; Bruening, M. L.; Baker, G. L. *Macromolecules* **2002**, *35*, 5410-5416.
(39) Osborne, V. L.; Jones, D. M.; Huck, W. T. S. *Chemical Communications* **2002**, 1838-1839.
(40) de las Heras Alarcon, C.; Farhan, T.; Osborne, V. L.; Huck, W. T. S.; Alexander, C. *Journal of Materials Chemistry* **2005**, *15*, 2089-2094.
(41) Zhou, F.; Zheng, Z.; Yu, B.; Liu, W.; Huck, W. T. S. *Journal of the American Chemical Society* **2006**, *128*, 16253-16258.
(42) Matyjaszewski, K.; Miller, P. J.; Shukla, N.; Immaraporn, B.; Gelman, A.; Luokala, B. B.; Siclovan, T. M.; Kickelbick, G.; Vallant, T.; Hoffmann, H.; Pakula, T. *Macromolecules* **1999**, *32*, 8716-8724.
(43) Edmondson, S.; Huck, W. T. S. *Journal of Materials Chemistry* **2004**, *14*, 730-734.
(44) Kong, X.; Kawai, T.; Abe, J.; Iyoda, T. *Macromolecules* **2001**, *34*, 1837-1844.
(45) Topham, P. D.; Howse, J. R.; Crook, C. J.; Parnell, A. J.; Geoghegan, M.; Jones, R. A. L.; Ryan, A. J. *Polymer International* **2006**, *55*, 808-815.
(46) Yu, W. H.; Kang, E. T.; Neoh, K. G. *Langmuir* **2004**, *20*, 8294-8300.

(47) Granville, A. M.; Boyes, S. G.; Akgun, B.; Foster, M. D.; Brittain, W. J. *Macromolecules* **2004**, *37*, 2790-2796.
(48) Boyes, S. G.; Brittain, W. J.; Weng, X.; Cheng, S. Z. D. *Macromolecules* **2002**, *35*, 4960-4967.
(49) Boyes, S. G.; Akgun, B.; Brittain, W. J.; Foster, M. D. *Macromolecules* **2003**, *36*, 9539-9548.
(50) Tomlinson, M. R. Surface-Grafted Polymer and Copolymer Assemblies with Gradient in Molecular Weight and Composition, PhD thesis, North Carolina State University, 2005.
(51) Tu, H.; Heitzman, C. E.; Braun, P. V. *Langmuir* **2004**, *20*, 8313-8320.
(52) Hair, M. L.; Tripp, C. P. *Colloids and Surfaces, A: Physicochemical and Engineering Aspects* **1995**, *105*, 95-103.
(53) Parikh, A. N.; Allara, D. L.; Azouz, I. B.; Rondelez, F. *Journal of Physical Chemistry* **1994**, *98*, 7577-7590.
(54) Lee, M.-T.; Ferguson, G. S. *Langmuir* **2001**, *17*, 762-767.
(55) Briggs, D. *Surface Analysis of Polymers by XPS and Static SIMS*; First ed.; Cambridge University Press: Cambridge, 1998.
(56) St. John, P. M.; Craighead, H. G. *Applied Physics Letters* **1996**, *68*, 1022-1024.
(57) Jeon, N. L.; Nuzzo, R. G.; Xia, Y.; Mrksich, M.; Whitesides, G. M. *Langmuir* **1995**, *11*, 3024-3026.
(58) Harada, Y.; Girolami, G. S.; Nuzzo, R. G. *Langmuir* **2004**, *20*, 10878-10888.
(59) Xia, Y.; Mrksich, M.; Kim, E.; Whitesides, G. M. *Journal of the American Chemical Society* **1995**, *117*, 9576-9577.
(60) Harada, Y.; Girolami, G. S.; Nuzzo, R. G. *Langmuir* **2003**, *19*, 5104-5114.
(61) Delamarche, E.; Schmid, H.; Bietsch, A.; Larsen, N. B.; Rothuizen, H.; Michel, B.; Biebuyck, H. *Journal of Physical Chemistry B* **1998**, *102*, 3324-3334.
(62) Gourianova, S.; Fuhrmann, J. *Macromolecules* **2004**, *37*, 1825-1830.
(63) Zhao, B.; He, T. *Macromolecules* **2003**, *36*, 8599-8602.

Chapter 5

Synthesis of Binary-Patterned Polymer Brushes

5.1 Introduction

The majority of methods for the synthesis of binary-patterned polymer brushes involve at least one photolithographic step[1-7]. The previous chapter describes attempts to synthesise a binary-patterned brush on silicon via direct microcontact printing of BMPUS, a silane-functionalised ATRP initiator. This approach was unsuccessful due to major difficulties with μCP of BMPUS. In view of this, it was decided to collaborate with Prof. Graham Leggett's group to try to develop a photodeprotection based method for the synthesis of binary-patterned polymer brushes.

The use of photolytic protecting groups was developed to allow the synthesis of solid state arrays of biomolecules such as peptides[8] and DNA[9,10]. Ahmad *et al.*[11] developed this approach to produce photopatternable surfaces. {N-[2-(2-Nitrophenyl)propan-1-oxycarbonyl]-3-aminopropyl}triethoxysilane (NPPOC-silane) forms SAMs on silicon. Exposure to ultra-violet light removes the NPPOC group, revealing an amine-terminated layer. Irradiation through a mask results in the production of a patterned NPPOC-/amine-terminated SAM.

Several groups have synthesised surface-bound initiators for ATRP by a two step method: first an (aminopropyl)triethoxysilane layer is allowed to self-assemble on silicon substrates, then the amine-terminated layer is reacted with suitable bromoester-functionalised acid halides or carboxylic acids to generate an α-bromoester-terminated surface which can initiate brush growth[12-17]. The amine-terminated SAM produced by deprotection of NPPOC-silane can be converted to an ATRP initiator by an analogous reaction with 2-bromoisobutyryl bromide. This gives an alternative route to the synthesis of binary-patterned polymer brushes, using the brush growth reactions discussed in Chapter 3.

The results presented in this chapter show that this approach can be used to produce binary-patterned PS/PMMA brushes (see p. 160 for the reaction scheme). This represents a proof of concept experiment: most of the reactions were not fully optimised, so further work would be needed to obtain good quality binary patterned polymer brushes. The samples were analysed by AFM, contact angles, XPS and SIMS.

5.2 Materials

Methyl methacrylate, styrene, copper(I) chloride, copper(I) bromide, 2,2'-bipyridine and $CuBr_2(dnNbpy)_2$ were prepared/synthesised as described in Chapter 3.

Anhydrous toluene, THF and DMF were obtained from a Solvent Purification System (Innovative Technology Inc., SPS-400-6 and SPS-200-6). Typical water contents were 10-16 ppm for toluene, 23-27 ppm for THF and 11 ppm for DMF.

All other reagents were obtained from Aldrich and used as received.

5.3 Experimental Methods

NPPOC-silane was synthesised by Lu Shin Wong and NPPOC-silane SAMs were prepared by Shahrul Ahmad. Photodeprotection of NPPOC-silane SAMs, to generate patterned and homogeneous amine-terminated SAMs was carried out by Shahrul Ahmad. All other synthesis was performed by the author.

PMMA and PS brushes were synthesised and dehalogenated using the methods described in Chapter 3. All reactions were performed in silver foil-covered carousel tubes (to prevent deprotection of NPPOC-silane coated areas), without stirring.

5.3.1 Synthesis of NPPOC-protected SAMs

{N-[2-(2-Nitrophenyl)propan-1-oxycarbonyl]-3-aminopropyl}triethoxysilane was synthesised according to the published method[8,11]. Pieces of silicon (or glass) were

cleaned and rendered hydrophilic by treatment with piranha solution for 45 minutes followed by RCA cleaning at 80 ºC for 40 minutes (see Chapter 3 and 4 for details of RCA and piranha solution). The cleaned silicon was then rinsed with ultrapure water and dried in an oven at 120 ºC for at least 24 hours.

Cleaned substrates were put into a Schlenk tube, evacuated to 10 mbar, then refilled with dry nitrogen. The cycle was repeated twice more to ensure complete removal of oxygen and water. A 1 mM solution of NPPOC-silane in dry toluene was added to the Schlenk tube by cannula (enough to cover all the pieces of silicon/glass). The substrates were left to react for 48 hours, at room temperature, in the dark. NPPOC-silane coated wafers were rinsed with toluene and ethanol, then dried in a vacuum oven at 120 ºC for 45 minutes. The NPPOC-functionalised wafers were light-sensitive, so they were stored in the dark to minimise degradation.

5.3.2 Photodeprotection of NPPOC-silane SAMs

NPPOC-silane coated wafers were exposed to light from a 325 nm laser at a power of 11 mW for 3 minutes (area of irradiation 1.78 cm^2), then rinsed with ethanol. Previous work indicated that this was sufficient to completely remove the NPPOC protecting group, leaving an amine-terminated SAM[11].

Patterned samples were produced by placing 1500 mesh electron microscope grids on the sample before irradiation. A quartz lens was used to hold the grids in intimate contact with the sample surface.

5.3.3 Synthesis of 3-(2-Bromoisobutyramido)propyl(triethoxy)silane SAMs

Amine-SAM or patterned amine/NPPOC-SAM coated substrates were placed shiny face down in clean dry carousel tubes. The tubes were covered with silver foil to exclude light, and sealed with rubber septa. Each tube was then flushed with nitrogen for at least 10 minutes (using needles as gas inlets and outlets).

Triethylamine (0.30 ml, 2.1 mmol) and dry THF (20 ml) were added to a round-bottomed flask, and degassed by bubbling nitrogen through the liquid for 10 minutes. 2-Bromoisobutyryl bromide (0.25 ml, 2.0 mmol) was then added by syringe. The reaction mixture immediately became cloudy. Then 3 – 5 ml of this solution was added to each carousel tube and left to react at room temperature for 3 hours. The wafers were removed from the reaction mixture and sequentially rinsed with THF, water, methanol and acetone.

5.4 Characterisation

Characterisation by contact angles, XPS, spectroscopic ellipsometry, and tapping mode AFM was performed as described in Chapter 3.

5.4.1 Lateral Force Microscopy

LFM AFM images were acquired using a Multimode AFM with an Extended Nanoscope 3A controller and Nanoscope V5.12r4 software. The images presented in this thesis were produced using Nanoscope V6.11r1 software. LFM images were produced in contact mode, using silicon nitride tips with four cantilevers (Veeco, NP) with spring constants of 0.06-0.58 N/m, and tip radii of 20 nm. To maximise the sensitivity of the measurement, samples were imaged using the long, thin cantilever.

5.4.2 SIMS

SIMS spectra and images were produced using an ION-TOF ToF.SIMS 5 instrument with a field emission bismuth cluster ion source with a cycle time of 100 ns. For each sample, positive and negative ion spectra were recorded at high mass resolution. Images (150 μm^2) were produced using burst mode, which has high lateral resolution, but lower mass resolution. To limit sample damage, each spectrum/image was recorded on a different part of the sample, and the total ion dose for each area was limited to 1 x 10^{12} cm^{-2} [18]. The SIMS instrument was operated by Tracie Whittle.

5.5 Results and Discussion

The use of photolabile protecting groups is well established in nucleic acid, carbohydrate and peptide chemistry. Controlled synthesis of well-defined sequences of multifunctional biomolecules requires that certain groups are prevented from reacting. This is done by the use of protecting groups: chemicals that selectively bind to, and block reaction of certain functionalities within a molecule. The protecting group must be quickly and easily removable, under conditions that do not affect the biomolecules, to allow subsequent reactions of the protected functionality. o-Nitrobenzyl derivatives have been used as protecting groups for hydroxyl, amino, thiol and carbonyl functionalities. The 2-nitrophenylpropyloxycarbonyl (NPPOC) group has been found to undergo rapid photodeprotection compared to 2-(o-nitrophenyl)ethoxycarbonyl (NPEOC) derivatives[19]. NPPOC has been used as a protecting group for nucleoside 5'-hydroxyls[9,19], allowing improved synthesis of DNA microarrays compared to 5'-O-((α-methyl-2-nitropiperonyl)oxy)carbonyl (MeNPOC) protected phosphoramidites[9,10]. Bhushan *et al*.[8] used NPPOC as a protecting group for the amine group of a series of amino acids. They found that the rate of NPPOC photolysis was at least twice that of nitroveratryloxycarbonyl (NVOC) protected amino acids, opening opportunities for improved solid phase peptide synthesis.

NPPOC undergoes rapid efficient photodeprotection by a mechanism that gives an alkene and carbon dioxide as by-products. This makes it more suitable for the protection of amine functionalities than other protecting groups such as NVOC and MeNPOC, which generate carbonyl compound by-products which can react with the deprotected amine to form imines (unless a reactive carbonyl scavenger is added)[11].

Ahmad *et al*.[11] developed the use of NPPOC-protected aminosilane monolayers for micro and nanopatterning on silicon surfaces. For this project, NPPOC-silane was synthesised according to the published method. NPPOC-silane SAMs were produced by immersing cleaned, surface-oxidised silicon or glass substrates in a 1 mM solution of NPPOC-silane in dry toluene under nitrogen in the dark. Previously published work showed that a limiting composition and morphology was reached after 48 hours. The resulting layer was smooth (rms roughness < 0.5 nm) with a contact angle of 75º. XPS analysis revealed the presence of carbon, silicon, nitrogen and oxygen. In particular, the

high resolution spectrum of the N 1s region showed two peaks at 400.0 and 406.2 eV, in approximately equal amounts. These signals were assigned to the amine and nitro groups respectively. Photolysis of the NPPOC group was monitored by comparing the size of the amine and nitro N 1s peaks by XPS, and by contact angles. For samples irradiated with a UV laser at a wavelength of 325 nm, a limiting value was reached after 3 minutes of light exposure[11].

The XPS of the deprotected amine-silane SAM is shown in Figure 5.1. The sample analysed was on a glass slide, explaining the presence of sodium, zinc, phosphorus and aluminium in the survey scan, and potassium near the C 1s region. The C: N ratio was 6.5: 1, which is more carbon-rich than predicted. The high resolution C 1s spectrum revealed the presence of four different carbon environments in a ratio of 3: 1: 0.2: 0.2. The main peaks, C1 and C2, can be assigned to saturated hydrocarbon (e.g. C-C) and $–CNH_2$ respectively. According to the expected structure of the SAM, these should occur in a 2: 1 ratio, not the 3: 1 ratio actually found. The remaining peaks were only present in small quantities: C3 has a chemical shift that fits the presence of an N-C-O linkage. This group is not present in amine-silane, but is present in the NPPOC-silane starting material. C4 could be due to a -C(=O)O group, which is also present in NPPOC-silane, although it is also possible that this is not a true peak, and is caused by noise leading up to the K 2p peak. The spectrum suggests that the surface was mainly covered by an amine-terminated layer, but that deprotection was incomplete, and a small amount of NPPOC-silane remained. This would also explain the excess amount of saturated hydrocarbon (C1).

Ahmad *et al.*[11] used XPS to follow the photolysis of NPPOC-silane by comparing the ratio of the N 1s peaks due to $–NO_2$ (406 eV) and $–NH_2$ (400 eV) with increasing UV exposure times. Even after 350 seconds exposure at 364 nm, some residual $–NO_2$ was detected. This was thought to be because there was some degree of multilayer formation, screening some of the nitro groups from UV exposure.

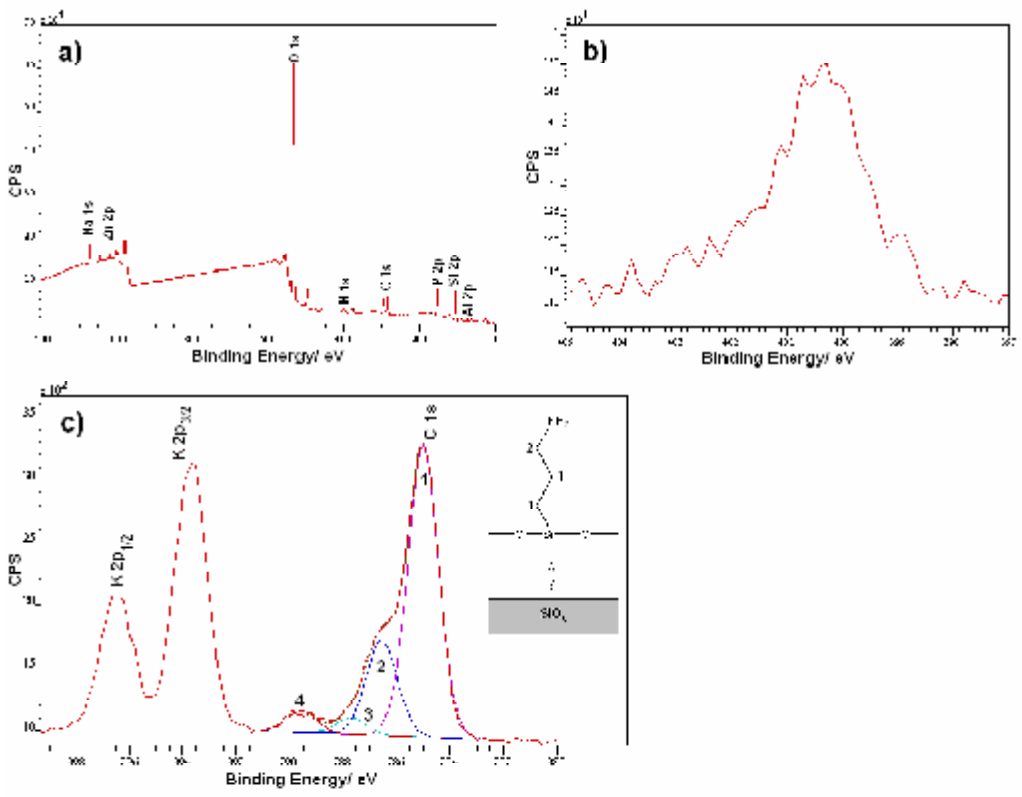

Figure 5.1 XPS of amine-SAM; a) Survey scan, b) high resolution spectrum of N 1s region, c) high resolution spectrum of C 1s region .

In Figure 5.1 b), the high resolution N 1s spectrum has a peak at 400.5 eV, which is consistent with an amine group. Unfortunately it does not show high enough binding energies to check the presence of nitro groups. However, the XPS of the bromo-silane SAM (shown in Figure 5.2) does show a second nitrogen environment, at approximately 406 eV, which gives more evidence for incomplete removal of the NPPOC group.

5.5.1 Synthesis of 3-(2-Bromoisobutyramido)propyl(triethoxy)silane SAMs

In Chapters 3 and 4, a surface-bound ATRP initiator was produced by allowing an α-bromoester-functionalised silane (BMPUS) to self-assemble on the substrate. An alternative approach is a two-step process to synthesise the initiator: 3-(Aminopropyl)triethoxysilane was allowed to react with a silicon substrate (using solution or vapour methods). The amine-terminated surface can then be reacted with 2-

bromoisobutyryl bromide[14], 2-bromo-2-methylpropionic acid[12,13] or 2-bromopropionyl bromide[15-17] in non-polar solvents, in the presence of a base, to produce an α-bromoester-terminated SAM that can initiate ATRP. This approach was used to convert amine-silane into an ATRP initiator. Deprotected amine-silane coated silicon wafers were reacted with 2-bromoisobutyryl bromide and triethylamine in dry THF for 3 hours. After addition of 2-bromoisobutyryl bromide, the reaction mixture became cloudy – this was thought to be due to reaction of 2-bromoisobutyryl bromide with traces of water, generating a precipitate of $Et_3N^+Br^-$. The reagents were present in massive excess compared to the number of surface-bound amine groups, so this side reaction did not effect the conversion, but it did necessitate extensive rinsing to ensure that no solid residue was left on the bromoester-silane coated substrates.

After reaction with 2-bromoisobutyryl bromide, the contact angle changed from 52 ± 4º for amine-silane, to 63 ± 7º. The XPS of the α-bromoester-silane SAM (shown in Figure 5. 2 below) had peaks due to carbon, nitrogen, oxygen, bromine, silicon (and sodium – probably indicating some surface contamination). As discussed in Chapter 2, XPS probes approximately the top 10 nm of the sample[20], resulting in the observation of silicon and oxygen signals from the oxidised silicon substrate. The carbon, nitrogen, and bromine peaks are present in an 11.7: 1: 0.16 ratio. The predicted structure should give a ratio of 7: 1: 1. The sample is more carbon-rich than expected, which is difficult to explain, especially as both the precursors (NPPOC-silane and amine-silane) have similar, or lower C: N ratios. The relatively low abundance of bromine suggests that the reaction is incomplete, with only ~ 20 % of the amine groups reacting with 2-bromoisobutyryl bromide.

The high resolution C 1s spectrum is also shown below. There are four different carbon environments in a ratio of 3.2: 1: 0.3: 0.3. The first two peaks can be assigned to saturated hydrocarbon (e.g. C-C) and $–CNH_2$ respectively (as in Figure 5.1). C3 can be assigned to the quaternary carbon adjacent to the bromine atom (or alternatively to an N-C-O linkage). C4 fits the amide carbon, or possibly a –C(=O)O group (the alternative assignments of these peaks represent groups found in the starting material, NPPOC-silane). The low intensity of these peaks compared to C1 and C2, and the lower than predicted amount of C1, again suggest that the reaction with

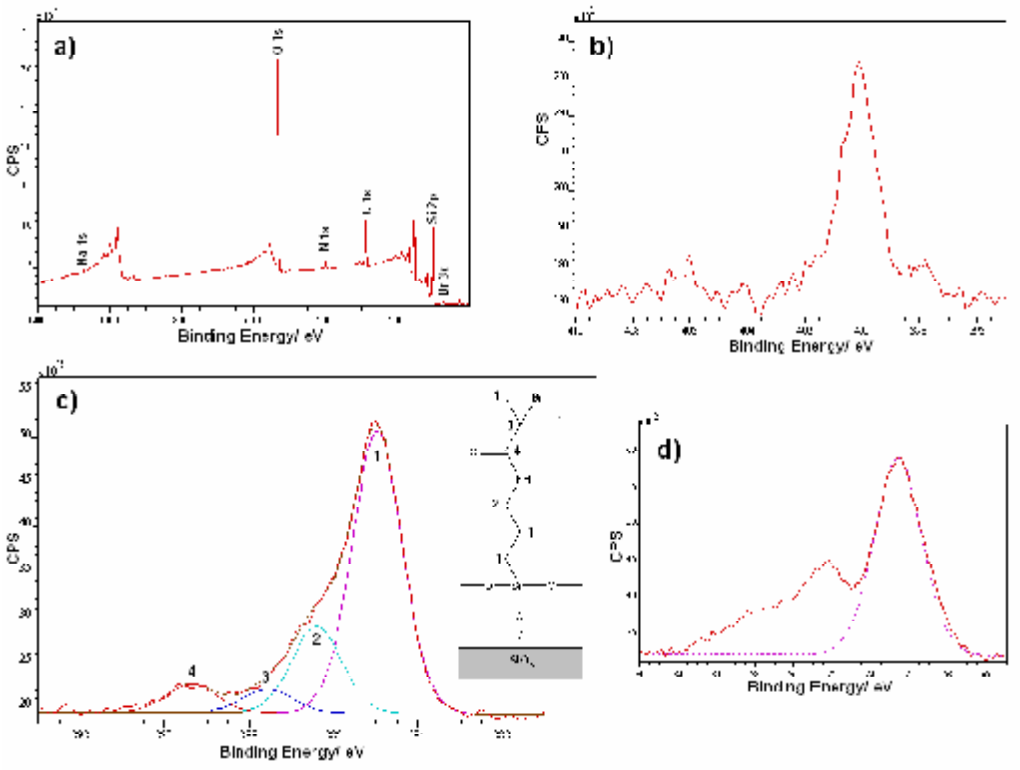

Figure 5.2 XPS of bromoester-silane SAM; a) survey scan, b) high resolution scan of N 1s region, c) high resolution scan of C 1s region, d) magnified view of Br 3d region of survey scan.

2-bromoisobutyryl bromide is incomplete. This low yield seems unlikely considering the large excess of reagents used, but it is possible that reaction of bulky 2-bromoisobutyryl bromide groups with the surface-bound amine groups is sterically hindered, or some interaction with the by-products of the reaction reduces their reactivity. A longer reaction time or more stringent conditions may help to improve the efficiency of the reaction. It is also known that bromine-terminated SAMs are susceptible to x-ray damage[21], which could explain some of the discrepancy in intensity for the Br 3d peak.

5.5.2 Growth of PMMA Brushes From 3-(2-Bromoisobutyramido) propyl(triethoxy)silane SAMs

The bromoester-silane coated wafers were then used to grow PMMA brushes, using the method described in Chapter 3. The pieces of silicon (and glass) used in this part of the

project were too small (3 – 4 mm^2) to use wire holders and the 8-necked flask, so initiator-coated substrates were placed face down in carousel tubes, covered with the reaction mixture and left to react without stirring, for the desired time. PMMA brush-coated wafers were then analysed by measurement of contact angles, ellipsometry, AFM and XPS.

There was a small change in contact angle from the α-bromoester-silane SAM (63 ± 7º) to PMMA brush (62 ± 5º), but, allowing for the experimental errors, this was not significant. The contact angle compares well with that of PMMA brush grown from BMPUS (59 ± 2º). PMMA brushes grown from bromoester-silane were much thinner than brushes grown from BMPUS under equivalent conditions, and the increase in brush thickness with time was not linear (shown below in Figure 5.3). In addition, there also appeared to be considerable variation in the thickness of the bromoester-silane layer between samples. However, only a small number of samples were measured, and they were very small (approximately the same size as the ellipsometer spot size), which could lead to errors in measurement. Further work would be needed to confirm these observations. If a lower thickness is consistently observed, this could be due to the low concentration of initiator groups on the surface (see p. 154). Calculations of the cross-sectional area of individual polymer chains in a brush suggest that each polymer chain

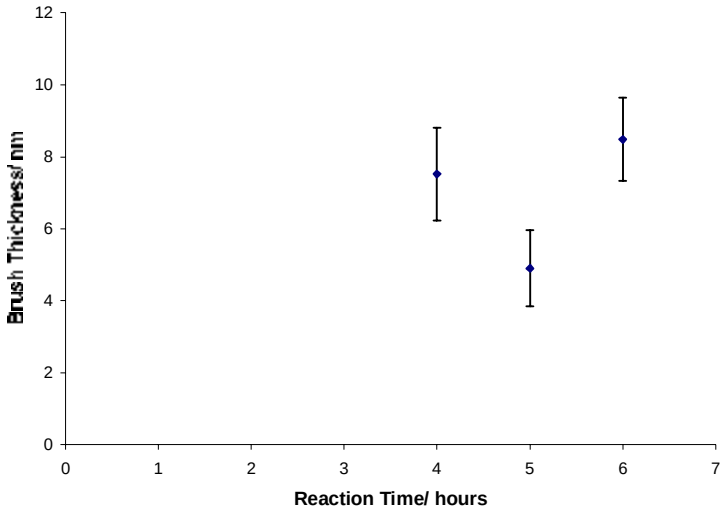

Figure 5.3 Uncorrected thickness of PMMA brush grown from bromoester-silane initiator. Error bars indicate the MSE.

blocks 10 – 12 initiator molecules[22,23]. This suggests that brushes grown from a SAM containing 10 % initiator groups should have the same thickness as those grown from 100 % initiator.

Jones *et al.*[22] and Bao *et al.*[24] investigated the effect of initiator density on brush thickness by growing polymer brushes from initiator SAMs diluted with an unreactive molecule. Both groups found that a lower initiator density resulted in lower brush thickness after equivalent reaction times. Low conversion of amine-silane to bromoester-silane is equivalent to a mixed SAM with a low percentage of initiator groups, resulting in a lower brush thickness (see Figure 4.10, p. 142).

AFM showed that the brush surface was relatively smooth, with an rms roughness of ~ 1.6 nm (not shown). There were more dust particles/raised features visible than on the PMMA brushes discussed in Chapter 3 (see p. 103), but no dramatic differences in appearance. These features were thought to be residues of material deposited during polymerisation, as the reaction mixture was not stirred.

The XPS of a bromoester-silane initiated PMMA brush 4.0 nm thick is shown in Figure 5.4. The survey scan has peaks due to silicon, oxygen, carbon, nitrogen and bromine (and sodium). In contrast to the XPS of PMMA brush grown using BMPUS as the initiator (see p. 106), chlorine was not detected. The Br 3d area is split into two peaks: the higher binding energy peak at ~ 74 eV suggested the surface was contaminated with BrO_3 or aluminium (although it is not clear where either of these species would have come from). A small amount of nitrogen was detected, presumed to be from the amine linkage within the initiator (and any unreacted NPPOC- and amine-silane).

The high resolution spectrum of the C 1s region corresponds with the previous spectrum for a PMMA brush, and with other examples of PMMA films[20]. Curve-fitting reveals four carbon environments in an approximate 2: 1: 1: 1 ratio, which can be assigned to saturated hydrocarbon (C-C), -C*-C(=O), C*-O-C(=O) and ester carbon (-C(=O)OR respectively, as shown below in Figure 5.4.

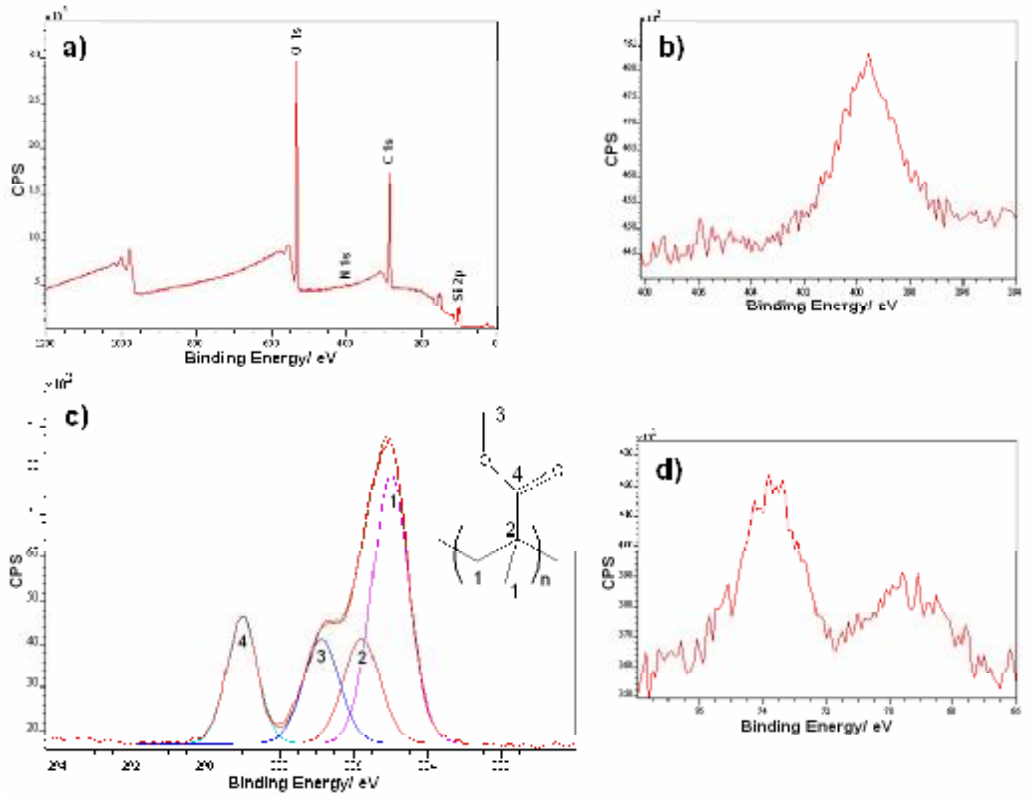

Figure 5.4 XPS of PMMA brush initiated by bromoester-silane; a) survey scan, b) high resolution scan of N 1s region, c) high resolution scan of C 1s region, d) magnified view of Br 3d region of survey scan..

There are clearly differences between PMMA brushes grown from bromoester-silane and BMPUS. It is likely that at least one of the reactions used to prepare bromoester-silane does not go to completion, which may explain the difference in thickness. Nevertheless, it is possible to synthesise PMMA (and PS) brushes from bromoester-silane. Optimisation, and a better understanding of this process could be a subject for further study, but it was decided to proceed with the production of patterned and binary-patterned polymer brushes.

5.5.3 Patterned and Binary-Patterned Polymer Brushes

As discussed on p. 28, binary-patterned polymer brushes have been synthesised by a variety of methods, most of which use photopatterning in some way[1,3-7,25]. One approach is to produce a homogeneous brush, then use UV light to selectively etch (or chemically alter[3]) the first brush, before growing a second brush[4,6,7]. However, etching

a thick polymer brush may be slow and is certainly wasteful. An alternative method is to grow a patterned brush by UV-induced free radical polymerisation through a mask, leaving areas of initiator that can later grow a second polymer brush[5]. However this method can only be used with (uncontrolled) free radical polymerisation and requires the masked sample to be immersed in the reaction mixture, which may cause problems. In addition, active initiator groups remain within the first brush. To prevent unwanted growth, it was found to be necessary to ensure that the first brush adopted a collapsed conformation during the second polymerisation. This could either be done if the first polymer was not soluble in the reaction mixture for the second polymerisation, or by chemical modification of the first brush[5], but it limits the combinations of polymer brushes that can be produced by this method.

The use of photopatternable NPPOC-silane SAMs should allow the development of a more general method for the synthesis of binary-patterned brushes. The proposed reaction scheme is shown in Scheme 5.1.

5.5.3.1 Synthesis and Modification of Patterned SAMs

To produce patterned NPPOC-/amine-silane surfaces, 1500 mesh copper electron microscope grids were used as masks. They were placed onto a NPPOC-silane coated silicon substrate and held in contact with the surface by a quartz lens. The system was exposed to UV laser light for 3 minutes, then the side products were removed by a quick rinse in ethanol. The grids used give a pattern of squares with a period of approximately 12 μm.

Tapping mode AFM (Figure 5.5 a) showed a smooth surface with no detectable pattern in the height or phase. LFM can be used to image samples with different frictional properties but low height variation, such as patterned SAMs[11,26-28]. This clearly showed a square pattern covering the sample, with a period of approximately 12 μm (Figure 5.5 b). There was also a small ‘droplet’ type feature on each square: this was thought to be surface contamination produced when locating the patterned part of the sample.

Scheme 5.1 Synthesis of binary-patterned polymer brushes

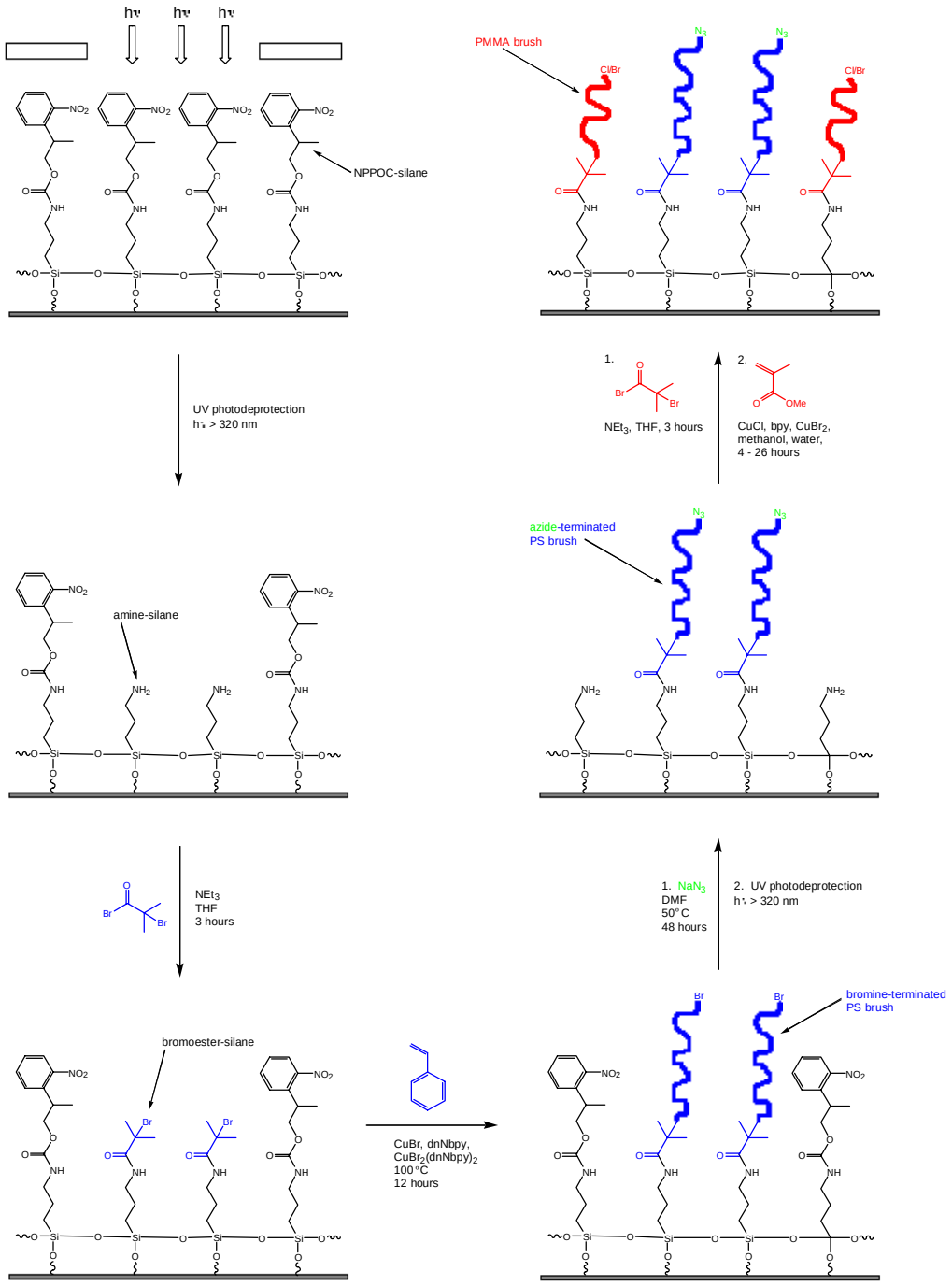

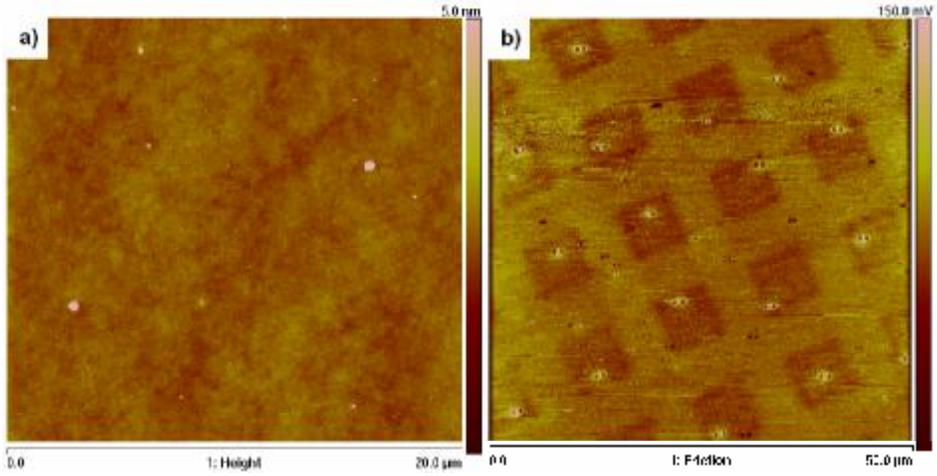

Figure 5.5 a) Tapping mode image of a patterned NPPOC-silane/amine-silane sample (R_a 0.18 nm, rms 1.0 nm), b) LFM image of the same sample.

SIMS is a versatile surface analysis technique, which can be used to identify and image the distribution of particular ions on a sample. It is very surface-sensitive, showing mainly the composition of the top 1 nm of the sample. The sample is bombarded with a beam of primary ions (or neutral atoms), causing a complex cascade of fragmentation and ionisation resulting in the emission of secondary ions (and neutral species). The secondary ions are captured and analysed by a time of flight mass spectrometer. SIMS imaging relies on measurement of the mass spectra of very small areas of the sample, which can then be used to map the spatial distribution of particular ions. For each sample, positive and negative ion spectra were recorded at high mass resolution (not shown). Images were produced using burst mode, which has high lateral resolution, but lower mass resolution. As the processes involved in secondary ion production are complex and not fully understood, the literature was used to identify likely fragments for each material. SIMS is not quantitative because some ion yields are much more intense than others. A selection of ion images (mainly those showing the best contrast) are presented for each sample. SIMS is an inherently destructive technique: ion bombardment and fragmentation cause progressive damage to the sample surface. To limit this, each spectrum/image was recorded on a different part of the sample, and the total ion dose for each area was limited to 1 x 10^{12} cm^{-2} [18].

The negative and positive ion images for a patterned NPPOC-/amine-silane SAM are shown in Figure 5.6 below:

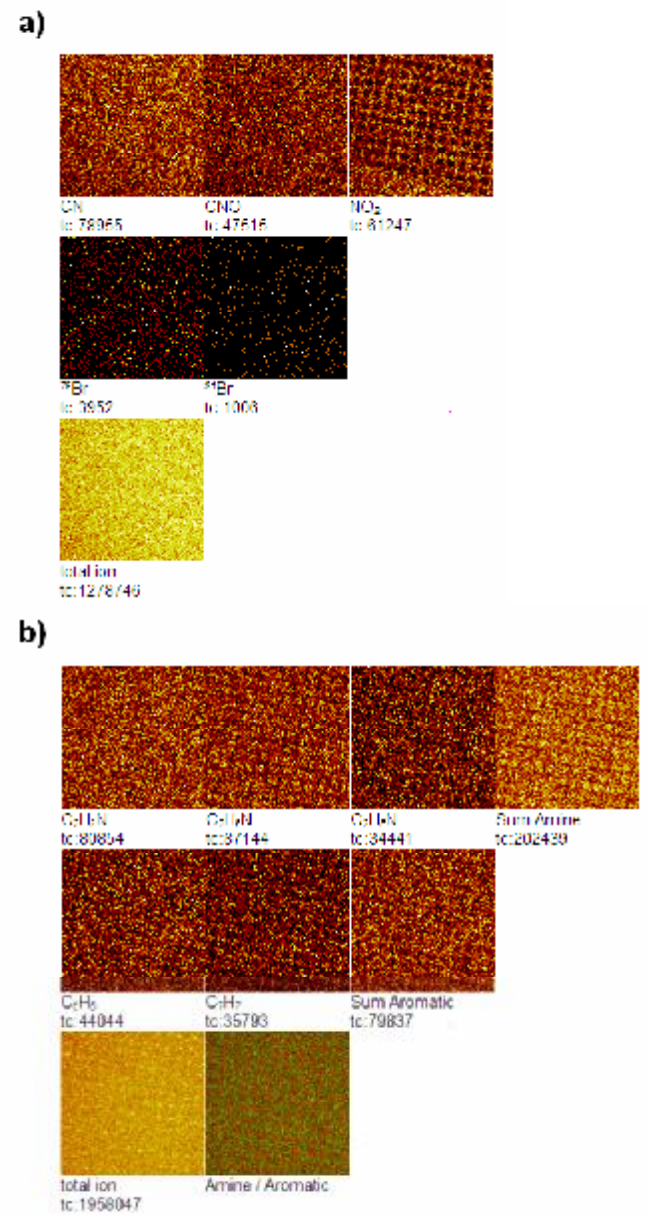

Figure 5.6 a) Negative and b) positive SIMS images of patterned NPPOC-silane/amine-silane SAM.

The pattern was clearly visible – in particular NO_2^- (m/z 46) and $C_7H_7^+$ (m/z 91) show NPPOC-silane forming the 'grid', and $C_2H_5N^+$ (m/z 43) (and others) show the amine-silane squares. CN^- (m/z 26) and CNO^- (m/z 42) gave a strong signal, but no visible pattern, presumably because these species could be generated by the fragmentation of either silane. There was no bromine signal.

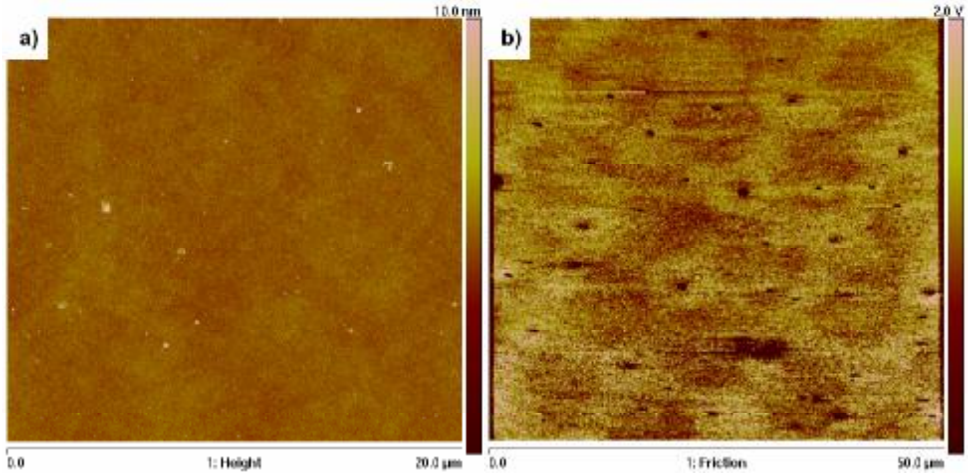

Figure 5.7 a) Tapping mode image of a patterned bromoester-silane/NPPOC-silane sample, (R_a 0.30 nm, rms 0.62 nm), b) LFM image of the same sample.

The samples were then reacted with 2-bromoisobutyryl bromide to produce bromoester-/NPPOC-silane SAMs. Tapping mode AFM again showed a smooth, featureless surface. The sample was difficult to image by LFM, but a faint pattern of squares could be seen (see Figure 5.7).

SIMS images (Figure 5.8), provided clear evidence for the successful incorporation of α-bromoester groups: there was now an intense bromine signal from the squares (bromine yields are typically high in SIMS). As before, NO_2^- showed the NPPOC-silane forming the grid of the pattern. Both NPPOC-silane and bromoester-silane can produce amine ions, hence the almost homogeneous signal observed for $C_2H_3N^+$, $C_2H_5N^+$ and $C_3H_5N^+$.

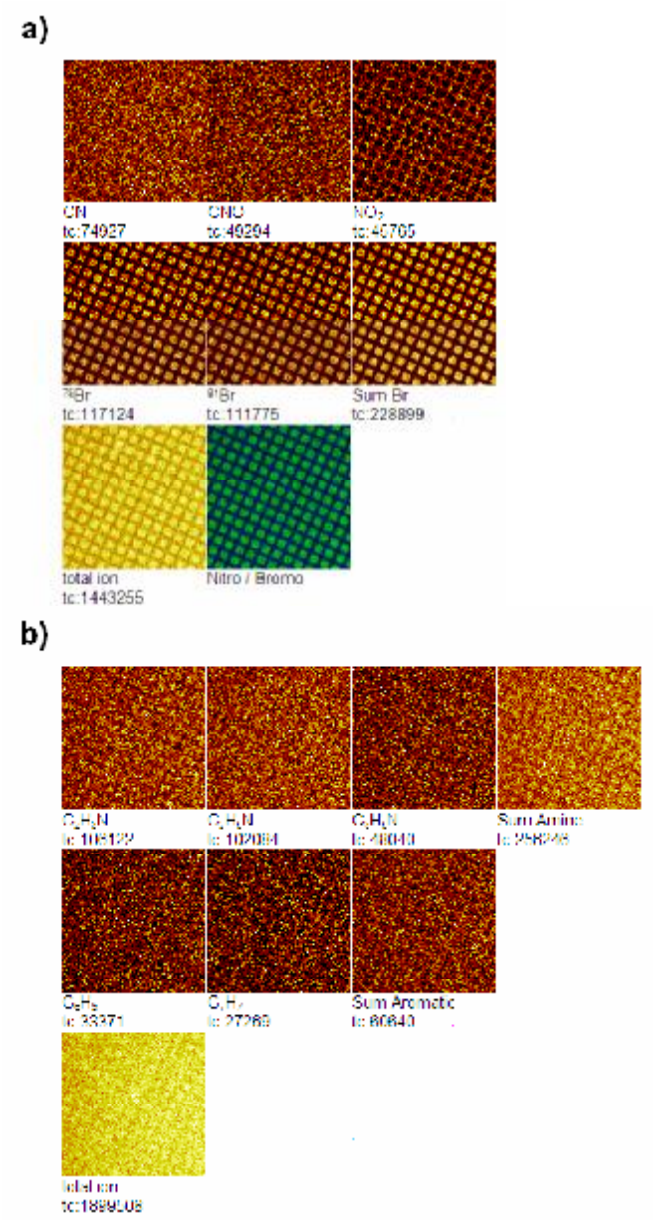

Figure 5.8 a) Negative and b) positive SIMS images of patterned bromoester-silane/NPPOC-silane SAM.

5.5.3.2 Patterned Brushes

PMMA and PS brushes were grown from the initiator-patterned wafers. In an initial experiment, PMMA brushes were grown for either 4 or 6 hours. This produced patterns of raised squares 7 – 8 μm across and ~ 4.5 nm high. There was no significant difference in thickness between the two samples: after 4 hours the squares were

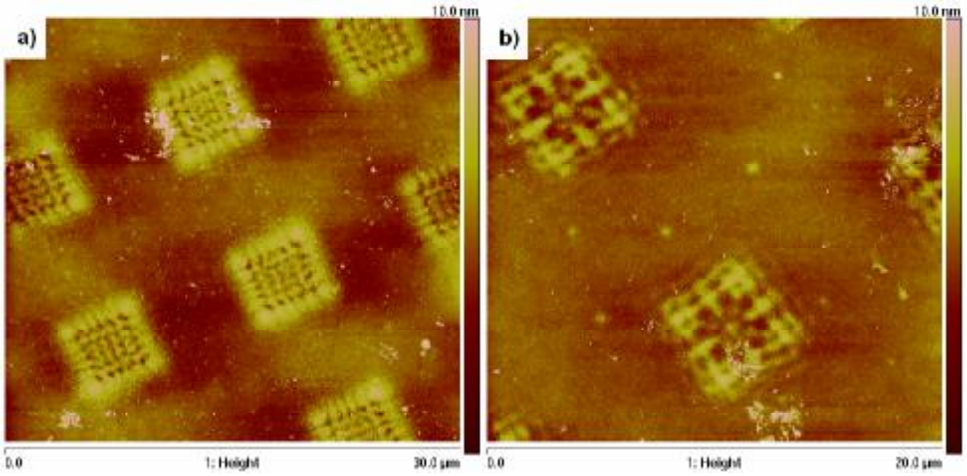

Figure 5.9 Tapping mode AFMs of patterned PMMA brushes grown for a) 4 hours, b) 6 hours.

4.5 ± 0.3 nm high, after 6 hours the average height was 4.3 ± 0.6 nm. The raised squares had some symmetrical micropatterning, which can be seen in Figure 5.9 above.

To allow the synthesis of binary-patterned polymer brushes, it was necessary to grow the PS brush first (see p. 115), so in subsequent reactions, patterned PS brushes were produced. A reaction time of 12 hours was predicted to produce homogeneous PS brush approximately 17 nm thick, but the patterned samples were only 3 – 7 nm thick. This was probably a consequence of the incomplete conversion of NPPOC-silane to bromoester-silane. As already discussed, a low surface concentration of initiator results in the growth of thinner brushes[22,24]. Production of a patterned brush can also affect the brush conformation and apparent thickness. Koutsioubas and Vanakaras[29] modelled the behaviour of polymer chains within a patterned brush for different pattern sizes and solvent conditions. Under good solvent conditions, the polymer chains extended out from the edges of the patterned regions, increasing the apparent width of the pattern. Under poor solvent conditions, the polymer chains were collapsed and formed dense, column-like structures with very limited lateral expansion. The patterned PS and PMMA brushes shown here were analysed in the absence of solvent, so should adopt a collapsed conformation, but any spreading of the brush onto the non-patterned areas would result in a reduction in apparent brush thickness.

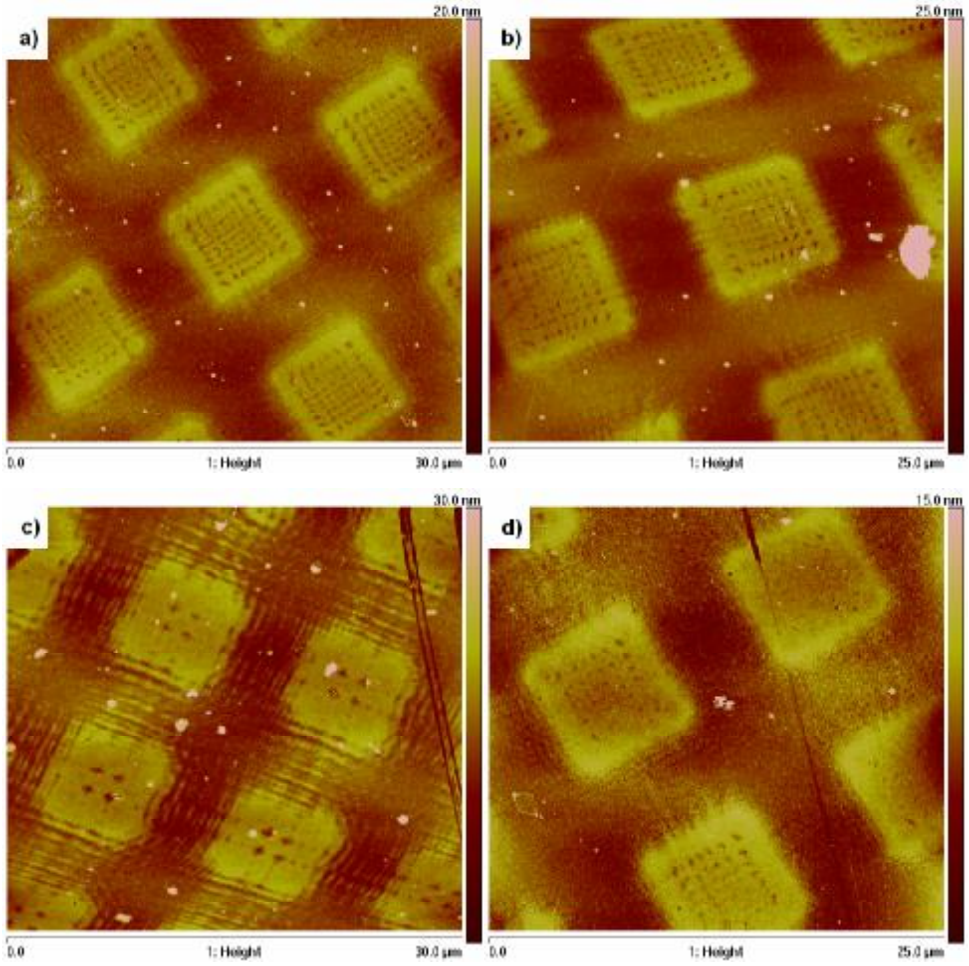

Figure 5.10 Tapping mode AFM images of patterned PS brushes. a) PS-N_3/amine-silane, b) and d) PS-N_3/bromoester-silane, c) PS-Br/NPPOC-silane.

All the samples were microstructured. The precise pattern formed varied between samples, but they all reflected the square geometry of the main pattern, and were larger than the wavelength of the light used to deprotect the NPPOC-silane SAM (325 nm). In some cases, the microstructuring spread beyond the edges of the squares, into areas originally covered by the mask, resulting in a 'tartan' pattern. Some examples of microstructured patterned PS brushes are shown above in Figure 5. 10 (both bromine and azide-terminated samples are included).

The micropatterning was not detectable by FFM, which showed that the squares were completely covered by polystyrene (albeit of varying thickness). No examples of

substructuring of patterned SAMs or polymer brushes could be found in the literature. Several possible explanations for this phenomenon are discussed below:

1. A quartz lens was used to hold the copper grid in contact with the sample during laser exposure. A reduced image of the grid could be formed at the surface of the lens and reflected back onto the sample. Variations in the relative position of the lens and the grid could alter the focal length, resulting in different patterns on different samples. However it is difficult to explain how this mechanism would produce the 'tartan' patterns, as these spread into the area covered by the grid.

2. Production of an intense laser beam requires a long path length through the active medium (to obtain sufficient overall gain). This is achieved by multiple reflections in an optical resonator. The length of the cavity defines the allowed resonant frequencies, or longitudinal modes of the laser. Each of these frequencies may be subdivided into transverse modes: an electric and magnetic field configuration at some position in the laser cavity, which on propagating one round trip in the cavity, returns to that position with the same pattern. Laguerre-Gaussian transverse modes have rectangular symmetry and can generate patterns which look similar to those seen in some examples of patterned brushes[30]. The transverse modes are a function of the size and shape of the resonant cavity, so it seems unlikely that the same laser would produce different patterns with different samples, and the patterns involved are quite complex. Also, other researchers using the same laser and patterning technique have not reported the formation of secondary patterns, although most of the other work has involved patterned SAMs, where it may not show up due to the low (or absent) height contrast.

3. The substructures may be due to formation of stationary patterns of diffusing reagents during the polymerisation reactions. Chemical patterns have been observed in complex, multi-step reactions such as the Belousov-Zhabotinsky or CIMA/CDIMA chemical oscillators. Dolnik *et al.*[31] investigated a two-dimensional reaction – diffusion model which produced regularly patterned standing waves (with square, rhombic, striped, or hexagonal morphologies).

The morphology found depended on the starting conditions, degree of supercriticality and many other parameters. A multi-step reaction mechanism was required to produce a system that exhibited a wave instability which could lead to standing wave formation. The polymerisation reactions used to produce polymer brushes were unstirred, which could allow standing waves to develop, but each sample was shaken several times during the course of a reaction, which would presumably destroy any local concentration gradients. Also, in the model system, patterns of several different symmetries could be produced depending on the randomly selected starting conditions, whereas all the micropatterned polymer brushes had square symmetry. If this mechanism applied to the synthesis of patterned polymer brushes by ATRP, it seems extremely unlikely that it has not been observed before and reported in the literature.

4. Laser irradiation can induce electromagnetic fields (evanescent waves) in metals[32] The grid structure could result in this field forming standing waves, which could result in the observed microstructuring. However, for this to be observed, the angle of incidence of the light must be low enough that total internal reflection occurs. This is highly unlikely, as the laser was mounted directly over the samples (angle of incidence close to 90º). No similar examples were found in the literature, and it is difficult to explain how irradiation of the same type of grid with the same laser could result in the production of so many different patterns.

5. Aberrations and defects in the lens used to hold the grid down could produce patterns, though these would probably not be regular and symmetrical.

6. The secondary patterns could be an artefact of TM AFM imaging. However, they were only observed on patterned brushes (not on homogeneous brushes and polymer blend films which were also imaged at the same time), and micropatterns were consistently observed on all patterned brushes, over several sessions, using different tips and AFM parameters. Each sample had a consistent microstructure, which was retained after further reactions: an example is shown in Figure 5.11.

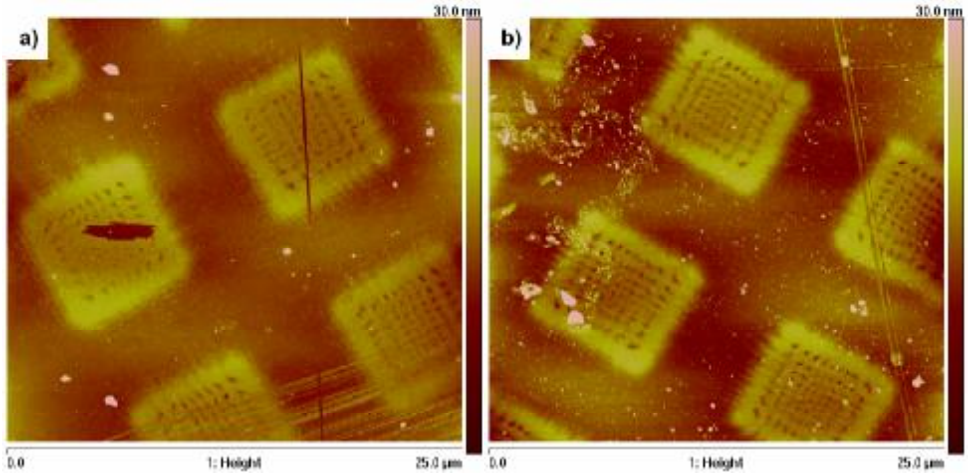

Figure 5.11 AFM images of a) patterned PS and b) PS/PMMA binary brush – sequential images of the same sample, showing retention of similar micropatterning.

None of these effects can completely explain the observed structures. It is possible that several factors combine to generate the micropatterns, but further study would be required to understand exactly how and why these micropatterns form.

SIMS also showed the production of patterned PS brushes (Figure 5.12). The images showed a patterned surface, with PS ions and Br^- found mainly on the squares of the pattern, and nitrogen-containing ions (from NPPOC-silane) on the grid. The patterns were less distinct than in the previous SIMS images (see Figure 5.8). This can be explained by looking at the AFM of this sample, shown in Figure 5.10 c, which showed that it was 'tartan' patterned, with PS covering part of the grid.

5.5.3.3 Towards Binary-Patterned Polymer Brushes

The patterned PS brushes were reacted with saturated sodium azide in DMF at 50 ºC for at least 48 hours to 'kill' the active polymer chains, then exposed to laser light for 3 minutes to remove the NPPOC protecting groups. There was no change in the appearance of the samples by AFM (see Figure 5.10 and Figure 5.11). SIMS was used to confirm the changes in surface chemistry. Initially, the PS brush was bromine-terminated, with characteristic ions for PS and Br observed on the squares. After reaction with NaN_3, PS ions were still emitted from the squares, but there was now no detectable bromine signal, suggesting complete debromination of the polymer chains.

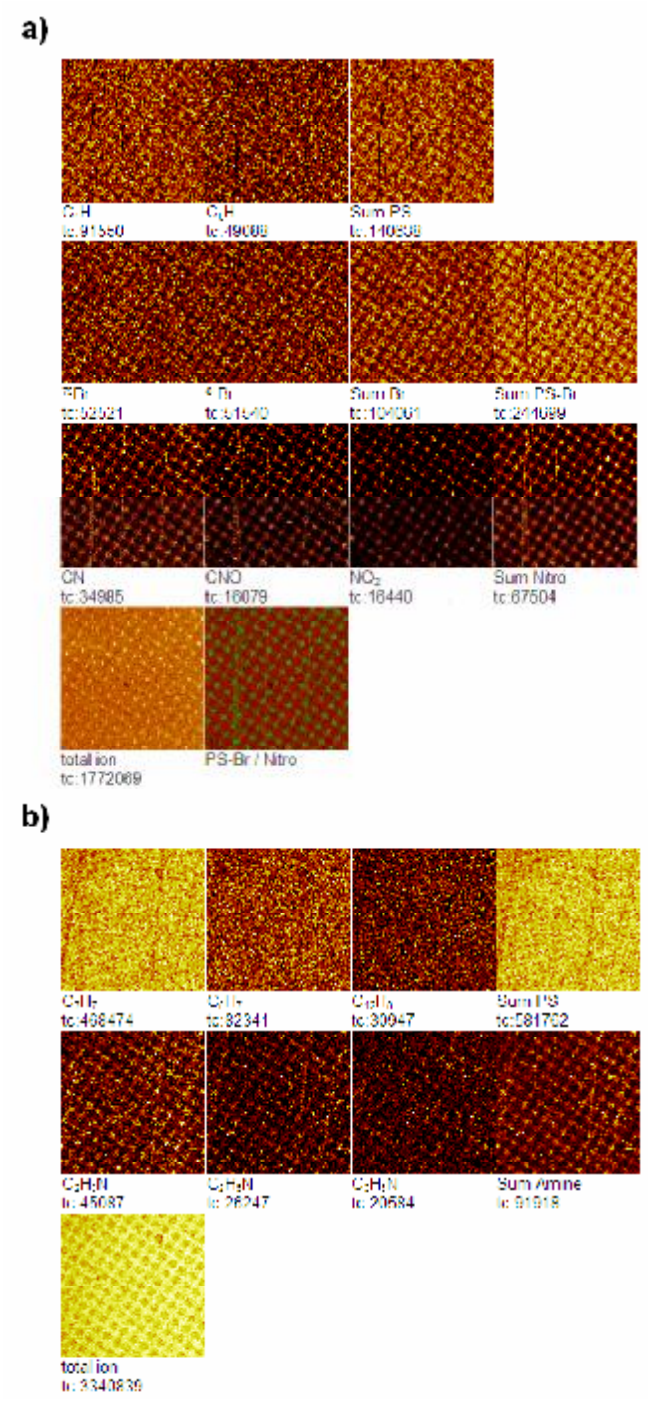

Figure 5.12 a) Negative and b) positive SIMS images for a patterned PS-Br/NPPOC-silane sample.

Irradiation resulted in an increase in the intensity of amine ions (especially $C_2H_3N^+$, $C_2H_5N^+$ and $C_3H_5N^+$), showing effective photolysis of NPPOC from the remaining areas

of the sample. There was also a weak signal for NO_2^-, which suggests that there may be some residual NPPOC-silane. The SIMS images are shown in Figure 5.13 below.

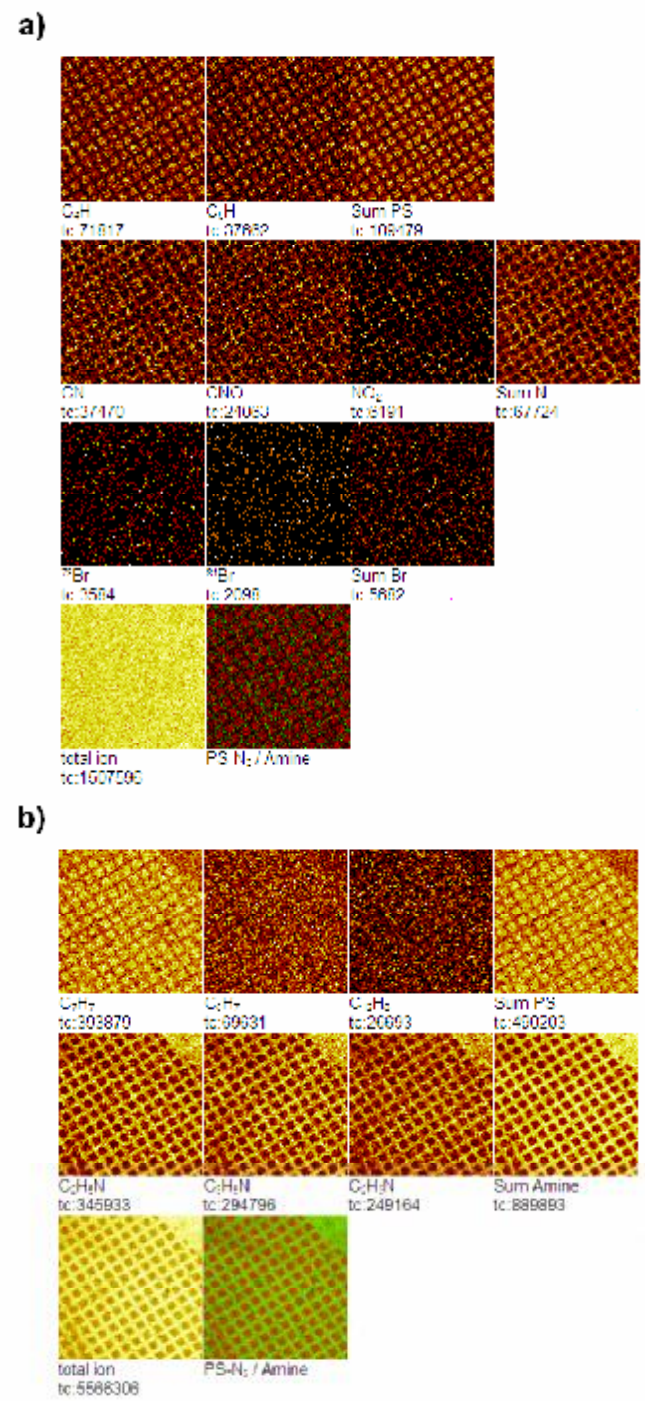

Figure 5.13 a) Negative and b) positive SIMS images for a patterned PS-N_3/amine-silane sample.

Reaction with 2-bromoisobutyryl bromide converted the remaining amine-silane to bromoester-silane. Bromine ions reappeared in the SIMS image (see Figure 5.14), now located on the grid. The signal seemed less intense than after the previous bromination reaction (see Figure 5.8). This could be due to variation between samples, but could also suggest that the second bromination reaction was less complete than the first.

It is possible that one of the previous reactions also affects the NPPOC-silane (or amine-silane), or a slow degradation over time reduces the amount of surface-bound groups that can react with 2-bromoisobutyryl bromide. Alternatively, the PS brush may hinder access to the surface amine groups – the bromination reaction is performed in THF, a good solvent for PS, so the brush will be swollen, and could spread laterally, covering part of the surface.

The patterned samples were finally used to grow PMMA brushes. SIMS analysis of a sample grown for 5 hours indicates the successful production of a binary-patterned PS/PMMA brush (Figure 5.15). Species characteristic of PMMA form the grid of the pattern, with PS found on the squares. Cl^- and Br^- are associated with the PMMA grid, suggesting that the ATRP reaction was controlled/'living', and the active chain ends were retained ($^{37}Cl^-$ appears indistinct, probably due to an overlap with C_3H^-, a characteristic PS ion, which occurs at the same m/z). A second binary brush, with the PMMA grown for 20 hours produced very similar SIMS images (though the halogen signal was less well-defined), showing that the synthesis was reproducible. AFM showed that the binary brushes were not smooth: there was no obvious change in surface morphology from the patterned PS brushes. Initially the PMMA brush was grown for 5 hours, predicted to produce PMMA brush around the same thickness as the PS features (5 – 10 nm). Longer reaction times were investigated to see if a flat binary brush (or even one with inverted topography) could be produced, but even 26 hours of PMMA growth did not significantly alter the appearance of the samples. Some AFM images of binary-patterned brushes are shown below in Figure 5.16.

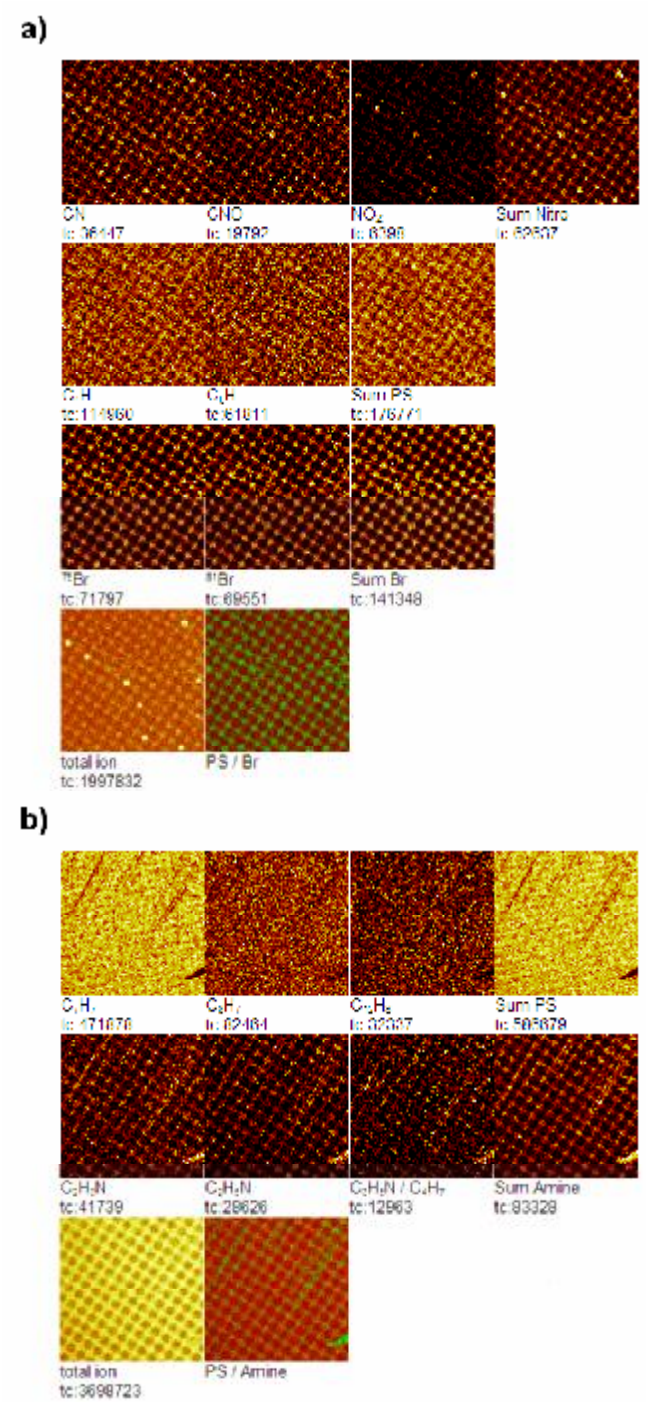

Figure 5.14 a) Negative and b) positive SIMS images for a patterned PS-N_3/ bromoester-silane sample.

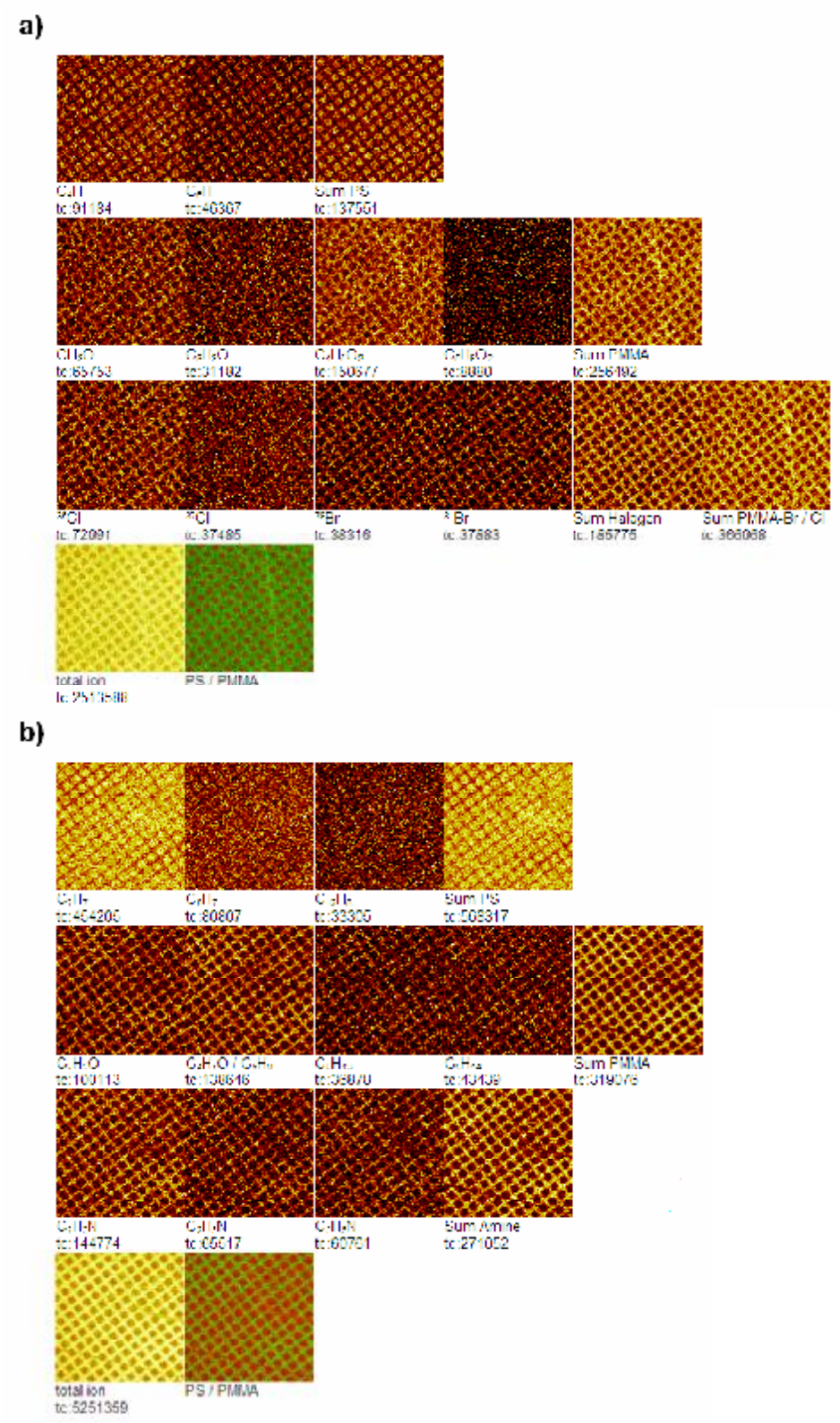

Figure 5.15 a) Negative and b) positive SIMS images for a binary-patterned PS/PMMA brush.

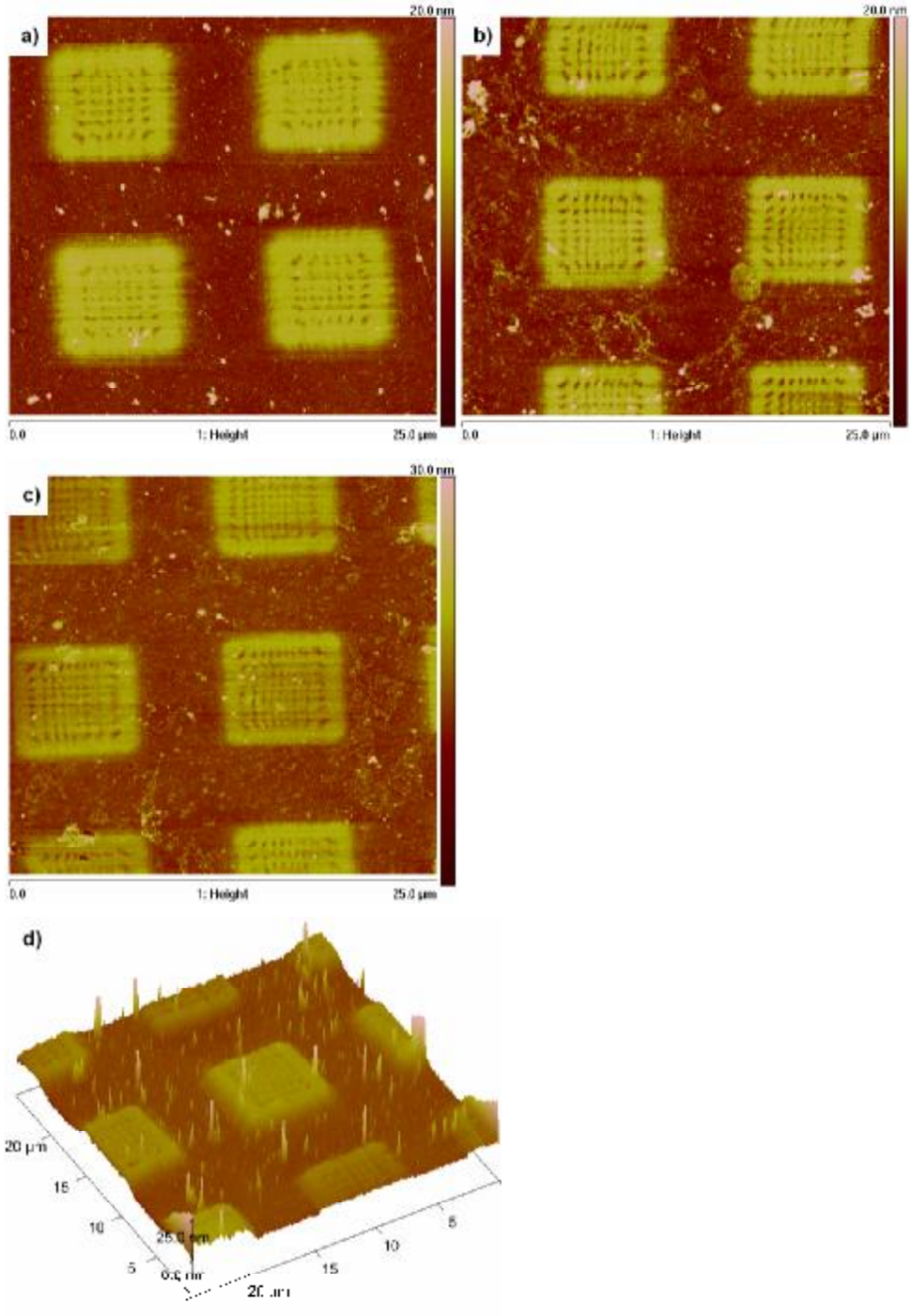

Figure 5.16 AFM images of binary-patterned PS/PMMA brushes. PS brushes grown for 12 hours, PMMA brushes grown for a) 12 hours, b), c) 20 hours, d) 5 hours .

5.6 Summary

Binary-patterned PS/PMMA brushes were successfully synthesised. The SIMS images showed that PMMA was chemically present, but AFM suggested that it formed a very thin layer, and did not increase in thickness with increasing reaction time. Some of the reaction steps used in preparing the functionalised surfaces were not 100 % efficient. Each additional step will amplify the inefficiency, resulting in a very low grafting density of PMMA, the surface-bound equivalent of a low yield. A polymer brush forms when polymer molecules are attached by one end to a substrate with a density of attachment points high enough that the chains are forced to adopt a stretched conformation[33,34]. At lower grafting densities, surface-attached molecules adopt a mushroom or pancake morphology, depending on the interaction of the polymer with the substrate[34]. In this case it would appear that the PMMA layer forms a 'pancake', and as the polymer chains grow longer, they spread further over the surface without any observable increase in thickness. Further work would be needed to optimise the synthesis: in particular there seemed to be problems with converting amine-silane into the bromoester-silane ATRP initiator. The efficiency of this reaction might be improved by using more aggressive reaction conditions, or reacting amine-silane with a less bulky molecule to produce an alternative surface-bound ATRP initiator.

This work has shown that it is possible to use this approach to synthesise binary-patterned polymer brushes. In principle, this method can be used to make binary brushes using any monomers that can be polymerised by ATRP. At present, the first polymerisation must use copper bromide as the catalyst to allow effective dehalogenation by reaction with sodium azide. It may be possible to modify amine-silane to produce initiators for alternative polymerisation reactions, increasing the range of accessible polymers. Patterning by irradiation through masks limits this technique to producing brushes on planar substrates, and means that the minimum feature size is dictated by the wavelength of light. This could be overcome by the use of near-field techniques such as scanning near-field photolithography (SNP) which allow maskless patterning to produce features much smaller than the wavelength of light[11,35].

5.7 References

(1) Xu, F. J.; Kang, E. T.; Neoh, K. G. *Journal of Materials Chemistry* **2006**, *16*, 2948-2952.
(2) Maeng, I. S.; Park, J. W. *Langmuir* **2003**, *19*, 9973-9976.
(3) Husemann, M.; Morrison, M.; Benoit, D.; Frommer, J.; Mate, C. M.; Hinsberg, W. D.; Hedrick, J. L.; Hawker, C. J. *Journal of the American Chemical Society* **2000**, *122*, 1844-1845.
(4) Zhou, F.; Jiang, L.; Liu, W.; Xue, Q. *Macromolecular Rapid Communications* **2004**, *25*, 1979-1983.
(5) Konradi, R.; Rühe, J. *Langmuir* **2006**, *22*, 8571-8575.
(6) Tovar, G.; Paul, S.; Knoll, W.; Prucker, O.; Rühe, J. *Supramolecular Science* **1995**, *2*, 89-98.
(7) Prucker, O.; Habicht, J.; Park, I.-J.; Rühe, J. *Materials Science & Engineering, C-Biomimetic and Supramolecular Systems* **1999**, *8-9*, 291-297.
(8) Bhushan, K. R.; DeLisi, C.; Laursen, R. A. *Tetrahedron Letters* **2003**, *44*, 8585-8588.
(9) Beier, M.; Hoheisel, J. D. *Nucleic Acids Research* **2000**, *28*, e11, i-vi.
(10) Beier, M.; Hoheisel, J. D. *Nucleic acids research* **1999**, *27*, 1970-7.
(11) Alang Ahmad, S. A.; Wong, L. S.; ul-Haq, E.; Hobbs, J. K.; Leggett, G. J.; Micklefield, J. *Journal of the American Chemical Society* **2009**, *131*, 1513-1522.
(12) Kong, X.; Kawai, T.; Abe, J.; Iyoda, T. *Macromolecules* **2001**, *34*, 1837-1844.
(13) Tu, H.; Heitzman, C. E.; Braun, P. V. *Langmuir* **2004**, *20*, 8313-8320.
(14) Zhao, J.; Shang, Z.; Gao, L. *Sensors and Actuators, A: Physical* **2007**, *A135*, 257-261.
(15) Sha, K.; Li, D. S.; Li, Y.; Wang, S.; Wang, J. *Journal of Materials Science* **2007**, *42*, 4916-4925.
(16) Lei, Z.; Bi, S. *Materials Letters* **2007**, *61*, 3531-3534.
(17) Zhang, K.; Li, H.; Zhang, H.; Zhao, S.; Wang, D.; Wang, J. *Materials Chemistry and Physics* **2006**, *96*, 477-482.
(18) Briggs, D. *Surface Analysis of Polymers by XPS and Static SIMS*; First ed.; Cambridge University Press: Cambridge, 1998.
(19) Hasan, A.; Stengele, K.-P.; Giegrich, H.; Cornwell, P.; Isham, K. R.; Sachleben, R. A.; Pfleiderer, W.; Foote, R. S. *Tetrahedron* **1997**, *53*, 4247-4264.
(20) http://www.casaxps.com/help_manual/manual_updates/xps_spectra.pdf.
(21) Lee, M.-T.; Ferguson, G. S. *Langmuir* **2001**, *17*, 762-767.
(22) Jones, D. M.; Brown, A. A.; Huck, W. T. S. *Langmuir* **2002**, *18*, 1265-1269.
(23) Kim, J.-B.; Bruening, M. L.; Baker, G. L. *Journal of the American Chemical Society* **2000**, *122*, 7616-7617.
(24) Bao, Z.; Bruening, M. L.; Baker, G. L. *Macromolecules* **2006**, *39*, 5251-5258.
(25) Xu, F. J.; Song, Y.; Cheng, Z. P.; Zhu, X. L.; Zhu, C. X.; Kang, E. T.; Neoh, K. G. *Macromolecules* **2005**, *38*, 6254-6258.
(26) Peach, S.; Polak, R. D.; Franck, C. *Langmuir* **1996**, *12*, 6053-6058.
(27) Sun, S.; Leggett, G. J. *Nano Letters* **2007**, *7*, 3753-3758.
(28) Sun, S.; Chong, K. S. L.; Leggett, G. J. *Nanotechnology* **2005**, *16*, 1798-1808.
(29) Koutsioubas, A. G.; Vanakaras, A. G. *Langmuir* **2008**, *24*, 13717-13722.
(30) Smith, F. G.; King, T. A.; Wilkins, D. *Optics and Photonics: An Introduction*; Second ed.; John Wiley and Sons, Ltd: Chichester, UK, 2007.

(31) Dolnik, M.; Rovinsky, A. B.; Zhabotinsky, A. M.; Epstein, I. R. *Journal of Physical Chemistry A* **1999**, *103*, 38-45.
(32) Duffin, W. J. *Electricity and Magnetism*; Fourth ed.; The McGraw-Hill Companies: London, 1990.
(33) Milner, S. T. *Science* **1991**, *251*, 905-914.
(34) Rühe, J. In *Polymer Brushes: Synthesis, Characterization, Applications*; Advincula, R. C., Ed.; Wiley-VCH: Weinheim, 2004.
(35) Leggett, G. J. *Chemical Society Reviews* **2006**, *35*, 1150-1161.

Chapter 6

Pattern-Directed Phase Separation

6.1 Introduction

The properties of a polymer blend depend firstly on whether it is homogeneous or phase-separated. For phase-separated blends, the properties depend on the domain morphology[1], and the strength of the interfaces between the domains[2].

Most blends of high molecular weight polymers are thermodynamically incompatible[3]. As the molecular weight is reduced, the polymers become miscible within a particular composition and temperature range. The phase separation behaviour of a blend is determined by the nature of the interactions between the two polymers, which can be discussed in terms of the Flory – Huggins interaction parameter, χ: when χ is positive, the polymers are immiscible. Different types of phase diagrams are produced according to the value and temperature dependence of χ (this is explained in more detail by Balsara[1]). PS/PMMA blends have positive χ which increases linearly with $1/T$[1]. Blends of intermediate molecular weight are miscible at the extremes of composition and show UCST behaviour in the mid-composition range[4]. Experimentally determined cloud points can be used to calculate the binodal curve and critical point of a blend.

As the thickness of a polymer blend film is reduced (below ~ 1 μm[5]), the interaction of the polymers with the surface and substrate begin to affect phase separation throughout the film[6]. In most cases, one of the polymers preferentially segregates to each interface[7], resulting in significant changes in morphology. The sample preparation and processing can also have significant effects on the observed structure. For example, spin coating produces blend films by the rapid evaporation of a common solvent, resulting in morphologies that may be far from thermodynamic equilibrium[8]. The phase separation behaviour of thin blend films is more varied, and affected by many more

factors than in the bulk. This makes it more challenging to understand the morphology of a polymer blend thin film, but offers the potential for more control over structure.

Control of the lateral microstructure of polymer blends is a subject of great interest for applications such as polymer LEDs[9], non-linear optical devices[10], polymer-based microelectronic circuits[11,12], optoelectronic devices[13] and templating in lithographic processes[13]. Phase separation in polymer mixtures can be altered by the presence of a substrate with a lateral pattern of surface energy[14]. Each polymer has a different affinity for the pattern, leading to preferential adsorption and segregation of each polymer on different areas of the patterned surface[15]. This pattern-directed phase separation has been studied both experimentally[9-22] and theoretically[16,23-25]. The key parameters for pattern replication are the ratio of the characteristic length scale of phase domains to the pattern periodicity, and the match of the blend composition to the area of the pattern[15].

Blends of PS/PMMA (with a wide range of molecular weights and compositions) have been extensively studied[1,4,8,12,19,26-48]. We used small-angle light scattering (SALS), AFM, nuclear reaction analysis (NRA), optical microscopy and SIMS to investigate the phase separation of a low molecular weight blend of PS/PMMA on homogeneous and patterned substrates. SALS was used to measure cloud points and determine the binodal curve and critical point of the bulk blend. AFM and NRA were used to investigate the morphology of thin films of the blend on silicon substrates. Blends were also spin-coated onto patterned SAMs and binary-patterned polymer brushes then AFM and optical microscopy or SIMS was used to measure the affect of the patterns on the domain structure.

6.2 Materials

Hydrogen-terminated PMMA, M_p 4900 g mol^{-1}, M_w 4960 g mol^{-1} (GPC), M_n 4530 g mol^{-1}, M_w/M_n 1.10, was obtained from Polymer Laboratories, Shropshire, UK. Polystyrene, M_n 5180 g mol^{-1}, M_w/M_n 1.04, was synthesised by Laurence Corvazier. Deuterated PS, M_w 5680 g mol^{-1}, M_n 5220, M_w/M_n 1.09 synthesised by Pierre Chambon was used to make samples for NRA.

Anhydrous toluene was obtained from a Solvent Purification System (Innovative Technology Inc., SPS-400-6 and SPS-200-6). Typical water content was 10-16 ppm.

Single crystal silicon wafers were obtained from Compart Technology Ltd (100 mm diameter, 525 μm thick, boron doped, <100> face polished).

Glass slides were Chance Coverglasses, 16 mm diameter, 1.5 thickness (0.155 – 0.185 mm), obtained from Agar Scientific.

6.3 Experimental Methods

All blend compositions are given as % PS / % PMMA (w/w).

6.3.1 Small Angle Light Scattering/Cloud Point Determination

PS and PMMA were weighed out to the desired compositions (30/70, 40/60, 50/50, 60/40, 70/30 w/w), then made up to 20 % (w/v) solutions with dry toluene. The polymers were left to dissolve for at least an hour. Glass slides were cleaned by sonicating for 15 minutes each in water, acetone and toluene, then dried with a stream of nitrogen. A single drop of 20 % (w/v) polymer solution was placed on the centre of a clean glass slide. Once most of the solvent had evaporated, a second drop was added to produce a thick polymer film. Samples were stored for at least two days, then heated to 115 ºC under vacuum overnight to remove any residual solvent (above T_g for both polymers). Samples were left to cool to room temperature under vacuum.

The polymer blend films were found to dewet the glass slides at high temperatures. To prevent this, small pieces of glass were placed around the edge of the slide, and used to support a second slide (see Figure 6.1). This limited the movement of the blend film during cloud point determination, and ensured that the laser beam passed through the polymer film.

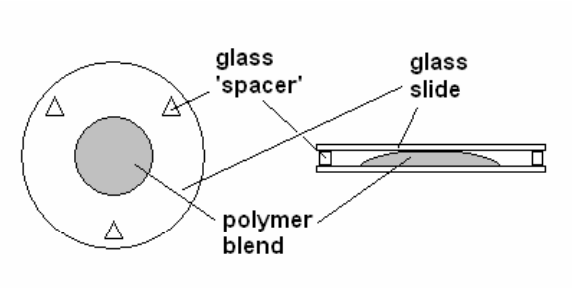

Figure 6.1 Sample preparation for SALS

A home-made SALS apparatus, built by Yoshii Ishii, was used to determine the cloud points of the blends. Light from a 20 mW He-Ne laser with a wavelength of 632.8 nm (Uniphase) was passed through optics to produce a homogeneous light source. The sample was mounted in the path of the laser on a Linkam THMS 600 hot stage with LNP and CI 93 temperature programmers (controlled by LinkSys 2.3a software). Light scattered by the sample fell onto a flashed opal diffuser (Comer) with a simple beam stop to prevent transmission of the unscattered beam. The scattering patterns were captured by a SITe 512 x 512 pixel camera (Princeton Instruments)[49] and integrated using WinView 32 software. The blend films were heated to 300 ºC under nitrogen, then the scattering pattern was captured every 30 s as the sample was cooled at 1 ºC/minute. The stage temperature was recorded at different frame numbers to allow calibration of the data. The cloud points were determined by examining plots of total scattering intensity – temperature for each sample.

6.3.2 Morphology of Thin Polymer Blend Films

PS and PMMA were weighed out to the desired compositions (30/70, 50/50, 70/30 w/w), then made up to 2 % (w/v) solutions with dry toluene. The polymers were left to dissolve for at least 30 minutes, then the solution was passed through a 0.45 μm microfilter before use.

The substrates were cleaned before use:

- Silicon wafers were cut into 1 cm^2 pieces, and rinsed with water, methanol, THF and acetone.
- Patterned NPPOC-silane/amine-silane coated samples were stored in the dark, then rinsed with ethanol immediately before use.

6. Pattern-Directed Phase Separation

- Binary-patterned polymer brushes were rinsed repeatedly in toluene (at least 5 rinses).

All samples were dried with nitrogen immediately before spin coating.

A substrate was mounted onto the spin coater, covered with 2 – 3 drops of polymer solution, then spun at 3000 rpm for 120 s. The acceleration and deceleration were set to equal values and kept constant for all samples. Samples were stored for at least 24 hours to allow the solvent to evaporate, then samples were annealed at 115 ºC under vacuum overnight and allowed to cool slowly to room temperature under vacuum.

6.3.2.1 Selective Dissolution

Information about the phase-separated morphology of polymer blend films was obtained by removing one of the components with a selective solvent. The sample was scratched with a scalpel blade, then the AFM tip was aligned with respect to the intersection of two scratches using an optical microscope (it was helpful to mark the position of the scratches, tip and other surface features on the optical microscope monitor screen). The sample was immersed in the selective solvent for 3 minutes: cyclohexane was used to dissolve PS, glacial acetic acid to remove PMMA[8,26]. Samples were rinsed quickly with cyclohexane or water respectively, then dried. The scratches and surface features were used to relocate and image the original area of the sample[8,26]. Results from selective dissolution experiments need to be treated with caution, as immersion in solvent is an invasive process that can introduce artefacts[15]. This is discussed in more detail below (see p. 189).

6.3.2.2 Phase Separation on Patterned SAMs

Samples were heated on a hot stage mounted on a reflection optical microscope. Images were captured every 30 s, starting when the temperature reached 100 ºC, and finishing after approximately 200 frames. All samples were heated using the same settings:

Heating Rate/ $^{o}C\ min^{-1}$	Limit/ ^{o}C	Time at Limit/ minutes	Frame Number When Limit Reached	Frame Number When Limit Changed
10	100	0	1	1
2	150	10	51	71
2	155	10	76	91
2	160	7.5	96	111
2	200	7.5	150	-

6.4 Characterisation

Characterisation by spectroscopic ellipsometry, tapping mode AFM and SIMS was performed as described in Chapters 3 and 5.

6.4.1 Reflection Optical Microscopy

Images were acquired using a Nikon Eclipse ME600 optical microscope with a PixeLINK camera and PixeLINK Capture OEM software. Blends on patterned SAMs were heated in situ using a Linkam THMS 600 hot stage with a TP 93 controller.

6.4.2 Nuclear Reaction Analysis

2 % (w/v) solutions of dPS/PMMA were spin-coated onto silicon wafers at 3000 rpm for 120 s (see above). NRA measurements were performed by Mark Geoghegan, Richard Thompson and Parvaneh Mokarian-Tabari using a National Electronics Corporation 5SDH series Pelletron accelerator facility at the University of Durham. $^{3}He^{2+}$ ions were accelerated to 700 keV before being incident on the polymer film at a glancing angle of 5º. Protons were detected and used to determine the depth profiles. The $^{3}He^{+}$ exposure delivered to the sample during any measurement was limited to 5 μC^{50}. Film thicknesses were measured by ellipsometry. The film thickness multiplied by the volume fraction dPS was used to define the area under the depth profile. This area was used to calibrate the data obtained from the ion beam experiments. Data were

fitted using a 100 % dPS profile measured at 750 keV. These conditions gave a depth resolution of ~ 5 nm.

6.5 Results and Discussion

6.5.1 Cloud Point Determination

PS/PMMA blends are immiscible at high molecular weight, and become fully miscible only when the weight-average molecular weights are reduced to 2950 g mol^{-1} and 2400 g mol^{-1} for PS and PMMA respectively[4].

The cloud point is defined as the temperature at which a blend first becomes cloudy[4], which can be taken to represent the onset of phase separation. SALS was used to measure cloud points and produce a phase diagram. Based on the work of Callaghan and Paul[4], the cloud points were predicted to be between 150 and 250 ºC. Samples were heated to 300 ºC under nitrogen, and the scattering patterns were recorded as the samples were cooled at 1 ºC/minute. The cloud point was determined by plotting the total scattering intensity against temperature. A sample plot is shown below in Figure 6.2.

The plot could be split into three sections: at high temperatures above the cloud point, the blend was clear, so the scattering intensity was low. As the temperature was reduced, the formation of phase-separated domains led to a rapid increase in scattering intensity. The cloud point was determined by calculating the intersection point of lines of best fit for each of these regions. An approximate solution was found by looking at the graph, then the fits were adjusted to maximise the R^2 value for both lines (it is worth noting that this only resulted in small changes in the determined temperature). As the temperature was further reduced, the progression of phase separation resulted in the polymer film becoming more opaque, eventually blocking the transmission of light, and slowly decreasing the scattering intensity.

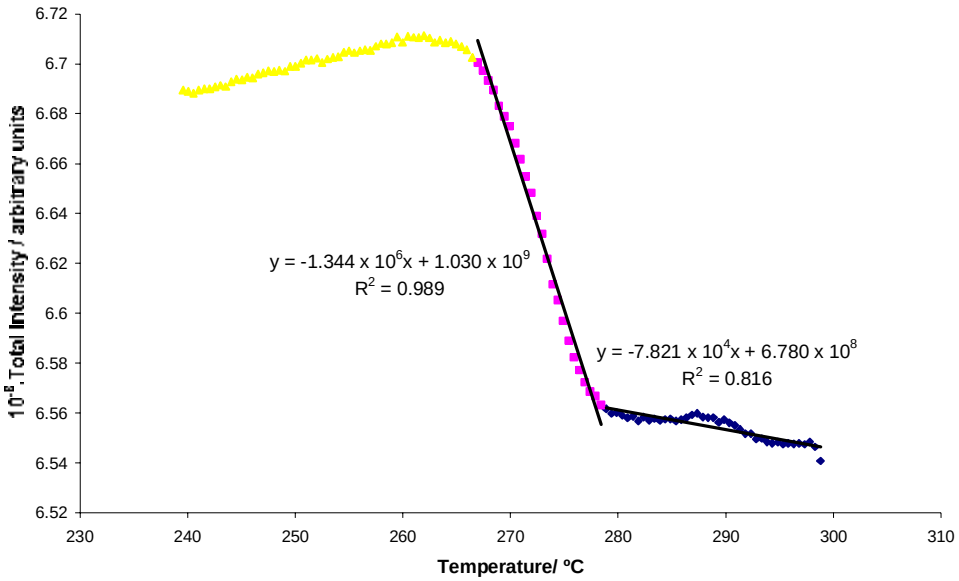

Figure 6.2 SALS profile to allow determination of the cloud point for 70/30 PS/PMMA. ♦ high temperature region, blend clear, ■ onset of phase separation, blend becoming cloudy, ▲ domain size increasing, blend becoming opaque.

Cloud points were determined for blends from 30 – 70 % (w/w) PS. At least two samples were measured for each composition. Cloud points agreed to within ± 3 ºC, except for 70/30 PS: PMMA where there was an uncertainty of ± 5 ºC over three measurements. The approximate phase diagram is shown below (Figure 6.3).

This represents the binodal curve for the blend. The critical point was found at approximately 290 ºC, 52 % PS. This was higher than expected: Callaghan and Paul reported a critical point of 250 ºC, ϕ_{PMMA} 0.57 for a blend of PS (M_w 9200) and PMMA (M_w 4250)[4]. It is possible that the discrepancy may be partially due to differences in experimental method (which was not completely explained in the reference). It is also possible that there were differences between the (measured) stage temperatures and the actual temperature of the samples, though any differences are likely to be small. PMMA is known to undergo thermal depolymerisation by several different mechanisms with significant rates at temperatures below 280 ºC[51,52], which could also affect the results (in fact, thermal depolymerisation can be used to recycle high yields of MMA from PMMA[53,54]). Use of a lower molecular weight blend was abandoned due to obvious changes in appearance after heating, so this may be a significant effect.

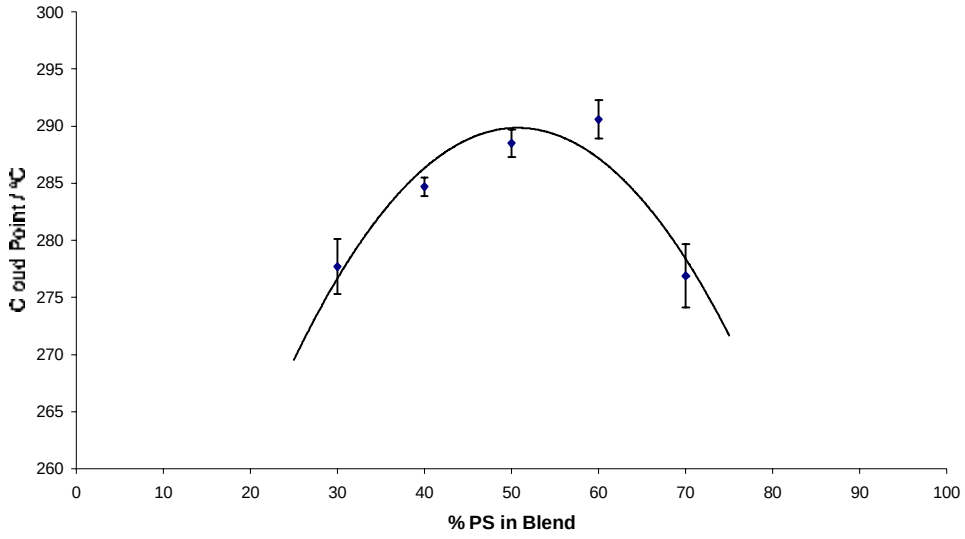

Figure 6.3 Measured cloud points for PS/PMMA blend, error bars as shown. Line of best fit is a second order polynomial, $R^2 = 0.87$.

6.5.2 Phase Separation in Thin Films

For bulk polymer blends, phase separation leads to the formation of an isotropic, disordered phase morphology with a characteristic length scale increasing in the course of the process[14]. As the film thickness is reduced, the interaction of the polymers with the substrate and the air interface begin to have significant effects on the process of phase separation[6]. There is generally preferential segregation of one component of the blend to each of the interfaces[7]. The polymer of lower surface energy is attracted to the surface[2] in order to minimise the air-polymer interfacial free energy[30,31]. One of the blend components is also likely to be adsorbed onto the substrate, again to minimise the interfacial energy, for example, for PS/PMMA blends, the more polar PMMA is attracted to hydrophilic silicon (oxide) substrates[8,30]. Changing the substrate can dramatically alter the morphology of a phase-separated blend[8,30,38].

In relatively thin films (thickness less than ~ 1 μm[5]) preferential segregation of one or other component of the blend to the interfaces can induce the formation of composition waves normal to the surface[6]. This surface-directed spinodal decomposition results in a layered structure, which coarsens over time due to the high interfacial energy of the composition waves[20,55]. For films that are thinner than the wavelength of the

composition waves (thickness < ~ 200 nm), surface-directed spinodal decomposition is suppressed, and lateral phase separation occurs within the plane of the film[20].

The morphology of a polymer blend film is affected by the chemical structure of the polymers and their molecular weights, the blend composition, nature of the substrate, film thickness, casting solvent, solution concentration, chain end groups and temperature[26,44]. Thin films of PS/PMMA blends have been extensively studied: different groups have investigated the effect of molecular weights[35,47], blend composition[32,40-42,48], substrate[8,30,38], casting solvent[8,44], film thickness[26,30], solution concentration[40,41,44], end groups[28], alternative preparation methods[27], the effect of block copolymer additives[34] and annealing time and temperature[31,35-37,39,48]. This project investigated the behaviour of thin films of three different compositions of a low molecular weight PS (M_n 5180)/ PMMA (M_n 4530) blend. Blends were spin-coated onto silicon substrates from toluene, then annealed 115 ºC under vacuum overnight, and allowed to cool slowly to room temperature. This is above the glass transition temperature of both polymers: based on DSC measurements of other low molecular weight PS and PMMA samples, T_g(PMMA) ~ 99 ºC, T_g(PS) 74 – 96 ºC[4], and so could be expected to have some affect on the domain structure. However the annealing conditions were quite mild, so any changes in structure could be expected to be relatively small. This was supported by AFM images of as-cast dPS/PMMA blends that appeared to be only slightly different to the annealed PS/PMMA films.

Film thicknesses, determined by AFM and ellipsometry were between 51 and 85 nm. AFM showed very similar morphologies for all the blend films. The surfaces were very smooth, with small circular raised features ~ 200 nm in diameter and ~ 5 nm high (or similar sized holes). The phase images (not presented here) were also very smooth, suggesting that there was a chemically homogeneous layer covering the surface. Selective dissolution was used to obtain more information about the internal phase morphology. Separate (but equivalent) samples were rinsed with either cyclohexane, which selectively dissolves PS[8,26], or glacial acetic acid, which is a good solvent for PMMA[8]. The original scan areas were then relocated and imaged, revealing the underlying phase morphology. Care must be taken when analysing selective dissolution images, as immersion in solvent can affect the film structure or introduce artefacts. These include damage to the remaining film morphology arising from partial solubility

and/or swelling of the non-selected polymer, the removal of thin surface layers of either polymer and the washing away of small inclusions of the insoluble phase suspended completely within the solvated polymer[15]. Sets of images, showing the initial and selective solvent treated morphologies are presented on the following pages: Figures 6.4 and 6.5 show the effects of cyclohexane and acetic acid treatment respectively.

Most samples had a few larger, irregularly-distributed features up to 1.5 μm across and 100 nm high. These were still visible after samples had been treated with either cyclohexane (e.g. Figure 6.4 a, b) or acetic acid (e.g. Figure 6.5 a, b), which suggests that they were probably caused by dust particles trapped in the polymer film during spin coating.

Treatment with cyclohexane selectively dissolved the PS, revealing the PMMA morphology. All samples showed an increase in surface roughness e.g. 30/70 PS/ PMMA (Figure 6.4 a) had an rms roughness of 1.16 nm, which increased to 3.74 nm after treatment with cyclohexane (Figure 6.4 b). There was no obvious lateral domain structure revealed. The 50/50 PS/PMMA blend was rougher than the other samples: cyclohexane rinsing revealed a network of irregularly-shaped depressions ~ 30 nm deep with raised rims ~ 30 nm above the height of the background across part of the image (see Figure 6.4 d).

Cyclohexane only becomes a good solvent for PS above ~ 35 ºC[56]. However, various different groups have used cyclohexane at unspecified temperatures (assumed to be room temperature) to selectively dissolve the PS component of polymer blend films[7,8,15,27,43,57] (in addition, Jerome *et. al*[45] used cyclohexane at 28 – 30 ºC to selectively dissolve PS from a PS/PMMA blend film). For the low molecular weight PS used in these experiments, three minutes exposure to room temperature cyclohexane seemed to dissolve the vast majority of a 100 % PS film. The success of the selective dissolution is further supported by the significant changes in morphology observed when blend films on binary-patterned brushes were rinsed with cyclohexane (see p. 204). However, the results should still be interpreted with caution. An interesting further test would be to treat the samples with warm cyclohexane (> 35 ºC) to see if this alters the observed morphologies.

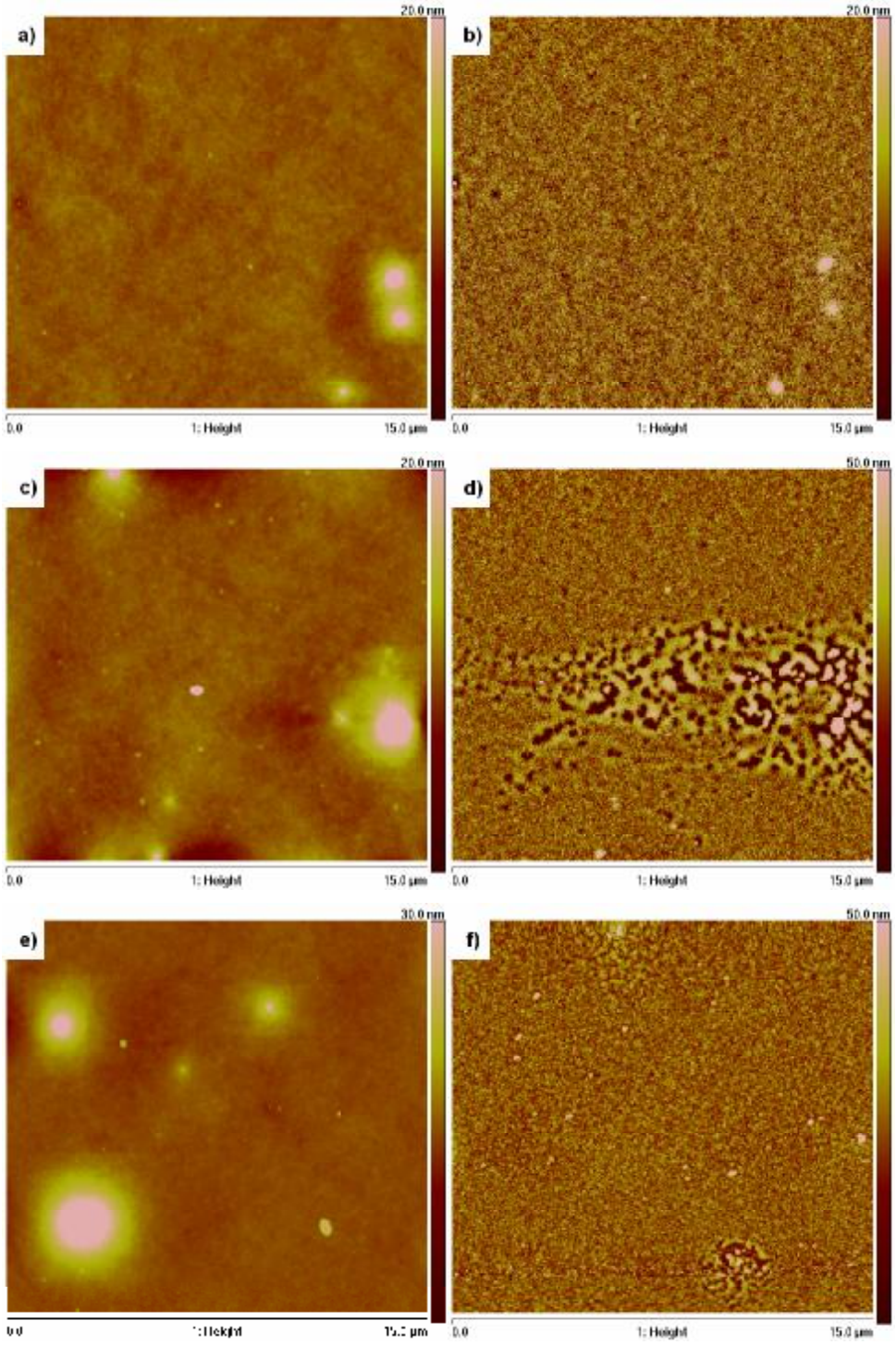

Figure 6.4 PS/PMMA blends on silicon. Images in the left-hand column show the complete blend film morphology, images in the right-hand column show the same areas after rinsing with cyclohexane. a), b) 30/70 PS/PMMA; b),d) 50/50 PS/PMMA; e), f) 70/30 PS/PMMA. Image sizes and scales as shown.

Treatment with acetic acid (a selective solvent for PMMA) resulted in dramatic changes in appearance, shown in Figure 6.5. Highly textured, irregularly-shaped interconnected domains 100 – 130 nm high were observed on 30/70 and 50/50 blends (one area). The depressed areas between these features were extremely smooth, and were thought to be the silicon substrate. 70/30 and a different part of the 50/50 sample showed a smooth surface layer covered by circular holes around 1.5 μm in diameter and 50 nm deep, with rims raised ~ 20 nm above the rest of the film. These images conflicted with the other evidence: some of the raised features were significantly higher than the total blend film thickness, but were not visible when the unmodified samples were imaged. In other words, if the PS and PMMA morphologies were added together, the result would not resemble the structure of the complete blend film. There were also difficulties in imaging films after treatment with acetic acid, especially for 50/50 blends (it took several attempts to successfully obtain the image presented in Figure 6.5 d): in some cases it looked like the film had been partially removed from the surface then redeposited. The results suggest that the low molecular weight PS used in this work was affected by acetic acid. This was tested by exposing a 100 % PS film to acetic acid for three minutes. Optical microscopy showed cracking and partial removal of the film (see Figure 6.6). The PS was completely removed in areas close to the scratches used to align the AFM tip, presumably because they allow acetic acid to reach the substrate and begin to undercut the polymer film. This means that the morphologies observed on samples exposed to acetic acid need to be treated with extreme caution, as the morphology shown is very likely to be different from the morphology of the PS domains within the blend film.

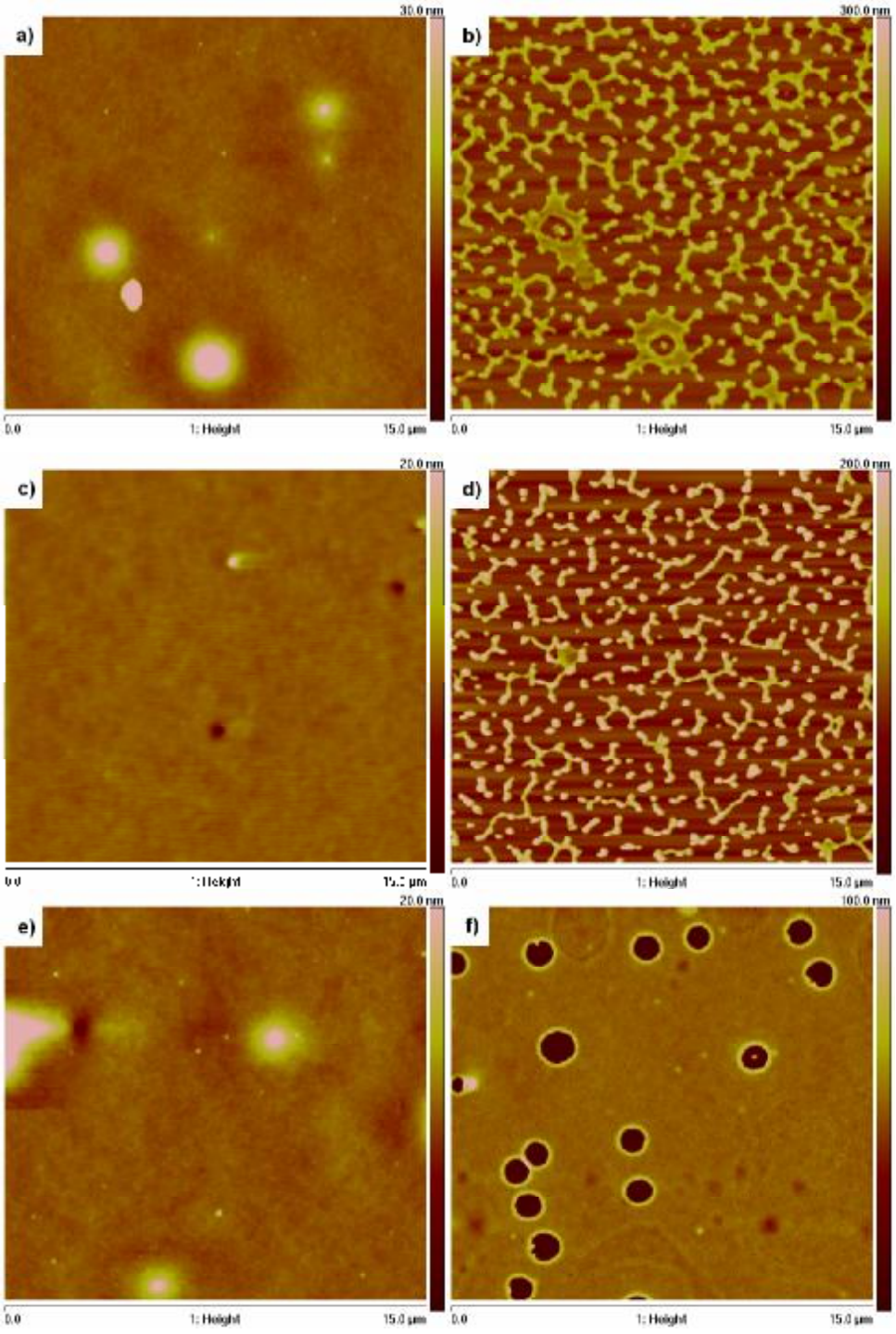

Figure 6.5 PS/PMMA blends on silicon. Images in the left-hand column show the complete blend film morphology, images in the right-hand column show the same areas after rinsing with acetic acid. a), b) 30/70 PS/PMMA; b),d) 50/50 PS/PMMA; e), f) 70/30 PS/PMMA. Image sizes and scales as shown.

Figure 6.6 Optical micrograph showing PS on silicon after treatment with acetic acid showing partial removal of the PS, and cracking of the film. The scratches were used to align the AFM tip on the surface. 10 x magnification.

NRA can be used to determine the composition of a sample as a function of depth[58]. One of the polymers must be deuterated to give contrast, so samples were made using dPS with M_w 5680 g mol^{-1}. The samples were analysed as cast, without any annealing. In NRA, the sample is bombarded by a monoenergetic $^3He^+$ beam at a low angle of incidence. When an ion hits the film surface it loses its second electron to form a $^3He^{2+}$ ion. At some depth within the polymer it reacts with deuterium to form an unstable lithium nucleus, which decays yielding a proton and an alpha particle, either of which can be detected (in these experiments, protons were detected):

$$^3He^{2+} + d \longrightarrow (^5Li^{3+})^* \longrightarrow \alpha + p \quad (6.1)$$

The protons emitted from the film have a characteristic energy spectrum which is dependent on the energy of the reaction and the depth at which the reaction occurred[50,59], which can be used to build up a volume fraction (ϕ) – depth composition profile for the sample. The depth profiles (Figure 6.7), showed that PMMA was enriched at the substrate, which could be expected due to a favourable interaction between the PMMA and the polar silicon substrate[30]. The thickness of this substrate layer, and the degree of enrichment depended on the composition of the blend: for 30/70 dPS/PMMA, $\phi_{PMMA} > 0.88$ in the bottom 24 nm of the sample; when the amount of PMMA was reduced to 50 %, this layer was only 9 nm thick. For the blend with 30 % PMMA, there was obviously some PS within the wetting layer at the substrate, but a layer 12 nm thick exceeded the bulk concentration of PMMA. Conversely, dPS was

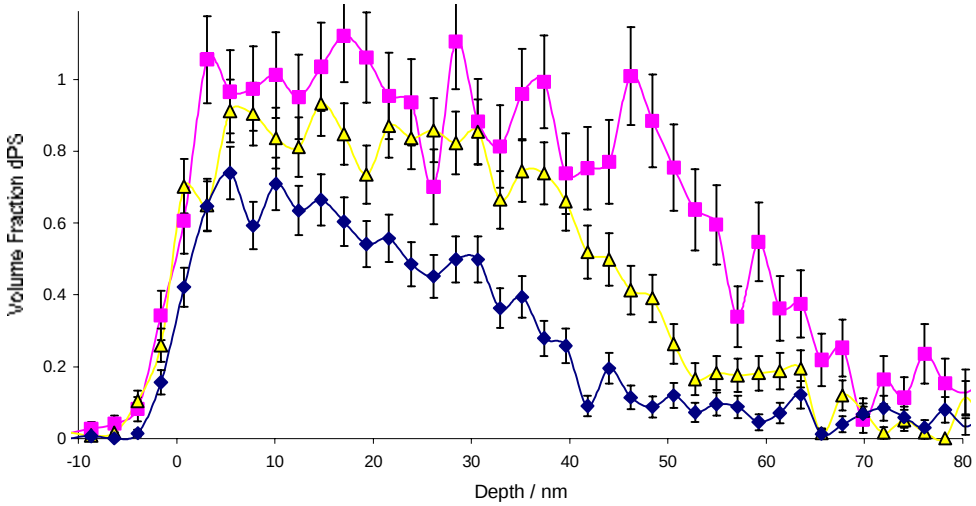

Figure 6.7 NRA depth profiles for dPS/PMMA blends on silicon. ♦ 30/70 dPS/PMMA (68 nm thick), ▲ 50/50 dPS/PMMA (73 nm thick), ■ 70/30 dPS/PMMA (75 nm thick).

enriched at the free surface. For 70/30 and 50/50 blends, there was an almost pure dPS layer (ϕ_{dPS} > 0.9) 24 and 15 nm thick respectively, at the surface. For 30/70 dPS/ PMMA, the surface layer contained more PMMA, but ϕ_{dPS} > 0.6 within 15 nm of the surface.

As discussed on p. 43, the morphology of thin films of phase-separated polymer blends is affected by many variables. For PS/PMMA blends spin-coated onto silicon (or other hydrophilic substrates such as mica) there appear to be three main effects:

- The attractive interaction between the carbonyl groups of PMMA and the polar silanol groups on the silicon substrate[30], which favours the formation of a PMMA wetting layer at the substrate.
- The relative solubility of PS and PMMA in the common solvent – the least soluble polymer will solidify earlier in the spin coating process, while the more soluble polymer is still swollen with solvent[8].
- The surface tension of the polymers – the lower surface free energy polymer is attracted to the air interface[2].

There is some debate in the literature about the role of surface tension for PS/PMMA blends. PS has lower surface tension, so should be enriched at the surface. However, the differences in surface tension are small, and in some cases insignificant e.g. PS (M_n 90k) γ = 40.2 mJ m^{-2}, PMMA (M_n 69k) γ = 41.2 mJ m^{-2} [30] or PS (M_v 44k) γ = 40.7 mJ m^{-2}, PMMA (M_v 3000) γ = 41.1 mJ m^{-2} [60]. Tanaka *et al.*[30] found evidence for surface enrichment of PS in bulk blends, but when the film thickness was reduced to 100 nm, there was lateral phase separation with both polymers present at the surface. This is supported by the work of Harris *et al.*[48] used near-edge x-ray absorption fine structure spectroscopy (NEXAFS) to rule out the presence of a homogeneous PS surface layer in annealed blends. For PS/PMMA blends, the relatively small differences in surface tension are dominated by substrate and solvent effects, and have little impact on the final film morphology.

When PS/PMMA blends are spin-coated onto silicon from toluene solution the solubility and solvent effects combine, favouring the formation of a bilayer morphology with a PMMA-rich layer at the substrate, with PS-rich layer deposited above. This bilayer structure is far from equilibrium. As the remaining solvent evaporates, or the film is annealed, the PS-rich layer becomes unstable and begins to dewet the PMMA-rich layer[27,44]. The equilibrium morphology is dewetted droplets of PS suspended in a PMMA-rich matrix[26,27,35,38,44,48]. However, the high viscosity of high molecular weight polymers may inhibit flow through the film, making changes very slow[26], which can kinetically trap a non-equilibrium morphology. Very different morphologies can be obtained when the solvent and substrate effects conflict. Ton-That *et al.*[31,41] spin-coated PS/PMMA blends onto mica substrates from chloroform solution. PS was deposited first onto the substrate due to its lower solubility in chloroform, leaving the surface rich in PMMA[31,41]. Annealing resulted in dewetting of the PMMA from the PS-rich phase, eventually producing a laterally phase-separated film with a continuous, but non-homogeneous PS layer at the surface[31]. However, for a similar system, Harris and co-workers[48] found that longer annealing at a higher temperature allowed it to reach the equilibrium morphology of PS droplets in a PMMA matrix. Large differences in molecular weight between the polymers can also alter the domain structure: high molecular weight PS/low molecular weight PMMA blends were PMMA-rich at the surface due to the lower entropic penalty for shorter polymer chains at the surface[47].

A diverse range of intermediate morphologies (and an equally wide range of explanations of these!) have been reported depending on the properties of the polymers, sample preparation conditions and annealing time and temperature. The polymers used in this work had very low molecular weights, so it can be assumed that they are less viscous and more mobile than higher molecular weight blends, resulting in a quicker approach to equilibrium during spin coating and annealing[35]. However, the annealing conditions used (115 ºC, ~ 12 hours) were mild, so the blends are unlikely to have reached equilibrium.

AFM showed that the film surfaces were almost featureless: quite different in appearance to most of the references (a similar structure; a gently undulating surface with small, raised circular features was found after annealing a 50/50 mixture of PS (M_w 100k)/ PMMA (M_w 120k) spin-coated onto mica from chloroform at 142 ºC for 2 hours[31], but this is probably only a superficial similarity as the polymer molecular weights and preparation methods were very different). Selective dissolution of PS with cyclohexane left rough PMMA layers with no large surface features, and reduced the total film thickness.

AFM images of samples rinsed with acetic acid produced highly textured morphologies that resembled different stages of dewetting. The most likely explanation for this is that the low molecular weight PS was partially soluble in acetic acid, and the observed PS morphology does not represent the structure of the blend. Alternatively, dissolution of PMMA molecules within the PS-rich phase may lead to changes in the structure. Finally, removal of the PMMA-rich layer at the substrate may physically lift and break up the overlying PS-rich layer (this probably occurred in some samples where solvent rinsing caused destruction of the polymer film). NRA suggested that there was a PMMA-rich layer wetting the substrate and a PS-rich layer at the surface. These results suggest that the blends formed bilayer structures, with PMMA-rich layers at the silicon substrate, and PS-rich layers at the free surface, and little, if any, lateral domain formation.

The morphology of the blend on PS and PMMA brushes was also (indirectly) studied. The domain structure was very different, and will be discussed in more detail from p. 201 onwards.

6.5.3 Phase Separation on Patterned Substrates

The production of laterally microstructured materials is a subject of great commercial interest for a wide range of applications, mainly in microelectronic and optoelectronic devices (see p. 41 and 50). The lateral morphology of a phase-separated polymer blend film can be controlled by breaking the symmetry of the substrate through heterogeneous chemical patterning of the surface energy or by topographical surface patterning[15]. This pattern-directed phase separation was first studied by Krausch *et al*. in 1994[10]. Since then, the effect of chemical and/or topographical patterning on phase separation has been investigated both experimentally[9-22] and theoretically[16,23].

Several parameters are important for pattern replication: there must be preferential segregation of at least one of the polymers to one of the areas of the chemically patterned surface[11,14]. Secondly, the periodicity of the substrate pattern must be comparable to the natural length scale for phase separation under the conditions used[9,11]. The natural length scale of phase separation can be altered by varying the film thickness or blend composition[15]. Finally, the blend composition should match the pattern area fraction (although this is less important than the match of the length scales)[15].

The phase separation of a PS/PMMA blend was investigated on patterned NPPOC-/amine-silane SAMs and binary-patterned PS/PMMA brushes (see Chapter 5 for details of the synthesis of these substrates). AFM images of the binary-patterned brushes were used to calculate the area fraction of the patterns. On average the squares were 6.92 μm across, and the grid was 5.58 μm across, giving a square repeat unit 12.50 μm across. This allowed calculation of the area fraction of the squares and the grid: $f_{squares} = 0.3$, $f_{grid} = 0.7$. The surface chemistry and dimensions of the patterns are shown in Figure 6.8. The pattern periodicity was significantly larger than the natural length scale of phase separation observed on unpatterned polymer brush substrates, but time constraints meant that smaller patterns could not be synthesised. However, this could be done via the use of a mask with smaller features.

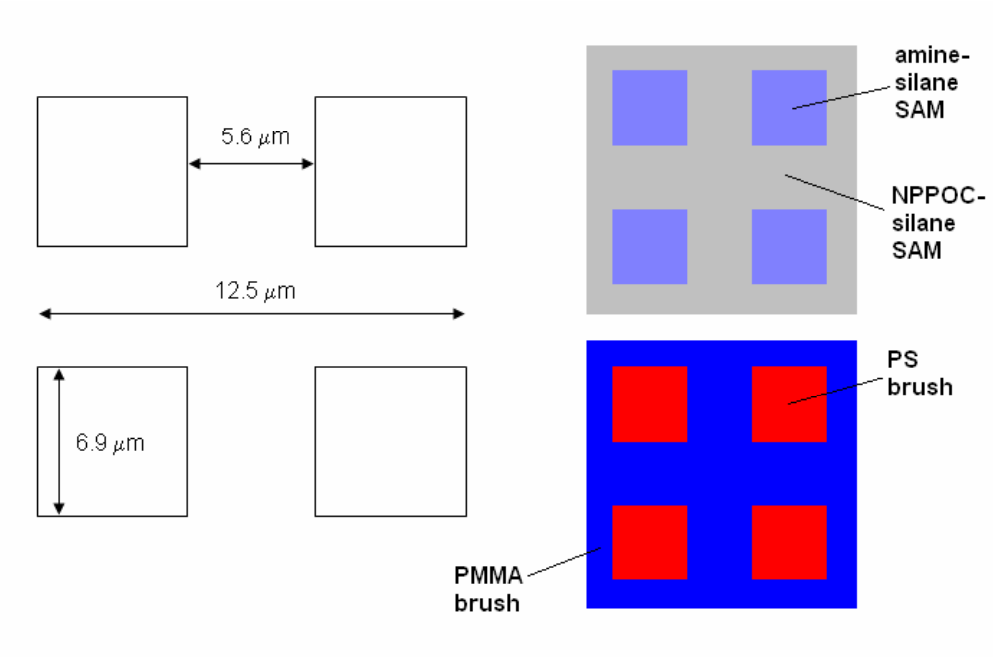

Figure 6.8 Schematic diagram showing patterned SAM and binary-patterned polymer brush substrates.

6.5.3.1 Phase Separation on Patterned SAMs

The behaviour of 30/70 PS/PMMA was investigated on patterned SAMs. The blend was spin-coated onto the patterned substrates, then heated to 115 ºC under vacuum overnight. After this there was no evidence of lateral phase separation: optical microscopy showed a smooth surface with a few tiny scattered holes and dust grains (see Figure 6.9 a) and AFM showed a largely smooth surface (rms roughness 1.98 nm) with some circular raised features and depressions about 1 μm in diameter (see Figure 6.10 a).

As there was no evidence of pattern replication, it was decided to slowly heat the samples, monitoring changes as they happened with optical microscopy. Heating a polymer blend in the two-phase region of the phase diagram, above the glass transition temperature for both polymers allows phase separation to progress[3]. As the sample was heated, there was an increase in the number of small holes (visible as bright spots in the microscope images), first noticeable at ~ 138 ºC (Figure 6.9 b). As the temperature was increased further, the number of holes and their diameter slowly increased. Smaller surface corrugations, which did not seem to pass through the entire thickness of the film

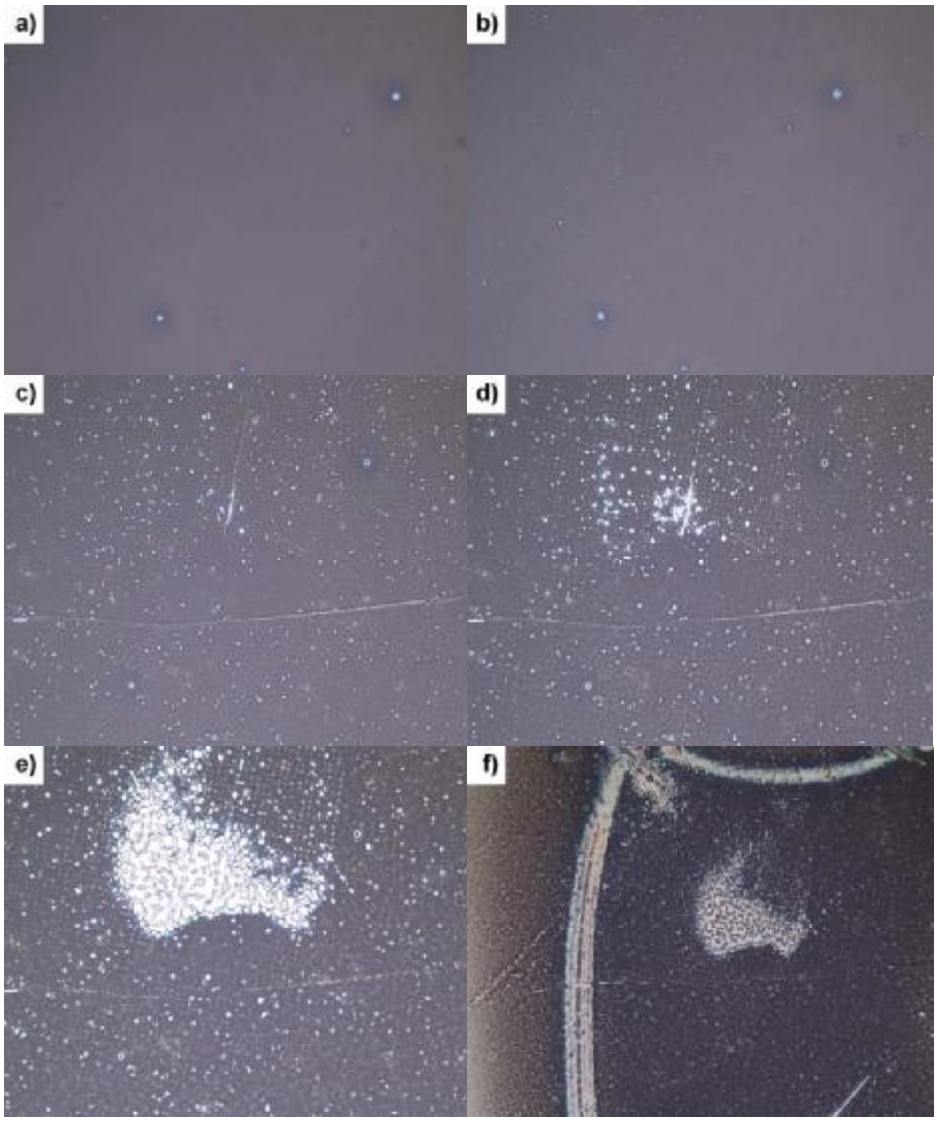

Figure 6.9 Optical microscopy images of heating 30/70 PS/PMMA on patterned SAM. All 10 x magnification except f) 5 x. a) as cast, b) 138 ºC, c) 160 ºC, d) 185 ºC, e) 200 ºC, f) structure after cooling to room temperature.

also began to appear. By ~ 185 ºC (Figure 6.9 c), it became apparent that the features in the upper part of the image were following a square lattice. The sample was then held at 200 ºC to allow the surface features to develop. Dewetting progressed on one part of the surface, starting from holes arranged in a square pattern. The rest of the sample showed a square pattern which appeared to consist of thinner and thicker regions of polymer (see Figure 6.9 d, e). A final image is included which shows the extent of the pattern, and the boundary between patterned and homogeneous NPPOC-silane regions of the substrate (Figure 6.9 f).

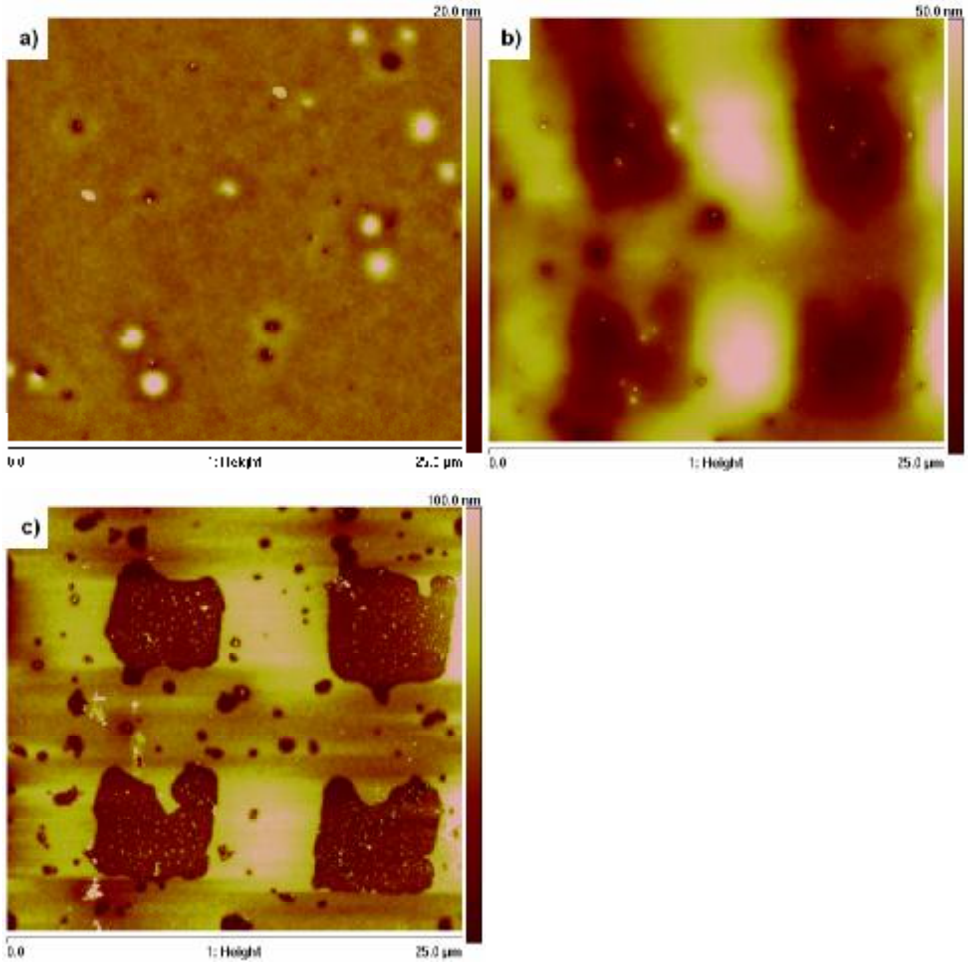

Figure 6.10 30/70 PS/PMMA on patterned NPPOC-silane/amine-silane substrates. a) as cast morphology, b) after heating to 200 ºC (see p. 180 for heating conditions), c) same area as b) after rinsing with cyclohexane. Image sizes and scales as shown.

After heating, AFM showed an undulating surface, with rounded square-shaped depressions arranged in a square lattice (Figure 6.10 b). Examination of the bright areas visible optically confirmed that these were dewet, with large irregularly-shaped droplets up to 400 nm high separated by areas of substrate covered in smaller droplets. PS was selectively dissolved with cyclohexane to give more information about the phase morphology (shown in Figure 6.10 c). This resulted in the square depressions becoming more clearly defined and approximately 15 nm deeper. The raised grid was less obviously affected, but there was an increase in the number of holes. This suggested that the squares were covered with a thin layer of PS, with PMMA attracted to the NPPOC-silane covered grid. The increased number of surface holes suggested that

there could be a PS overlayer or secondary domains of PS located on the PMMA coated grid. There were also small secondary PMMA domains left on the square part of the pattern. The dewet areas suggest that these were transient morphologies and that the blend film was unstable on the amine-silane SAM.

The heating experiments were repeated with several samples. The conditions used were decided on by watching the behaviour of the first sample. Although this was fairly arbitrary, all samples were heated using the same conditions, allowing some comparison. Similar patterned/dewet areas were produced by heating different samples, but the onset of changes occurred at varying temperatures and times. In one case, there was no detectable patterning, even after around 25 minutes at 200 ºC. The behaviour of the samples appeared to be very sensitive to local variations such as fluctuations in layer thickness, variation in substrate properties and the presence of defects such as dust particles and scratches – this can be seen in Figure 6.9 – some areas were dewetted, initiating from a small scratch on the surface, where other areas retained a continuous, but corrugated polymer layer.

The wetting/dewetting behaviour of thin polymer films is important to applications such as coatings, paints, dielectric layers, thin film lubrication and microelectronic and optoelectronic devices[7]. It is known that bilayers of PS and PMMA on silicon are unstable and undergo dewetting[12,61] (whatever the order of the layers). In the case of PS/PMMA blends spin coated onto NPPOC-silane/amine-silane patterned SAMs, it would seem that during spin coating and at temperatures below ~ 130 ºC the polymer film is stable on the patterned substrate. As the temperature is increased, the blend eventually dewets from the pattern, beginning from the amine-silane-covered squares. It is difficult to comment further on the phase separation morphology, although it seems likely that PMMA is preferentially attracted to the NPPOC-silane regions.

6.5.3.2 Phase Separation on Binary-Patterned Polymer Brushes

Next, the phase separation of the blend was investigated on binary patterned PS/PMMA brushes. These substrates were both chemically and topographically patterned: the PS brush squares were around 9 nm higher than the PMMA brush grid. There has been some study of the behaviour of polymer thin films on substrates that are both

chemically and topographically patterned (see p. 49)[19,62,63], but there has been little study of phase separation on binary-patterned brushes, possibly because they are relatively new materials and they are still challenging to synthesise. Edwards[64] and Stoykovich[65] studied the behaviour of PS-*block*-PMMA copolymers[64] and ternary blends of block copolymers and homopolymers[65] on patterns produced by photolithographic treatment of 'grafted to' PS brushes. They found that well-ordered structures were produced providing the pattern periodicity was close to the natural length scale of phase separation. Fukunaga *et al*.[18] investigated phase separation on a randomly patterned binary polymer brush produced by physisorption of a poly(styrene-*block*-2-vinylpyridine-*block*-*tert*-butyl methacrylate) triblock copolymer onto silicon. Spin coating this microphase separated brush with a PS/poly(*tert*-butyl methacrylate) blend resulted in a significant reduction in domain size compared to the morphology found on silicon substrates.

PS/PMMA blends of three different compositions (30/70, 50/50, 70/30) were spin-coated onto the binary-patterned PS/PMMA brushes and annealed at 115 ºC overnight. The morphologies were examined by optical microscopy, AFM and SIMS. Changes were immediately detected as the patterns became clearly visible: this is shown by the optical micrographs in Figure 6.11 below.

AFM showed different morphologies on PS and PMMA brush, and for each of the three

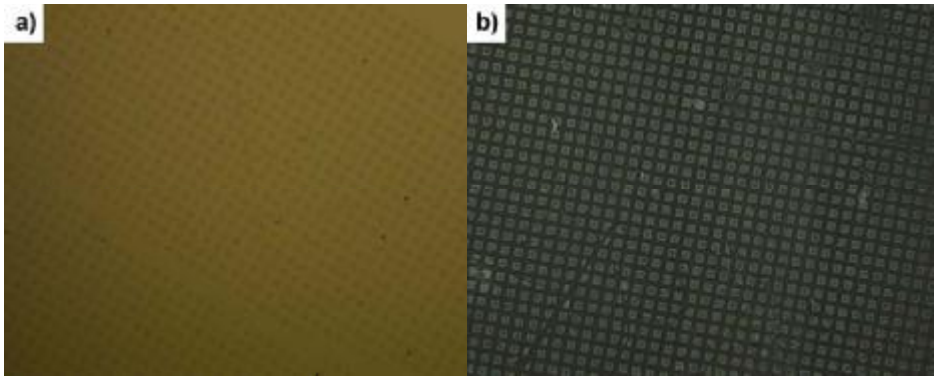

Figure 6.11 Optical micrographs of a) PS/PMMA binary-patterned polymer brush, b) 50/50 PS/PMMA blend spin-coated onto PS/PMMA binary-patterned polymer brush – note how the pattern is much more clearly visible in b). Both 10 x magnification.

blend compositions. The 30/70 PS/PMMA sample most closely matched the area fraction of the patterned brush (assuming that PS is attracted to PS brush etc), so could be expected to give the best pattern replication[15]. The squares (PS brush) were clearly visible and (on average) higher than the PMMA brush grid. The grid was covered by a relatively smooth layer, though there was some smaller scale structure visible on most samples. The squares were covered by a raised polymer layer with irregularly distributed holes, ~ 25 nm deep and ~ 1 μm in diameter (e.g. Figure 6.12 a). However there was some variation between samples, probably due to differences between the substrates, for example, one sample had much higher relief than the others: the squares were about 30 nm higher than the grid, and the holes were up to 75 nm deep and 1.5 μm in diameter (see Figure 6.12 c).

Samples were then rinsed with cyclohexane, to reveal the PMMA morphology. There were no major changes, but the microstructure on the grid became much more clearly defined. The morphology on the squares remained the same, but the depth of the holes increased, typically by ~ 10 nm, suggesting that there was a layer of PS at the bottom of the holes. There was little change in the height difference between the squares and the grid (see Figure 6.12 b).

The samples were also rinsed with acetic acid to remove the PMMA. Acetic acid was found to alter the morphology of PS/PMMA blends and pure PS films on silicon substrates (see p. 191), so the results need to be interpreted with caution as they may not be a true representation of the PS morphology. However, in this case (Figure 6.12 d), the morphology revealed was complementary to the PMMA structure described above. On the PS brush squares, there were isolated cylinders ~ 1.5 μm across in the same places as there had been circular holes in the complete blend film. The top of these features was dish-shaped, with a raised rim and depressed centre. This suggested that the PMMA layer at the surface was dewetting, and pulling up the underlying PS, producing raised cylinders with curved menisci. The background level of the squares was about 20 nm above the background of the grid. On the grid there were many smaller features 100 - 120 nm high. This suggested that the PS brush was covered by a continuous layer of PS, but that it was less favourable for PS to be at the surface of the

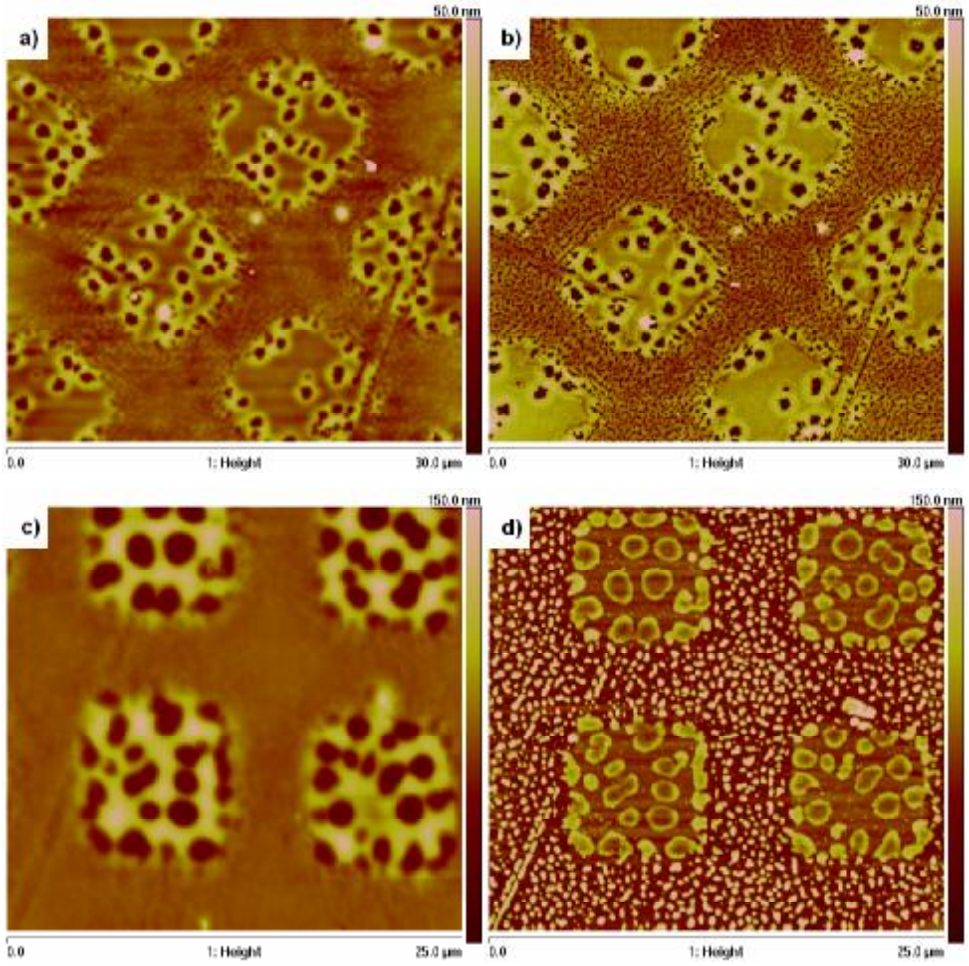

Figure 6.12 30/70 PS/PMMA blends on binary-patterned polymer brush. a), c) As-cast, b) same area as a) after rinsing with cyclohexane, d) same area as c) after rinsing with acetic acid. Image sizes and scales as shown.

PMMA brush, so it formed smaller, more raised domains to reduce the unfavourable contact. The PMMA-rich phase formed a continuous layer at the surface, almost completely covering the underlying structure and leaving an almost smooth film surface on the grid.

SIMS was also used to map the distribution of characteristic PS and PMMA ions on the samples. It was decided to map the same ions used to identify the chemistry of the binary-patterned PS/PMMA brushes (though other ion images were also looked at). The ion images, presented in Figure 6.13, show PS forming a homogeneous layer covering the sample, suggesting that there could be a very thin layer of PS covering the

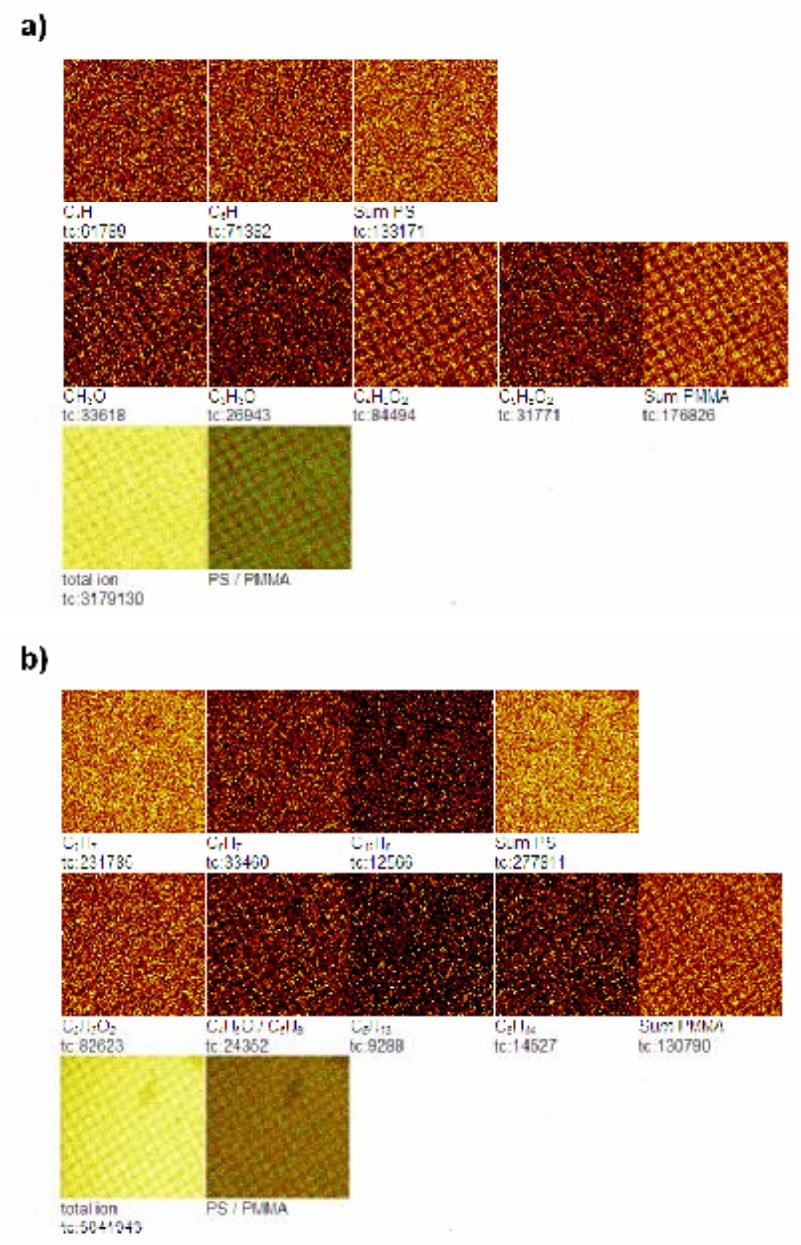

Figure 6.13 a) Negative and b) positive SIMS images of 30/70 PS/PMMA spin-coated onto binary-patterned PS/PMMA brush.

whole surface. PMMA was clearly patterned, and appeared to be mainly located on the squares. SIMS is very surface-sensitive[66], so any surface layer of PS would have to be extremely thin (< 1 nm), or it would prevent detection of the PMMA ions. However, the lateral resolution of SIMS is around 60 nm, which may not be sensitive enough to detect the small scale patterning on the grid. The larger, micron scale structure on the

squares could be detected, showing the PMMA-rich surface. The topography of the samples may also have some effect on the recorded ion images.

AFMs of the samples coated with 50/50 PS/PMMA had less obvious surface features than those of the 30/70 blend (see Figure 6.14 a, c). The squares and grid were still clearly visible, but the edges of the squares were less clearly defined. Some structure was visible on the surface of the squares, and smaller scale patterning could be detected on the grid regions. The height difference between the squares and the grid was 15 – 25 nm, but varied quite a lot between samples, and was as much as 35 nm in one case – as mentioned earlier, this is probably due to differences between the individual substrates.

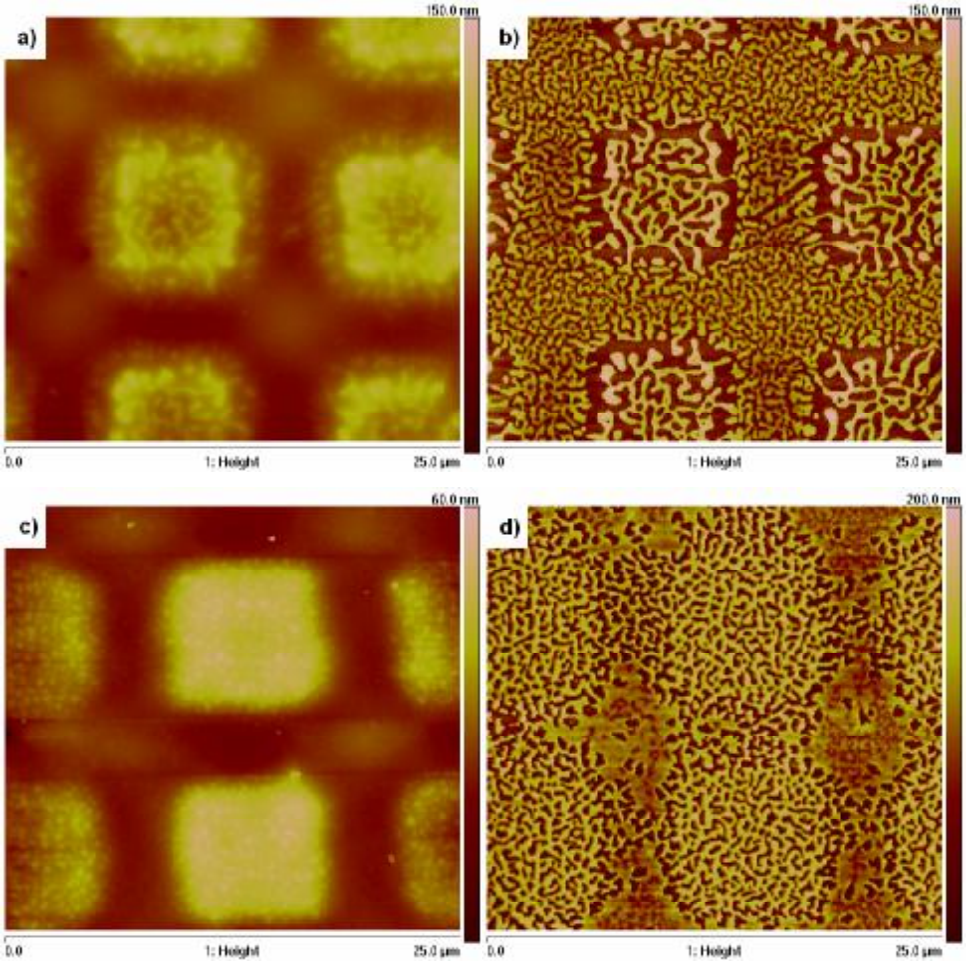

Figure 6.14 50/50 PS/PMMA on binary-patterned polymer brush. a), c) As-cast, b) same area as a) after rinsing with cyclohexane, d) same area as c) after rinsing with acetic acid. Image sizes and scales as shown.

Rinsing with cyclohexane revealed an interconnected network of PMMA domains (Figure 6.14 b). The domains were larger on the PS brush squares (typically ~ 500 nm across and ~ 100 nm high) than on the PMMA brush grid (~ 300 nm across, 40 nm high), but the general morphology was similar. Treatment with acetic acid revealed a complementary interconnected morphology on the squares, and spreading over the grid. The centre of the grid regions were covered by a continuous layer with scattered holes (see Figure 6.14 d). The AFM images suggest that there was a higher percentage coverage of PMMA domains on the PMMA grid, but this is difficult to measure. SIMS again showed a homogeneous PS layer, with squares faintly visible in the PMMA signal (though they were less clear than for 30/70) – see Figure 6.15.

The samples were covered by an interconnected and interpenetrating network of phase-separated PS and PMMA. Surprisingly, there seemed to be little preferential adsorption of either polymer on the PS or PMMA brush surface. SIMS suggested that the PS brush squares were enriched in PMMA at the free surface, so there may be a PS-rich layer next to the brush. On the PMMA brush, the domains were smaller. AFM and SIMS suggested that the substrate was slightly enriched in PMMA, and that PS almost completely covered the PMMA structure, resulting in the smooth surface observed by AFM, and the lack of PMMA ions from the grid in SIMS.

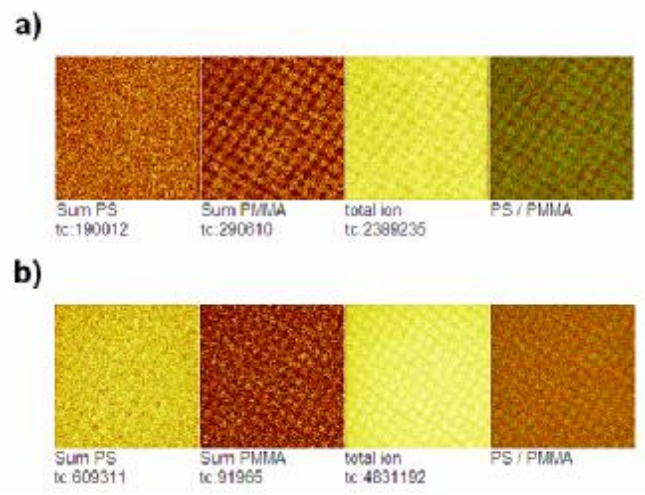

Figure 6. 15 a) Negative and b) positive SIMS ion images of 50/50 PS/PMMA on binary-patterned polymer brush. Images presented are the sums of the same ions as shown in Figure 6.13.

Finally, 70/30 PS/PMMA was spin-coated onto the patterned substrates. In this case there was a large mismatch between the pattern area fraction and the blend composition (assuming that PS is attracted to PS brush etc). AFM (Figure 6.16 a, c), clearly showed the expected pattern. The squares were covered by small raised circular features up to 300 nm in diameter. There was no surface structure on the grid – this was confirmed by looking at the blend morphology on the homogeneous PMMA brush at the edge of the patterned region, which showed a gently undulating surface with a few small circular blobs – similar in appearance to Figure 6.4 a, c. Removal of PS by rinsing with cyclohexane showed that the surface was densely covered with small round PMMA domains (Figure 6.16 b). These were up to 100 nm high, and 200 – 300 nm in diameter

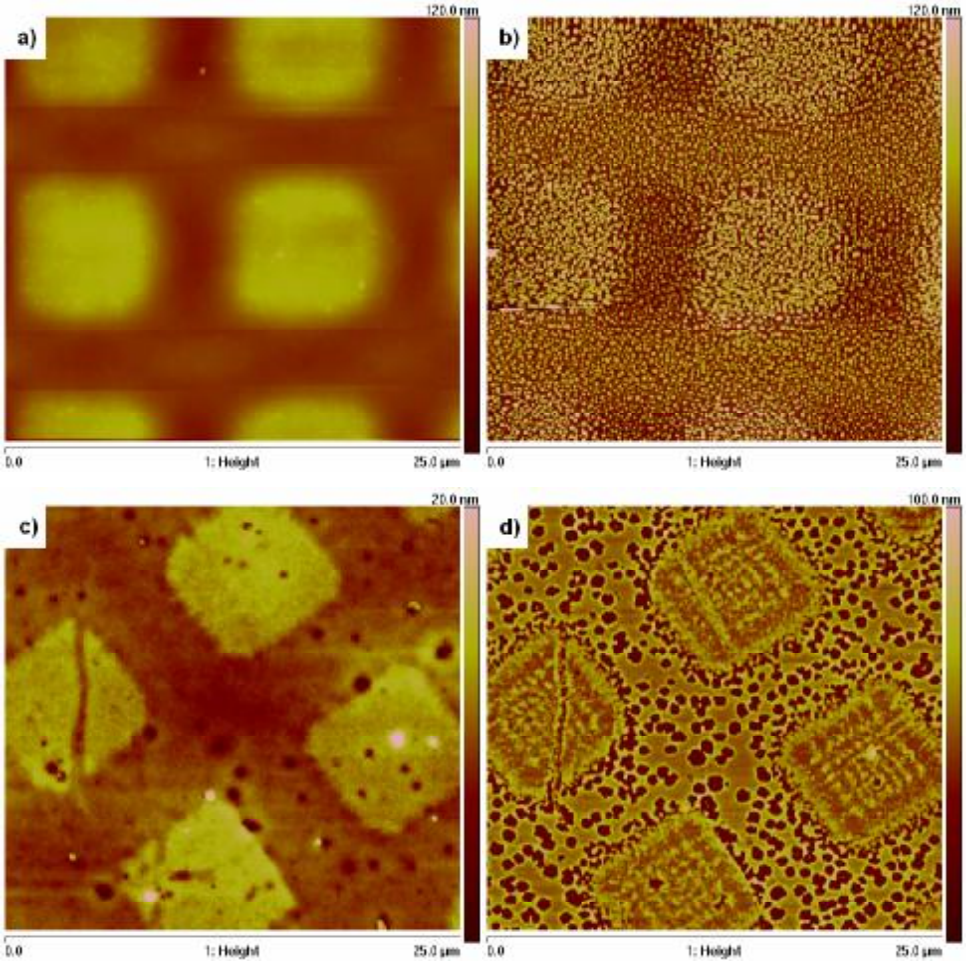

Figure 6.16 70/30 PS/PMMA on binary-patterned polymer brush. a), c) As-cast, b) same area as a) after rinsing with cyclohexane, d) same area as c) after rinsing with acetic acid. Image sizes and scales as shown.

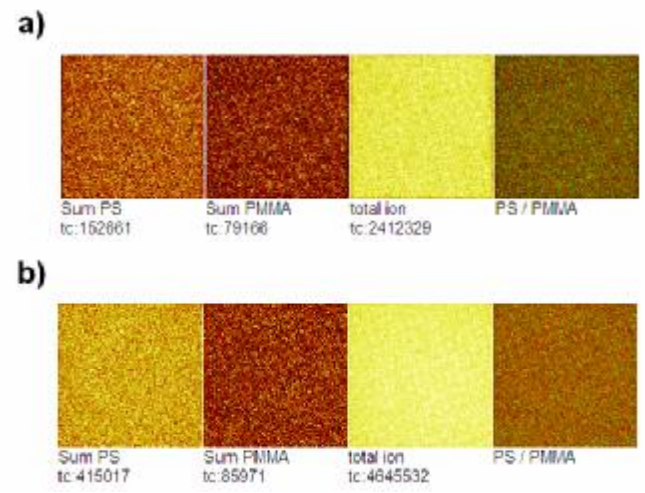

Figure 6.17 a) Negative and b) positive SIMS ion images for 70/30 PS/PMMA on binary-patterned polymer brush. Images presented are the sums of the same ions as shown in Figure 6.13.

on the squares, and slightly smaller (~ 200 nm diameter, 60 nm high) on the grid. Rinsing with acetic acid produced a highly structured surface (see Figure 6.16 d): the squares were covered by a continuous layer, which showed the microstructure of the underlying PS brush (see p. 166). On the grid there was a polymer layer covered in circular holes with raised rims (similar to those seen in Figure 6.5 f).

As discussed earlier, the low molecular weight PS used in these experiments was affected by exposure to acetic acid. For these samples, the PMMA morphology and the morphology revealed by rinsing in acetic acid were not complementary, suggesting that that exposure to the solvent had altered the PS domain morphology. Also the appearance of this sample (both before and after solvent treatment) was different to other examples of this blend. Possible reasons for this are discussed below.

SIMS images (Figure 6.17), showed that both PS and PMMA ions were present at the surface, but there was no detectable pattern, and the PMMA signal was noticeably weaker than for the other blends. This can be explained in part by the lower amount of PMMA present in the blend, but it also suggests that there is a homogeneous PS rich layer covering the surface (within the lateral resolution of the technique).

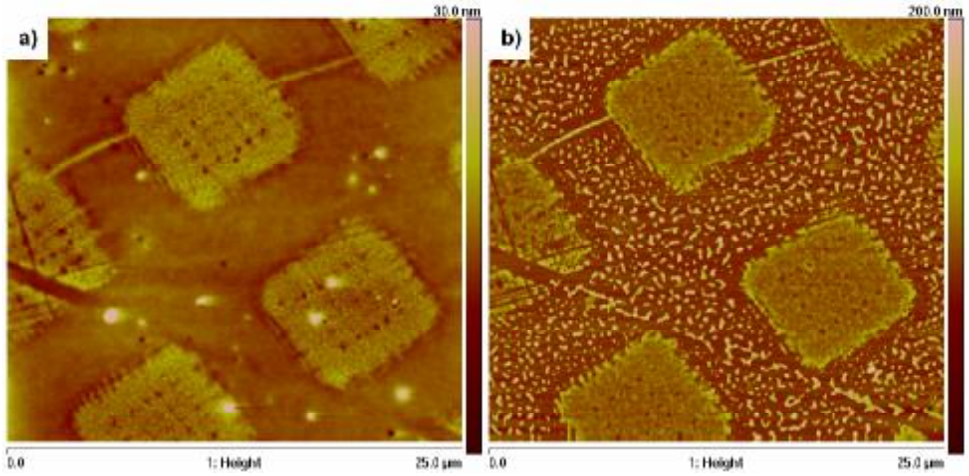

Figure 6.18 50/50 PS/PMMA on binary brush: recoated sample. a) As-cast, b) same area as a) after rinsing with acetic acid.

In some cases, different morphologies were observed for the same blend composition spin-coated onto two different samples. This may be caused by small chemical and physical differences between the individual patterned substrates. Only a small number of binary-patterned polymer brush samples were made, so in some cases it was necessary to clean and recoat samples. The first blend film was removed by repeatedly rinsing samples with toluene. A second blend composition was then spin-coated onto the cleaned substrates. There is some evidence that this affected the blend morphology, for example, a sample recoated with 50/50 PS/PMMA had a different morphology to the same blend on a new substrate – compare the images in Figure 6.18 above to Figure 6.14 c, d.

The sample shown in Figure 6.16 c and 6.16 d had also been recoated, and again seemed to have a different morphology from a fresh sample. It is possible that during spin-coating, the free polymer chains penetrate the brush (which will become swollen by toluene), and become trapped/entangled. They may then be very difficult to remove, even after extensive rinsing with a good solvent for the brush and the free polymer, as diffusion of the free chains out of the brush may be very slow. Another possibility is that the polymer brushes are permanently affected by exposure to cyclohexane and/or acetic acid, resulting in altered properties when a second polymer blend is placed on the substrate.

Very different morphologies were observed for each of the different composition PS/PMMA blends on the PS and PMMA regions of the binary-patterned polymer brushes. As already discussed, the morphology of thin films of polymer blends are affected by many different parameters including the chemistry and topography of the substrate, blend composition and the nature of the common solvent[26,44]. In addition, films prepared by spin-coating may be far from equilibrium[8], so annealing at temperatures above the glass transition temperatures of the polymers can lead to large changes in blend morphology[31]. The results discussed in this chapter were produced by annealing samples at a relatively low temperature, so the morphologies were still likely to be far from equilibrium. The observed morphologies of phase-separated PS/PMMA blends on binary-patterned brushes can be explained by considering the different solubility of the polymers in the common solvent, the match of the blend composition to the area of the pattern, and the preferential attraction of the polymers to different areas of the substrates.

For 30/70 PS/PMMA, the blend composition was matched to the area fraction of the binary-patterned polymer brush. The domain structure was mainly determined by the chemical (and topographical) differences across the substrates. The PS brush was completely covered by a PS-rich layer, with a layer of PMMA at the air interface. Bilayers of PMMA on PS are unstable and can undergo spinodal dewetting[61]. This may have produced the holes seen in the AFM images, and also deformed the underlying PS layer. On the PMMA brush, the domain size was much smaller: the substrate was covered by smaller domains of PMMA, with a surface layer of PS. It seems likely that both polymers were present at the brush interface, although the data presented here cannot rule out the presence of a thin PMMA layer covering the substrate. This suggested that there was a weaker attraction between free PMMA and PMMA brush than between PS and PS brush – a surprising result. The PMMA brush on the patterned substrates was very thin, and probably does not adopt the stretched conformation of a true polymer brush. To test that the brush conformation/thickness did not affect the phase morphology, the blends were spin-coated onto thicker PMMA brush samples (~ 10 nm thick), which resulted in almost identical morphologies. A schematic diagram of the phase-separated structure is shown below in Figure 6.19.

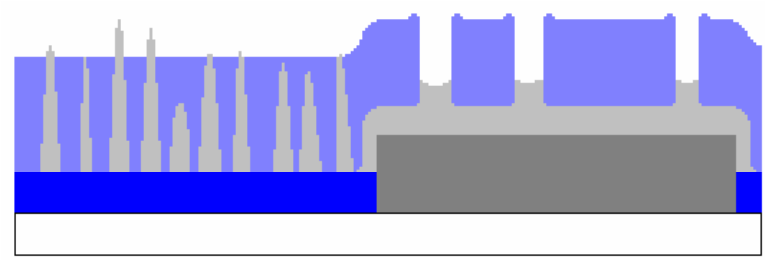

Figure 6.19 Schematic diagram showing the phase-separated structure of 30/70 PS/PMMA on PS/PMMA binary brush. PS brush: dark grey, PMMA brush: dark blue, PS pale grey, PMMA pale blue. Not to scale, but vertical scale is much exaggerated compared to the horizontal scale.

The 50/50 blend formed an interpenetrating network structure, with domains of each polymer present next to the brush (see Figure 6.20). The general morphology was the same on both PS and PMMA brush, although the feature size was slightly smaller, and there may have been a slight excess of PMMA, next to the PMMA brush surface. This suggested that, under the conditions used, the patterned substrates had little effect on the phase separated morphology. The laterally phase-separated structure also suggested that there was not a strong preferential attraction between the free polymers and either of the polymer brushes, although thin wetting layers could not be detected by the techniques used here.

For 70/30 PS/PMMA, AFM and SIMS results suggested that PMMA was deposited at the brush surface, forming a discontinuous layer of small domains, which were then covered by an almost smooth PS overlayer. PMMA is less soluble than PS in toluene, so was deposited earlier in the spin coating process[8]. For this blend there was a large

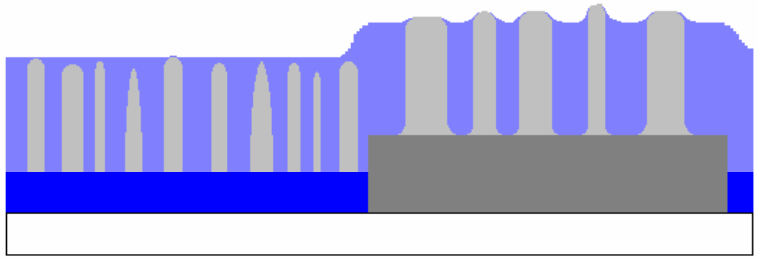

Figure 6.20 Schematic diagram showing the phase-separated structure of 50/50 PS/PMMA on PS/PMMA binary brush. PS brush: dark grey, PMMA brush: dark blue, PS pale grey, PMMA pale blue. Not to scale, but vertical scale is much exaggerated compared to the horizontal scale.

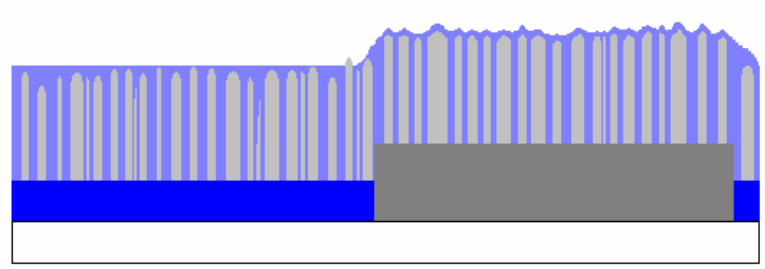

Figure 6.21 Schematic diagram showing the phase-separated structure of 70/30 PS/PMMA on PS/PMMA binary brush. PS brush: dark grey, PMMA brush: dark blue, PS pale grey, PMMA pale blue. Not to scale, but vertical scale is much exaggerated compared to the horizontal scale.

mismatch between the pattern area fraction ($f_{PS} = 0.3$) and the blend composition ($\phi_{PS} \approx 0.7$). The observed structure of the blend suggests that in this case, the difference in solubility had a greater effect on the domain morphology than the surface patterning or preferential attraction of either polymer to the brush surfaces (see Figure 6.21).

6.6 Summary

Phase separation in thin films of polymer brushes is affected by many different variables. In this chapter, the effect of blend composition and substrate chemistry was investigated for thin films of a low molecular weight PS/PMMA blend. The blend was spin-coated onto binary-patterned polymer brushes to see if the patterns would affect the domain structure of the blend. Very different morphologies were observed on each substrate, and for different blend compositions.

On silicon the blend formed a bilayer structure, with a PMMA-rich layer wetting the silicon substrate, and a PS-rich layer at the free surface. The degree of enrichment and the thickness of the layers depended on the blend composition.

30/70 PS/PMMA was spin-coated onto patterned NPPOC-/amine-silane SAMs. There was no evidence of pattern replication, or of a difference in morphology on the NPPOC-silane and amine-silane coated areas. Heating resulted in dewetting, beginning from the

amine-silane coated squares. Further study is required to gain a more complete understanding of the behaviour of the blend on these substrates.

The morphologies observed on binary-patterned PS/PMMA brushes were complex. Different structures were found on the PS and PMMA brush regions, and for each blend composition. The eventual structure was determined by the interaction of the polymers with the substrate and solubility effects. Where the blend composition matched the area fraction of the pattern, there was some evidence of preferential segregation of each polymer to the chemically equivalent brush. Where there was a large mismatch between composition and area fraction, solubility effects seemed more important, resulting in a laterally phase-separated structure covering both polymer brushes.

Surface chemical patterns may direct the phase separation of a polymer blend when the natural length scale for phase separation under the conditions used is close to the periodicity of the pattern[9]. In the system discussed above, the period of the pattern was significantly larger than the natural length scale of phase separation of the polymer blend, so pattern-directed phase separation, as defined in the literature, did not occur. Different morphologies were observed on PS and PMMA brush substrates, but identical morphologies were observed on the large homogeneous regions of brush at the edges of the samples and on the corresponding parts of the pattern.

The challenges involved in the synthesis of binary-patterned polymer brushes mean that only a few samples have been produced, and the pattern size has not been optimised. The results presented in this thesis suggest that phase separation of polymer blends on binary-patterned polymer brushes is an interesting field for further study. However, it would first be necessary to solve the problems associated with the synthesis of binary-patterned polymer brushes, allowing the reproducible production of samples with predetermined thickness of both polymer brushes, and varied pattern size. In these experiments, the patterns were produced using electron microscope grids as masks, but there is no reason why smaller features (or different shapes) could not be produced by using different structures as masks. It would then be interesting to see if reduction of the pattern periodicity (or increase in the blend domain size) would result in an altered morphology, and under which conditions this might occur. The effect of brush thickness and height changes on phase separation could be studied by deliberately

synthesising topographically patterned samples. It might also be useful to investigate the role of blend film thickness on morphology and pattern replication. Finally, samples could be annealed for different times and at different temperatures to investigate how the blend morphology develops as the film approaches equilibrium.

The results presented in this chapter show that a wide range of phase-separated morphologies can be produced by varying the composition of a low molecular weight PS/PMMA blend and the chemistry of the substrate. There has been little previous study of the interaction of polymer blends with polymer brushes. The binary-patterned polymer brushes had a pattern periodicity that was too large to direct phase separation by templating the PS/PMMA domain structure, but the observed structures may still lead to useful applications.

6.7 References

(1) Balsara, N. P. In *Physical Properties of Polymers Handbook*; Mark, J. E., Ed.; AIP Press: New York, 1996.
(2) Jones, R. A. L.; Richards, R. W. *Polymers at Surfaces and Interfaces*; Cambridge University Press: Cambridge, 1999.
(3) Strobl, G. *The Physics of Polymers: Concepts for Understanding Their Structures and Behaviour*; Third ed.; Springer: Berlin, 2007.
(4) Callaghan, T. A.; Paul, D. R. *Macromolecules* **1993**, *26*, 2439-2450.
(5) Tanaka, K.; Yoon, J.-S.; Takahara, A.; Kajiyama, T. *Macromolecules* **1995**, *28*, 934-938.
(6) Müller-Buschbaum, P.; Gutmann, J. S.; Stamm, M. *Macromolecules* **2000**, *33*, 4886-4895.
(7) Li, X.; Han, Y.; An, L. *Polymer* **2003**, *44*, 5833-5841.
(8) Walheim, S.; Böltau, M.; Mlynek, J.; Krausch, G.; Steiner, U. *Macromolecules* **1997**, *30*, 4995-5003.
(9) Fichet, G.; Corcoran, N.; Ho, P. K. H.; Arias, A. C.; MacKenzie, J. D.; Huck, W. T. S.; Friend, R. H. *Advanced Materials* **2004**, *16*, 1908-1912.
(10) Krausch, G.; Kramer, E. J.; Rafailovich, M. H.; Sokolov, J. *Applied Physics Letters* **1994**, *64*, 2655-2657.
(11) Böltau, M.; Walheim, S.; Mlynek, J.; Krausch, G.; Steiner, U. *Nature* **1998**, *391*, 877-879.
(12) Higgins, A. M.; Jones, R. A. L. *Nature* **2000**, *404*, 476-479.
(13) Shou, Z.; Chakrabarti, A. *Polymer* **2001**, *42*, 6141-6152.
(14) Budkowski, A.; Bermasik, A.; Cyganic, P.; Rysz, J.; Brenn, R. *e-Polymers* **2002**, Paper No 6, 1-21.
(15) Andrew, P.; Huck, W. T. S. *Soft Matter* **2007**, *3*, 230-237.
(16) Karim, A.; Douglas, J. F.; Lee, B. P.; Glotzer, S. C.; Rogers, J. A.; Jackman, R. J.; Amis, E. J.; Whitesides, G. M. *Physical Review E: Statistical Physics, Plasmas, Fluids, and Related Interdisciplinary Topics* **1998**, *57*, R6273-R6276.
(17) Ermi, B. D.; Nisato, G.; Douglas, J. F.; Rogers, J. A.; Karim, A. *Physical Review Letters* **1998**, *81*, 3900-3903.
(18) Fukunaga, K.; Elbs, H.; Krausch, G. *Langmuir* **2000**, *16*, 3474-3477.
(19) Rockford, L.; Liu, Y.; Mansky, P.; Russell, T. P.; Yoon, M.; Mochrie, S. G. J. *Physical Review Letters* **1999**, *82*, 2602-2605.
(20) Nisato, G.; Ermi, B. D.; Douglas, J. F.; Karim, A. *Macromolecules* **1999**, *32*, 2356-2364.
(21) Cyganik, P.; Bernasik, A.; Budkowski, A.; Bergues, B.; Kowalski, K.; Rysz, J.; Lekki, J.; Lekka, M.; Postawa, Z. *Vacuum* **2001**, *63*, 307-313.
(22) Jaczewska, J.; Budkowski, A.; Bernasik, A.; Raptis, I.; Moons, E.; Goustouridis, D.; Haberko, J.; Rysz, J. *Soft Matter* **2009**, *5*, 234-241.
(23) Kielhorn, L.; Muthukumar, M. *Journal of Chemical Physics* **1999**, *111*, 2259-2269.
(24) Yan, L.-T.; Li, J.; Li, Y.; Xie, X.-M. *Macromolecules* **2008**, *41*, 3605-3612.
(25) Li, J.-L.; Yan, L.-T.; Xie, X.-M. *Polymer* **2009**, *50*, 2172-2180.
(26) Li, X.; Han, Y.; An, L. *Applied Surface Science* **2004**, *230*, 115-124.
(27) Li, Y. X.; Yang, Y. M.; Yu, F. S.; Dong, L. S. *Journal Of Polymer Science Part B: Polymer Physics* **2006**, *44*, 9-21.

(28) Kailas, L.; Bertrand, P. *Applied Surface Science* **2006**, *252*, 6648-6651.
(29) Heriot, S. Y.; Jones, R. A. L. *Nature Materials* **2005**, *4*, 782-786.
(30) Tanaka, K.; Takahara, A.; Kajiyama, T. *Macromolecules* **1996**, *29*, 3232-3239.
(31) Ton-That, C.; Shard, A. G.; Daley, R.; Bradley, R. H. *Macromolecules* **2000**, *33*, 8453-8459.
(32) Sugihara, H.; Oya, K.; Murase, H.; Akabori, K.; Tanaka, K.; Kajiyama, T.; Takahara, A. *Applied Surface Science* **2008**, *254*, 3180-3183.
(33) Madbouly, S. A.; Chiba, T.; Ougizawa, T.; Inoue, T. *Polymer* **2000**, *42*, 1743-1750.
(34) Seo, Y.-S.; Kim, E.; Kwon, S. Y.; Jing, H.; Shin, K. *Ultramicroscopy* **2008**, *108*, 1186-1190.
(35) Li, X.; Han, Y.; An, L. *Polymer* **2003**, *44*, 8155-8165.
(36) Kailas, L.; Nysten, B.; Bertrand, P. *Surface and Interface Analysis* **2004**, *36*, 1227-1230.
(37) Kailas, L.; Nysten, B.; Audinot, J. N.; Migeon, H. N.; Bertrand, P. *Surface and Interface Analysis* **2005**, *37*, 435-443.
(38) Winesett, D. A.; Ade, H.; Sokolov, J.; Rafailovich, M.; Zhu, S. *Polymer International* **2000**, *49*, 458-462.
(39) Winesett, D. A.; Zhu, S.; Sokolov, J.; Rafailovich, M.; Ade, H. *High Performance Polymers* **2000**, *12*, 599-602.
(40) Liu, D.; Yang, P. Y.; Luscombe, C. K. *Journal Of Physical Chemistry C* **2008**, *112*, 7886-7894.
(41) Ton-That, C.; Shard, A. G.; Teare, D. O. H.; Bradley, R. H. *Polymer* **2000**, *42*, 1121-1129.
(42) Li, H. M.; Wang, Z.; Chen, X. C.; Xie, Z. D.; Shu, D. J.; Wang, M.; Peng, R. W.; Ming, N. B. *European Physical Journal-Applied Physics* **2009**, *45*, 20501/1-4.
(43) Walheim, S.; Schaffer, E.; Mlynek, J.; Steiner, U. *Science* **1999**, *283*, 520-522.
(44) Cui, L.; Ding, Y.; Li, X.; Wang, Z.; Han, Y. *Thin Solid Films* **2006**, *515*, 2038-2048.
(45) Jerome, J.; Zhu, S.; Seo, Y. S.; Ho, M.; Pernodet, N.; Gambino, R.; Sokolov, J.; Rafailovich, M. H.; Zaitsev, V.; Schwarz, S.; DiNardo, R. *Macromolecules* **2004**, *37*, 6504-6510.
(46) Ugur, S.; Pekcan, O. *Journal of Applied Polymer Science* **2006**, *100*, 2104-2110.
(47) Tanaka, K.; Takahara, A.; Kajiyama, T. *Macromolecules* **1998**, *31*, 863-869.
(48) Harris, M.; Appel, G.; Ade, H. *Macromolecules* **2003**, *36*, 3307-3314.
(49) Ishii, Y. Processing of Polyphenylene Ether with Thermoset Resins, PhD thesis, University of Sheffield, 1999.
(50) Chappell, J.; Lidzey, D. G.; Jukes, P. C.; Higgins, A. M.; Thompson, R. L.; O'Connor, S.; Grizzi, I.; Fletcher, R.; O'Brien, J.; Geoghegan, M.; Jones, R. A. L. *Nature Materials* **2003**, *2*, 616-621.
(51) Chiantore, O.; Guaita, M. *Polymer Bulletin* **1988**, *20*, 201-206.
(52) Holland, B. J.; Hay, J. N. *Polymer Degradation and Stability* **2002**, *77*, 435-439.
(53) Smolders, K.; Baeyens, J. *Waste Management* **2004**, *24*, 849-857.
(54) Kaminsky, W.; Franck, J. *Journal Of Analytical And Applied Pyrolysis* **1991**, *19*, 311-318.
(55) Geoghegan, M.; Jones, R. A. L.; Clough, A. S. *Journal of Chemical Physics* **1995**, *103*, 2719-2724.
(56) Brandrup, J.; Immergut, E. H.; Grulke, E. A. *Polymer Handbook*; Fourth ed.; John Wiley and Sons, Inc.: New York, 1999.

(57) Lambooy, P.; Phelan, K. C.; Haugg, O.; Krausch, G. *Physical Review Letters* **1996**, *76*, 1110-1113.
(58) Higgins, A. M.; Martin, S. J.; Thompson, R. L.; Chappell, J.; Voigt, M.; Lidzey, D. G.; Jones, R. A. L.; Geoghegan, M. *Journal of Physics: Condensed Matter* **2005**, *17*, 1319-1328.
(59) Wendlandt, M.; Kerle, T.; Heuberger, M.; Klein, J. *Journal Of Polymer Science Part B-Polymer Physics* **2000**, *38*, 831-837.
(60) Wu, S. *Journal Of Physical Chemistry* **1970**, *74*, 632-638.
(61) Wang, C.; Krausch, G.; Geoghegan, M. *Langmuir* **2001**, *17*, 6269-6274.
(62) Zhang, Z.; Wang, Z.; Xing, R.; Han, Y. *Surface Science* **2003**, *539*, 129-136.
(63) Geoghegan, M.; Wang, C.; Rehse, N.; Magerle, R.; Krausch, G. *Journal of Physics: Condensed Matter* **2005**, *17*, S389-S402.
(64) Edwards, E. W.; Montague, M. F.; Solak, H. H.; Hawker, C. J.; Nealey, P. F. *Advanced Materials* **2004**, *16*, 1315-1319.
(65) Stoykovich, M. P.; Müller, M.; Kim, S. O.; Solak, H. H.; Edwards, E. W.; de Pablo, J. J.; Nealey, P. F. *Science* **2005**, *308*, 1442-1446.
(66) Briggs, D. *Surface Analysis of Polymers by XPS and Static SIMS*; First ed.; Cambridge University Press: Cambridge, 1998.

Chapter 7

Summary and Conclusions

Binary-patterned polymer brushes are an interesting and little studied class of micropatterned materials. Since the first example was reported in 1995[1], there have only been 12 papers reporting their synthesis and properties. The first papers reporting applications of binary-patterned polymer brushes were published in 2009, suggesting that certain systems can be used to template chemical vapour deposition of metals, or as antifouling/selective adsorption surfaces for biochemical applications[2,3].

This thesis describes the development of a novel method for the synthesis of binary-patterned polymer brushes on silicon substrates. Firstly, well-controlled, reproducible methods for the growth of unpatterned PS and PMMA brushes by homogeneous surface-initiated ATRP were identified. Binary-patterned PS/PMMA brushes were synthesised via the use of a photopatternable SAM. A NPPOC-silane monolayer was allowed to self-assemble on silicon. It was then selectively deprotected by exposure to UV light through a mask, producing a chemical pattern of amine-terminated and NPPOC-terminated regions. The exposed amine groups were reacted with 2-bromoisobutyryl bromide to generate an α-bromoester-functionalised surface which could be used to initiate the growth of PS or PMMA brushes by ATRP. The NPPOC-protected regions of the SAM were (relatively) unaffected by the reactions required to grow the first brush. The protecting groups could subsequently be removed by exposure to UV light, and the surface modification reactions repeated to generate a binary-patterned polymer brush. As ATRP is a 'living' polymerisation, it was necessary to dehalogenate, or 'kill', the first brush by reaction with sodium azide to prevent the formation of block copolymer brushes during the second polymerisation. This was only found to be possible for bromine-terminated polymer brushes, so the PS brush had to be grown first. A mixed halogen system was used to grow PMMA brushes, so the polymer chains were terminated by both bromine and chlorine. There are, however, literature methods for the synthesis of PMMA brushes that use copper(I) bromide as the catalyst, which would produce bromine-terminated PMMA brushes and remove this restriction.

Although chemical analysis (by SIMS) indicated the presence of both PS and PMMA, AFM measurement showed that the second brush (PMMA) formed a very thin layer, and that the layer thickness did not increase with increasing reaction time. Homogeneous polymer brushes grown from bromoester-silane were significantly thinner than brushes grown from BMPUS under equivalent conditions. These results suggest that the reaction of 2-bromoisobutyryl bromide with amine-SAM was inefficient, and that the density of surface-bound initiator groups was low. This was thought to be because attachment of bulky bromoisobutyrate groups to the surface would quickly hinder further reaction of the surface-bound amines. Surface-initiated ATRP from the bromoester-silane SAM resulted in a polymer layer with a grafting density too low to force the polymer chains to adopt the stretched configuration of a true polymer brush. Improving the efficiency of this reaction is essential for further development of this system. It may be possible to use more aggressive reaction conditions to increase the amount of surface-attached bromoester groups, or use a longer alkyl 'spacer' to increase the conformational flexibility of the SAM, and allow a greater number of bulky groups to be incorporated. Many different halogen-containing groups can be used as ATRP initiators, so another option might be to react the amine-SAM with a less bulky reagent to produce a surface-attached alkyl halide which can initiate ATRP. Extension of this method to allow the synthesis of other binary-patterned polymer brushes (for example those containing temperature or pH responsive groups) is likely to lead to interesting 'smart' materials with a range of practical applications.

One of the original goals of this work was the synthesis of binary-patterned polymer brushes without the use of photolithography. At the start of this project this had not been done (although two different methods have since been reported[4,5]). Attempts were made to use μCP to print BMPUS, then grow patterned brushes by surface-initiated ATRP. It did not prove possible to produce good-quality patterned brushes by this method, so an alternative approach was pursued (see above). The failure of this approach was surprising, as other groups have successfully printed other silane-functionalised ATRP initiators including 2-bromo-2-methylpropionic acid 3-trichlorosilanylpropyl ester[6]. However, self-assembly of alkyltrichlorosilanes on silicon is very complicated and is affected by many different variables (which can be hard to

control). It is possible that a more systematic study of the reaction, and printing under more controlled conditions might allow this approach to succeed in the future.

It has been shown that chemical patterns can direct the phase separation of polymer blends. Controlled, regular domain structures can self-assemble provided that there is preferential segregation of at least one of the polymers to one of the areas of the chemically patterned surface[7,8], and the periodicity of the substrate pattern is comparable to the natural length scale for phase separation under the conditions used[7,9]. Pattern-directed phase separation has been demonstrated for a range of polymer blends on patterned SAMs. A controlled domain structure has been shown to improve the efficiency of polymer LEDs[9-11] and bulk heterojunction solar cells[12]. There has been little study of the behaviour of polymer blends on polymer brushes. Polymer brushes allow access to a greater range (and density) of functional groups than is possible for SAMs. In addition, the polymer molecules in the brush can change their configuration according to the conditions. This has been shown to lead to interesting behaviour such as autophobic dewetting[12-16].

This thesis presents a preliminary investigation of the phase separation of a PS/PMMA blend on a binary-patterned polymer brush. The phase separation of the blend was investigated on silicon, patterned NPPOC-/amine-silane SAMs and binary-patterned polymer brushes. NRA and AFM showed that the blend formed a bilayer structure on silicon, with a PMMA-rich layer wetting the substrate and a PS-rich layer at the free surface. On binary-patterned PS/PMMA brushes, domains rich in each polymer were present at the surface. Different morphologies were found on the PS and PMMA brush regions and for each blend composition. Where the blend composition matched the patterned area fraction (e.g. 30/70 PS/PMMA), there was some evidence of preferential segregation of PS to PS brush, and vice versa. Unfortunately, the pattern periodicity was too large for true pattern-directed phase separation to occur. This meant that the blend morphology was the same on an unpatterned PS or PMMA brush and on the equivalent part of the pattern. Smaller scale binary-patterned polymer brushes could be synthesised using the methods described herein (via use of a mask with smaller features), but this was not done due to time constraints. A more thorough understanding of the system is needed before applications can be developed. Further study should investigate how changing the pattern periodicity affects the blend morphology as it

approaches the characteristic length scale of phase separation. It would also be interesting to investigate the effect of altering the properties of the blend, for example by changing the film thickness, the molecular weights of the polymers in the blend and annealing time and temperature.

The original goals of this project were to synthesise binary-patterned polymer brushes and to use them to investigate pattern-directed phase separation of a polymer blend. After working to overcome significant difficulties and gaining an improved understanding of ATRP reactions, brush synthesis, self-assembly, polymer blends and pattern-directed phase separation, both these goals were achieved. Further work is required to improve the quality of the binary-patterned PS/PMMA brushes, and to fully understand how the patterned substrate influences the phase separation of the blend.

7.1 References

(1) Tovar, G.; Paul, S.; Knoll, W.; Prucker, O.; Rühe, J. *Supramolecular Science* **1995**, *2*, 89-98.
(2) Liu, Z.; Hu, H.; Yu, B.; Chen, M.; Zheng, Z.; Zhou, F. *Electrochemistry Communications* **2009**, *11*, 492-495.
(3) Liu, Z.; Khan, N.; Hu, H.; Yu, B.; Liu, J.; Chen, M.; Zhou, F. *Macromolecular Rapid Communications* **2008**, *29*, 1937-1943.
(4) Zhou, F.; Zheng, Z.; Yu, B.; Liu, W.; Huck, W. T. S. *Journal of the American Chemical Society* **2006**, *128*, 16253-16258.
(5) Liu, Y.; Klep, V.; Luzinov, I. *Journal of the American Chemical Society* **2006**, *128*, 8106-8107.
(6) Hamelinck, P. J.; Huck, W. T. S. *Journal of Materials Chemistry* **2005**, *15*, 381-385.
(7) Böltau, M.; Walheim, S.; Mlynek, J.; Krausch, G.; Steiner, U. *Nature* **1998**, *391*, 877-879.
(8) Budkowski, A.; Bermasik, A.; Cyganic, P.; Rysz, J.; Brenn, R. *e-Polymers* **2002**, Paper No 6, 1-21.
(9) Fichet, G.; Corcoran, N.; Ho, P. K. H.; Arias, A. C.; MacKenzie, J. D.; Huck, W. T. S.; Friend, R. H. *Advanced Materials* **2004**, *16*, 1908-1912.
(10) Corcoran, N.; Ho, P. K. H.; Arias, A. C.; Mackenzie, J. D.; Friend, R. H.; Fichet, G.; Huck, W. T. S. *Applied Physics Letters* **2004**, *85*, 2965-2967.
(11) Yim, K.-H.; Zheng, Z.; Friend, R. H.; Huck, W. T. S.; Kim, J.-S. *Advanced Functional Materials* **2008**, *18*, 2897-2904.
(12) Chen, F.-C.; Lin, Y.-K.; Ko, C.-J. *Applied Physics Letters* **2008**, *92*, 023307/1-023307/3.
(13) Maas, J. H.; Fleer, G. J.; Leermakers, F. A. M.; Stuart, M. A. C. *Langmuir* **2002**, *18*, 8871-8880.
(14) Voronov, A.; Shafranska, O. *Langmuir* **2002**, *18*, 4471-4477.
(15) Sharma, S.; Rafailovich, M. H.; Sokolov, J.; Liu, Y.; Qu, S.; Schwarz, S. A.; Eisenberg, A. *High Performance Polymers* **2000**, *12*, 581-586.
(16) Reiter, G.; Auroy, P.; Auvray, L. *Macromolecules* **1996**, *29*, 2150-2157.